

University of Southampton Research Repository

Copyright © and Moral Rights for this thesis and, where applicable, any accompanying data are retained by the author and/or other copyright owners. A copy can be downloaded for personal non-commercial research or study, without prior permission or charge. This thesis and the accompanying data cannot be reproduced or quoted extensively from without first obtaining permission in writing from the copyright holder/s. The content of the thesis and accompanying research data (where applicable) must not be changed in any way or sold commercially in any format or medium without the formal permission of the copyright holder/s.

When referring to this thesis and any accompanying data, full bibliographic details must be given, e.g.

Thesis: Author (Year of Submission) "Full thesis title", University of Southampton, name of the University Faculty or School or Department, PhD Thesis, pagination.

Data: Author (Year) Title. URI [dataset]

University of Southampton

Faculty of Environmental and Life Sciences

School of Ocean and Earth Science

A Charged Topic: Application of Electrokinetic Remediation for Removal of Difficult-to-Measure Radionuclides at Nuclear Sites

by

Shaun Daniel Hemming

ORCID ID <u>0000-0001-5826-8710</u>

Thesis for the degree of Doctor of Philosophy

October 2025

"Every puzzle has an answer"

– Professor Hershel Layton

University of Southampton Abstract

Faculty of Environmental and Life Sciences
School of Ocean and Earth Science

<u>Doctor of Philosophy</u>

A Charged Topic: Application of Electrokinetic Remediation for Removal of Difficult-to-Measure Radionuclides at Nuclear Sites

by

Shaun Daniel Hemming

As the number of nuclear sites across the world requiring decommissioning increases, so do the challenges faced by site operators whilst safely dismantling facilities. One common issue are difficult-to-measure radionuclides (DTMRs), which emit pure alpha, pure beta, low-energy gamma, or a combination of these radiation types during decay. This makes their *in situ* detection problematic, requiring complex analysis in laboratories to quantify activities present. DTMRs can be abundant at nuclear sites and so effective remediation technologies are essential for meeting both small-scale and site-wide decommissioning objectives. Whilst numerous decontamination techniques are currently deployed at nuclear facilities, the context-specific nature of many remedial challenges mean that no single approach is appropriate for every scenario. Electrokinetic remediation (EKR) is a more sustainable and lower-cost decontamination technology compared to traditional approaches. A low-voltage direct current is applied to a contaminated material, inducing electromigration (movement of ions), electrophoresis (movement of charged colloids) and electroosmosis (movement of water). Whilst previous EKR work has focussed on easy-to-measure radionuclides (ETMRs), much less attention has been paid to DTMR remediation.

This thesis explores the applications of EKR on DTMRs, some for the first time in this context, that are present within materials commonly found at nuclear sites – namely, groundwaters, cements (as part of concretes), and sediments. H-3, Sr-90, and Tc-99 all showed good EKR-amenability in groundwaters, although transportation rates varied between each. For both homogeneous- and surface-contaminated cements, Cs-137 displayed clear migration whilst H-3, Sr-90, I-129, and U-236 showing a lesser degree or no mobilisation. In an aged, authentically contaminated coastal sediment core, Tc-99 and Pu showed greater remediation capability with a citric acid electrolyte, with Am-241 more mobile with seawater and Cs-137 demonstrating little or no remobility in either setting. Overall, low-voltage EKR showed the greatest potential when treating environmental materials (i.e. groundwaters and sediments), with a trade-off existing between the voltage used and both the remedial project duration and financial cost. The time between contamination and treatment of the material is also shown to be important, highlighting the potential of EKR as an effective emergency response technology for radionuclide leaks. Future work should look at in situ applications of the technique as well as larger pilot-scale trials to further promote EKR use as a diverse remedial tool at nuclear sites.

Table of C	Contents	S	4
Table of T	ables		11
Table of F	igures		12
Research	Thesis:	Declaration of Authorship	14
Acknowle	edgemer	nts	15
Definition	ns and A	bbreviations	17
Chapter 1	Introd	luction	19
1.1 Rad	lionuclid	es at Nuclear Sites	20
1.1.1	Radionu	clide Generation	20
1.1.2	Decomr	nissioning Challenges	20
1.2 Diff	icult-to-I	Measure Radionuclides (DMTRs)	22
1.2.1	Definition	on	22
1.2.2	Scaling	factors	23
1.2.3	Tradition	nal Remediation Approaches	24
1.3 Elec	ctrokinet	ic Remediation (EKR)	26
1.3.1	Principle	9S	26
	1.3.1.1	Electromigration	27
	1.3.1.2	Electrophoresis	27
	1.3.1.3	Electroosmosis	28
	1.3.1.4	Electrolysis	28
	1.3.1.5	Benefits	28
1.3.2	Previous	s Studies	29
	1.3.2.1	Common Metrics of EKR Effectiveness	29
	1.3.2.2	Application on Radionuclides	30
	1.3.2.3	Common Experimental Setups	33
	1.3.2.4	Summary of Studied Radionuclides in EKR Literature	34
1.4 The	sis Aims	and Objectives	

1.5	The	sis Struc	cture	36
1.6	Ref	erences.		36
Chap	oter 2	2 Instru	ument Methodologies for Radionuclide Quantificatio	n 45
2.1	Intr	oductior	n	46
2.2	Ехр	erimenta	al Setup and Parameters Used	46
2.3	Qua	ality Con	trol During Analysis	46
2.4	Alp	ha Spect	trometry	47
2.5	Liqu	uid Scint	tillation Counting (LSC)	47
2.6	Gar	nma Spe	ectrometry	48
2.7	Ind	uctively (Coupled Plasma Mass Spectrometry (ICP-MS)	49
2.8	Ref	erences.		50
Chap	oter 3	B Migra	ation of Aqueous Radionuclide Contaminants	51
3.1	Intr	oduction	n	52
;	3.1.1	Sellafiel	ld Case Study	52
		3.1.1.1	Background	52
		3.1.1.2	Geology and Hydrogeology	52
		3.1.1.3	Groundwater contamination	53
;	3.1.2	Electrok	kinetic remediation (EKR)	55
;	3.1.3	Radionu	uclides of Interest	56
3.2	Met	hods		58
;	3.2.1	Material	ls and Reagents	58
;	3.2.2	Experim	nental Setup	58
;	3.2.3	Analysis	s 60	
3.3	Res	ults	•••••••••••••••••••••••••••••••••••••••	61
;	3.3.1	Distribu	ıtion Profile Quantification	61
;	3.3.2	Tube cu	ırrents, pHs, and Electrolyte Evaporation	62
;	3.3.3	Tritium	64	
;	3.3.4	Strontiu	ım-85	65

	3.3.5	5 Technetium-99	65
3.4	Dis	scussion	66
	3.4.1	1 Tritium 66	
	3.4.2	2 Strontium-85	66
	3.4.3	3 Technetium-99	67
	3.4.4	4 Radionuclide Comparisons and Future Work	68
3.5	Cor	onclusions	69
3.6	a Ack	knowledgements	70
3.7	' Ref	ferences	70
Cha	ntor	4 Investigation into Padionuclida Migration Through Co	monto Hoing
Cila	iptei 2	4 Investigation into Radionuclide Migration Through Ce Electrokinetic Remediation	_
4.1		troduction	
		1 Electrokinetic Remediation (EKR)	
	4.1.2	2 Radionuclides of Focus	
		4.1.2.1 H-3	
		4.1.2.2 Sr-90	80
		4.1.2.3 I-129	80
		4.1.2.4 Cs-137	81
		4.1.2.5 Uranium	81
4.2	. Met	ethods	82
	4.2.1	1 Core Descriptions	82
		4.2.1.1 Reagents	83
	4.2.2	2 Core Creation and Contamination	83
	4.2.3	3 Electrokinetic Treatment	84
	4.2.4	4 Core Sampling	85
4.3	8 Ana	nalysis	86
	4.3.1	1 Autoradiography	86
	4.3.2	2 Radionuclide Analysis	86

		4.3.2.1	H-3 and I-129	86
		4.3.2.2	Sr-90, Cs-137, and U-236	87
		4.3.2.3	Sr-90 and U-236 (Continued)	87
		4.3.2	2.3.1 Sr-90 Purification	88
		4.3.2	2.3.2 U-236 Purification and Electrodeposition	88
4.4	Res	sults		88
	4.4.1	Soaking	Set Contamination	88
	4.4.2	Visual O	Observations	89
	4.4.3	Current	and pH	90
	4.4.4	Autorad	liography	90
	4.4.5	Discrete	e Radionuclide Analysis	92
		4.4.5.1	H-3	92
		4.4.5.2	Sr-90	92
		4.4.5.3	I-129	92
		4.4.5.4	Cs-137	93
		4.4.5.5	U-236	93
4.5	Dis	cussion.		100
	4.5.1	Autorad	liography	100
	4.5.2	Discrete	e Radionuclide Analysis	101
		4.5.2.1	H-3	101
		4.5.2.2	Sr-90	102
		4.5.2.3	I-129	102
		4.5.2.4	Cs-137	103
		4.5.2.5	U-236	104
	4.5.3	Radionu	uclide Comparison and Future Work	105
4.6	Coi	nclusions	s	107
4.7	Ref	erences.		108

Chapter 5 Application of Electrokinetic Remediation for Clean-up of

Medium- and Long-Lived Radionuclides in Coastal Sediments 115

5.1	1 Inti	roduction	1	116
	5.1.1	Electrok	cinetic remediation (EKR)	117
5.2	2 Ma	terials an	nd Methods	118
	5.2.1	Core Co	llection and Experimental Set Up	118
	5.2.2	Analysis	3 122	
		5.2.2.1	Reagents	122
		5.2.2.2	X-ray Fluorescence (XRF)	122
		5.2.2.3	Caesium-137 and Americium-241	122
		5.2.2.4	Organic Matter and Carbonate Content	122
		5.2.2.5	Plutonium	123
5.3	3 Res	sults and	Discussion	123
	5.3.1	Visual O	Observations	123
	5.3.2	Current	and pH Measurements	123
	5.3.3	XRF	124	
		5.3.3.1	Core Composition	125
		5.3.3.2	Redox Sensitive Elements	125
	5.3.4	Initial Ra	adionuclide Distributions	126
	5.3.5	Defining	Peaks of Elevated Radionuclide Activities	126
	5.3.6	Caesiun	n-137	127
	5.3.7	Plutoniu	ım	129
	5.3.8	Americi	um-241	133
	5.3.9	Electroly	yte Comparison and Upscaling Requirements	136
5.4	4 Ref	erences.		138
Cha	apter (6 Reme	ediation of Tc-99 in Legacy Coastal Sediments Through	the
			f Electrokinetic Remediation	
6.1	1 Intı		1	
20		Tc-99	151	
	- •	6.1.1.1	Environmental Geochemistry	151
			•	

		6.1.1.2 Analytical Complexities	152
6	6.1.2	Electrokinetic Remediation (EKR)	153
6.2	Met	thods	155
6	6.2.1	Materials and Apparatus Setup	155
6	6.2.2	Analysis 157	
		6.2.2.1 X-ray Fluorescence (XRF)	157
		6.2.2.2 Tc-99	157
		6.2.2.2.1 Reagents	157
		6.2.2.2.2 Quantification Using Tc-99m Tracer	158
		6.2.2.2.3 Quantification Using Stable Re Tracer	158
		6.2.2.4 Defining Regions of Elevated Activity	160
6.3	Res	sults	160
6	6.3.1	Visual EKR Observations	160
6	6.3.2	XRF Analysis	161
6	6.3.3	Tc-99m and Re Tracer Comparison	162
6	6.3.4	Sediment Core Tc Distributions	163
6.4	Disc	cussion	165
6	6.4.1	Visual EKR Observations	165
6	6.4.2	Tc-99m and Re Tracer Comparison	165
6	6.4.3	Sediment Core Tc Distributions	166
6	6.4.4	Comparison Between Electrolytes and Future Work	168
6.5	Con	nclusions	169
6.6	Ack	knowledgements	170
6.7	Ref	ferences	170
Chan	oter 7	7 Conclusions and Future Work	177
7.1		erall Conclusions	
7.2		ntributions to EKR Knowledge	
7.3		ure Work	
/.4	Ket	ferences	

App	endix A Supp	oorting Information for Chapter 3	185
A.1	Radionuclid	e Solution Preparation	186
A.2	Preliminary	Experiments with Stable Sr and Re	187
	A.2.1 Introduc	ction	187
	A.2.2 Methods	s 187	
	A.2.3 Results	188	
	A.2.3.1	Cell pHs	188
	A.2.3.2	Sr and Re Concentrations	188
	A.2.4 Discuss	ion	191
	A.2.5 Conclus	sions	192
	A.2.6 Referen	ces	192
Арр	endix B Supp	oorting Information for Chapter 4	196
B.1	Analytical M	lethods	197
	B.1.1 H-3 and	I-129	197
	B.1.2 Sr-90, C	s-137, and U-236	197
	B.1.3 Sr-90 an	nd U-236 (Continued)	198
	B.1.3.1	Sr-90 Purification	198
	B.1.3.2	U-236 Purification and Electrodeposition	199
Арр	endix C Supp	oorting Information for Chapters 5 and 6	202
C. 1	References.		223
Арр	endix D Towa	ards the application of electrokinetic remediation for	
- •		ar site decommissioning	224
Арр	endix E Curr	ent and emerging technologies for the remediation of	
	diffici	ult-to-measure radionuclides at nuclear sites	247

Table of Tables

Table of Tables

Table 3.1 – Summary for radionuclides of focus57	7
Table 3.2 – Summary of each tube used in the experiments)
Table 3.3 – Tube pHs at the beginning and end of the experiment62	<u>)</u>
Table 3.4 – SGWS additions to each cell63	3
Table 3.5 – Final radionuclide distributions within each tube64	1
Table 4.1 – Summary of the properties for radionuclide of focus, as well as the activities us	sed to
contaminate each core used in this study82	2
Table 4.2 – Radionuclide uptakes for the Soaking Set cement cores89)
Table 5.1 – Summary for radionuclides of focus118	3
Table 5.2 – Summary table for definition and range of radionuclide regions of elevated acti	vity,
and extent of radionuclide remobilisation for each core135	5
Table 6.1 – Summary of chemical tracers that can be used for Tc-99 analysis153	3
Table 6.2 – Summary of the yellow liquids produced from the EKR cores during treatment.	161
Table 6.3 – Summary table for the extent of remobilisation in each of the three 'peaks'	
containing elevated levels of Tc-99 activity165	5

Table of Figures

Figure 1.1 – The radioactive waste hierarchy22
Figure 1.2 – Schematic showing the three main transportation mechanisms that occur during EKR
Figure 1.3 – Periodic table showing the state of progress since 2009 for EKR on elements with isotopes commonly found at nuclear sites (excluding those with half-lives of < 1 year)
Figure 2.1 – Schematic of an ICP-MS50
Figure 3.1 – Sellafield groundwater monitoring data from 2020-202254
Figure 3.2 – EKR schematic55
Figure 3.3 – Experimental setup for the EKR cells60
Figure 3.4 – Heat map results for all eight tubes
Figure 4.1 – Schematic of the fundamental EKR principles
Figure 4.2 – Schematic showing the naming system for each of the cores created per set.83
Figure 4.3 –Schematic of electrokinetic remediation setup; Side-on view on the Homogeneous Set Cathode core prior to EKR; Top-down view of the four Homogeneous Set cores
Figure 4.4 – Schematic showing how the core was subsampled for analysis86
Figure 4.5 – Autoradiography for the Homogeneous Set and Soaking Set cores91
Figure 4.6 – activity concentrations present in each cement core section
Figure 5.1 – Summary diagram of electrokinetic remediation
Figure 5.2 – Map of the Ravenglass Saltmarsh core sampling location map; Photo from the core sampling location
Figure 5.3 – Schematic showing how the collected core was divided up; Photo of the experimental setup; Photo of the citric acid core electrolyte 'bridge' 121
Figure 5.4 – Photo, radiograph, and µ-XRF data for key stable elements in the control core.126

Table of Figures

Figure 5.5 – Radionuclide distributions in the control core, seawater core, and citric acid core
127
Figure 6.1 – Map of the Esk Estuary and Ravenglass Saltmarsh151
Figure 6.2 – Schematic for the principles of electrokinetic remediation154
Figure 6.3 – Schematic of the divided sediment core; Photo of the experimental setup; Photo of
the citric acid core electrolyte 'bridge'
Figure 6.4 – Photograph, radiograph, and elemental and ratioed XRF data for key nuclides (XRF)
in the control core162
Figure 6.5 – Sediment Tc-99 activities when using Re and Tc-99m tracers163
Figure 6.6 – Quantitative Tc data and semi-quantitative XRF Mn and Fe measurements 164
Figure 7.1 – periodic table showing EKR amenability based on work presented within this thesis
180
Figure 7.2 – Periodic table showing the state of progress since 2009 for EKR on elements with
isotopes commonly found at nuclear sites181

Research Thesis: Declaration of Authorship

Research Thesis: Declaration of Authorship

Print name: Shaun Daniel Hemming

Title of thesis: A Charged Topic: Application of Electrokinetic Remediation for Removal of Difficult-to-Measure Radionuclides at Nuclear Sites

I declare that this thesis and the work presented in it are my own and has been generated by me as the result of my own original research.

I confirm that:

- This work was done wholly or mainly while in candidature for a research degree at this University;
- 2. Where any part of this thesis has previously been submitted for a degree or any other qualification at this University or any other institution, this has been clearly stated;
- 3. Where I have consulted the published work of others, this is always clearly attributed;
- 4. Where I have quoted from the work of others, the source is always given. With the exception of such quotations, this thesis is entirely my own work;
- 5. I have acknowledged all main sources of help;
- 6. Where the thesis is based on work done by myself jointly with others, I have made clear exactly what was done by others and what I have contributed myself;
- 7. None of this work has been published before submission.

C: +	Date:
Sionattire	Date.

Acknowledgements

Firstly, I would like to thank the Natural Environmental Research Council for my funding through the University of Southampton INSPIRE DTP. I would also like to thank the TRANSCEND Consortium for the networking and funding opportunities, allowing me to meet so many incredible people in the nuclear community, both nationally and internationally.

My thanks also go to Andy Cundy and Phil Warwick for their invaluable advice and support you've offered me over the years. To Andy especially, from the (often wet and windy) Tenby fieldtrips to my many, hour-long "I promise this will only take five minutes this time" meetings, it has been a blast. You offered me my undergraduate 4th year research project (which feels like a lifetime ago now!) and, later, the PhD which gave me the opportunity to develop into the scientist I am today – "thank you" doesn't begin to cover how appreciative I am for everything.

Reflecting on the early days, I'd like to thank Jamie Purkis for all his help during the 'tutorial level' (1st year) of the PhD, teaching me how to be a proper chemist, and recently helping me out with feedback on thesis drafts. My thanks also go to Sarah Lu for thesis feedback as well as introducing me to two things: STEM outreach and working at NOCS until it closed for the night. As much as I could *sometimes* complain about both, outreach is still one of my PhD highlights.

I'd like to extend my gratitude to all the GAU-Radioanalytical staff for their patience in the lab with me, willingness to answer my never-ending list of questions, and for the occasional leftover sandwiches after any training events. I would also like to thank James Graham from the National Nuclear Laboratory for his advice throughout the project, and for organising trips to various nuclear sites – the latter was the 'cherry on the cake' for my time as a PhD student.

To the Compass Crew – Clara, William, and Harry (with special guests Ash, Vestri, and Molly & Jacob) – thanks for all the fun times, from the big things such as summer BBQs and movie nights to little things like the many random hallway/staircase conversations and continuously finding plastic babies hidden around the kitchen. It was such a fun house dynamic, and I will always miss it (almost as much as I miss William's big TV).

Whilst there's so many of the PGR community I'd like to thank for the fun lunch times and PG Coffees, a few key names come to mind – Mark, Phoebe, and Izzy. Through the highs and lows, you were always ready to have a laugh and make the days seem brighter (even if it normally involved the most chaotic conversations imaginable). Also, to Jamie, thanks for all the evenings teaching me navy slang and chatting about rugby, even if you repeatedly tried and failed (at time of writing) to convert me to being a coffee drinker. Continuing the rugby theme, I'd like to thank Joe for the work distractions (in a good way) with games evenings and getting me hooked on the

Acknowledgements

Premiership (COYQ!). Shout outs are also deserved for both the Monday quiz team and Thursday quiz/games night gang – sometimes I think it is a miracle I got any PhD work done.

Finally, I'd like to thank my family for always being there for me and being so supportive of my ambitions. I hope I've made you proud. Plus, as an added bonus, I will finally stop going on about "EKR" and "DTMRs" now, as if they are normal things everyone knows about.

To everyone mentioned, as well as office mates past and present, and those I've forgotten to mention (oops, sorry), you've helped to make this journey an unforgettable one. Thank you.

Definitions and Abbreviations

Bq...... Becquerel CPS Counts per second DTMR...... Difficult-to-Measure Radionuclide EDTA..... Ethylenediaminetetraacetic acid EKR..... Electrokinetic remediation ETMR Easy-to-measure radionuclide HLW High level waste IAEA......International Atomic Energy Agency IAEA......International Atomic Energy Agency ICP-MS Inductively coupled plasma mass spectrometry ILW Intermediate level waste K_d...... Partition coefficient LLW Low level waste LOD Limit of detection LSC.....Liquid scintillation counting m/z mass to charge ratio MQ Milli Q water MSSS Magnox Swarf Storage Silo NDA...... Nuclear Decommissioning Authority NORM...... Naturally occurring radioactive material P&T..... Pump and treat pCi..... Picocurie ppb......parts per billion by mass (i.e. nanograms per gram) ppm......parts per million by mass (i.e. micrograms per gram) PRB permeable reactive barrier

SGWS Sellafield groundwater simulant

Definitions and Abbreviations

TEVA	Tetravalent Actinide extraction chromatographic resin
UTEVA	Uranium and Tetravalent Actinide extraction chromatographic resin
WHO	World Health Organisation
XRF	X-ray fluorescence

Chapter 1 Introduction

This chapter uses work from Purkis et al. (2021) and Hemming et al. (2023) (papers included in full in Appendix D and Appendix E, respectively).

1.1 Radionuclides at Nuclear Sites

1.1.1 Radionuclide Generation

Since the end of World War II, 50 countries around the world have built nuclear power plants to generate electricity, as of 2023 (IAEA, 2023). Nuclear reactors function by bombarding fissile nuclear fuel such as U-235 or Pu-239 with neutrons, causing nuclei instability and consequent fission. As well as releasing thermal energy, the fissile nucleus breaks into two or more pieces, each with a chance of being unstable and needing to undergo radioactive decay to achieve stability (known as a radionuclide). The probability of particular isotopes being created, known as the fission yield, has been highly studied and, as such, these values are well known (IAEA, 2025). A wide range of chemical elements and isotopes can be created as result of fission, with the latter having half-lives between fractions of a second to septillions of years. Whilst in the reactor, U and Pu isotopes can absorb neutrons and subsequently undergo beta minus decay to produce elements with greater atomic numbers. These are referred to as the transuranics and range from U to Cm on the periodic table (z = 92-96).

As well as nuclear fuel, neutrons can also collide with stable atoms surrounding the reactor, such as those in concrete bioshielding or coolant systems, potentially causing them to absorb the neutron and become a radionuclide. These are known as activation products and can be present as many different isotopes and chemical elements depending on the materials present near the reactor.

Over the operational lifetime of a nuclear reactor, successive fuel rod burnup and increased neutron bombardment of reactor casing produces a variety of wastes. After this, site decommissioning is commenced which requires these materials are decontaminated to ensure their safe long-term disposal.

1.1.2 Decommissioning Challenges

With the backdrop of the Cold War, weapons production was the main priority for a significant part of many early nuclear reactors' operational lifetimes. As such, remediation and clean-up projects were often sidelined and have consequently resulted in technical challenges in the present day (e.g. Magnox fuel left in storage ponds for years at the Sellafield nuclear site, resulting in containment degradation and pond contamination (Jackson et al., 2014)). In addition, the inevitability of every nuclear site eventually requiring dismantling means that effective decontamination, along with the site-specific complexities that may come with this, will be required for both the present and future. It is viewed that safe remediation of material is

required now, rather than making the issue a problem for future generations (e.g. NDA, 2021). However, the nature of radionuclides means they cannot be broken down or destroyed like some organic (Megharaj et al., 2011; Newman and Reynolds, 2004) and inorganic contaminants (Srichandan et al., 2022). Further, the range of different chemistries, half-lives, and toxicities present in different materials (Korolev, 2009; Purkis et al., 2021b) at nuclear sites makes decommissioning strategies and approaches context-specific, meaning generic plans that were effective at one facility may not be suitable for other sites.

Over the last few decades, sustainability has become of increasing importance in the nuclear sector. Ellis and Hadley (2009) defined sustainability as a remedy to a problem that maximises the net benefits to both humans and the environment whilst using only minimal resources. In 2008, the European Union produced legislation to emphasise sustainability when considering radioactive waste. A waste hierarchy was created (Figure 1.1) to show the pathway deemed most appropriate when considered with waste. Prevention of waste generation was the top priority, with remaining priorities being minimisation, re-use, recycling and disposal. In the UK, this philosophy was adopted by the Nuclear Decommissioning Authority (NDA), which implemented it into its core strategy for management and decommissioning of its nuclear sites across the UK (NDA, 2023). Remediation of waste is of clear benefit, as it firstly minimises the volumes that would otherwise enter limited capacity waste disposal sites but may also allow previously contaminated or partially decontaminated material to be re-used. This fulfils two of the top three criteria in the waste hierarchy and should therefore be prioritised as a present and future area of research and development.



Figure 1.1 – The radioactive waste hierarchy, a priority list in how to manage waste to create sustainable practices. Waste prevention is considered the ideal outcome, with reuse, recycle, and disposal further down the hierarchy (NDA, 2023).

1.2 Difficult-to-Measure Radionuclides (DMTRs)

1.2.1 Definition

Difficult-to-measure radionuclides (DTMRs) are isotopes than emit either pure alpha, pure beta, low-energy gamma, or a combination of these three radiation types during radioactive decay. This results in an absence of penetrating high-energy gamma emissions, which can escape some chemical matrices and be detected by a gamma spectrometer without the need for destructive sample analysis. DTMRs therefore need to be chemically separated from their host matrix as well as, in most cases, other radionuclides in order to be quantified. This can be complex and time consuming, as transportation to laboratories must be performed (whilst mitigating any risks to operators and the public associated with mobilising *in situ* radioactive samples and moving them between locations both on- and off-site) and analysis undertaken (likely taking days or weeks depending on the desired radionuclide(s)). In comparison to both *in situ* and *ex situ* quantification of easy-to-measure radionuclides (ETMRs), which can take as little as minutes or hours, the length of time required for DTMR mapping can make both emergency response and remediation scenarios challenging.

There currently is no exact definition for what constitutes 'difficult to measure', as this is context-dependent on the abundance, gamma emission energy, and gamma emission probability for a given radionuclide, as well as the sensitivity of the detector, which all contribute to the instrument counting efficiencies. Further, if multiple gamma emitters with similar radiation energies exist within a sample, accurate quantification of each can be difficult without additional gamma peaks from the same radionuclides to use in spectra peak deconvolution. It is agreed that pure alpha and pure beta emitters (e.g. H-3, C-14, Sr-90 (ISO, 2007; Leskinen et al., 2020; Thierfeldt and Deckert, 1996)) are challenging to quantify but ambiguity comes when determining a threshold limit for easily measurable gamma. The maximum gamma energy in previous work with an emission probability of > ~ 0.1 % has ranged from 100-200 keV depending on the context of the work and radionuclides investigated (e.g. Leskinen et al., 2020; Thierfeldt and Deckert, 1996), although many DTMRs have energies much below these values. Alternatively, a definition of gamma emissions < 100 keV has been previously used as a compromise between including many key radionuclides relevant to nuclear sites whilst ensuring challenging quantification still remained true (Hemming et al., 2023). As advancements in detection technology progress over time, such as reduced limits of detection and more efficient instrument shielding, it is likely that any DTMR definition would change. However, due to naturally occurring radioactive material (NORM), Compton scattering (partial deposition of gamma energy into gamma spectrometer; see Section 2.4), and radionuclides' xray emissions making backgrounds on gamma spectra an inevitability, as well as the existence of pure alpha and beta emitters, a form of DTMR definition will likely always exist. This thesis will use a modified definition of the one proposed by Hemming et al. (2023) – a DTMR here is a radionuclide with a < 0.1 %probability of emitting gamma radiation greater than 100 keV per radiative decay.

1.2.2 Scaling factors

One approach for estimating the activity of a DTMR in a scenario is to determine the ratio between the DTMR and an ETMR (e.g. Sr-90 : Cs-137), called a scaling factor (IAEA, 2009). This allows subsequent samples to only undergo ETMR analysis, with DTMR activities estimated based on the ETMR abundance and the scaling factor. This can reduce the number of samples that require laboratory analysis, reducing both the cost and timescale of remediation. However, this approach requires two conditions: the scaling factor can be accurately determined, and there is little or no variation in scaling factors between individual samples. Failure to meet both prerequisites (e.g. if Sr-90 migration rate in a sediment were much lower than that of Cs-137) can cause inaccurate estimations and may delay decommissioning and remediation projects if all samples must undergo DTMR analysis following issues with scaling factors. Further, UK

nuclear sites such as Winfrith, Harwell, and Dounreay are examples of facilities that performed research on various reactor designs (NDA, 2019), meaning scaling factors for typical British nuclear power plants cannot be relied upon in these contexts. As such, this technique becomes much more limited in its applications and any scaling factors that are used must be checked frequently to ensure accurate DTMR estimation are being made.

1.2.3 Traditional Remediation Approaches

Technologies discussed in this section are focussed only on medium- or long-term immobilisation, dispersion, or removal of radionuclides, as approaches such as sediment capping, in-ground barriers, or monitored natural attenuation focus more on passive containment or in-action (ONR, 2020) instead of active decontamination.

For water soluble radionuclides sometimes found in groundwater contamination such as Sr-90, Tc-99, and I-129, in addition to H-3 which primarily exists as tritiated water, pump-and-treat (P&T) is the most commonly applied ex situ technique at nuclear sites (Dushenkov, 2003; Pearce et al., 2020). For this, groundwater is pumped to a treatment facility where ion exchange, adsorption, or chemical processes extract contaminants, and the clean water is released into surface waters or back into the subsurface. Whilst the technique has been commonly deployed due to its success for a wide range of radionuclides, set up and maintenance costs (which may be multiple decades for long-term projects) for the piping and treatment facility can be expensive and is consequently not considered a sustainable remediation technique (Hemming et al., 2023). An alternative more sustainable, in situ approach are permeable reactive barriers (PRBs), which involves creating a trench in the path of groundwater flow that is filled with a reactive medium that causes adsorption of precipitation of radionuclides and allows clean groundwater to pass through (Faisal et al., 2018; Obiri-Nyarko et al., 2014). However, this method relies on accurate contaminant mapping and suitable placement to avoid migration around the barrier, as well as previous authors reporting loss of permeability over time due to mineral precipitation within the PRB (e.g. Henderson and Demond, 2007; Phillips et al., 2003), making it less suitable for large plumes. Phytoremediation has also been used previously for immobilising, volatilising, and changing speciation of radionuclides for medium and long time periods through the use of plants and associated microbial and fungal communities (Ali et al., 2013; Alkorta et al., 2004; Macci et al., 2020; Salt et al., 1995). This can be considered one of the most passive in situ techniques and offers secondary benefits such as increased biodiversity (Cundy et al., 2021) but is limited to remediating shallow groundwater contamination as well as low activities of volatile radionuclides to avoid inhalation risks to site operators or the public (Hemming et al., 2023).

For radionuclides with higher affinities to sediment, such as Pu and Am in most soils and Cs in clays, alternative techniques must be used. Soil washing is a simple approach involving spraying of a material with both water and chelating agents to mobilise or complex radionuclides into a solution phase (ONR, 2020). This can work well for weakly-bound contaminants and can be performed both in situ and ex situ, but the possible loss of surfactants into the subsurface if performed in situ may raise concerns with site regulators and will likely only be an effective technique if all the radionuclides concentrate efficiently into the washings or (ex situ only) particular sediment grain sizes or phases (Liu et al., 2022; ONR, 2020). Solidification and stabilisation can also be performed, involving immobilisation through either physical (encasement in materials such as cement) or chemical (e.g. redox reactions or gaseous reduction for conversion to a less mobile oxidation state) means, respectively (ONR, 2020; Tajudin et al., 2016). These can be deployed both in situ or ex situ and can be effective at sequestering radionuclides to ensure no subsequent remobilisation is likely to occur, with the latter option allowing for mixing with additives beforehand to ensure homogeneous distributions (ONR, 2020). However, solidification can create much larger waste forms than if material were directly treated, and the efficacy of chemical treatment can be limited if the contaminated medium has a low porosity or a high buffering capacity to any changes in redox or pH conditions (Hong and Um, 2023). Further, in both cases radionuclides remain within their original medium, meaning the material may need replacing if the treated area is removed after project completion, and the long-term durability of the material may be affected by factors such as weathering if left in situ (ONR, 2020).

Structural materials for buildings such as concretes require different approaches. Concrete remediation can be broken into two broad divisions. The first is physical techniques, which generally target contamination on outer surfaces. This includes less intrusive methods such as washing, scrubbing with surfactants, or applying peelable foam-gels, removing weakly bound contaminants (NEA, 1999). Residual contamination can then be removed through more aggressive approaches such as surface removal by blasting, grinding or scabbling. These simple approaches, particularly washing, can be effective whilst having minimal impact on the concrete's structural properties which make it an ideal *in situ* technique. However, if radionuclides display high levels of retention, physical removal of material is required which would likely create potential health risks to workers through dust generation (Sow *et al.*, 2020). Care is also needed to avoid the removal of clean concrete deeper within the structure alongside contaminated surficial material (NRC, 2001) as this will increase total waste volumes. These methods also do not remediate radionuclides deeper within the concrete, making them entirely unsuitable in cases involving activated concrete, where radionuclides can be found > 1 m into the structure (*e.g.* Kim *et al.*, 2008; PGE, 1995). Alternatively, chemical techniques can be

used, which involve either *ex situ* submersion or *in situ* application of reagents onto the material (Attallah *et al.*, 2018; NEA, 1999). This can be done to a solid monolith to address surface and near-surface contamination, or on crushed material to treat contamination that would be otherwise inaccessible (unless fractures were present that could act as a preferential chemical transportation pathway) (NEA, 1999). The concentration of reagent(s) used can be chosen based on the volume of contaminated material and the radionuclide resilience to aqueous phase uptake. However, the volume of cleaning agents required to achieve sufficient remediation may be significant if using lower concentrations, and higher concentrations may involve additional measures put in place to prevent operator harm whilst in use as well as secondary treatment and waste minimisation (Hong and Um, 2023). Further, the use of acids will dissolve the concrete rather than target specific radionuclides, potentially producing large waste volumes depending on the starting mass of contaminated material, as well as impacting the post-treatment concrete's structural properties (Hong and Um, 2023; NEA, 1999). Chemical approaches will only affect radionuclides in the near-surface, reducing the efficacy of concrete bioshielding decontamination.

Whilst every remediation technique has its strengths and niches for optimal use, each also has disadvantages, making the ideal technology for a given remedial project highly context specific. As such, it is important for site operators to have a variety of approaches available to them so they can make informed decisions on which is best for their context. Emerging technologies are therefore vital to this goal – newer techniques able to support areas in which traditional methods are generally weaker, as well an incorporating greater sustainability into nuclear sector practices.

1.3 Electrokinetic Remediation (EKR)

1.3.1 Principles

Electrokinetic remediation (EKR) is an emerging technology that can be considered more sustainable than many traditionally applied decontamination approaches. EKR involves the application of a direct current into a contaminated material through electrodes placed within the medium (Acar *et al.*, 1995; Acar and Alshawabkeh, 1993; EPA, 1995). Typically, either a constant amperage or constant voltage is applied, although both achieve the same purpose as they are intrinsically linked through equation 1.1:

$$V = IR \tag{1.1}$$

Where V is the voltage (V), I is the current (A), and R is the resistance (Ω). If the contaminated material is permeable, three main transportation processes can occur (see below).

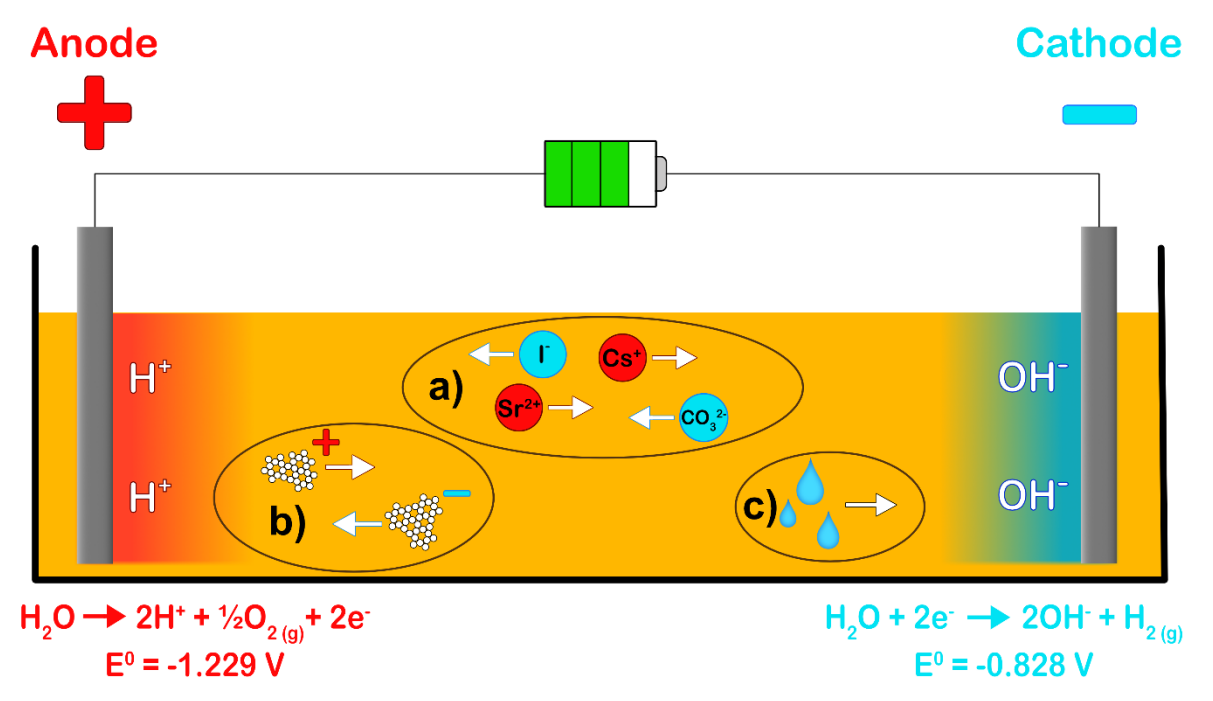


Figure 1.2 – Schematic showing the three main transportation mechanisms that occur during EKR: a) electromigration; b) electrophoresis; and c) electroosmosis. Electrolysis of water results in hydronium ion generation at the anode and hydroxide ion creation at the cathode, which migrate towards each other as a result of electromigration, resulting in the formation of a pH gradient across the cell over time.

1.3.1.1 Electromigration

Electromigration is the movement of dissolved ions throughout the system, caused by electrostatic attraction towards an electrode (Figure 1.2; Sun *et al.*, 2023). Cations will migrate towards the cathode (electrode(s) with a negative charge) and anions migrating towards the anode (electrode(s) with a positive charge) (Purkis *et al.*, 2021b; Vane and Zang, 1997). Migration rates can be affected by an ion's diffusion coefficient, concentration, resorption/desorption rates, charge, the material's porosity, grain size, tortuosity and temperature, and the voltage gradient applied (Acar and Alshawabkeh, 1993; Sun *et al.*, 2023; Thepsithar, 2006). Electromigration is the major cause of electrical current flow in a system with a moderate concentration of electrolytes (Pamukcu *et al.*, 1997).

1.3.1.2 Electrophoresis

Electrophoresis is similar to electromigration, but instead involves the movement of charged colloids (small particles typically 1-5000 nm in size (Lee, 2019)) throughout a solution (Figure 1.2). Colloidal material can consist of clay particles, microorganisms, surfactant micelles and electrolytes (Vane and Zang, 1997). Due to the larger size of the colloid in respect to an ion, the factors controlling migration rates differ; the transportation rate during electrophoresis depends on fluid viscosity, particle zeta potential and radius, and voltage gradient (Acar and Alshawabkeh, 1993; Brett and Brett, 1993; Delgado *et al.*, 2007).

1.3.1.3 Electroosmosis

Electroosmosis is the movement of water molecules caused by electric double layer (EDL) migration. EDLs can form when cations are attracted to negatively charged grains such as the sediment particles (Martin *et al.*, 2019; Oldham, 2008). This creates two cationic layers – the inner layer is strongly bound to the particle surface, whilst the outer layer is shielded from it, allowing hydrated ions to form which makes the outer layer more diffuse and mobile. When an electrical current is applied, electromigration causes the diffuse outer layer of cations to migrate towards the cathode (Martin *et al.*, 2019). Electroosmosis is the only one of the discussed processes to be able to transport contaminants without a charge, through advection (Pamukcu *et al.*, 1997). Since the process transports water towards the cathode, cationic migration is aided by electroosmosis whilst anionic migration is hindered. However, electroosmosis is a much slower transportation process than electromigration (Sun *et al.*, 2023), resulting in an overall minor effect on electromigrative processes.

1.3.1.4 Electrolysis

Electrolysis occurs at both electrodes, but the products generated are dependent on the polarity. Equations 1.2 and 1.3 show the half-equations for the cathode and anode, respectively, with potentials quoted relative to the standard hydrogen electrode (Acar and Alshawabkeh, 1993).

$$H_2O + 2e^- \rightarrow 2OH^- + H_2$$
 (E⁰= -0.828 V) (1.2)

$$H_2O \rightarrow 2H^+ + 1/2O_2 + 2e^-$$
 (E⁰ = -1.229 V) (1.3)

Gaseous H_2 and O_2 are produced, along with aqueous OH^- and H^+ which, due to their charges, then migrate towards the oppositely charged electrode. With a great enough voltage and time, this migration can form a pH gradient across the contaminated material.

1.3.1.5 Benefits

EKR can be quicker at remediating low-permeability materials such as clay than other technologies that involve fluid flow (e.g. Xu et al., 2021), as it allows ions to migrate without the need for a hydraulic gradient, and also assists cation migration through movement of the EDL when a current is applied. The approach can be considered low-cost compared to traditional technologies such as P&T (e.g. average set up and annual maintenance costs of 32 United States Environmental Protection Agency P&T sites in North America of $\sim £3.8$ million (\$4.9 million) and $\sim £610,000$ (\$770,000), respectively, in 2001 (EPA, 2001), vs estimated thousands of pounds for operator labour costs and borehole drilling, and tens to hundreds of pounds for

equipment for the entire project (electricity, steel or graphite electrodes, and wiring) in 2020 (Purkis *et al.*, 2021a, 2021b)).

When considering the radioactive waste hierarchy (EU, 2008; NDA, 2023; ONR, 2015), EKR is appealing due to it being able to remediate a material and allow it to be either minimised or reused, with potentially little or no impact on the material's properties. This approach is accepted across the UK and European Union is being an ideal outcome for contaminated material.

However, despite relatively simple fundamental principles, computer modelling of EKR in real-world systems can be very complex which results in models having to focus on specific contaminants instead of understanding entire systems (López-Vizcaíno *et al.*, 2017). As such, practical work and field trials are necessary to accurately determine both the efficacy, and scale-up requirements and parameters, of EKR.

1.3.2 Previous Studies

1.3.2.1 Common Metrics of EKR Effectiveness

Literature studies generally quantify EKR efficacy through either the proportion of radionuclide(s) remobilised or the proportion of radionuclide(s) removed. The first of these terms describes the extent of initially stationary contamination that is successfully transported away from its starting location, whilst the latter defines the quantity of contamination migrated to a specific area of the EKR cell deemed "outside" of the starting location (with the "outside" location determined on a case-by-case basis). For proof-of-concept and bench-scale experiments, the remobilisation percentage can be used to quantify whether a radionuclide shows any affinity to EKR. However, for scaled-up trials, removal percentage is a more suitable assessor as it describes the radionuclide activity removed from a material (or, at least, the proportion migrated to another area deemed more suitable to hold the contamination e.g. migrating radionuclides to the edge of a medium where the edge material can be subsequently removed to leave the central parts decontaminated). A middle-ground metric for these two methods is the proportion of material considered sufficiently decontaminated after treatment (with the exact criteria of "decontaminated" determined by the individual scenario), but this is not commonly used as it requires greater characterisation of the material volume to determine activity reductions compared to remobilisation and removal percentages. The proportions of remobilisation and removal may be the same value if a contaminant fully migrates without issue, but will differ if interaction with the host material occurs. Whilst both metrics are equally valid for quantifying EKR effectiveness, previous studies have generally used remobilisation

percentage for smaller and proof of concept work, and removal percentage for larger, scaled-up trials targeting specific nuclear industry problems.

1.3.2.2 Application on Radionuclides

EKR has been applied many times in non-nuclear contexts for remediation of heavy metals (e.g. Abou-Shady et al., 2025; Rosestolato et al., 2015; Sun et al., 2023) and organic compounds (e.g. Cameselle and Gouveia, 2018; Pham and Sillanpää, 2015; Zhou et al., 2025) but radionuclide applications have been less common. Some of the earliest known EKR trials on nuclear site material were performed on artificially spiked sediment from the Hanford site (Washington, USA). Under a 200 V electric field (22.8 cm cell; 7 V/cm gradient) induced by two flat-plate electrodes that "sandwiched" the material for 200 hours, Co-60 and Cs-137 both migrated approximately 10 cm toward the cathode, leaving notable portions of the soil decontaminated (Buehler et al., 1994). More recently, Jung et al. (2015) demonstrated that 68 days of EKR on Cs-133-contaminated Hanford soil reduced radionuclide concentrations by up to 55 %, with removal efficiencies higher in silty-clayey fractions (51 %) compared to sandy ones (38 %). The setup for this used a more conventional approach of having anode and cathode cylinders in small electrolyte tanks that are bridged by a chamber containing the contaminated material, held in place with porous dividers to allow ions to migrate whilst keeping the media stationary. Despite the success of Buehler et al. and Jung et al., both used small experimental setups (< 25 cm), limiting conclusions that could be drawn on their scalability. Sandia National Laboratories investigated the removal of uranium from a rectangular cell containing Hanford sand, with a 2.11 mA/cm² current gradient applied for 55 days (Booher et al., 1997). The final removal efficiency was > 70 % and required that a sufficient supply of citrate electrolyte was maintained. Inadequate citrate concentrations resulted in the uranium complex dissociating, causing the radionuclide to precipitate in the cell. Soils surrounding the Korean Atomic Energy Research Institute (KAERI) were treated by Kim et al. in 2009 and 2010. EKR using custom-made, multitank electrokinetic-flushing equipment achieved 57–94 % Cs-137 removal efficiencies from simulant soils in sandstones with a nitric acid electrolyte over a 20–50 day treatment period, with waste effluent generated at ~ 2.5 mL/g (Kim et al., 2009a). Scaling from a 10 L to a 50 L pure-EKR system with plate electrodes maintained efficiency under similar conditions (0.01 M HNO₃ electrolyte and 55-day treatment), though effluent production increased to ~5 mL/g (Kim et al., 2010b). Kim et al. (2011) have also examined U remediation in soils from around the KAERI facility, using the same 50 L equipment. They found the EKR process was hindered by U metal oxide formation when it co-precipitated with CaO on the cathode, requiring a 75 µm metal oxide particulate filter to mitigate this impact. Filtering was used in later work alongside pH control (preventing alkaline conditions which induce precipitation) to treat 50 L of U-contaminated soil. Using a 0.01 M nitric acid electrolyte and a 28 V electric field for 28–49 days, the authors

achieved > 99 % U removal. Scaling the EKR system up to 800 L (Kim et al., 2015) and 1.2-tonne systems (Kim et al., 2016) and including an additional soil washing system maintained the high remediation efficiency, with U removal reaching 94 % (800 L, 30 days) and up to 83 % (1.2 tonnes, 40 days). Work has also been performed on U-contaminated gravel, which constitutes 20–30 % of the soil near South Korea's KAERI facility (Park et al., 2015). Kim et al. (2014) aimed to reduce U-238 contamination from ~ 10 Bq/g to below the 0.43 Bq/g landfill disposal limit. After 20 days at 20 V supplied by plate electrodes in a nitric acid electrolyte, uranium removal in the 200 L reactor reached up to 83 %, with an average efficiency of 37 %, depending on the pretreatments used. In 2011, Agnew et al. performed ex situ field-scale work on transuranicscontaminated sediment at a UK Atomic Weapons Establishment site. Four tonnes of soil were treated with a ten-cylinder-electrode array for 60 days using 19.2 V and a citric acid electrolyte (Agnew et al., 2011). Gross alpha activities showed Pu (and likely Am due to beta decay of Pu-241 into Am-241 (IAEA, 2025)) migration, resulting in ~ 60 % of the soil being reclassified as 'exempt' waste (< 0.4 Bq/g above background), with remediation costs estimated at £2054/m³ (as of 2019), significantly lower than the anticipated £6054 (as of 2019) for conventional excavation and disposal. Valdovonis et al. (2016) used EKR for Na-24 and Tc-99m (as analogues for longer-lived Na-22 and Tc-99) in Mexican phaeozemic soil contaminated with scintillation fluids from interim storage in the 1970s and 1980s. In the ~ 32 V system applied, 72 % of Na-24 concentrated at the cathode after 4 hours of treatment, whilst 61 % of added Tc-99m accumulated at the anode. However, due to their short half-lives, Na-24 and Tc-99m likely did not have enough time to interact with the sediment before being treated, making further trials with the longer-lived isotopes important. Advancements for EKR with radionuclides in recent years (2020-2025) have been much less frequent. Purkis et al. (2021a) examined bench-scale EKR for stable Cs and Sr remediation in contaminated soils simulating those from the Fukushima prefecture, following the 2011 accident at the Fukushima Daiichi Nuclear Power Plant. In the rectangular cells with single cylinder electrodes, Cs remediation was shown to be high (> 80 %) in spiked soils, whereas Sr had a more limited remobilisation extent (up to 51 % removal). Bench-scale EKR trials have been performed on U tailing mine soils with 30 V using plate electrodes in chambers connected to the contaminated material (Wang et al., 2023) and artificially spiked U contaminated groundwaters with 18 V delivered by a multi-cylinderelectrode array in a rectangular cell (Zhang et al., 2022), each achieving up to 70-85 % removal efficiencies. EKR has also been combined with phytoremediation in a bench-scale trials using artificially spiked U contaminated paddy soil with ryegrass (Zhou et al., 2024). 60 V was applied for 8 hours per day for 7 days, through plate electrodes in electrolyte tanks adjacent to the material, before the electrode polarity was reversed and maintained for 7 days at 8 hours per day. Of the UO2, UO2(NO3)2, and UO3 phases examined, only the latter was found to be remobilised which would equate to a total U uptake of 0.08 % per batch of ryegrass. EKR

combined with permeable reactive barriers (EKR-PRB) containing adsorbent gels have also been performed in a remediation approach for artificially spiked U in topsoil. Bench-scale EKR was performed for 6 days with a 1.5 V/cm gradient and an electrolyte of 0.1 mol/L tartaric acid and 0.08 mol/L FeCl₃. PRB material was made of sodium alginate with activated carbon and hydroxyapatite adsorbent gels. It was found the setup without gel only removed 18 % of the U, whereas 82 % could be extracted with the PRB adsorbents in place.

Some of the earliest publicly accessible EKR work on nuclear site concretes was performed by Acar et al. in 1992 (described in Acar et al. (1995)). Georgia kaolinite was spiked with uranyl, thorium, and radium salts and treated for 85-550 hours at 127 µA/cm² using single electrodes in electrolyte tanks connected to the part containing the soil. Significant U migration towards the cathode was observed in multiple trials with various activities, although most showed precipitation prior to reaching the electrode as a result of the alkaline conditions generated through electrolysis. However, Th and Ra did not exhibit any migration, suggesting that acidic conditions and/or a chelating may be needed to enable dissolution. Th-contaminated flooring at the Mound facility (Ohio, USA) was treated by Lomasney et al. (1996) by placing flat plate electrodes either side of the concrete and using 7.5 V alongside an electrolyte of 5 % HNO₃ + 0.2 M citric acid for 12 hours. Results showed a three-fold improvement on Th extraction rates compared to a control that underwent identical electrolyte soaking but without EKR applied. DePaoli et al. (1996) later tried migrating U, as well as stable Co, Sr and Cs, through ~ 1-cmthick concrete disks at either 100 mA or 500 V. After trial times ranging from 14 – 54 hours in electrolytes of 0.5 M and 1 M Na₂CO₃, and 0.025 M EDTA, U consistently showed 0 % removal due to precipitation onto the concrete disk. Co showed a similar behaviour in distilled water and 0.016 M NaOH, but Sr and Cs had removals in 0.016 M NaOH of 18 % and ≥90 %, respectively. Yurchenko et al. (2009) applied EKR on steel-reinforced concrete from a uranium processing facility in Moscow, treating 98 kg of contaminated material by crushing, sodium carbonate washing, and EKR (0.22 A/cm²) for 30 days. The experimental setup utilised a tank containing the concrete, with a compartment at each end separated by permeable "diaphragms" that housed the electrodes as well as piping to and from smaller tanks containing buffer solutions to prevent a pH gradient from forming. This remedial process reduced the uranium activity by 95 % while generating minimal waste (3.5–3.8 mL effluent per gram of treated concrete), highlighting scalability potential. Kim et al. (2009b) investigated Co-60 and Cs-137 removal from concrete using EKR with a similar setup to Depaoli et al. (1996), achieving 81 % and 55 % efficiency, respectively, with a 0.01 M acetic acid electrolyte over 15 days at 4 V/cm. However, when a pretreatment of 3 M HCl was applied prior to treatment in a flow-system with the same electrolyte, removal was enhanced to > 99 % for both radionuclides. Further studies by Kim et al., (2010a) demonstrated similar efficiencies when using 3 M H₂SO₄ pre-treatment with a 0.01 M HNO₃

electrolyte. Kim *et al.* (2013) also explored the application of EKR for the treatment of incinerated waste ash contaminated with Cs-134 and Cs-137. In bench-scale experiments using a similar setup to their earlier work, nitric acid pre-treatment and then EKR for seven days resulted in a 75 % removal efficiency for both radionuclides. When trials were scaled up to a 10-day EKR in a 200 L washing/EKR system, the removal efficiency increased to 94 % with a 2 M nitric acid electrolyte. Parker *et al.* (2017) showed that K^+ ions in 0.4 M KCl electrolytes facilitated Cs-137 desorption, increasing removal from 19 % to ~ 60 % through ion exchange. However, high concentrations of competing ions may hinder radionuclide uptake during effluent treatment. Since then, despite promising developments in the decade prior, no new studies could be found looking at developing radionuclide focussed EKR on concrete.

1.3.2.3 Common Experimental Setups

Whilst many different electrode setups have been tested in non-nuclear EKR settings (e.g. Sun et al., 2024; Turer and Genc, 2005), much of the bench-scale work described in this section used single anode and cathode rods in a rectangular cell (e.g. Booher et al., 1997; Jung et al., 2015; Purkis et al., 2021a). This configuration is commonly applied as it makes the systems simple and, therefore, straightforward to predict and understand observed radionuclide migration behaviour(s). This approach is commonly performed through one of two setups – either by inserting the electrodes directly into the material (e.g. Purkis et al., 2021a; Zhang et al., 2022), or by placing electrodes in electrolyte tanks that are connected together by a section containing the contaminated material, with permeable barriers allowing ion flow whilst containing the solid media (e.g. Parker et al., 2017; Zhou et al., 2024). Electrodes are commonly cylinder shaped (e.g. Agnew et al., 2011; Jung et al., 2015) as they are easy to insert into a contaminated material and promote radionuclide concentration into a single point, although flat plates or mesh (e.g. Buehler et al., 1994; Kim et al., 2015) offer an alternative that apply an electrical current across a greater material volume but with the downside of accumulating radionuclides to a larger surface area. Field-scale trials may use more complicated geometries and electrode configurations to best suit the individual circumstances (e.g. Kim et al., 2015, 2009a) and can consequently be more varied.

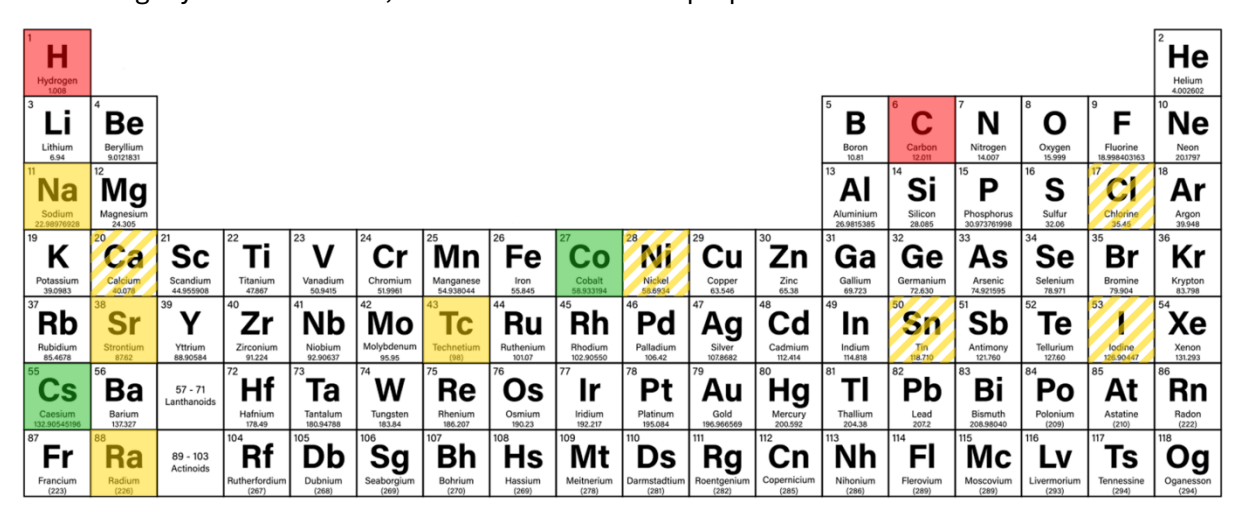
Whilst physical setups generally fit into a few distinct categories, recordings of electrical parameters are much less standardised in the literature. The majority of authors report the current or voltage value that was kept constant throughout the experiments, allowing the other value to vary to compensate for any changes to electrical resistivity in the contaminated material throughout the experiment (see equation 1.1). However, since neither the variable value nor the resistivity are often reported, direct comparisons between all previous work is not possible. Further, even if a voltage or current is applied, the distance between the electrodes

may not be provided which therefore makes determination of a voltage or current gradient across the cell challenging to determine. Despite this, for studies that do report these values, Purkis *et al.* (2021a) defined voltage gradients of < 1 V/cm as "low-energy" due to the frequent adoption of 1 V/cm in non-nuclear laboratory EKR studies that have demonstrated effective remediation. Further, the authors demonstrated remobilisation potential using only ~ 0.5 V/cm, indicating the technique is viable on radionuclides using minimal electrical usage and may not require more extreme gradients such as some previously seen (e.g. 4 V/cm used by Kim *et al.* (2009b) and 7/ V/cm used by Buehler *et al.* (1994)).

1.3.2.4 Summary of Studied Radionuclides in EKR Literature

When summarising previous EKR nuclear site / nuclear material applications, Purkis et al. (2021b) produced a summary schematic (based on the standard periodic table) to show the work performed between 2009 and 2019 with EKR for radionuclides commonly found at nuclear sites; an updated version of this schematic to reflect work up to 2025 has been included in Figure 1.3. Of the elements highlighted as being key in nuclear decommissioning and remediation contexts, Co, Cs, and U, elements with prominent radionuclides classified as ETMRs (Co-60, Cs-137, and U-235 (IAEA, 2025)), have been most studied. This is likely due both their prominence at nuclear sites (Carroll, 2001; Kim et al., 2010b, 2010a; NCRP, 2006), making their effective remediation a priority, and their ETMR status making trials with radioactive material easier to handle and analyse. Comparatively, elements with DTMRs as their most commonly encountered isotopes such as H-3, Sr-90, and Tc-99 are much less studied, despite their abundance at nuclear sites, due to the challenges associated with activity quantification. Further, 17 of the 20 elements listed have at least one radionuclide classed as a DTMR (Na, Co, and Ra being the exceptions to this), therefore assessing EKR's applications for DTMR clean-up would produce a more accurate assessment of the technology's efficacy on a range of key radionuclides in the nuclear sector. The benefits of this include additional tools for site operators when preparing and executing remediation and decommissioning projects, potentially allowing for more efficient, quicker and cheaper decontamination for a range of materials commonly found at nuclear sites. In addition, work can highlight uses for EKR as a mitigation and remediation technology for contemporary radionuclide leaks and discharges as

well as legacy contamination, enhanced nuclear site preparedness in the event of an incident.



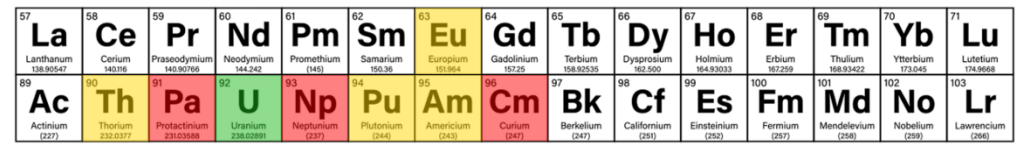


Figure 1.3 – Periodic table showing the state of progress since 2009 for EKR on elements with isotopes commonly found at nuclear sites (excluding those with half-lives of < 1 year). Elements in green have been demonstrated as EKR-amenable in multiple studies, solid yellow shows limited work, striped yellow displays work performed on stable isotopes only, and red indicates further work is needed. Modified from Purkis *et al.* (2021b).

1.4 Thesis Aims and Objectives

This work aims to address the lack the EKR trials performed on media contaminated with DTMRs (defined here by a \leq 0.1 % probability of producing a gamma emission > 100 keV per radioactive decay event). EKR will be applied to DTMRs to understand how the process (re)mobilises them, and how the technique may be optimised for future use with different electrolytes, materials, voltage gradients, or electrode polarities. The materials and radionuclides examined have been selected based on the challenges associated with their decommissioning at nuclear sites, both in the UK and globally. To emphasise the sustainability aspect of EKR, 0.5 V/cm (where cm is the spacing between the electrodes) will be the standard voltage gradient applied.

The thesis aims will be achieved through the following objectives:

- Investigate EKR usage at different voltage gradients for simulated radionuclide contamination in groundwaters at the Sellafield nuclear site (Cumbria, UK).
- 2. Apply EKR to artificially contaminated cement cores, looking at scenarios where radionuclides are retained either by primarily sorption mechanisms or primarily mineral phase incorporation.

3. Examine the efficacy of EKR on real-world, aged coastal sediment, with different electrolytes applied to understand the benefits of complexation for enhancing radionuclide remobilisation.

1.5 Thesis Structure

Chapter 2 will introduce the background behind the analytical techniques used for laboratory work. Subsequent chapters then build the system complexity that EKR is applied to, with Chapter 3 focussing on H-3, Sr-90, and Tc-99 management/remediation in simplified, simulated groundwater systems found at the Sellafield nuclear facility (objective 1). Chapter 4 then investigates deployment of EKR on cementitious material, where radionuclides are retained through different mechanisms (objective 2). Chapters 5 and 6 build EKR maturity further by looking at treatment of authentic, legacy contamination of coastal sediment in proximity to the Sellafield site (objective 3). Chapter 5 addresses actinide and Cs-137 remobilisation, whilst Chapter 6 targets Tc-99 and validation of its activity measurements. Chapter 7 draws the discussed work together, presenting overall conclusions and suggestions for future (including scale up) work.

1.6 References

Abou-Shady, A., Eissa, D., Yaseen, R., Ibrahim, G.A.Z., Osman, M.A., 2025. Scaling up soil electrokinetic removal of inorganic contaminants based on lab chemical and biological optimizations. Int. J. Environ. Sci. Technol. https://doi.org/10.1007/s13762-025-06357-w

Acar, Y.B., Alshawabkeh, A.N., 1993. Principles of electrokinetic remediation. Environ. Sci. Technol. 27, 2638–2647. https://doi.org/10.1021/es00049a002

Acar, Y.B., Gale, R.J., Alshawabkeh, A.N., Marks, R.E., Puppala, S., Bricka, M., Parker, R., 1995. Electrokinetic remediation: Basics and technology status. Journal of Hazardous Materials, Soil Remediation: Application of Innovative and Standard Technologies 40, 117–137. https://doi.org/10.1016/0304-3894(94)00066-P

Agnew, K., Cundy, A.B., Hopkinson, L., Croudace, I.W., Warwick, P.E., Purdie, P., 2011. Electrokinetic remediation of plutonium-contaminated nuclear site wastes: Results from a pilot-scale on-site trial. Journal of Hazardous Materials 186, 1405–1414. https://doi.org/10.1016/j.jhazmat.2010.12.016

Ali, H., Khan, E., Sajad, M.A., 2013. Phytoremediation of heavy metals—Concepts and applications. Chemosphere 91, 869–881. https://doi.org/10.1016/j.chemosphere.2013.01.075

Alkorta, I., Hernández-Allica, J., Becerril, J.M., Amezaga, I., Albizu, I., Garbisu, C., 2004. Recent Findings on the Phytoremediation of Soils Contaminated with Environmentally Toxic Heavy Metals and Metalloids Such as Zinc, Cadmium, Lead, and Arsenic. Re/Views in Environmental Science and Bio/Technology 3, 71–90. https://doi.org/10.1023/B:RESB.0000040059.70899.3d

Attallah, M.F., Rizk, S.E., Shady, S.A., 2018. Separation of 152+154Eu, 90Sr from radioactive waste effluent using liquid–liquid extraction by polyglycerol phthalate. Nuclear Science and Techniques 29. https://doi.org/10.1007/s41365-018-0423-z

Booher, W.F., Lindgren, E.R., Brady, P.V., 1997. Electrokinetic removal of uranium from contaminated, unsaturated soils (No. SAND-97-0122). Sandia National Lab. (SNL-NM), Albuquerque, NM (United States), New Mexico, USA. https://doi.org/10.2172/434445

Brett, C.M.A., Brett, A.M.O., 1993. Electrochemistry: Principles, Methods, and Applications. Oxford University Press.

Buehler, M.F., Surma, J.E., Virden, J.W., 1994. In situ soil remediation using electrokinetics. Presented at the 33rd hanford Symposium on Helath and the Environment, Richland, Washington.

Cameselle, C., Gouveia, S., 2018. Electrokinetic remediation for the removal of organic contaminants in soils. Current Opinion in Electrochemistry, Environmental Electrochemistry - Solar Cells 11, 41–47. https://doi.org/10.1016/j.coelec.2018.07.005

Carroll, L.R., 2001. Predicting long-lived, neutron-induced activation of concrete in a cyclotron vault. AIP Conference Proceedings 576, 301–304. https://doi.org/10.1063/1.1395309

Cundy, A.B., LaFreniere, L., Bardos, R.P., Yan, E., Sedivy, R., Roe, C., 2021. Integrated phytomanagement of a carbon tetrachloride-contaminated site in Murdock, Nebraska (USA). Journal of Cleaner Production 290, 125190. https://doi.org/10.1016/j.jclepro.2020.125190

Delgado, A.V., González-Caballero, F., Hunter, R.J., Koopal, L.K., Lyklema, J., 2007. Measurement and interpretation of electrokinetic phenomena. Journal of Colloid and Interface Science, Elkin 06, International Electrokinetics Conference, June 25-29, Nancy, France 309, 194–224. https://doi.org/10.1016/j.jcis.2006.12.075

DePaoli, D.W., Harris, M.T., Ally, M.R., Morgan, I.L., Cate, N., Ellis, M.E., Heath, K., Hovist, D.W., Kabalka, G.W., Anderson, C.L., Tang, C., 1996. Testing and Evaluation of Electrokinetic Decontamination of Concrete (No. DOE/ORO/2036). Oak Ridge National Laboratory, Oak Ridge, Tennessee.

Dushenkov, S., 2003. Trends in phytoremediation of radionuclides. Plant and Soil 249, 167–175. https://doi.org/10.1023/A:1022527207359

Ellis, D.E., Hadley, P.W., 2009. Sustainable remediation white paper—Integrating sustainable principles, practices, and metrics into remediation projects. Remediation 19, 5–114. https://doi.org/10.1002/rem.20210

EPA, 2001. Cost Analyses for Selected Groundwater Cleanup Projects: Pump and Treat Systems and Permeable Reactive Barriers (No. EPA 542-R-00-013). U. S. Environmental Protection Agency.

EPA, 1995. In Situ Remediation Technology: Electrokinetics. United States Environmental Protection Agency, Washington D.C., USA.

EU, 2008. Directive 2008/98/EC of the European Parliament and of the Council.

Faisal, A.A.H., Sulaymon, A.H., Khaliefa, Q.M., 2018. A review of permeable reactive barrier as passive sustainable technology for groundwater remediation. Int. J. Environ. Sci. Technol. 15, 1123–1138. https://doi.org/10.1007/s13762-017-1466-0

Hemming, S.D., Purkis, J.M., Warwick, P.E., Cundy, A.B., 2023. Current and emerging technologies for the remediation of difficult-to-measure radionuclides at nuclear sites. Environ. Sci.: Processes Impacts 25, 1909–1925. https://doi.org/10.1039/D3EM00190C

Henderson, A.D., Demond, A.H., 2007. Long-Term Performance of Zero-Valent Iron Permeable Reactive Barriers: A Critical Review. Environmental Engineering Science 24, 401–423. https://doi.org/10.1089/ees.2006.0071

Hong, S., Um, W., 2023. Decontamination of neutron-activated radioactive concrete waste by separating Eu, Co, Fe, and Mn-containing sand particles using dense medium separation.

Journal of Hazardous Materials 443, 130183. https://doi.org/10.1016/j.jhazmat.2022.130183

IAEA, 2025. IAEA Nuclear Data Services. URL https://www-nds.iaea.org/ (accessed 13.1.25).

IAEA, 2023. Country Nuclear Power Profiles (Text No. CNPP/2023), Country Nuclear Power Profiles. International Atomic Energy Agency, Vienna.

IAEA, 2009. Determination and Use of Scaling Factors for Waste Characterization in Nuclear Power Plants (No. NW-T-1.18), Nuclear Energy Series. International Atomic Energy Agency, Vienna.

ISO, 2007. Nuclear energy — Nuclear fuel technology — Scaling factor method to determine the radioactivity of low- and intermediate-level radioactive waste packages generated at nuclear power plants.

Jackson, S.F., Monk, S.D., Riaz, Z., 2014. An investigation towards real time dose rate monitoring, and fuel rod detection in a First Generation Magnox Storage Pond (FGMSP). Applied Radiation and Isotopes 94, 254–259. https://doi.org/10.1016/j.apradiso.2014.08.019

Jung, H.B., Yang, J.-S., Um, W., 2015. Bench-scale electrokinetic remediation for cesium-contaminated sediment at the Hanford Site, USA. J Radioanal Nucl Chem 304, 615–625. https://doi.org/10.1007/s10967-014-3852-0

Kim, D.J., E. Warwick, P., Croudace, I.W., 2008. Tritium Speciation in Nuclear Reactor Bioshield Concrete and its Impact on Accurate Analysis. Anal. Chem. 80, 5476–5480. https://doi.org/10.1021/ac8002787

Kim, G.-N., Choi, W.-K., Lee, K.-W., 2010a. Decontamination of radioactive concrete using electrokinetic technology. J Appl Electrochem 40, 1209–1216. https://doi.org/10.1007/s10800-010-0088-8

Kim, G.-N., Kim, I., Kim, S.-S., Choi, J.-W., 2016. Removal of uranium from contaminated soil using indoor electrokinetic decontamination. J Radioanal Nucl Chem 309, 1175–1181. https://doi.org/10.1007/s10967-016-4707-7

Kim, G.-N., Kim, S., Moon, J.-K., Hyun, J., 2015. Removal of uranium from soil using full-sized washing electrokinetic separation equipment. Annals of Nuclear Energy 81, 188–195. https://doi.org/10.1016/j.anucene.2015.01.046

Kim, G.-N., Kim, S., Park, H.-M., Kim, W.-S., Park, U.-R., Moon, J.-K., 2013. Cs-137 and Cs-134 removal from radioactive ash using washing–electrokinetic equipment. Annals of Nuclear Energy 57, 311–317. https://doi.org/10.1016/j.anucene.2013.02.016

Kim, G.-N., Lee, S.-S., Shon, D.-B., Lee, K.-W., Chung, U.-S., 2010b. Development of pilot-scale electrokinetic remediation technology to remove 60Co and 137Cs from soil. Journal of Industrial and Engineering Chemistry 16, 986–991. https://doi.org/10.1016/j.jiec.2010.05.014

Kim, G.-N., Park, U.-R., Kim, S., Kim, W.-S., Moon, J.-K., Hyun, J., 2014. Decontamination of gravels contaminated with uranium. Annals of Nuclear Energy 72, 367–372. https://doi.org/10.1016/j.anucene.2014.05.031

Kim, G.-N., Shon, D.-B., Park, H.-M., Lee, K.-W., Chung, U.-S., 2011. Development of pilot-scale electrokinetic remediation technology for uranium removal. Separation and Purification Technology 80, 67–72. https://doi.org/10.1016/j.seppur.2011.04.009

Kim, G.-N., Yang, B.-I., Choi, W.-K., Lee, K.-W., 2009a. Development of vertical electrokinetic-flushing decontamination technology to remove 60Co and 137Cs from a Korean nuclear facility site. Separation and Purification Technology 68, 222–226. https://doi.org/10.1016/j.seppur.2009.05.015

Kim, G.-N., Yang, B.-I., Choi, W.-K., Lee, K.-W., Hyeon, J.-H., 2009b. Washing-Electrokinetic Decontamination For Concrete Contaminated With Cobalt and Cesium. Nuclear Engineering and Technology 41, 1079–1086. https://doi.org/10.5516/NET.2009.41.8.1079

Korolev, V.A., 2009. Electrokinetic Removal of Radionuclides, in: Electrochemical Remediation Technologies for Polluted Soils, Sediments and Groundwater. John Wiley & Sons, Ltd, pp. 127–139. https://doi.org/10.1002/9780470523650.ch5

Lee, E., 2019. Chapter 1 - Electrophoresis of a Single Rigid Particle, in: Lee, E. (Ed.), Interface Science and Technology, Theory of Electrophoresis and Diffusiophoresis of Highly Charged Colloidal Particles. Elsevier, pp. 3–45. https://doi.org/10.1016/B978-0-08-100865-2.00001-1

Leskinen, A., Salminen-Paatero, S., Gautier, C., Räty, A., Tanhua-Tyrkkö, M., Fichet, P., Kekki, T., Zhang, W., Bubendorff, J., Laporte, E., Lambrot, G., Brennetot, R., 2020. Intercomparison exercise on difficult to measure radionuclides in activated steel: statistical analysis of radioanalytical results and activation calculations. J Radioanal Nucl Chem 324, 1303–1316. https://doi.org/10.1007/s10967-020-07181-x

Liu, J., Zhao, L., Liu, Q., Li, J., Qiao, Z., Sun, P., Yang, Y., 2022. A critical review on soil washing during soil remediation for heavy metals and organic pollutants. Int. J. Environ. Sci. Technol. 19, 601–624. https://doi.org/10.1007/s13762-021-03144-1

Lomasney, H.L., SenGupta, A.K., Yachmenev, V., 1996. Electrokinetic decontamination of concrete (No. DOE/MC/30162-97/C0804; CONF-9610231-4). Isotron Corp., New Orleans, LA (United States), New Orleans, Los Angeles, USA.

López-Vizcaíno, R., Yustres, A., León, M.J., Saez, C., Cañizares, P., Rodrigo, M.A., Navarro, V., 2017. Multiphysics Implementation of Electrokinetic Remediation Models for Natural Soils and Porewaters. Electrochimica Acta 225, 93–104. https://doi.org/10.1016/j.electacta.2016.12.102

Macci, C., Peruzzi, E., Doni, S., Masciandaro, G., 2020. Monitoring of a long term phytoremediation process of a soil contaminated by heavy metals and hydrocarbons in Tuscany. Environ Sci Pollut Res 27, 424–437. https://doi.org/10.1007/s11356-019-06836-x

Martin, L., Alizadeh, V., Meegoda, J., 2019. Electro-osmosis treatment techniques and their effect on dewatering of soils, sediments, and sludge: A review. Soils and Foundations 59, 407–418. https://doi.org/10.1016/j.sandf.2018.12.015

Megharaj, M., Ramakrishnan, B., Venkateswarlu, K., Sethunathan, N., Naidu, R., 2011. Bioremediation approaches for organic pollutants: A critical perspective. Environment International 37, 1362–1375. https://doi.org/10.1016/j.envint.2011.06.003

NCRP, 2006. Cesium-137 in the Environment: Radioecology and Approaches to Assessment and Management (No. 154), NRCP Releases Report. National Council on Radiation Protection and Measurements, Maryland, USA.

NDA, 2023. NDA strategic position on radioactive waste treatment: August 2023. Nuclear Decommissioning Authority, Cumbria, UK.

NDA, 2021. Nuclear Decommissioning Authority Strategy 2021 (No. SG/2021/48). Nuclear Decommissioning Authority, Cumbria, UK.

NDA, 2019. Nuclear Provision: the cost of cleaning up Britain's historic nuclear sites. Nuclear Decommissioning Authority, Bootle, UK.

NEA, 1999. Decontamination Techniques Used in Decommissioning Activities. Nuclear Energy Agency, Paris, France.

Newman, L.A., Reynolds, C.M., 2004. Phytodegradation of organic compounds. Current Opinion in Biotechnology 15, 225–230. https://doi.org/10.1016/j.copbio.2004.04.006

NRC, 2001. Inventory of Materials with Very Low Levels of Radioactivity Potentially Clearable From Various Types of Facilities (No. NRC-04-01-049). Nuclear Regulatory Commission, Virginia, USA.

Obiri-Nyarko, F., Grajales-Mesa, S.J., Malina, G., 2014. An overview of permeable reactive barriers for in situ sustainable groundwater remediation. Chemosphere 111, 243–259. https://doi.org/10.1016/j.chemosphere.2014.03.112

Oldham, K.B., 2008. A Gouy–Chapman–Stern model of the double layer at a (metal)/(ionic liquid) interface. Journal of Electroanalytical Chemistry 613, 131–138. https://doi.org/10.1016/j.jelechem.2007.10.017

ONR, 2020. Remediation Techniques for Radioactive Contaminated Land on Nuclear Licensed Sites (No. NT/7225002059/R2043 Issue 1). Office for Nuclear Regulation, Bootle, UK.

ONR, 2015. Basic principles of radioactive waste management An introduction to the management of higher activity radioactive waste on nuclear licensed sites (No. Revision 2). Office for Nuclear Regulation, Bootle, UK.

Pamukcu, S., Weeks, A., Wittle, J.K., 1997. Electrochemical extraction and stabilization of selected inorganic species in porous media. Journal of Hazardous Materials, Electrochemical Decontamination of Soil and Water 55, 305–318. https://doi.org/10.1016/S0304-3894(97)00025-3

Park, U.-R., Kim, G.-N., Kim, S.-S., Moon, J.-K., 2015. Decontamination of Uranium-Contaminated Gravel. Journal of Nuclear Fuel Cycle and Waste Technology 13, 35–43. https://doi.org/10.7733/jnfcwt.2015.13.1.35

Parker, A.J., Joyce, M.J., Boxall, C., 2017. Remediation of 137Cs contaminated concrete using electrokinetic phenomena and ionic salt washes in nuclear energy contexts. Journal of Hazardous Materials 340, 454–462. https://doi.org/10.1016/j.jhazmat.2017.07.007

Pearce, C.I., Moore, R.C., Morad, J.W., Asmussen, R.M., Chatterjee, S., Lawter, A.R., Levitskaia, T.G., Neeway, J.J., Qafoku, N.P., Rigali, M.J., Saslow, S.A., Szecsody, J.E., Thallapally, P.K., Wang, G., Freedman, V.L., 2020. Technetium immobilization by materials through sorption and redox-driven processes: A literature review. Science of The Total Environment 716, 132849. https://doi.org/10.1016/j.scitotenv.2019.06.195

PGE, 1995. Trojan Nuclear Plant Radiological Site Characterization Report Rev 0.1. Portland General Electric, Oregon, USA.

Pham, T.D., Sillanpää, M., 2015. Electrokinetic remediation of organic contamination. Environmental Technology Reviews 4, 103–117. https://doi.org/10.1080/21622515.2015.1105306

Phillips, D.H., Watson, D.B., Roh, Y., Gu, B., 2003. Mineralogical Characteristics and Transformations during Long-Term Operation of a Zerovalent Iron Reactive Barrier. Journal of Environmental Quality 32, 2033–2045. https://doi.org/10.2134/jeq2003.2033

Purkis, J.M., Tucknott, A., Croudace, I.W., Warwick, P.E., Cundy, A.B., 2021a. Enhanced electrokinetic remediation of nuclear fission products in organic-rich soils. Applied Geochemistry 125, 104826. https://doi.org/10.1016/j.apgeochem.2020.104826

Purkis, J.M., Warwick, P.E., Graham, J., Hemming, S.D., Cundy, A.B., 2021b. Towards the application of electrokinetic remediation for nuclear site decommissioning. Journal of Hazardous Materials 413, 125274. https://doi.org/10.1016/j.jhazmat.2021.125274

Rosestolato, D., Bagatin, R., Ferro, S., 2015. Electrokinetic remediation of soils polluted by heavy metals (mercury in particular). Chemical Engineering Journal 264, 16–23. https://doi.org/10.1016/j.cej.2014.11.074

Salt, D.E., Blaylock, M., Kumar, N.P.B.A., Dushenkov, V., Ensley, B.D., Chet, I., Raskin, I., 1995. Phytoremediation: A Novel Strategy for the Removal of Toxic Metals from the Environment Using Plants. Bio/Technology 13, 468–474. https://doi.org/10.1038/nbt0595-468

Sow, M., Leblois, Y., Bodiot, C., Motzkus, C., Ritoux, S., Gensdarmes, F., 2020. Aerosol release fraction by concrete scarifying operations and its implications on the dismantling of nuclear facilities. Journal of Hazardous Materials 400, 123077.

https://doi.org/10.1016/j.jhazmat.2020.123077

Srichandan, H., Singh, P.K., Parhi, P.K., Mohanty, P., Adhya, T.K., Pattnaik, R., Mishra, S., Hota, P.K., 2022. Environmental remediation using metals and inorganic and organic materials: a review. Journal of Environmental Science and Health, Part C 40, 197–226. https://doi.org/10.1080/26896583.2022.2065871

Sun, Z., Xu, S., Zhang, J., Eugene, B.D., Li, S., 2024. Effect of Electrode Positioning on Electrokinetic Remediation of Contaminated Soft Clay with Surface Electrolyte. Toxics 12, 758. https://doi.org/10.3390/toxics12100758

Sun, Z., Zhao, M., Chen, L., Gong, Z., Hu, J., Ma, D., 2023. Electrokinetic remediation for the removal of heavy metals in soil: Limitations, solutions and prospection. Science of The Total Environment 903, 165970. https://doi.org/10.1016/j.scitotenv.2023.165970

Tajudin, S.A.A., Azmi, M.A.M., Nabila, A.T.A., 2016. Stabilization/Solidification Remediation Method for Contaminated Soil: A Review. IOP Conf. Ser.: Mater. Sci. Eng. 136, 012043. https://doi.org/10.1088/1757-899X/136/1/012043

Thepsithar, P., 2006. A Study of the Electrokinetic Treatment Process for Soil Remediation (PhD). University of Manchester, Manchester, UK.

Thierfeldt, S., Deckert, A., 1996. Radionuclides difficult to measure in waste packages. Final report. Swedish Nuclear Power Inspectorate, Stockholm, Sweden.

Turer, D., Genc, A., 2005. Assessing effect of electrode configuration on the efficiency of electrokinetic remediation by sequential extraction analysis. Journal of Hazardous Materials 119, 167–174. https://doi.org/10.1016/j.jhazmat.2004.12.003

Valdovinos, V., Monroy-Guzmán, F., Bustos, E., 2016. Electrokinetic removal of radionuclides contained in scintillation liquids absorbed in soil type Phaeozem. Journal of Environmental Radioactivity 162–163, 80–86. https://doi.org/10.1016/j.jenvrad.2016.05.017

Vane, L.M., Zang, G.M., 1997. Effect of aqueous phase properties on clay particle zeta potential and electro-osmotic permeability: Implications for electro-kinetic soil remediation processes. Journal of Hazardous Materials, Electrochemical Decontamination of Soil and Water 55, 1–22. https://doi.org/10.1016/S0304-3894(97)00010-1

Wang, S., Gao, B., Jiang, W., Huang, D., Ma, W., Liu, S., Zhang, B., 2023. Electrochemical leaching remediation and bioaccessibility study of uranium-contaminated soil. J Radioanal Nucl Chem 332, 3215–3225. https://doi.org/10.1007/s10967-023-09015-y

Xu, H., Zhao, P., Ran, Q., Li, W., Wang, P., Luo, Y., Huang, C., Yang, X., Yin, J., Zhang, R., 2021. Enhanced electrokinetic remediation for Cd-contaminated clay soil by addition of nitric acid, acetic acid, and EDTA: Effects on soil micro-ecology. Science of The Total Environment 772, 145029. https://doi.org/10.1016/j.scitotenv.2021.145029

Yurchenko, A.Yu., Karlin, Yu.V., Nikolaev, A.N., Karlina, O.K., Barinov, A.S., 2009. Decontamination of radioactive concrete. At Energy 106, 225–230. https://doi.org/10.1007/s10512-009-9156-8

Zhang, Y., Li, M., Hua, Y., Wu, X., Zhang, X., Fang, Q., Cai, T., 2022. A novel solar-powered electrochemical mineralization system for persistent remediation of uranium-contaminated groundwater. Journal of Environmental Radioactivity 250, 106909. https://doi.org/10.1016/j.jenvrad.2022.106909

Zhou, M., Chen, R., Huang, Q., Cang, L., 2025. Peroxymonosulfate enhanced electrokinetic remediation of PAHs-contaminated soil: Effects of periodic electric field. Journal of Industrial and Engineering Chemistry 145, 551–560. https://doi.org/10.1016/j.jiec.2024.10.050

Zhou, S., Yang, Y., Tang, H., Duan, Y., Yuan, H., Yan, J., Yu, X., Li, Y., 2024. Mechanism of remediation of U(VI) contaminated simulated soil by AC-nHAP gel microsphere as PRB combined electrokinetic technology. J Radioanal Nucl Chem 333, 6133–6148. https://doi.org/10.1007/s10967-024-09788-w

Chapter 2 Instrument Methodologies for Radionuclide Quantification

2.1 Introduction

Experimental parameters used consistently across the work performed for this thesis are defined in section 2.2, analytical quality control is described in section 2.3, and radionuclide counting and quantification techniques are described in sections 2.4 – 2.7.

2.2 Experimental Setup and Parameters Used

The standard voltage gradient used in this work is 0.5 V/cm (where cm is the spacing between the electrodes), as this is the lowest voltage that has been used in multiple successful remedial trials (see section 1.3.2.3) and will therefore emphasise the sustainability aspect of EKR. Due to the smaller-scale nature of the work presented in this thesis, a single anode and cathode will be used, with rectangular cells created unless another geometry for the trials is more suitable. The electrodes will be inserted into the material as this offers the closest setup to one that could be expected for scaled-up *in-situ* trials. Due to the varying physical and chemical characteristics of samples in each data chapter, their preparation for analysis is described in each respective methodology section in Chapters 3 to 6.

2.3 Quality Control During Analysis

Sample contamination and loss are risks during analysis preparation. To mitigate these, every batch of samples that could not be directly quantified in the form they were collected in (*i.e.* samples that required chemical or physical preparation in order to be counted) had a QC standard and a 'blank' sample prepared alongside. Both of these contained an identical matrix to that of the samples (or a similar matrix, if an identical one could not be used), with the QC standard containing a known activity of the analyte(s) of interest and the blank containing none. These underwent the same analytical methods as the unknown samples. To demonstrate an effective procedure with no contamination, the final QC standard measurement was expected to be within uncertainty of the activity initially added and the blank should have an activity at background levels. Unless stated otherwise, if the QC standard condition was not met or if the blank sample activity was greater than ~ 1 % of the unknown sample activities and therefore not suitable for using as a background subtraction for the unknowns, the batch was disregarded and a new one made.

In addition, unless stated, every sample that required a form of chemical or physical preparation before counting was spiked with a known amount of tracer solution prior to any chemistry being performed. The tracer was a different isotope of the same element to that of the radionuclide of interest (or, failing that, a different element that had a very similar chemical

behaviour to the radionuclide of interest). This was added such that if a portion of the radionuclide was lost during chemical separation (e.g. through incomplete sample transfer between beakers, incomplete removal from a separation column, etc.), an equal proportion of the tracer isotope would also be lost as the two nuclides would behave identically. After analysis, the tracer in each sample was quantified and used to determine the portion lost during chemistry, known as the chemical recovery, which was then used to calculate the unknown radionuclide activities in a 100 % recovered sample. Tracer was put in every blank and standard sample to verify the procedure worked as expected; The batch was disregarded and a fresh one made if this was not the case.

2.4 Alpha Spectrometry

Alpha spectrometry is used to quantify the emission energy of alpha particles produced during radioactive decay. Alpha emissions are monoenergetic, meaning that whilst multiple distinct emission energies may be released by a given isotope, the energy released in each case is transferred entirely to the alpha particle. Alpha spectrometry analysis here was performed with EG&G ORTEC Octete PC alpha spectrometers, with subsequent peak analysis performed using MAESTRO software (ORTEC; Aix-en-Provence, France). These instruments have silicon detectors, allowing for the production of electron-hole pairs in detector atoms during alpha particle collision. The number of electron-hole pairs created are proportional to the energy of the alpha particle, allowing for quantification of the energy deposited. A vacuum is created in each sample chamber during counting to prevent the alpha particle from interacting with the air and losing energy before colliding with the detector. For the work performed in this thesis, energy calibrations were performed using U-236, Pu-242, and Am-241 at least once a year to correct for instrument energy drift over time.

2.5 Liquid Scintillation Counting (LSC)

Liquid scintillation counting (LSC) can determine the activity of radionuclides that undergo beta minus, beta plus, and alpha decay (the lattermost of these is more commonly counted in an alpha spectrometer due to its lower limits of detection, but may be measured in an LSC if the ratio of alpha and beta peaks are of interest for analysis). Beta minus emissions are generated from the conversion of a neutron to a proton and beta plus are created from the reverse process, producing an electron (beta minus particle) and an anti-neutrino, or a positron (beta plus particle) and a neutrino, respectively. Whilst the total energy released during this process is a distinct value, the energy is randomly distributed between the electron + anti-neutrino or positron + neutrino. As such, beta particles generally have a broader range of observed spectral

energies compared to alpha or gamma spectrometry. LSC analysis here involved measuring samples in darkness in WALLAC 1220 Quantulus™ Ultra low Level Liquid Scintillation Counters and analysed with EasyView software. In most cases after radionuclide separation chemistry had been performed liquid samples were mixed with a scintillation cocktail before being placed into counters. When a beta minus particle collides with the organic solvent in the cocktail it transfers a portion of its energy which, in turn, is passed to the scintillator. The excited scintillant releases this energy as photons in the UV or visible light range, which can pass through a glass or clear plastic vial and be detected by two photomultiplier tubes (PMTs). The more photons that are emitted by a single beta particle, the higher the energy of the original beta particle. Alternatively, some high energy betas such as Y-90 do not need a scintillation cocktail to be measured in an aqueous sample, instead relying on PMT measurements of Cherenkov radiation (photon emission caused by a charged particle travelling faster than the speed of light in a medium). Whilst the work for this thesis was performed, counting efficiencies for the radionuclides of interest were determined at least once a year by producing a set of calibration standard samples. Each sample would contain the same activity of a given radionuclide but would have varying levels of nitromethane added to provide differing levels of quench, and, thus, differing instrument counting efficiencies. The 1220 Quantulus can provide an external Standard Quench Parameter (SQPE) value for each sample, which can be used as a proxy for the total quench, and this can be compared to the theoretical vs measured calibration standard samples to produce a calibration curve plotting SQPE against counting efficiency. Once this has been obtained, this equation can be used with samples to determine the counting efficiency for that particular sample.

2.6 Gamma Spectrometry

Gamma spectrometry quantifies the activity of gamma-emitting radionuclides in a sample, which work in a similar principle to Si detectors for alpha spectrometry (described in section 2.4), and NaI(Tl) scintillators, which use a similar mechanism to detectors in LSCs (described in section 2.5). HPGe detectors used for this thesis were Canberra well-type gamma-ray spectrometers, with spectra deconvolution performed in Fitzpeaks software (JF Computing; Stanton in the Vale, UK) and the NaI(Tl) detector was a HIDEX AMG gamma spectrometer that had spectra analysed with HidexAMG software (Turku, Finland). For HPGe detectors, gamma radiation interacts with the HPGe crystal through the photoelectric effect (deposition of all energy), Compton scattering (partial deposition of energy), or production of an electron-positron pair (can occur if gamma emission is > 1.022 MeV), all creating electron-hole pairs which can be collected and quantified. In the alternative approach, excitation of a NaI crystal and the subsequent energy transfer, excitation and deexcitation of the Tl doped into the lattice releases

a photon that can be detected by two PMTs. For the work performed here, energy calibrations were performed weekly using a mixed gamma source to account for instrument energy drift over time.

2.7 Inductively Coupled Plasma Mass Spectrometry (ICP-MS)

Inductively coupled plasma mass spectrometry (ICP-MS) can be used to quantify of both stable isotopes and radionuclides. Mass spectrometry analysis in this thesis was performed on an Agilent 8800 ICP-QQQ-MS, with data processing occurring in MassHunter software (Agilent; Santa Clara, USA). The advantage of a triple quad instrument over a traditional single quad mass spectrometer is its higher efficiency at removing interferences such as isobars (different chemical elements with the same mass), dimers (two atoms of the same element, each half the mass of the isotope of interest, forming a polyatomic ion that has the same mass to charge ratio (m/z) as the isotope of interest) and divalent ions (an atom with double the mass of the isotope of interest undergoing double ionisation to form an ion with the same m/z as the isotope of interest). In this instrument, aqueous samples are first converted to an aerosol in a nebuliser using argon gas before being passed to the induction coil where both vaporisation of compounds into individual atoms and subsequent conversion to positively charged ions occurs. These then go through three quadrupoles under vacuum, organised in a configuration of: analyser, reaction cell, analyser. The first analyser quadrupole acts as a filter by oscillating the electrical charges of each pole at the specific frequency required to retain isotopes with the desired m/z ratio and cause deflection of other ions. The reaction cell can be filled with a gas such as H, He or O which can be used to preferentially react with either the isotope(s) of interest or interferents to create a mass differentiation between the two. The second analyser then acts as another filter to remove all but the m/z of the isotope(s) of interest. The filtered ions finally reach the detector where the number of collisions is recorded. For the work performed in this thesis, standard samples for quantifying the nuclide(s) of interest were prepared and analysed at the beginning of every run. Further details for each specific run can be found in the respective data chapters.

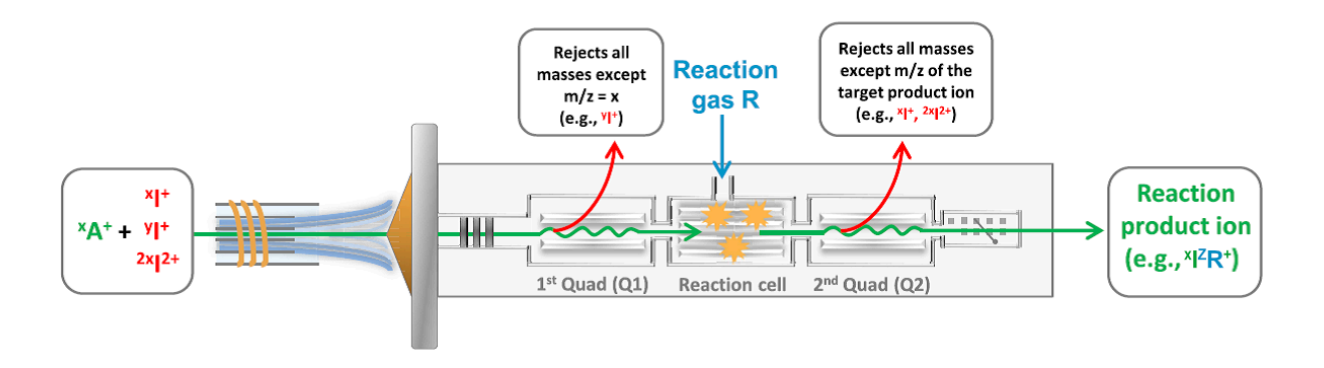


Figure 2.1 – Schematic of an ICP-MS. ^XA⁺ represents ionised argon gas, ^XI⁺ and ^YI⁺ represent ions with different masses, ^{2X}I²⁺ represents an ion with both double the mass and charge of ^XI⁺ which would result in identical m/z ratios, and R is the reaction gas (e.g. H, He, O). Modified from (Ghent University, 2025).

2.8 References

Ghent University, 2025. Tandem ICP-mass spectrometry (ICP-MS/MS) [WWW Document]. URL (accessed 3.3.25).

Chapter 3 Migration of Aqueous Radionuclide Contaminants

3.1 Introduction

Leaks-to-ground at nuclear sites can introduce a wide variety of contaminants into the subsurface, including radionuclides (e.g. Sellafield Ltd., 2017; USDOE, 2024). Whilst some chemical elements with high affinities for particles can be retained in proximity to the leak site (e.g. Pu, Am (USEPA, 1999)), those that do not interact readily with the environment can be transported from the source through groundwater flow. This can present immediate contamination issues to the facility itself, potentially causing disruptions to site operations as well as health risks to workers. Further, if left unmitigated, radionuclides may migrate out of site boundaries and pose hazards to health for both local populations and ecosystems.

3.1.1 Sellafield Case Study

3.1.1.1 Background

The Sellafield site (Cumbria, UK) was initially built as a munitions factory but was later repurposed at the start of the nuclear age, producing Pu for the UK's atomic weapons' program. Reprocessing facilities were built to separate U and Pu from fission products present in irradiated Magnox and Advanced Gas-cooled Reactor (AGR) fuels (Sellafield Ltd., 2016; Shaw, 1990). The Magnox Swarf Storage Silo (MSSS) stores waste Magnox fuel cladding (known as swarf) after reprocessing, submerged in cover water (Gray et al., 1995; ONR, 2023). Over subsequent years, further waste management approaches were deployed such as building additional storage silos and ponds as well as treatment plants e.g. Site Exchange Effluent Plant (SIXEP) and Enhanced Actinide Removal Plant (EARP) (Morley, 2004). After power generation to the National Grid was ceased in 2003, efforts turned towards completing reprocessing of spent fuel which was achieved in July 2022 (Sellafield Ltd., 2024; Williamson, 2008). Work now focusses on total site decommissioning by 2120 (NDA, 2018).

3.1.1.2 Geology and Hydrogeology

The Sellafield subsurface is comprised of a Triassic Sherwood Sandstone bedrock, Quaternary glacial deposits, and overlying 'made ground' (tarmac, concrete, timber *etc.*) (Sellafield Ltd., 2017). The sandstone group mainly comprises aeolian, poorly consolidated lithologies that are weathered in the upper portions, proximally to overlain units (Chaplow, 1996; Sellafield Ltd., 2017). Quaternary deposits contain up to 60 m depth of heterogeneous sands and gravels along with silt and clay lenses that vary in size both laterally and vertically (Sellafield Ltd., 2017). Surface material is generally anthropogenic and can range in thickness from 10 cm to > 5 m depending on the land's use (road, building foundations *etc.*).

The primary aquifer in the area runs through the sandstone layer, with a smaller aquifer also present within the glacial material (Sellafield Ltd., 2017). These are generally separated by an impermeable clay layer, although due to the bed's lateral discontinuity under Sellafield, some groundwater exchange can occur. Groundwater is sourced from rainfall originating from the Cumbrian Fells as well as anthropogenic leakage from process water at the centre of site, which ultimately discharges into the Irish Sea or surface waters. Flow rates for groundwater vary considerably due to subsurface heterogeneity, with travel times between the northern Sellafield site boundary and the Irish Sea estimated to be 10-20 years (Sellafield Ltd., 2017).

3.1.1.3 Groundwater contamination

Over decades of site operations, spills and infrastructure failure (e.g. containment facilities and pipes) have released radionuclides into the subsurface (Sellafield Ltd., 2024, 2017, 2006-2021). Most contamination originates from the centre of site, known as the Separation Area, which contains many legacy buildings e.g. MSSS and First Generation Magnox Storage Pond (FGMSP) (NDA, 2011; Sellafield Ltd., 2024, 2017). As such, the Separation Area often contains the greatest groundwater activities for most radionuclides, with those that are water soluble also in lower concentrations downgradient of the source area (Sellafield Ltd., 2017). The most recent major release of radionuclides occurred from MSSS in 2019 which contained predominantly H-3, C-14, Cl-36, Sr-90 and Cs-137 (Sellafield Ltd., 2024). The foremost three of these are likely to migrate at a similar rate to the silo liquor plume as they do not bind to sediment; Sr-90 and Cs-137 are expected to migrate much slower due to their high affinities for the clay present in the Sellafield subsurface. Water contained within the silos is categorised as intermediate level waste (ONR, 2023), giving the liquid an activity of > 4 GBq/tonne of total alpha radiation and/or > 12 GBq/tonne of combined total beta and gamma (ONR, 2015). Maximum plume activities recorded in boreholes within the vicinity of MSSS as a result of the leak for H-3, C-14, Cl-36, and Tc-99 were \sim 12,000, \sim 14, \sim 35, \sim 3.5, Bq/L. However, these were recorded in 2020 and 2021, with downgradient boreholes in 2022 and early 2023 showing reductions in maximum activities (Sellafield Ltd., 2023). As of 2023, liquor was being lost to ground at a rate of 2.3-2.5 m³/day and may get worse as site infrastructure ages, with the leak anticipated to continue until the majority of MSSS waste is removed from the silos in 2045-2050 (ONR, 2023).

Legacy and contemporary contamination pose a potential health hazard for on-site and off-site groundwaters, both in the present as well as the future. Hemming *et al.* (2023; Appendix E) have discussed at length current remediation techniques for H-3, Sr-90, and Tc-99 at nuclear sites, and so only a brief summary will be provided here. Pump and treat is the most commonly used approach, with groundwater extracted, contaminants stripped through the use of ion exchange resins or adsorbents, and then clean water released either back into the ground or surface

waters. Whilst the process is generally effective for Sr-90 and Tc-99, H-3 cannot be treated through these means (the radionuclide is present as tritiated water molecules rather than an extractable ion present in water) and the set up and maintenance costs make it expensive to operate, especially over annual and decade timescales (if required). More sustainable and lower-cost techniques can sometimes be used, such as permeable reactive barriers (PRBs) and phytoremediation which both require less infrastructure and can treat radionuclides *in situ*. However, PRBs are only effective on redox sensitive elements and phytoremediation is only suitable for elements with a low bioaccumulation risk in humans, or a high bioavailability. As such, no single technique exists for the effective clean-up of key radionuclides H-3, Sr-90 and Tc-99 that are present within the Sellafield subsurface (Figure 3.1) due to varying (geo)chemistries, site conditions, *etc.* between radionuclides. It is therefore important that emerging technologies are developed to broaden the suite of remediation tools available to site operators in the event of radionuclide leaks to ground.

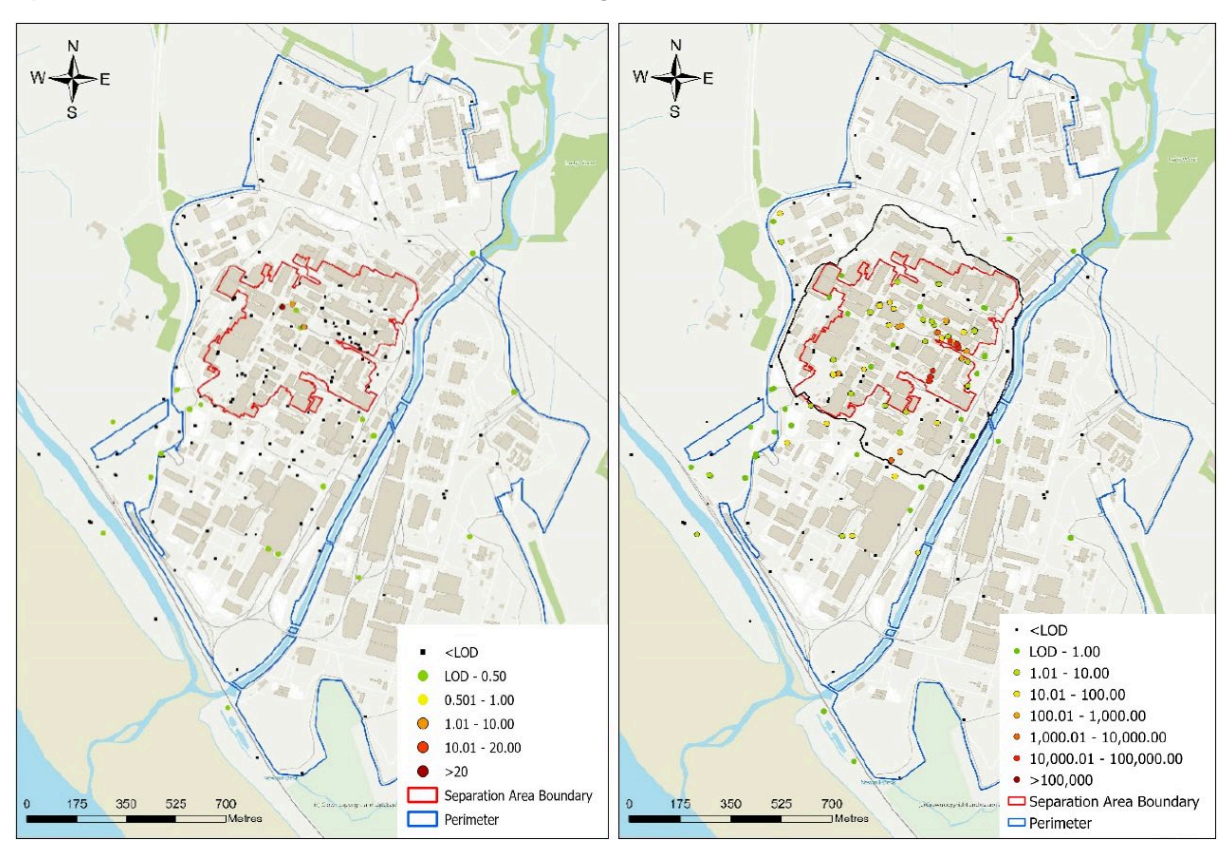


Figure 3.1 – Sellafield groundwater monitoring data from 2020-2022 showing the three-year averaged total alpha and total beta activities (all activities quoted in Bq/L), with most legacy contamination originating from the Separation Area (outer boundary marked by red line) (Sellafield Ltd., 2023). A significant portion of total alpha activities are made up of Pu and Am which have high affinities for sediment (USEPA, 1999) and so show little migration away from the Separation Area, whereas more soluble beta emitters migrate with groundwater flow towards the Irish Sea.

3.1.2 Electrokinetic remediation (EKR)

Electrokinetic remediation (EKR) is a cost-effective and sustainable alternative to traditional remediation methods (Purkis et al., 2021). This technique involves applying a direct current to a medium, inducing (re)mobilisation and migration of contaminants toward specific areas within the material (Figure 3.2). Three primary transport mechanisms occur during the remediation process: Electromigration, electrophoresis and electroosmosis. Electromigration is the movement of ions within the contaminated material, with cations and anions migrating towards their respective oppositely charged electrodes. Electrophoresis involves the transport of charged colloidal particles, typically ranging in size from 1 to 5000 nm (Lee, 2019), within the material. Finally, electroosmosis is the movement of water molecules towards the cathode, caused by the double diffuse layering around sediment particles. This layering is created by the negative surface charge of grains attracting enough cations to form a strongly bound, immobilised coating around the particles as well as a diffuse region directly above where cations are weakly attracted but still mobile (Li and Wu, 2000). When an electric current is applied the diffuse layer, along with the surrounding hydrating layer, migrates towards the cathode. Water tension causes additional aqueous layers to be dragged along, creating a net flow in the electrokinetic cell. When water encounters either electrode, electrolysis occurs which produces hydronium ions at the anode and hydroxide ions at the cathode. Their respective charges cause migration toward the opposite electrodes, creating a pH gradient within the medium over time.

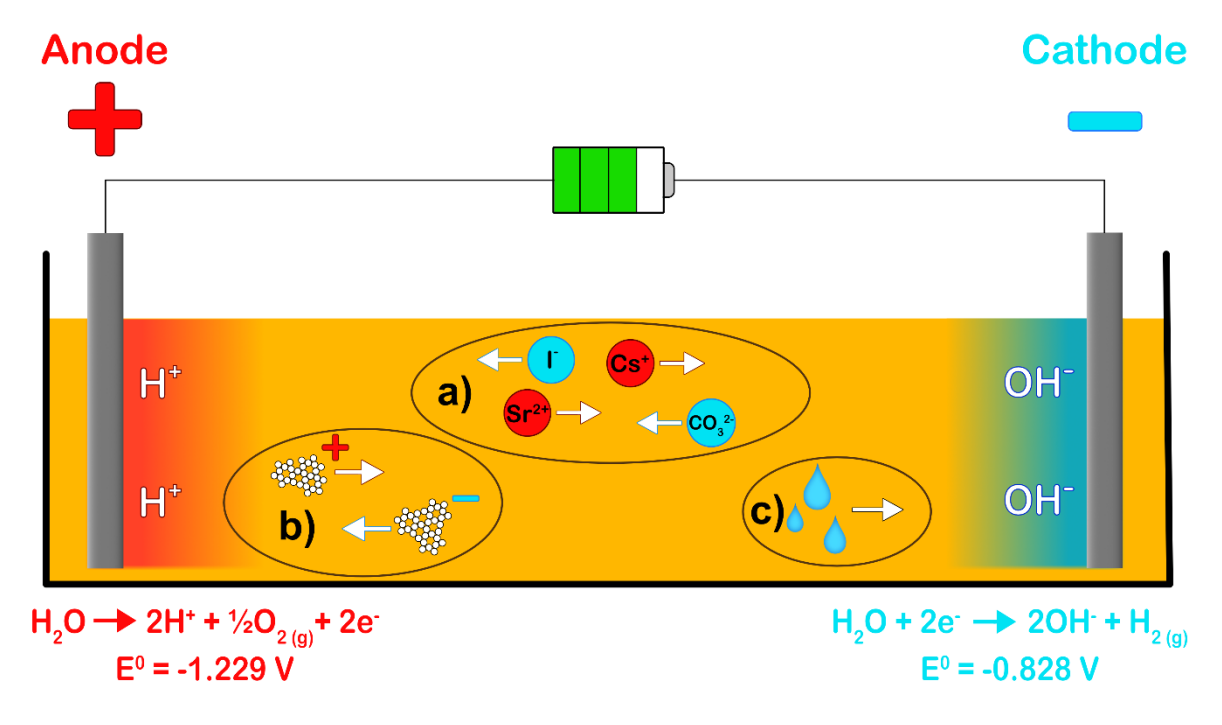


Figure 3.2 – EKR schematic, modified from Purkis *et al.* (2021), showing a) – electromigration, b) – electrophoresis, c) – electroosmosis. Electrolysis equations shown create protons and hydroxide ions, which eventually form a pH gradient across the cell.

The primary mechanisms for remediation of contaminants involve either direct precipitation an adsorptive subsurface barrier (e.g. FIRS – Ferric Iron Remobilisation and Stabilisation (Purkis et al., 2023)) or sediment, electrokinetic fencing (EKF; maintaining an electrical current indefinitely to hold contaminants at the electrodes (Cameselle, 2015; Lageman, 2014)), or in combination with other remediation techniques (e.g. permeable reactive barriers (Ghaeminia and Mokhtarani, 2018)). Previous work has demonstrated effective mobilisation of stable elements and molecules in groundwaters (e.g. Reynolds and Gent, 2017; Xu et al., 2022) but comparatively few studies have evaluated applications involving radionuclides, despite the fundamental technical similarities with EKR of non-radioactive contaminants. Development in this area could broaden the remedial techniques available to nuclear site operators and enhance the overall success of clean-up projects.

This paper evaluates EKR as a potential remediation technique for key radionuclides H-3, Sr-90, and Tc-99 within Sellafield sediments. Groundwater simulant and real-world subsurface material collected proximally to the site were used to enhance authenticity to the conditions found under the facility. Preliminary proof-of-concept work using stable analogues for radionuclides showed evidence for migration and trapping within the treatment cell (Section A.2) but the cells suffered from extensive evaporation which limited the conclusions that could be drawn. The work presented here reports results from a revised experimental design for radionuclide-specific work, which minimised both evaporative effects and the volume of contaminated material / activities used, while providing robust data on radionuclide transport under applied EKR.

3.1.3 Radionuclides of Interest

Radionuclide	Half- life ^[a]	Predominant mobile oxidation state(s) in groundwater	Kd range in environmental conditions	Highest three-year average activity in Sellafield groundwater between 2020 and 2022 (Bq/L) [1]	WHO drinking water standard (Bq/L) [j, k]
H-3	12.32 years	O [p]	0 ^[e]	36,600	10,000
Sr-90	28.91 years	(II) ^[c]	10-25 (quartz- rich) ^[f] ~ 10 ³ (clay) ^[g]	60,600	10

Tc-99	211,000	(VII) ^[d]	0-1 ^[h]	57.5	100
10-99	years	(VII) * 3	0-1 - 7		

Table 3.1 – Summary for radionuclides of focus. [a] – iaea.nds (2024); [b] – Sellafield Ltd. (2017); [c] – Gupta *et al.* (2018); [d] – Banerjee *et al.* (2016); [e] – Serne (2007); [f] – Serne *et al.* (1993); [g] – Wallace *et al.* (2012); [h] – Cantrell *et al.* (2003); [i] – Sellafield Ltd. (2023); [J] – WHO (2022); [k] – Sellafield Ltd. (2022).

A detailed description of environmental behaviours for the radionuclides of interest, alongside a discussion on using partition coefficients (K_d ; Equation 3.1) is given in Hemming *et al.* (2023) but summarised here. Partition coefficients are used to describe the affinity of a radionuclide to bind to a solid phase instead of remaining in a liquid.

$$K_d = \frac{\text{radionuclide on adsorbent at equilibrium (mg/g)}}{\text{radionuclide in solution at equilibrium (mg/mL)}}$$
 (3.1)

A K_d of 1 mL/g would show a radionuclide was found in equal proportions on the solid and liquid phases, with values < 1 mL/g showing a preference for the aqueous phases and values > 1 mL/g showing an affinity for the solid phases.

A summary of the radionuclides of focus can be found in Table 3.1 and described here. H-3 (half-life – 12.32 years (IAEA, 2025)) primarily exists in groundwaters as tritiated water ((H-1)(H-3)O) due to the radionuclide undergoing isotopic exchange with H-1 in light water (Sellafield Ltd., 2017), which gives it, by definition, a K_d of 0 (Serne, 2007). This can increase if the radionuclide exists as organically-bound tritium (OBT), with the K_d then dependent on the properties of the entire molecule (Croudace et al., 2012). Sr-90 (half-life - 28.91 years (IAEA, 2025)) will primarily exist as Sr(II) cations that are present as hydrated ions) or organic compounds (Gupta et al., 2018), with observed K_ds of 10-25 mL/g in quartz rich sediment (Serne et al., 1993). However, when bound to organic material or clays, solid phase retention is increased e.g. K_d of ~ 10³ estimated in the Sellafield subsurface (Guillén et al., 2015; Wallace et al., 2012). Finally, Tc-99 (half-life – 211,100 years) can exist either as Tc(IV) or Tc(VII) in environmental conditions, although only the latter is mobile in groundwaters, existing as TcO₄. Tc(VII) typically has K_ds of 0-1 mL/g (Banerjee et al., 2016; Cantrell et al., 2003; Serne, 2007), whereas in reducing conditions Tc(IV) has a much higher affinity for sediment e.g. estimations of 15-280 mL/g at Laxemar-Simpevarp and Forsmark sites in Sweden (Sheppard et al., 2011). The high groundwater mobilities for all three radionuclides of focus emphasise the need for effective remediation techniques, of which EKR may be capable of filling this niche.

3.2 Methods

3.2.1 Materials and Reagents

To make the experiments as authentic to the Sellafield subsurface as possible, sediment was sourced from Peel Place Quarry (Holmrook, Cumbria, UK, CA19 1YD), an area of land ~ 5 km from Sellafield, with the same Triassic sandstones as those at the nuclear site (Purkis *et al.*, 2023). Characterisation has been performed on these previously by Purkis *et al.* (2023) and Smith *et al.* (2020) and so was not repeated here. The material selected for use was medium sand primarily comprised of quartz, with some feldspars, kaolinite, and micas also present. The sediment was homogenised by leaving 500 g in a plastic bottle overnight on rollers at 30 RPM, simplifying the complex nature of the Sellafield subsurface. A Sellafield groundwater simulant (SGWS) was also prepared to optimise authenticity, with the simulant created using a modified recipe from Chaplin *et al.* (2022) (Table A.1).

Whilst radionuclides of focus H-3 and Tc-99 were used in this experiment, Sr-85 was used as an analogue for Sr-90. Sr-85 (half-life 64.85 days; IAEA (2025)) was selected as its gamma radiation can be measured more rapidly and easily than Sr-90, which is conventionally quantified through counting of the Cherenkov radiation emitted by Y-90, its daughter nuclide (Lu, 2023).

For radionuclides, H-3 and Sr-85 were purchased from Physikalisch-Technische Bundesanstalt (Braunschweig, Germany) and Tc-99 from Amersham (now GE Healthcare; Chicago, USA), with each prepared with the method described in Section A.1. Regarding, reagents, and SGWS constituents, nitric acid were acquired from NaHCO₃ from Fisher Scientific (now Thermo Fisher Scientific; Pennsylvania, USA); NH₄NO₃ from Acros Organics (now Thermo Fisher Scientific; Pennsylvania, USA); CaCl₂·2H₂O and SrCl₂.6H₂O from Merck Group (Darmstadt, Germany); H₃PO₄, KHCO₃, and MgSO₄ from British Drug Houses Ltd. (now Merck Group; Darmstadt, Germany); and Gold Star scintillation cocktail from HIDEX (Turku, Finland). Silicon tubing was acquired from Altec (Cornwall, UK) and graphite electrodes from Marvellous (Taiyuan, China).

3.2.2 Experimental Setup

In total, experiments were performed (Table 3.2). All three radionuclides had an EKR cell operating at 0.5 V/cm (7 V total; chosen to reduce costs and make the experiments as economically feasible as possible for scale-up work) and a diffusion-only cell with no EKR applied. In addition, Sr-85 and Tc-99 also had 1 V/cm (14 V total; chosen to investigate migration enhancement with greater voltages), but due to concerns about potential volatilisation of tritiated water through electrolysis, a trial at this higher voltage gradient with H-3 was not

performed. An extra two control cells containing no radionuclides were created to provide a background activity in the sediments and SGWS.

Tube Number	Radionuclide Used	EKR Voltage Gradient Applied
		(V/cm)
1	H-3	N/A (diffusion only)
2	H-3	0.5
3	Sr-85	N/A (diffusion only)
4	Sr-85	0.5
5	Sr-85	1.0
6	Tc-99	N/A (diffusion only)
7	Tc-99	0.5
8	Tc-99	1.0
9	None	N/A (diffusion only)
10	None	N/A (diffusion only)

Table 3.2 – Summary of each tube used in the experiments.

Each cell was made of silicone tubing (20 x 0.8 cm, length x internal diameter), with the dimensions selected to avoid unnecessary contamination of non-radioactive sediment and to minimise groundwater evaporation during the experiment (Figure 3.3). The tubing was cut and filled with enough Peel Place Quarry sand to fill 14 cm of length. The tube was then bent into a 'U' shape (done to minimise the potential of leaks from either end compared to blocking up at least one tube end, as well as to make SGWS 'top-ups' easier to perform), with the sand redistributed by tapping, twisting, and shaking to fill the middle of the tube. SGWS was added until all but the top ~ 1 cm of tubing was saturated before the tubing was twisted three times whilst still maintaining its 'U' shape to release any trapped air within the sediment. The pH of SGWS in each end was taken with indicator paper, radionuclide solution containing either H-3, Sr-85 or Tc-99 was then added into one end, graphite electrodes were placed in the EKR cells, and SGWS was introduced at both ends until the tubes were completely filled with liquid. All cells had both tube ends covered with parafilm to minimise SGWS evaporation (EKR cells had a hole pierced in the parafilm to allow the electrodes to protrude), the current was switched on for the applicable cells and all tubes were left for 96 hours (4 days). Once per day, SGWS in each cell was topped up if the water level had decreased by > 1 cm. This was done to keep the hydraulic head in both ends of the tube consistent and avoid a hydraulic gradient transporting

contaminants instead of diffusion, electromigration, and/or electroosmosis. The pH was measured at the start and end of the experiments using indicator paper. This was done as it required a smaller volume to yield a measurement compared to a pH probe, as well as avoiding the possibility of contaminating the probe. Since the primary purpose of this was to determine the presence of a pH gradient across the cells, a precise measurement was not required.

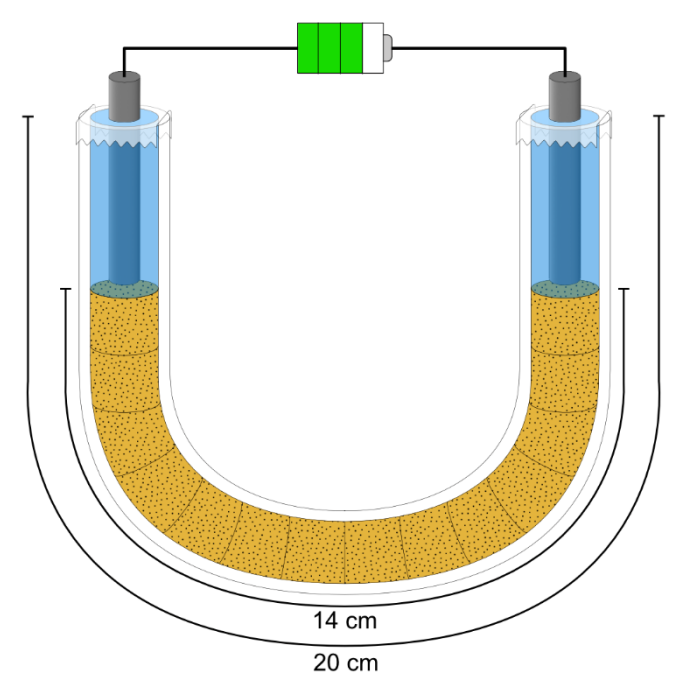


Figure 3.3 – Experimental setup for the EKR cells. Diffusion-only tubes had a similar setup but without electrodes. The location of radionuclide addition and EKR electrode polarity were chosen to promote transport through the sediment *i.e.* H-3 and Sr-85 were added to the anodic tube end and the Tc-99 was added to the cathodic end.

3.2.3 Analysis

At the end of the 96 hours, electrodes were removed from the EKR cells and standing water above the SGWS-sediment interface was extracted with a pipette. Sr-85 samples were directly counted on a HIDEX AMG gamma spectrometer and analysed with HidexAMG software, whereas the H-3 and Tc-99 were mixed with 12 mL and 15 mL Gold Star scintillation cocktail, respectively, and were measured in a Wallac 1220 Quantulus liquid scintillation counter (LSC) and analysed with WinQ software. The tubes were resealed with fresh parafilm and placed in a freezer to minimise radionuclide migration and SGWS spillage during future handling. After, the tubes were removed and cut into 1-cm-thick sections for sediment analysis. Subsequent procedure depended on the radionuclide and analysis method:

 For H-3, the sediment from each section was pushed into a scintillation vial and the tubing washed with 10 mL of 0.1 M HNO₃ (chosen as acidic conditions improve H-3

- dissolution but can break down scintillation cocktail (Warwick *et al.*, 2010)). This was left overnight to equilibrate before an 8 mL aliquot was taken and mixed with 10 mL of scintillation cocktail for LSC measurements.
- Sr-85 measurements involved pushing sediment from the tube into a scintillation vial, placing the tube section into the vial, and counting each sample on a gamma spectrometer. A calibration sample was created, which involved spiking clean sediment and a 1-cm-thick section of tubing with a known activity of Sr-85, and positioned in the vial to mimic the geometry of the samples (*i.e.* sand at the bottom of the vial with tubing on top) as closely as possible.
- For each Tc-99 sample, the sand and tube were digested in 25 mL of 8 M HNO₃ on a 100 °C hotplate for three hours. The digests were then extracted through 0.22 μm syringe filters and put into clean beakers where they were evaporated to dryness. After, the precipitates were redissolved in 5 mL of SGWS, 3 mL of 2 M H₃PO₄ (to reduce the yellow colour caused by Fe compounds and produce a more transparent and, therefore, less quenched sample) and 12 mL of Gold Star before undergoing LSC. Due to the proof-of-concept nature of the work, the chemistry was kept as simple as possible, and so no Re yield recovery tracer was used. However, a sample with a known amount of Tc underwent the aforementioned procedure with each batch of Tc samples, giving an indicator for the recoveries expected in the samples.

3.3 Results

3.3.1 Distribution Profile Quantification

For describing the distribution profiles of each tube, the proportion of radionuclide leaving the initial aqueous radionuclide input zone, the proportion of radionuclide reaching the end aqueous zone, and the median travel distance were used. The first two of these quantify how much radionuclide enters and is fully transported through the sediment, whilst the median shows the middle distance that the radionuclide has travelled.

For determining areas of enrichment within the EKR cells, a 'peak' was defined as sediment sections that had at least 2 % of the total recovered activity within the tube. This cut-off value was chosen to avoid including broad tailing than spanned across multiple sections whilst only contributing a minor portion to the 'peak' activity.

3.3.2 Tube currents, pHs, and Electrolyte Evaporation

	Н-3				Sr-85						Tc-99						
	Diffusion		usion 0.5 V/cm		Diffusion 0.5		0.5 V).5 V/cm		1 V/cm		Diffusion		0.5 V/cm		cm	
	Init	Fin	An	Cat	Init	Fin	An	Cat	An	Cat	Init	Fin	An	Cat	An	Cat	
Initial pH	6	6	6	6	6	6	6	6	6	6	6	6	6	6	6	6	
Final pH	6	6	3	9	5	5	2-3	9	2	10-11	6	5-6	3	9	2	11	
pH Change	0	0	-3	+3	-1	-1	-3.5	+3	-4	+4.5	0	-0.5	-3	+3	-4	+5	
Final pH gradient across entire cell	0		6		0		6.5		8.5		0.5		6		9		

Table 3.3 – Tube pHs at the beginning and end of the experiment. An = anode, Cat = cathode, Init = initial aqueous zone, Fin = final aqueous zone. A pH range was put if the result of the indicator paper did not clearly show a single pH value. 'Final pH gradient across the entire cell' was calculated by the difference in final pH values between both ends of the tube.

The pHs before and after each experiment are shown in Table 3.3. To summarise, the diffusion tubes showed little to no change in pH, whilst the EKR cells formed typical pH gradients of \sim 3 to \sim 9 at the anode and cathode, respectively. Whilst all EKR cells recorded electrical currents of 0.000 A throughout the experimental duration, clear pH gradients in the treated tubes show electrolysis, and therefore EKR, was occurring.

SGWS addition (mL)	H-3				Sr-85						Tc-99					
	Diffusion		0.5 V/cm		Diffusion		0.5 V/cm		1 V/cm		Diffusion		0.5 V/cm		1 V/cm	
	An	Cat	An	Cat	An	Cat	An	Cat	An	Cat	An	Cat	An	Cat	An	Cat
Initial	6.0		4.5		6.0		4.5	1	4.6	•	6.0		4.3	•	4.8	
After 24 hrs	_	_	_	_	_	_	_	_	0.3	0.1	_	_	_	_	_	_
After 48 hrs	_	_	_	_	_	_	_	_	0.5	_	_	_	_	_	_	_

After 72 hrs	_	_	0.8	0.3	_	_	0.3	0.1	0.3	_	_	_	0.1	0.3	_	0.3
Total Top-up	_	_	0.8	0.3	ı	ı	0.3	0.1	1.1	0.1	ı	ı	0.1	0.3	I	0.3

Table 3.4 – SGWS additions to each cell. An = anode, Cat = cathode. Initial volumes are listed as a total across the entire cell, whilst subsequent SGWS top-ups are subdivided into anode and cathode additions.

SGWS volumes added to each tube are shown in Table 3.4. As a summary, ~ 6 mL of simulant was initially added to each diffusion setup and ~ 4.5 mL added to each EKR cell as a result of volume reduction caused by electrodes. These values, combined with ~ 0.1 mL of radionuclide solution, saturated the sediment and completely filled the tubes with liquid. Throughout the experiments all diffusion cells maintained their SGWS levels, whilst all EKR cells required a least one simulant top-up. In each case, the location of radionuclide addition was the tube-end that required a larger SGWS top-up.

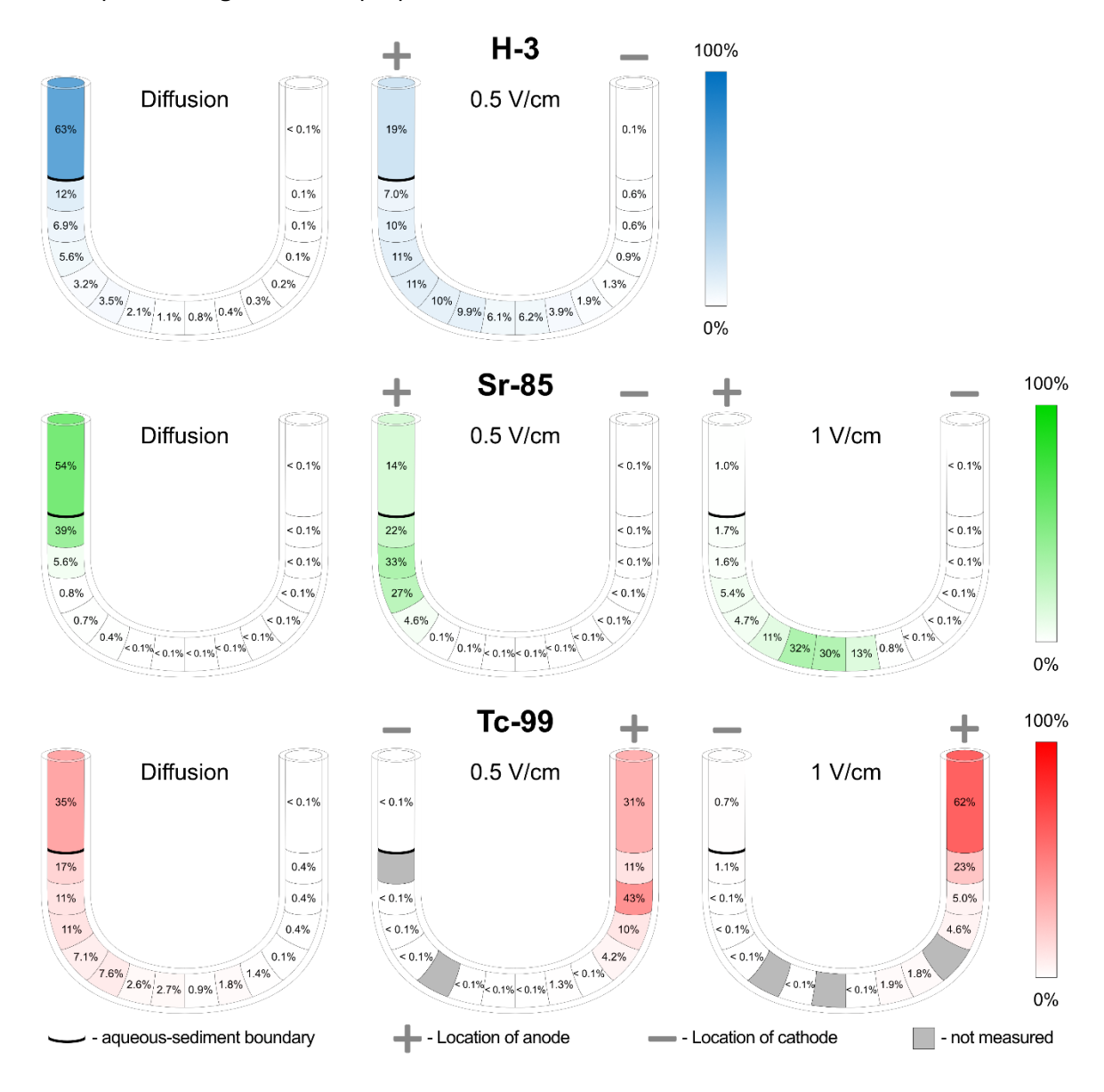


Figure 3.4 – Heat map results for all eight tubes. Percentage of the total recovered activity in each section is marked on each section. In every case, the radionuclide was introduced in the aqueous zone in the top left of each schematic. Where applicable, electrodes were placed to aqueous areas at each end of the tube to promote electromigration/ electroosmosis through the sediment. The aqueous-sediment boundary marks the point where the radionuclide moved from the initial introduction region to the Sellafield subsurface material. For tabled results see Table A.3.

SGWS addition (mL)	H-3		Sr-85			Tc-99			
	Diff	0.5 V/cm	Diff	0.5 V/cm	1 V/cm	Diff	0.5 V/cm	1 V/cm	
Radionuclide proportion that diffused/ electromigrated from initial zone (%)	37 +/- 4	81 +/- 1	46 +/- 2	86 +/- 1	99 +/-0	65+/- 7	100 +/- 0	99 +/- 0	
Proportion of radionuclide that diffused/ electromigrated to the end aqueous zone (%)	< 0.1	0.1 +/-	< 0.1	< 0.1	< 0.1	< 0.1	31 +/- 5	62 +/- 7	
Section containing median of tube's cumulative activity (cm)	Start	3-4	Start	1-2	5-6	0 – 1	12 – 13	End	
'Peak' of elevated activity in each tube (cm)	Start – 6	Start – 9	Start – 2	Start – 4	2-8	Start – 7	10 – End	11 – End	

Table 3.5 – Final radionuclide distributions within each tube. Diff = diffusion-only tube. For more information see section 3.3.1. As samples were not run in replicate, uncertainties presented here are analytical uncertainties for a single measurement.

3.3.3 Tritium

For the diffusion-only tube, 63% of the final activity was present in the starting aqueous fraction of the tube and < 0.1 % present in the end aqueous fraction, with the cumulative activity median found in the starting aqueous zone, and an elevated activity peak present between the starting aqueous zone and 7 cm, and. (Figure 3.4; Table 3.5, columns 1 and 2). The 0.5 V/cm cell retained 81 % of the final activity in its initial aqueous zone and 0.1 % in the end aqueous

fraction. The concentration gradient within the diffusion tube was much shallower than that in the diffusion cell, creating a broad, shallow H-3 peak between the initial aqueous zone and 9 cm with a median located at 3-4 cm.

3.3.4 **Strontium-85**

The diffusion-only tube had 46% of Sr-85 transported away from the radionuclide input area, with < 0.1 % reaching the other end of the tube, a median in the initial aqueous zone, and the peak between the starting aqueous fraction and 2 cm of sediment (

Figure 3.3; Table 3.5, columns 3-5). With the 0.5 V/cm cell, 86 % of Sr had migrated from the initial aqueous area, of which < 0.1 % had reached the end aqueous fraction. The median was found in section 1-2 cm, with the peak located between the start area and 4 cm into the sediment. In contrast, the 1 V/cm cell had a 99 % movement from the initial fraction and < 0.1 % reaching the opposite end of the tube, with a median at 5-6 cm and a peak at 2-8 cm. The diffusion tube has a sharp drop in activity within 1 cm of the aqueous-sediment boundary, whilst the EKR cells both show asymmetrical peaks in Sr-85, skewed towards the cathode.

3.3.5 Technetium-99

Diffusion away from the radionuclide input zone of the control tube was found to be 65 %, with < 0.1 % reaching the end of the tube, 0-1 cm containing the median, and the initial aqueous region and 10 cm containing the peak (

Figure 3.3; Table 3.5, columns 6-8). Due to logistical issues during measurement preparation, five samples across the EKR cells could not be analysed. Despite this, treatment with 0.5 V/cm showed a 100 % Tc movement from the start area, a 31 % collection in the end aqueous fraction, a median at 12-13 cm, and a peak between 11 cm and the final aqueous fraction at > 14 cm. Similarly, the 1 V/cm cell had a 99 % radionuclide input zone migration, 62 % of which accumulated in the final aqueous fraction, a median in the final aqueous fraction, and a peak located at 11 cm to the end aqueous region at > 14 cm. The diffusion-only and 1 V/cm profiles are broadly mirror images of each other, whilst the 0.5 V/cm displays an apparent 'double peak' in both the 12-13 cm and end aqueous fractions.

3.4 Discussion

3.4.1 Tritium

The diffusion-only tube showed little movement of H-3 away from the radionuclide addition zone, which is to be expected since H-3 exists as tritiated water and therefore acts as a proxy to light water, illustrates the lack of water flux between the aqueous and sediment regions. In comparison, the 0.5 V/cm EKR cell showed an increased H-3 mobility out of the initial aqueous zone compared to the diffusion tube by 44 %, in addition to a more gradual change in concentration gradient, and a broad, shallow peak of elevated activity. The large distance over which the peak occurs makes precise quantification difficult (see Table 3.5, bottom row), but, based on the peak boundary distances (which are defined here as the minimum and maximum distances the peak could be found in, i.e. for a peak found at 0-6 cm, the peak boundaries would be 0 and 6 cm), the diffusion tube has a migration rate of 0.0 - 0.8 cm/day $(0.0 - 8.7 \times 10^{-6}$ cm/s; calculated by dividing the peak boundaries by the length of time the experiment duration) and the 0.5 V/cm tube with a rate of 0.0 - 2.3 cm/day $(0.0 - 2.6 \times 10^{-5}$ cm/s). Transport towards the cathode is consistent with the expected movement direction from electroosmosis. However, SGWS addition data (Table 3.4, columns 1 and 2) shows water loss from the anode end of the cell, which may have caused remaining H-3 to diffuse into the sediment quicker before simulant levels were replenished. Despite this, the diffusion-only tube demonstrates that H-3 movement in the absence of EKR is minor at distances > ~ 3 cm, suggesting that enhanced transport of the radionuclide at distances greater than > ~ 4 cm from the aqueous-sediment boundary is likely primarily controlled by electroosmosis. Further, although light water ((H-1)₂O) will preferentially evaporate relative to tritiated water ((H-1)(H-3)O), both will escape the system during water loss, which would mitigate the formation of a greater concentration gradient either side of the aqueous-sediment boundary. Whilst this enhancement of transportation is evident, the technique has shown a lack of H-3 accumulation across the cell, suggesting that a much longer time period than this 4-day trial is required for effective remediation of the radionuclide. No EKR trials for H-3 in sediments could be found for assessing to what extent an increased voltage gradient would increase electroosmotic rates.

3.4.2 Strontium-85

Sr-85 showed little diffusion through the sediment, with 46 % of the radionuclide passing through the aqueous-sediment boundary and yet only 8 % travelling > 1 cm through the solid phase. This is consistent with site observations that Sr adsorbs to clays in the Sellafield subsurface, slowing its diffusion rate (ONR, 2023; Sellafield Ltd., 2023). However, enhanced

mobilities out the zone of radionuclide addition with 0.5 V/cm and 1 V/cm voltage gradients (increases of 40 % and 53 %, respectively) are observed for the EKR cells. Both have asymmetrical activity profiles that are skewed towards the cathode, which, in the absence of moving groundwater, suggests that electromigration is occurring alongside diffusion. Using peak boundaries, the diffusion rate of Sr was determined as 0.0 – 0.5 cm/day (0.0 – 5.8x10⁻⁶ cm/s), while cells with applied voltages of 0.5 V/cm and 1 V/cm produced rates of 0.0 - 1.0cm/day $(0.0 - 1.2 \times 10^{-5} \text{ cm/s})$ and $0.5 - 2.0 (5.8 \times 10^{-6} - 2.3 \times 10^{-5} \text{ cm/s})$ respectively. Improved transportation rates compared to the control tube demonstrate the efficacy of EKR in migrating radiostrontium and mitigating adsorption onto finer sediments. For a more precise migration rate estimation, the highest-activity sediment section in both cells (1-2 cm for 0.5 V/cm and 5-6 cm for 1 V/cm) were used. The distance between these sections shows that doubling the voltage gradient increases the migration rate by 2.5 – 6 times. Whilst previous work looking at the kinetics of Sr in sediments, non-linear migration rates with varying voltage gradients have been observed in previous EKR trials using similarly behaving heavy metals e.g. Cd (Yan et al., 2024), highlighting that a compromise between treatment cost and time is required for electrokinetic treatment to be as successful as possible.

3.4.3 Technetium-99

The majority of Tc passing through the sediment-aqueous boundary by the end of all trials suggests that the radionuclide has little interaction with the Sellafield sediment under the conditions present here. This is to be expected, as sediment grain surfaces are generally negatively charged (Naidu *et al.*, 1994) and would therefore repel TcO_4 : molecules, retaining them in the aqueous phase. This is also seen when Tc plumes have migrated through the Sellafield site (Cruikshak, 2012). Both EKR cells showed high remediation efficiencies (> 99 %), although the 1 V/cm was more effective at electromigrating Tc into the final aqueous region where the anode was located. Determined by using peak boundaries (Table 3.5), the diffusion rate of Tc is 0.0 - 1.8 cm/day (0.0 - 2.0x10-5 cm/s), with the migration rates for 0.5 V/cm and 1 V/cm being > 0.5 cm/day (> 0.5 cm/s) and > 0.5 cm/day (> 0.5 cm/s), respectively. Due to both EKR cells having significant Tc reaching the end of the cell as well as an absence of obtainable EKR literature on Tc-99 migration, the relationship between voltage gradients and migration rates cannot be quantified beyond stating that transportation with 1 V/cm is more rapid than with 0.5 V/cm.

Due to the high efficacy of radionuclide mobilisation to the anode, the EKR sediment sections that were not analysed likely contained only a very small fraction of the total Tc and consequently had little or no effect on the interpretations of the results. However, whilst the diffusion-only and 1 V/cm tubes show smooth activity gradients across the cells, the 0.5 V/cm

distribution profile is more erratic. No tracer was added to the samples to determine the final recovery, but the method standard sample (a known amount of Tc added to an otherwise blank sample of Sellafield sand, wetted with SGWS, and silicone tubing, that underwent the same chemistry as the rest of the solid-phase samples) from each batch of sediment analysis was used as a proxy for determining loss. Whilst these correction factors appear to have worked well with the diffusion and 1 V/cm tubes, the recovery of individual samples significantly differing from that of the method standard could explain the irregularly shaped profile of the 0.5 V/cm profile. Whilst this makes exact quantification of Tc activities in sediment sections less precise, the aqueous phases are unaffected by this, as they were measured immediately after tube extraction and the addition of a scintillation cocktail, making the overall conclusion that 1 V/cm is more effective than 0.5 V/cm still valid.

3.4.4 Radionuclide Comparisons and Future Work

Of the diffusion cells, H-3 showed the lowest migration rate out from the radionuclide input zone, with Sr-85 being slightly more mobile and Tc-99 having the greatest initial transport. This is to be expected as electroosmosis has been shown to be a slower process than electromigration (Sun et al., 2023). Once in the solid phase, however, H-3 and Tc-99 had similar distribution profiles which matches migration observations seen at Sellafield (Sellafield Ltd., 2023, 2022). This suggests that the sediment charge repulsion of TcO_4 makes it behave conservatively in the Sellafield material, allowing it to potentially migrate large distances unless there is a change in redox conditions. Given the similar radionuclide distributions through the sediment, a greater migration out of the radionuclide addition zone for Tc-99 compared to H-3 (which is a proxy for water movement) initially seems counter intuitive. However, this can be explained by the greater mass of Tc-99 added to the tubes relative to the H-3 (~ 4.5 Bq of Tc-99 = ~ 7.1 x10⁻⁹ g, ~ 200 Bq of H-3 = $\sim 5.6 \times 10^{-13}$ g) which results in a greater concentration gradient between the aqueous and sediment fractions of the tube at the beginning of the experiment, and, therefore, a greater extent of initial diffusion. With regards to Sr, its high affinity for clay fractions drastically reduces its diffusion rate compared to the other radionuclides of focus. When treated with EKR, both voltage gradients show Tc-99 as the easiest radionuclide to mobilise and Sr-85 as the most difficult, with H-3 at 0.5 V/cm having an intermediate rate. If movement of H-3 at 0.5 V/cm is assumed to be the combined rate of electroosmosis and diffusion, and Sr-85 is transported by both these factors in addition to electromigration, then the significantly lower migration rate of Sr demonstrates its strong retardation in Sellafield material which must be considered if EKR were to be deployed at the site. Nevertheless, all three radionuclides show some extent of promise for effective EKR in these idealised conditions, even if the remediation timescales vary. Whilst precise quantification of each sediment section was not possible to due potential water

movement and H-3 diffusion whilst being stored in the freezer, alongside issues with accurately determining Tc-99 sample yield recoveries, aqueous zone data and relative values from solid-phase data effectively demonstrates EKR as a potentially viable remediation technique for groundwater contamination. Sr-85 migration rates have been well defined, but H-3 and Tc-99 require further work to quantify their transport rates. This will be important for encouraging pilot EKR trials at field scales, as optimising treatment periods will be key for making the process as effective and appealing to site operators as possible. Further, the relationship between voltage gradient and migration rate will likely play a significant role in determining EKR efficacy in various media, making the determination of this for both H-3 and Tc-99 important for future upscaling work. Additional studies should also look at EKR efficacy in flowing groundwater, particularly when the (electro)migration direction is opposing or perpendicular to a hydraulic gradient. Once performed, trialling the same work performed here in a bench-scale, 2-dimensional system will add a realistic complexity to the system that will determine more accurate migration rates for radionuclides. This will give site operators the confidence to apply EKR in real-world scenarios, offer a potentially versatile tool for groundwater remediation.

3.5 Conclusions

This chapter investigated the efficacy of EKR for H-3, Sr-90, and Tc-99 in simulated groundwaters and authentic subsurface material from the Sellafield nuclear site. Diffusion-only control experiments showed H-3 and Tc-99 were able to travel through the entirety of the sediment, although most remained in the first \sim 6 cm, whilst Sr-85 was retained in < 1 cm of sediment likely resulting from strong sorption to clays. In contrast, results from the 0.5 V/cm trials demonstrated Tc-99 migration rates of > 2.5 cm/day; H-3 and Sr were also mobilised, with rates of 0.0-2.3 cm/day and 0.0-1.0 cm/day (up to 3x and 2x faster migration compared to diffusion tubes), respectively. Doubling the voltage gradient to 1 V/cm resulted in migration rates of 0.5-2.0 cm/day and > 2.8 cm/day for Sr-90 and Tc-99, respectively, leading to 2.5-6x faster migration of Sr compared to 0.5 V/cm and an unquantifiable amount faster rate for Tc.

H-3 behaviour can be explained through electroosmosis towards the cathode, making migration much slower than Sr-90 and Tc-99 which underwent electromigration. EKR of H-3 at 0.5 V/cm was much more effective at mobilising this radionuclide than diffusion alone, producing a broad, shallow plume throughout approximately 2/3rd of the core. Sr-90 demonstrated a reduced migration rate towards the cathode, likely as a result of sorption onto clays. Sr migration is accelerated by using EKR, with 1 V/cm movement being 2.5 – 6 times faster than 0.5 V/cm. Tc-99 had the greatest migration rates of the radionuclides investigated here, instead

migrating towards the anode. This was likely caused by repulsion between TcO₄⁻ and negatively charged sediment particles, minimising its contact with the any potential sorption sites.

Overall, all radionuclides showed improvement in migration rates compared to their diffusion-only counterparts under the experimental conditions used here, but differences in their transportation speeds have repercussions on future scaled-up work. Improved Sr, and to a lesser extent Tc, migration rates between 0.5 and 1 V/cm suggest there is a trade-off between the voltage applied and treatment time, which has implications for financial cost when scaled up. Understanding this compromise and optimising it for a nuclear context should be undertaken to build the case for EKR scale-up for groundwater applications and increasing site operator confidence in eventual site deployment

3.6 Acknowledgements

The authors would like to thank Dr. James Graham (National Nuclear Laboratory) for providing the Peel Place Quarry sediment used in these experiments.

3.7 References

Banerjee, D., Kim, D., Schweiger, M.J., Kruger, A.A., Thallapally, P.K., 2016. Removal of TcO4–ions from solution: materials and future outlook. Chem. Soc. Rev. 45, 2724–2739. https://doi.org/10.1039/C5CS00330J

Cameselle, C., 2015. Electrokinetic remediation and other physico-chemical remediation techniques for *in situ* treatment of soil from contaminated nuclear and NORM sites, in: van Velzen, L. (Ed.), Environmental Remediation and Restoration of Contaminated Nuclear and Norm Sites, Woodhead Publishing Series in Energy. Woodhead Publishing, pp. 161–184. https://doi.org/10.1016/B978-1-78242-231-0.00008-9

Cantrell, K.J., Serne, R.J., Last, G.V., 2003. Hanford Contaminant Distribution Coefficient Database and Users Guide (No. PNNL-13895 Rev. 1). Pacific Northwest National Laboratory, Richland, Washington.

Chaplin, J.D., Berillo, D., Purkis, J.M., Byrne, M.L., Tribolet, A.D.C.C.M., Warwick, P.E., Cundy, A.B., 2022. Effective 137Cs+ and 90Sr2+ immobilisation from groundwater by inorganic polymer resin Clevasol® embedded within a macroporous cryogel host matrix. Materials Today Sustainability 19, 100190. https://doi.org/10.1016/j.mtsust.2022.100190

Chaplow, R., 1996. The geology and hydrogeology of Sellafield: an overview. Quarterly Journal of Engineering Geology and Hydrogeology 29, S1–S12.

https://doi.org/10.1144/GSL.QJEGH.1996.029.S1.01

Croudace, I.W., Warwick, P.E., Morris, J.E., 2012. Evidence for the Preservation of Technogenic Tritiated Organic Compounds in an Estuarine Sedimentary Environment. Environ. Sci. Technol. 46, 5704–5712. https://doi.org/10.1021/es204247f

Cruikshak, J., 2012. The Sellafield Contaminated Land and Groundwater Management Project: Characterisation of a Complex Nuclear Facility. Presented at the Radiological characterisation for Decommissioning, Studsvik, Nykoping, Sweden.

Ghaeminia, M., Mokhtarani, N., 2018. Remediation of nitrate-contaminated groundwater by PRB-Electrokinetic integrated process. Journal of Environmental Management 222, 234–241. https://doi.org/10.1016/j.jenvman.2018.05.078

Gray, J., Jones, S.R., Smith, A.D., 1995. Discharges to the environment from the Sellafield site, 1951-1992. J. Radiol. Prot. 15. https://doi.org/10.1088/0952-4746/15/2/001

Guillén, J., Baeza, A., Corbacho, J.A., Muñoz-Muñoz, J.G., 2015. Migration of 137Cs, 90Sr, and 239+240Pu in Mediterranean forests: influence of bioavailability and association with organic acids in soil. Journal of Environmental Radioactivity 144, 96–102.

https://doi.org/10.1016/j.jenvrad.2015.03.011

Gupta, D.K., Schulz, W., Steinhauser, G., Walther, C., 2018. Radiostrontium transport in plants and phytoremediation. Environ Sci Pollut Res 25, 29996–30008.

https://doi.org/10.1007/s11356-018-3088-6

Hemming, S.D., Purkis, J.M., Warwick, P.E., Cundy, A.B., 2023. Current and emerging technologies for the remediation of difficult-to-measure radionuclides at nuclear sites. Environ. Sci.: Processes Impacts 25, 1909–1925. https://doi.org/10.1039/D3EM00190C

IAEA, 2025. IAEA Nuclear Data Services [WWW Document]. URL https://www-nds.iaea.org/(accessed 1.13.25).

Lageman, R., 2014. PRELIMINARY ASSESSMENT OF THE APPLICATION OF AN ELECTROKINETIC RING FENCE FOR THE REMOVAL OF RADIONUCLIDES FROM GROUNDWATER AT FUKUSHIMA DAIICHI NUCLEAR POWER PLANT. Lambda Consult, Netherlands.

Lee, E., 2019. Chapter 1 - Electrophoresis of a Single Rigid Particle, in: Lee, E. (Ed.), Interface Science and Technology, Theory of Electrophoresis and Diffusiophoresis of Highly Charged Colloidal Particles. Elsevier, pp. 3–45. https://doi.org/10.1016/B978-0-08-100865-2.00001-1

Li, S.F.Y., Wu, Y.S., 2000. ELECTROPHORESIS | Capillary Electrophoresis, in: Wilson, I.D. (Ed.), Encyclopedia of Separation Science. Academic Press, Oxford, pp. 1176–1187. https://doi.org/10.1016/B0-12-226770-2/04321-0

Lu, S.E., 2023. Development of novel microfluidic systems for radionuclide detection (Doctoral Thesis). University of Southampton, Southampton, UK.

Morley, B., 2004. Best practicable means (BPM) and as low as reasonably practicable (ALARP) in action at Sellafield*. J. Radiol. Prot. 24, 29. https://doi.org/10.1088/0952-4746/24/1/003

Naidu, R., Bolan, N.S., Kookana, R.S., Tiller, K.G., 1994. Ionic-strength and pH effects on the sorption of cadmium and the surface charge of soils. European Journal of Soil Science 45, 419–429. https://doi.org/10.1111/j.1365-2389.1994.tb00527.x

NDA, 2018. The Nuclear Decommissioning Authority: progress with reducing risk at Sellafield. Nuclear Decommissioning Authority, Cumbria, UK.

NDA, 2011. Sellafield Plan (No. LD215). Nuclear Decommissioning Authority, Cumbria, UK.

ONR, 2023. ONR's Regulatory Position on MSSS Original Building Leak to Ground (No. ONR-SDFW-PAR-22-003 Revision 3). Office for Nuclear Regulation, Bootle, UK.

ONR, 2015. Basic principles of radioactive waste management An introduction to the management of higher activity radioactive waste on nuclear licensed sites (No. Revision 2). Office for Nuclear Regulation, Bootle, UK.

Purkis, Burrell, F., Brydie, J.R., Graham, J., Hopkinson, L., Cundy, A.B., 2023. Electrokinetic generation of iron-rich barriers in soils: realising the potential for nuclear site management and decommissioning. Environmental Science: Advances 2, 652–662. https://doi.org/10.1039/D2VA00308B

Purkis, J., Robinson, C., Shaw, S., Lloyd, J., Graham, J., Morris, K., Cundy, A., 2023. Characterisation data for sediments collected from Peel Place Quarry, Cumbia, UK – A Sellafield nuclear site analogue. https://doi.org/10.17632/xn63xpnkbx.1

Purkis, J.M., Warwick, P.E., Graham, J., Hemming, S.D., Cundy, A.B., 2021. Towards the application of electrokinetic remediation for nuclear site decommissioning. Journal of Hazardous Materials 413, 125274. https://doi.org/10.1016/j.jhazmat.2021.125274

Reynolds, H.D., Gent, G., 2017. Pilot test of Electrokinetically Delivered Thermally Activated Persulfate, EK-TAP Final Report (No. 1223009824 Ver–2). NIRAS, Allerod, Denmark.

Sellafield Ltd., 2024. Sellafield Ltd. Annual Review of Environmental Performance 2023/24. Sellafield Ltd., Cumbria, UK.

Sellafield Ltd., 2023. Triennial Groundwater Monitoring Report 2020-2022, Triennial Groundwater Monitoring Reports. Sellafield Ltd., Cumbria, UK.

Sellafield Ltd., 2022. Monitoring Our Environment - Discharges and Environmental Monitoring 2021. Sellafield Ltd., Cumbria, UK.

Sellafield Ltd., 2017. Groundwater Monitoring Annual Data Review 2016 (No. LQTD000758). Sellafield Ltd.

Sellafield Ltd., 2016. Summary for Cumbria MWLP Examination, Dec 2016. Sellafield Ltd., Cumbria, UK.

Sellafield Ltd., 2006. Annual Discharge Monitoring Reports 2006-2021. Sellafield Ltd.

Serne, R.J., 2007. Kd Values for Agricultural and Surface Soils for Use in Hanford Site Farm, Residential, and River Shoreline Scenarios (No. PNNL-16531). U.S Department of Energy.

Serne, R.J., LeGore, V.L., Cantrell, K.J., Lindenmeiser, C.W., Campbell, J.A., Amonette, J.E., Conca, J.L., 1993. Solid-waste leach characteristics and contaminant-sediment interactions. Volume 1, Batch leach and adsorption tests and sediment characterization (No. PNL-8889-Vol.1). Pacific Northwest Lab., Richland, Washington.

Shaw, R.D., 1990. Corrosion prevention and control at Sellafield nuclear fuel reprocessing plant. British Corrosion Journal 25, 97–107. https://doi.org/10.1179/000705990798269676

Sheppard, S., Sohlenius, G., Omberg, L.G., Borgiel, M., Grolander, S., Nordén, S., 2011. Solid/liquid partition coefficients (Kd) and plant/soil concentration ratios (CR) for selected soils, tills and sediments at Forsmark (No. SKB R-11-24). Swedish Nuclear Fuel and Waste Management Co., Stockholm.

Smith, N.T., Shreeve, J., Kuras, O., 2020. Multi-sensor core logging (MSCL) and X-ray computed tomography imaging of borehole core to aid 3D geological modelling of poorly exposed unconsolidated superficial sediments underlying complex industrial sites: An example from Sellafield nuclear site, UK. Journal of Applied Geophysics 178, 104084. https://doi.org/10.1016/j.jappgeo.2020.104084

Sun, Z., Zhao, M., Chen, L., Gong, Z., Hu, J., Ma, D., 2023. Electrokinetic remediation for the removal of heavy metals in soil: Limitations, solutions and prospection. Science of The Total Environment 903, 165970. https://doi.org/10.1016/j.scitotenv.2023.165970

USDOE, 2024. Hanford Site Groundwater Monitoring Report For 2023 (No. DOE/RL-2023-54). U.S. Department of Energy, Richland, Washington.

USEPA, 1999. Understanding variation in partition co-efficient Kd values. Volume II: review of geochemistry and available Kd values for cadmium, cesium, chromium, lead, plutonium, radon, strontium, thorium, tritium and uranium (No. EPA402- R-99– 004B). U. S. Environmental Protection Agency, Washington D.C.

Wallace, S.H., Shaw, S., Morris, K., Small, J.S., Fuller, A.J., Burke, I.T., 2012. Effect of groundwater pH and ionic strength on strontium sorption in aquifer sediments: Implications for 90Sr mobility at contaminated nuclear sites. Applied Geochemistry 27, 1482–1491. https://doi.org/10.1016/j.apgeochem.2012.04.007

Warwick, P.E., Kim, D., Croudace, I.W., Oh, J., 2010. Effective desorption of tritium from diverse solid matrices and its application to routine analysis of decommissioning materials. Analytica Chimica Acta 676, 93–102. https://doi.org/10.1016/j.aca.2010.07.017

WHO, 2022. Guidelines for drinking-water quality: fourth edition incorporating the first and second addenda (Guidelines for drinking water quality). World Health Organisation, Geneva, Switzerland.

Williamson, E.J., 2008. Calder Hall Cooling Tower Demolition: Landmark Milestone for Decommissioning at Sellafield", Proc. of the Waste Management Symposia 2008, 8497, Phoenix, AZ (2008). Presented at the Waste Management 2008, Waste Management Symposia, Phoenix, Arizona.

Xu, H., Zhang, C., Zhang, H., Qiao, H., Zhang, L., Zhao, Y., 2022. Enhanced electrokinetic remediation of heterogeneous aquifer co-contaminated with Cr(VI) and nitrate by rhamnolipids. Journal of Environmental Chemical Engineering 10, 108531. https://doi.org/10.1016/j.jece.2022.108531

Yan, K., Chai, Z., Li, T., Duan, B., Xiao, C., Liu, Xiangyu, Liu, Xinyu, 2024. Effect of voltage gradients on EK-PRB remediation: Experimental and molecular dynamics simulations. Environmental Research 252, 119085. https://doi.org/10.1016/j.envres.2024.119085

Chapter 4 Investigation into Radionuclide Migration Through Cements Using Electrokinetic Remediation

Hemming, S. D., Burke, I.T., Burrell, F.M., Marsh, R.I., Warwick, P.E., & Cundy, A.B.

Prepared for submission as a paper to Journal of Hazardous Materials.

Author contributions:

Hemming, S. D. – experimental design, data collection and processing, interpretation, manuscript writing

Burke, I. T. – experimental design, data interpretation and manuscript editing

Burrell, F. M. – experimental design, data collection and processing, interpretation, manuscript editing

Marsh, R. I. – experimental design, data collection and processing

Warwick, P. E. – experimental design, data interpretation, manuscript editing

Cundy, A. B. - experimental design, data interpretation, manuscript editing

4.1 Introduction

Activities performed as part of the nuclear fuel cycle generate large volumes of radionuclide-contaminated concretes globally (IAEA, 2015; Min *et al.*, 2010). The extent of radionuclide contamination varies – for example, as of 2022, concrete and rubble made up 88 % of the UK's very low level waste inventory volume, 29 % of the low level waste volume, and a minority component of the intermediate level waste inventory (NDA, 2023). Further, with many nuclear facilities across the world either having reached, or are close to reaching, the end of either operation lifetimes (Han *et al.*, 2020), the volume of contaminated material will continue to increase over time.

Pathways and characterisation of radionuclide-contaminated concretes can vary depending on the context in which the concrete is used, but broadly fit into two categories (Lee et al., 2018). The first is cementitious material with radionuclides incorporated within mineral phases, known as activated concrete. This arises from neutron-bombardment of stable elements within bioshielding surrounding a nuclear reactor during operational use (Lee et al., 2018; Pantelias and Volmert, 2015), creating activation products including H-3, C-14, Ca-41, Co-60, Eu-152, and Eu-154 (Harms and Gilligan, 2010; IAEA, 1998). The quantities of activation products created depends on the initial concentrations of pre-cursor stable elements present in the concrete as well as the duration and intensity of neutron-bombardment (Lee et al., 2018). Generally, activities decrease exponentially with increasing depth from the surface but can penetrate up to > 1 m into the material (e.g. Kim et al., 2008; PGE, 1995). Radionuclide contamination can be extensive and long lasting due to the half-lives of some constituents (e.g. Trojan nuclear site (Oregon, USA) total bioshield activity of 3.57x10¹³ Bq at measurement date after 9 effective full power years and estimated activity of 1.22x10¹¹ Bq after 100 years of natural attenuation (PGE, 1995)). The second category of concrete contamination is via surface or nearsurface sorption of radionuclides in solution. Various scenarios can lead to such contamination, including leaks within nuclear fuel storage ponds, and spills onto concrete walls and floors (IAEA, 1998; Lee et al., 2018). Radionuclides and activities present will be context specific, dictated primarily by the source and pathway of contamination, but are more likely to contain major fission products (e.g. Sr-90, Cs-137) and actinides (e.g. U, Pu, Am) (Jackson et al., 2014; Lee et al., 2018). In these scenarios, the primary retention mechanisms are sorption onto cementitious minerals, particularly calcium silica hydrate (C-S-H) phases, and precipitation as hydroxides (Atkins and Glasser, 1992). One example of storage pond leakage is at the Hunterston-A site (Ayrshire, UK), where Magnox fuel cladding, which is prone to water corrosion

(Jackson *et al.*, 2014), degraded and released radionuclides into the pond (Denman, 2023). The primary contaminants to the concrete lining were Sr-90 and Cs-137, with Sr contained primarily on the surficial painted coating and Cs associated with aggregates in the near-surface of the concrete (Bower *et al.*, 2016; Denman, 2023). Depending on the activities and half-lives of radionuclides present, similar issues to activated concretes regarding the high dose rate over centuries and millennia may be seen.

Numerous decontamination methods exist for concretes, with factors including radionuclide(s) distribution profile and extent of cleaning required driving decisions on which technique is most suitable. Methods can be divided into physical and chemical decontamination approaches. The first category of physical decontamination approaches involves cleaning the top surface of the concrete through wiping, washing, or scrubbing with chemical surfactants (NEA, 1999). If this is deemed insufficient then surface removal techniques can be adopted, including drilling, scabbling (scraping the top layer away mechanically), and grit blasting. Whilst both categories can be effective at dealing with surface contamination, neither is capable of treating radionuclides deeper within the concrete, and a precise location for the contaminants is needed for treatment to be optimal. Further, more aggressive approaches such as drilling and scabbling may cause dust generation, potentially leading to health risks for workers if not carefully managed. Alternatively, chemical treatment can be performed by either circulating reagents through a material or by submerging ex situ sections into a tank and then agitating (NEA, 1999). This allows remobilisation of contamination present deeper within the concrete, dependant on porosity, and different combinations or stages of reagents can be used to leach multiple radionuclides simultaneously. However, aggressive chemicals such as concentrated acids or corrosive reagents raise additional hazards and may be restricted/ prohibited at nuclear sites, and milder chemicals may require longer treatment times to achieve the desired decontamination level. Further, the generation of contaminated liquids throughout treatment may result in a larger volume of waste material than that present in the starting volume of concrete, if not carefully managed. This waste may have to be carefully managed and disposed (or treated further) due to the potentially hazardous nature of the reagent(s), causing further issues with the approach. Emerging techniques such as strippable gels and coatings have been deployed previously, which were found to be effective but produced vast quantities of aqueous waste during post-decontamination rinsing (Mahrous et al., 2023). As such, development of new and additional emerging technologies should be encouraged to diversify the options available to site operators, leading to greater success in remediation projects.

4.1.1 Electrokinetic Remediation (EKR)

EKR is a sustainable and cost-effective alternative approach to conventional remediation (Purkis *et al.*, 2021). Direct current is applied to a contaminated material, resulting in migration of pollutants towards designated regions within the material (see Figure 4.1). Three primary transport mechanisms govern the process. Electromigration involves the movement of ions, with cations and anions migrating towards the cathode and anode, respectively. Electrophoresis is the transport of charged colloidal particles – typically 1–5000 nm in size (Lee, 2019) – through the material. Electroosmosis describes the movement of water molecules towards the cathode, driven by a double diffuse layer of cations and water around matrix particles. Cations are attracted to the negative surface charges of grains, creating a tightly bound inner layer and a more diffuse, mobile outer layer (Li and Wu, 2000). Under the influence of the applied electric field, the diffuse layer and its associated hydration shell migrate towards the cathode, dragging additional water molecules along through water tension, thus generating a net flow within the cell. Water molecules at either electrode will undergo electrolysis, producing hydronium ions at the anode and hydroxide ions at the cathode that create a pH gradient within the medium over time.

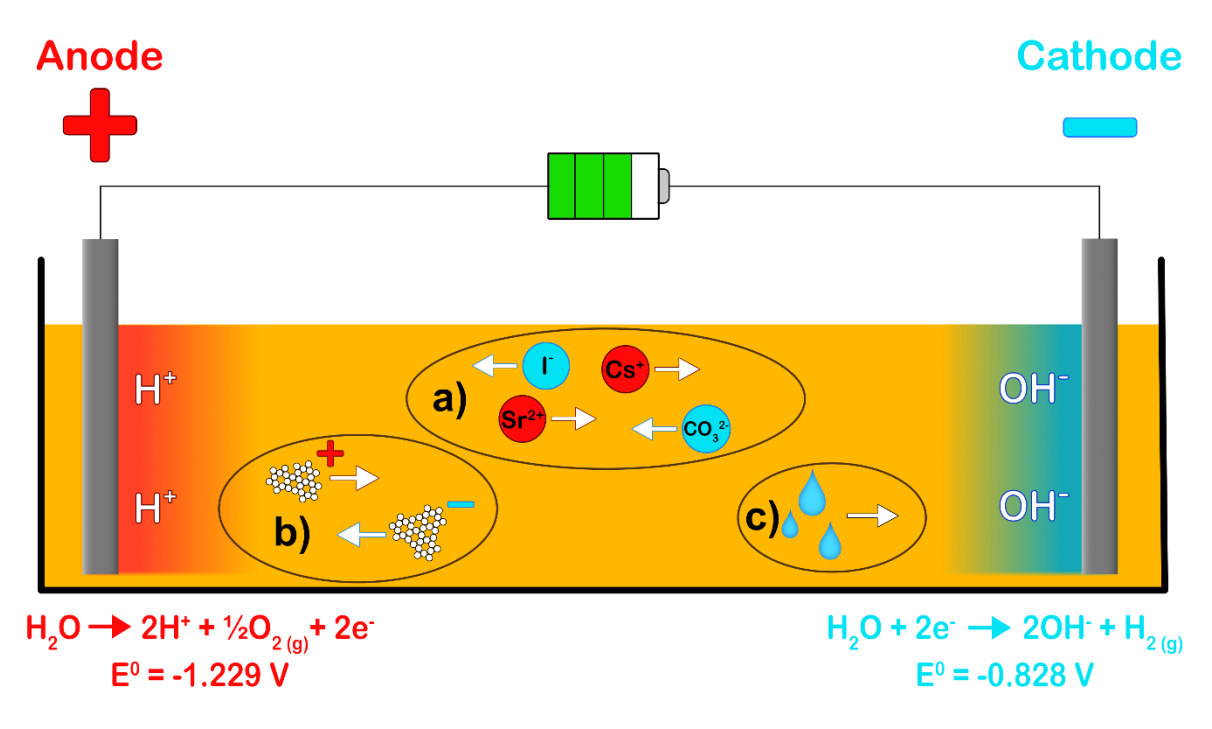


Figure 4.1 – Schematic of the fundamental EKR principles, showing a) electromigration, b) electrophoresis, and c) electroosmosis. Modified from Purkis *et al.* (2021).

EKR has been trialled on radionuclide-contaminated concrete several times, most commonly containing Co-60, Cs-137, and U (e.g. Acar et al., 1995; DePaoli et al., 1996; Frizon et al., 2005; Kim et al., 2010, 2009; Parker et al., 2017). Both Co-60 and Cs-137 emit high-energy gamma radiation during decay (IAEA, 2025), making them easy-to-measure radionuclides (ETMRs) when

performing *in situ* radiometric analysis. In comparison, much less EKR work has focussed on difficult-to-measure radionuclides (DTMRs), which emit pure alpha, pure beta, or low-energy gamma (the definition of low-energy is dependent on the sensitivity of individual gamma spectrometers, but has been previously defined by Hemming *et al.* (2023) as < 100 keV) during radioactive decay. DTMRs can be as abundant at nuclear sites as ETMRs (*e.g.* cumulative U-235 thermal fission yields of Sr-90 and Cs-137 being 5.7 % and 6.2 %, respectively (IAEA, 2025)) but their chronic underdevelopment compared to easier-to-measure counterparts such as Cs-137 and Co-60 (Kim *et al.*, 2018) must be addressed to achieve effective EKR treatment for multiple radionuclides simultaneously.

Here, EKR is trialled as a proof-of-concept for remediation of DTMRs H-3, Sr-90, I-129, and U-236 (the lattermost being used as an analogue for naturally occurring U-235 and DTMR U-238). Cs-137 was also included as it is an ETMR that has undergone successful EKR trials previously in concrete, adding comparability between this work and others. Sets of cores were created to represent concretes with either incorporated activation products or primarily sorbed surface contamination, to understand EKR efficacy in both contexts. Ordinary Portland cement (OPC) was chosen as the target media as it is a major constituent in OPC concretes, is the most common cement type used in radioactive waste cementation (Glasser and Atkins, 1994), and removes the requirement for aggregate addition to form concrete, which can add heterogeneity and variation to the resultant concrete through the addition of aggregate-specific mineral phases. Since the DTMRs of focus here are largely or wholly unreported in the electrokinetics literature, the system was kept as simple as possible in this proof-of-concept trial.

4.1.2 Radionuclides of Focus

4.1.2.1 H-3

H-3 (half-life of 12.32 years (IAEA, 2025)) is primarily created at nuclear sites through both ternary fission and Li-6(n, α)H-3 nuclear reactions in concrete bioshielding (Kim et al., 2008). The radionuclide primarily exists as tritiated water, either weakly sorbed onto or incorporated within hydrated cement mineral phases (Furuichi et al., 2006; Kim et al., 2008; Takata et al., 2005). H-3 can undergo isotopic exchange with stable H-1 nuclei, acting as a mechanism for both mobilisation and immobilisation (Eichholz, 1988; Takata et al., 2005).

H-3 is not susceptible to electromigration, as tritiated water does not have a charge, making electroosmosis the migratory process during EKR. DePaoli *et al.* (1996) published a report stating that EKR was unlikely to be able to completely decontaminate H-3 from concretes due to the extent of isotopic substitution that occurs with H-1 in water present within the cementitious phases. The only documented work with H-3 that could be found was by Wattez *et al.* (2013),

which had success with electrokinetic transportation through concrete, albeit with only 30 mm concrete thickness and with a high voltage gradient of 3.7 V/cm. However, this trial was focussed on radionuclide migration rates and so was not concerned about complete remediation of the concrete.

4.1.2.2 Sr-90

Sr-90 (half-life of 28.91 years (IAEA, 2025)) can be either a fission product or an activation product of stable Sr impurities in concrete (IAEA, 2025; Wieland *et al.*, 2008). Despite the chemical similarities between Sr-90 and Ca, a major constituent in cement, Sr has a more soluble nature in alkaline conditions makes precipitation as Sr(OH)₂ within concrete pores unlikely (Atkins and Glasser, 1992). Instead, coprecipitation, incorporation, and sorption onto and into cement hydrates as Sr(II) are expected to be the primarily immobilisation mechanisms.

No EKR experiments could be found that examined activated Sr, and only few investigating surface-contamination of radiostrontium. The most significant was performed by Popov *et al.* (2008) on an *in situ* section of concrete floor at Mound facility (Ohio, USA) containing multiple $\sim 1.2 \times 1.5 \, \text{m}$ "hot-spots" of Sr-90, amongst other radionuclides. After pre-treatment with sodium citrate and H_2O_2 , and 100 minutes of EKR with a citric acid electrolyte, 85 % of Sr-90 had been removed. However, complete remobilisation of Sr proved difficult as the radionuclide does not form citrate complexes, and an applied voltage of 110 V (which, although the exact value cannot be confirmed as electrode spacing was not quoted, is likely to form a voltage gradient greater than values of $\sim 0.5 \, \text{V/cm}$) is much greater than what may be considered acceptable for a sustainable approach.

4.1.2.3 I-129

I-129 is a fission product with a half-life of 1.57x10⁷ years (IAEA, 2025). Radioiodine retention in cements is highly dependent on the abundance of Al and Fe phases (AFm) present in the concrete, which are minority assemblages (2-8 wt%) within OPC (Alonso *et al.*, 2020; Atkins and Glasser, 1992). Weaker interactions with C-S-H and the mineral Ettringite can also result in I-129 immobilisation. Within concretes, the radionuclide is expected to exist solely as I⁻ in the alkaline, reducing conditions found in porewaters (Berner, 1992; Ma *et al.*, 2018; Takeno, 2005).

No previous EKR trials for I-129 could be found, despite concerns raised about its poor sorption in contexts such as retention within geological disposal facilities (Asmussen *et al.*, 2022; Liu and Gunten, 1988). This is an important knowledge gap when considering the high degree of retention expected in concretes with high Al and Fe content.

4.1.2.4 Cs-137

Cs-137 (half-life of 30.08 years (IAEA, 2025)) is a fission product created inside a nuclear reactor. In almost all aqueous conditions, Cs is expected to exist as a monovalent cation (Takeno, 2005). The primary mechanisms for retention in concretes are sorption to clay minerals and cement binders, giving the possibility of more heterogeneous distributions compared to other radionuclides discussed, depending on the clay content of the aggregate used (Bower et al., 2016; Nikolaev et al., 2012). As such, the extent of Cs adsorption in OPC is likely lower due to the lack phyllosilicates available.

Stable Cs has been used multiple times in previous EKR work on concrete (Castellote *et al.*, 2002; Kim *et al.*, 2009; Popov *et al.*, 2006) but few examples exist for treatment of radiocaesium, and even less for scaled-up trials. Kim *et al.* (2010) performed EKR on 20-year-old crushed concrete, achieving removal efficiencies of ~ 80 % after washing with 3 M H₂SO₄ and treating for 20 days in a 0.01 M HNO₃ electrolyte. This was sufficient enough for the Korea National Institute of Nuclear Safety to deem the material below the 100 Bq/kg 'safe' threshold. However, a high 4 V/cm voltage gradient and pre-washing with acid does not necessarily reflect the conditions present for *in situ* deployments, raising the question of how EKR would perform in more alkaline conditions or pre-washes.

4.1.2.5 Uranium

U-234, U-235, and U-238 (half-lives of 2.46x10⁵ years, 7.04x10⁸ years, and 4.47x10⁹ years, respectively (IAEA, 2025)) are naturally present in concretes due to their (low) abundance in the Earth's crust (IAEA, 1998). Each of these isotopes can absorb neutrons, but only U-235 produces a long-lived product as a result (U-236; half-life of 2.34x10⁷ years) (IAEA, 2025), resulting in three potential isotopes present in reactor bioshielding. The use of U fuel in reactors has also given rise to contamination in storage ponds, where corrosion of containment has occurred e.g. Magnox storage ponds at Sellafield (Cumbria, UK) (Jackson *et al.*, 2014). Speciation in cements is dependent on the conditions present, with fresh cement creating reducing conditions that generate U(IV) uraninite (UO₂), and aged cement producing more oxidising conditions in which U(VI) minerals can form, such as uranophane (CaO·2UO₃·SiO₂·6H₂O), and calcium uranium oxide hydrates (Ca₂UO₅·xH₂O) (Berner, 1992).

Limited EKR pilot trials have been performed, with most remediating crushed concrete (DePaoli et al., 1996; Yurchenko et al., 2009). However, Popov et al. (2008) reported on the in situ treatment of concrete flooring containing several $\sim 1.2 \times 1.5 \text{ m}$ "hot-spots" of contamination at Mound facility (Ohio, USA). Pre-treatment of sodium citrate and H_2O_2 was performed before 500 minutes of treatment with a citric acid electrolyte, which extracted 100 % of U within the time

interval between 100 minutes and 300 minutes of EKR. However, the use of oxidising agents (H_2O_2) and strong acids (citric acid pH of ~ 1.5) create risks that could make EKR in these conditions less appealing so site operators, and alternative, less hazardous approaches should be investigated to ensure the optimal approach can be deployed.

Radionuclide	Half-life (years)	Primary decay modes ^[a]	DTMR? (defined by < 0.1 % probability of a > 100 keV gamma emission during decay)	Activity used in core contamination solution (per core, Bq)
H-3	12.32	β-	Yes	5600
Sr-90	28.91	β-	Yes	570
I-129	1.57x10 ⁷	β-	Yes	1900
Cs-137	30.08	β-, γ	No	570
U-236	2.3x10 ⁷	α	Yes	9.4

Table 4.1 – Summary of the properties for radionuclide of focus, as well as the activities used to contaminate each core used in this study. [a] – IAEA (2025).

4.2 Methods

4.2.1 Core Descriptions

Each cement core was contaminated with 5.6 kBq of H-3, 570 Bq of Sr-90, 1.9 kBq of I-129, 570 Bq of Cs-137, and 9.4 Bq of U-236 (Table 4.1). These values were chosen to allow a minimum of one percent total activity to still be measurable in cement sub-samples when analysed. Cores were contaminated in one of two ways to create either a uniform distribution of radionuclides throughout the cores (which represents bioshielding), hereafter referred to as the Homogeneous Set, or surface and near-surface contamination (which represents storage pond contamination), referred to hereafter as the Soaking Set. The Homogeneous and Soaking sets contained four cement cores each, all $11 \times 6 \text{ cm}$ (D x H) (Figure 4.2). Both sets had a Control core, which were made and contaminated with radionuclides without being exposed to an electrolyte, to understand the initial distribution of radionuclides in the cement. Diffusion cores were contaminated and placed in electrolyte for 41 days to understand the diffusive mobility of the radionuclides. The final cores underwent electrokinetic treatment for the same 41-day duration; the current polarity was set up such that the Cathode cores had the central graphite electrode acting as the cathode, and *vice versa* for the Anode cores.

4.2.1.1 Reagents

All acids, ammonia, NaI, NaOH, and NaSO₄ were purchased from Thermo Fisher Scientific (Pennsylvania, USA); SrCl₂·6H₂O from Merck Group (Darmstadt, Germany); ammonium oxalate from Sigma-Aldrich (Missouri, USA); 1x8 100-200 mesh anion exchange resin (Cl form), UTEVA, and Sr resins from TrisKem (Brittany, France); H-3, Sr-85, Sr-90 and I-129 from Physikalisch-Technische Bundesanstalt (Braunschweig, Germany); Cs-137, U-232 and -236 from AEA Technology (now Ricardo-AEA; Oxfordshire, UK); Gold Star scintillation cocktail from HIDEX (Turku, Finland); general purpose cement powder from Blue Circle (London, UK); graphite electrodes from Marvellous (Taiyuan, China); 304 stainless steel mesh from F. H. Brundle (Rainham, UK). All chemical reagents were analytical grade or higher.

4.2.2 Core Creation and Contamination

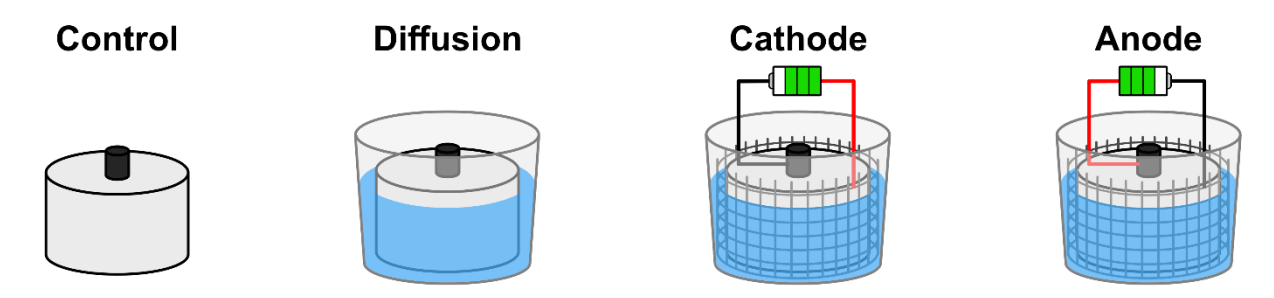


Figure 4.2 – Schematic showing the naming system for each of the cores created per set. Both Homogeneous and Soaking sets contained a Control (cast and contaminated, then placed in a freezer), Diffusion (contaminated and kept in electrolyte without an electrical current), Cathode (contaminated, placed in electrolyte and underwent EKR; central graphite electrode is the cathode) and Anode (contaminated, placed in electrolyte and underwent EKR; central graphite electrode is the anode).

Eight high-density polyethylene bottles (11 cm diameter) were cut in half and their bases partially filled with epoxy resin to prevent electrolyte and radionuclide flow through the bottom of the cores during treatment. A graphite rod was placed in the centre of each of these molds as the resin solidified, creating free standing electrodes. Once the resin had set, a quarter of each core's allocated Ordinary Portland Cement (OPC; \sim 200 g), Milli Q water (MQ; \sim 70 g) and either the solution containing the desired radionuclides (Homogeneous Set only) or further Milli Q (Soaking Set only) (20 g for each) were added to the molds and mixed. The next quarter-portion of material (\sim 200 g OPC; \sim 70 g MQ; 20 g of either radionuclide solution or additional MQ) was then added, and so on until all constituents had been added in full to the mold (final liquid : OPC ratio = 3: 7 = 0.43). Cores had clingfilm loosely placed over the top of the molds and were left to cure for 28 days.

Contamination of the cured Soaking Set cores (the set that had not had radionuclides added to them during casting) was done by leaving them for 42 days in a separate 'bath' containing the

radionuclides of interest dissolved in 0.1 M NaOH. Alkaline conditions were chosen to recreate the pH found in pond waters (Parker *et al.*, 2017), with the submersion period selected to balance sufficient diffusion of radionuclides with minimising the timeframe require for the experiments. All cement cores were then removed before starting EKR (where appliable).

The diffusion cores from both sets were submerged in a 0.1 M NaOH electrolyte for 41 days. Similarly to the Soaking Set contamination solution, these conditions were chosen to recreate pond water pH and enable radionuclide diffusion whilst reducing the experimental duration.

4.2.3 Electrokinetic Treatment

Per core, one electrode was the graphite rod located in the centre of the cement and the other was a stainless-steel mesh that was bent around the core (Figure 4.3). This setup promoted radial migration of radionuclides throughout the core rather than a linear pathway created by using two graphite rods. A voltage of 3.2 V (0.5 V/cm voltage gradient) was applied to test EKR efficacy whilst minimising power consumption and cement heating. Cores were treated in 0.1 M NaOH for 41 days before analysis.

Electrolyte pH measurements before and after treatment were recorded with a HANNA HI98301 probe (uncertainty +/- 0.2), whilst weekly measurements were performed with indicator paper (uncertainty +/- 0.5) to avoid excessive radioactive contamination of the pH probe. The HANNA probe could record a maximum pH of 14, whilst the indicator paper only measured up to 11.

 $A \sim 5 \times 5$ cm piece of steel mesh used for the surrounding electrode was kept in a beaker filled with electrolyte for 41 days to act as a control for any electrode degradation that occurred during EKR.

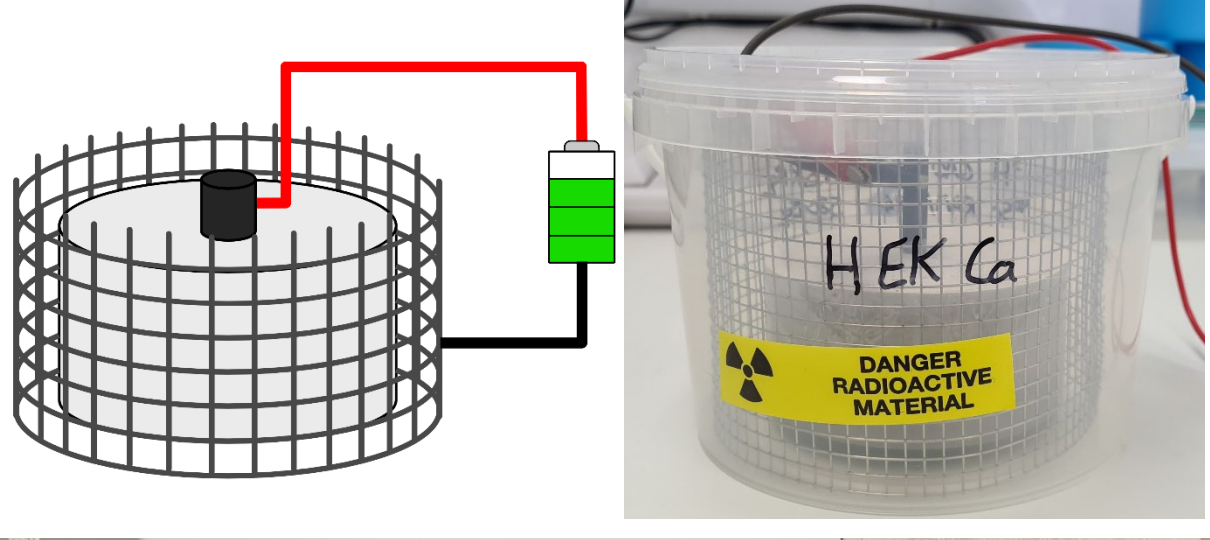




Figure 4.3 – Top left: schematic of electrokinetic remediation setup. One electrode was present as a graphite bar in the cement of the cement, whilst the other was a steel mesh surrounding core. Top right: side-on view on the Homogeneous Set Cathode core prior to EKR. Bottom: top-down view of the four Homogeneous Set cores.

4.2.4 Core Sampling

The cores were sub-sampled as shown in Figure 4.4. Each core was removed from the freezer and had its top and bottom removed to exclude radionuclide 'edge-effects' in the material caused by intermittent submersion in electrolyte due to evaporation and cement-resin interactions. This left a 3.5-cm-thick cylinder that had two vertical 'tram lines' cut, one either side of the electrode, with a 1-cm spacing between them. The remaining slice was sub-sampled into 6 sections. Core sections 1-5 (each $1 \times 1 \times 3.5 \text{ cm}$, 1×1

assumed that radial migration of radionuclides occurred and, thus, the distribution in core section 6 will be a mirror image of that in sections 1-5.

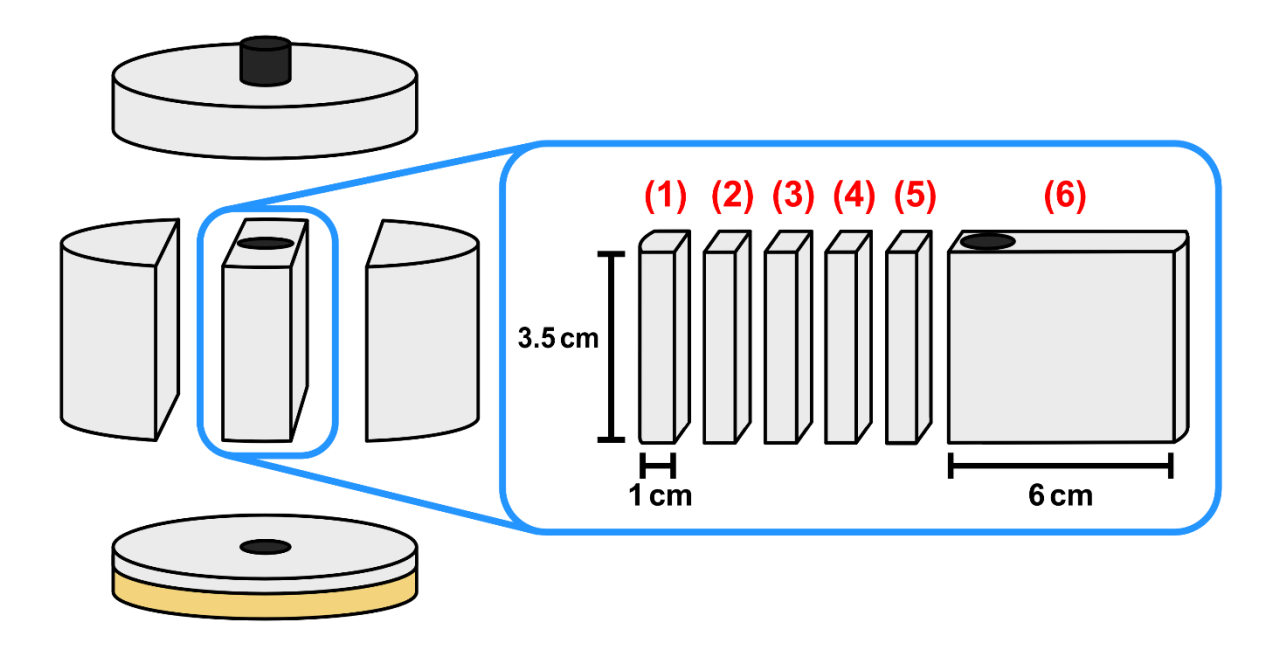


Figure 4.4 – Top: schematic showing how the core was subsampled for analysis. Core sections 1-5 were used for quantified activity measurements whilst core section 6 was used for autoradiography.

4.3 Analysis

4.3.1 Autoradiography

The 6×3.5 cm (L \times W) cement slices (see Figure 4.4) taken from each core were imaged via autoradiography at the British Geological Survey (Keyworth, UK), where samples were measured on a tritium plate for one week to optimise the detection of the DTMRs.

4.3.2 Radionuclide Analysis

Individual cement sections were removed from the freezer and ground into a powder using an agate mortar and pestle, before subsamples were taken for radionuclide analysis. Samples were not made in replicate and so all uncertainties presented here are analytical and counting uncertainties.

4.3.2.1 H-3 and I-129

For cement samples, the method performed by Kim *et al.* (2008) for H-3 analysis was followed. Radionuclides were volatilised using a RADDEC Pyrolyser-6 Trio™ with a 5.5-hour programme ramping the sample zone from 50 °C to 900 °C and maintaining the catalyst zone at 800 °C. Air was chosen as the flow-through gas, with H-3 and I-129 captured in 20 mL of 6 mmol Na₂CO₃

solution. A portion of this solution was used for direct counting of I-129, while the remainder underwent distillation to separate tritiated water, which was also counted. For electrolyte and soaking solution samples, TrisKem Cl-Resin™ loaded with AgNO₃ was used to extract both I-129 and stable iodine used as a tracer from the acidified samples (pH 5–6), followed by washing and elution with 0.35 M Na₂S. Stable iodine was analysed via ion chromatography, and remaining eluent was mixed with scintillation cocktail for I-129 quantification in a Wallac 1220 Quantulus™ Ultra Low-Level Liquid Scintillation Counter (2-hour count times). Tritium peak analysis was performed using LSC+ software (Raddec; Romsey, UK) and I-129 peak analysis with WinQ software (LKB-Wallac, Australian Capital territory, Australia).

4.3.2.2 Sr-90, Cs-137, and U-236

The analysis method for Sr-90 is based off work by Hateley (2021), and U-236 method from by Hateley (2021) (sample digestion and iron hydroxide precipitation) and Croudace et al. (2006) (separation columns), but described here with any minor deviations included. Whilst Cs-137 does not necessarily require preparation for gamma spectrometry, analysis was performed on aqueous solutions to ensure all samples had more consistent and better calibrated geometries in the instrument compared to solid cement blocks (Cao et al., 2022). For sequential analysis of U-232, Cs-137, and Sr-90, cement samples were spiked with U-232 and Sr-85, digested twice with aqua regia (30 g per digestion) on a hotplate, and centrifuged, with supernatants combined and evaporated to ~ 20 g. To ensure acid digestion was sufficient for total Sr extraction, one batch of samples had their filtered cement residues collected and fusion digested, involving ignition at 450 °C, fusion with lithium metaborate, quenching in water, and dissolution in 8 M HNO_3 , as described by Hateley (2021). The resultant solutions were combined with the original aqua regia digests, and all samples were analysed for Cs-137 using well-type HPGe gamma spectrometers (3-hour count times for samples above limit of detection (LOD), 12-hour times for samples close to, or below, LOD) and analysed with Fitzpeaks software (JF Computing, Stanton in the Vale, UK).

4.3.2.3 Sr-90 and U-236 (Continued)

After Cs-137 counting, the digests were acidified to pH < 4 with HNO_3 , and stable $SrCl_2 \cdot 6H_2O$ and $FeCl_3$ were added as carriers. Bromocresol green was used as an indicator, and ammonia was added to adjust the pH > 4, forming Fe and actinide precipitates. The cooled precipitates were centrifuged, separating Sr (in the supernatant) from U (in the precipitate).

4.3.2.3.1 Sr-90 Purification

For cement samples, Sr supernatant was evaporated to dryness, redissolved in HNO₃ and HCl, and diluted with Milli Q water. Ammonium oxalate and bromocresol green were added, followed by ammonia to adjust the pH (4–5), forming a precipitate that was coagulated, filtered, and ignited overnight at 450 °C. The residue was dissolved in HNO₃ and loaded onto a TrisKem Sr Resin™ column, with Sr eluted using Milli Q water and Y-90 separation times recorded for decay correction. Sr recovery was determined using Sr-85 gamma spectrometry using a HIDEX AMG gamma spectrometer (2-hour sample count times), and Sr-90 activity was measured via Cerenkov counting on a Wallac 1220 Quantulus™ Ultra Low Level Liquid Scintillation Counter (1.5-hour sample count times) and analysed with WinQ software. For electrolyte and soaking solutions, a similar procedure was followed, involving a repetition of the acid additions and evaporation stages before filtration, column separation, and activity measurement as described for cement samples.

4.3.2.3.2 U-236 Purification and Electrodeposition

The U-containing residues were dissolved in concentrated HNO₃ and diluted with 8 M HNO₃ before being loaded onto an anion exchange column, followed by a UTEVA column. After washing with 8 M HNO₃, the anion columns were removed, and the UTEVA columns were loaded with 6 M HCl before eluting U using 0.02 M HNO₃. The eluents had Na₂SO₄ added and were then evaporated, dissolved in HCl, and combined with ammonium oxalate. The mixtures underwent electrodeposition onto stainless steel discs, which were then counted through alpha spectrometry in EG&G ORTEC Octete PC alpha spectrometers (150,000-second count time) and analysed with MAESTRO software.

4.4 Results

4.4.1 Soaking Set Contamination

After the 42-day contamination period, prior to EKR treatment, samples of the radionuclide bath solutions were analysed to determine the change in activities in the solutions and, assuming that what was no longer present in the solution was therefore in the cement cores, the cementitious uptake. The transfer extent to each core is presented in Table 4.2. In summary, H 3 and Sr-90 showed low affinities for cement (28 % average uptake each), Cs-137 had very low uptakes (5 % average), and I-129 and U-236 were well retained in the cement (73 % and 100 % average uptake, respectively). These transfer rates were calculated based on the assumption

that no volatilisation or precipitation of radionuclides occurred, which may not be true for all tested radionuclides, as H-3 and I-129 are known to be volatile chemical elements.

Radionuclide	Uptake into cement core (%)							
	Control	Diffusion	Cathode	Anode	Average			
H-3	30 ± 2	30 ± 2	26 ± 2	26 ± 2	28 ± 5			
Sr-90	26 ± 8	30 ± 8	32 ± 8	24 ± 9	28 ± 17			
I-129	73 ± 2	72 ± 2	70 ± 2	75 ± 2	73 ± 3			
Cs-137	5 ± 3	4 ± 2	3 ± 3	8 ± 2	5 ± 7			
U-236	100 ± 1	100 ± 1	100 ± 1	100 ± 1	100 ± 3			

Table 4.2 – Radionuclide uptakes for the Soaking Set cement cores. All radiometric measurements were single replicates, with analytical uncertainties shown. Sr-90 uncertainties are larger than other radionuclides to account for a greater variance in instrument quality control data reproducibility.

4.4.2 Visual Observations

On day six of Homogeneous Set treatment, a white precipitate was observed in the electrolytes of both electrokinetic cores and remained for the six-week experiment duration. Gross alpha beta counting showed the precipitate contained negligible activity levels.

Both cathode cores formed (broadly) concentric orange rings, 3-5 mm thickness, on the top cement surface within 3 weeks of treatment. When the top ~ 1.5 cm of each core was removed during sectioning no oranges rings were seen, suggesting the rings are a surface or near-surface feature only. This was likely caused by electromigration of dissolved Fe(II) in reducing conditions towards the cathode (Furcas *et al.*, 2022), which was subsequently exposed to more oxidising conditions closer to the surface and precipitated as orange-brown Fe(III) (Takeno, 2005). This does however support the assumption of radial migration within the cement cores (section 4.2.4).

When the central electrode served as the anode, graphite corrosion into a black sludge was observed. This was first noticed after approximately four weeks of treatment for the Homogeneous core and approximately 1 week for the Soaking core.

After 41 days submerged in the electrolyte, the piece of steel mesh used as a control for electrolyte degradation of the electrode showed no visible signs of degradation.

4.4.3 Current and pH

Electrical current variations in the EKR cells are shown in Figure B.1. After fluctuations in the first 24 hours, both Cathode cores stabilised at ~ 15 mA, and both Anode cores stabilised at ~ 8 mA. The Homogeneous Set cells maintained these values for the experimental duration but both Soaking Set cements showed a gradual reduction in current, with the Soaking Set Cathode recording a final sixth week reading of 9 mA and the Anode cell measuring 1 mA.

Cell pHs are shown in Figure B.2. The Diffusion cores for both sets, along with the Anode core for the Homogeneous Set, showed similar pH behaviours of ~ 12.5 initially and 11+ in the following five weekly indicator paper tests, with final Diffusion core measurements on the sixth week of ~ 12.5 and the Homogeneous Anode core of 11.8. The Homogeneous Set Cathode cement had an initial pH of 12.6 and remained at 11+ for four weeks, before measuring 10-11 on the fifth week and 10.5 on the sixth week. Similarly, the Soaking Set Cathode core also had an initial 12.3 reading, followed by 11+ for the first and second weekly tests, 10-11 in the third and fourth, 10 in the fifth, and 10.1 at the experiment end. Finally, the Anodic counterpart cell started at 12.2 and maintained 11+ measurements for three weeks before decreasing to 10-11 for the remaining indicator paper tests and finishing at 10.3. Across both Sets, the decrease in pH is expected in the Cathode cores, since the anode (mesh electrode) would be generating hydronium ions through electrolysis which would partially neutralise the alkaline solution. However, in the Diffusion and Anode cements, this neutralisation would not occur.

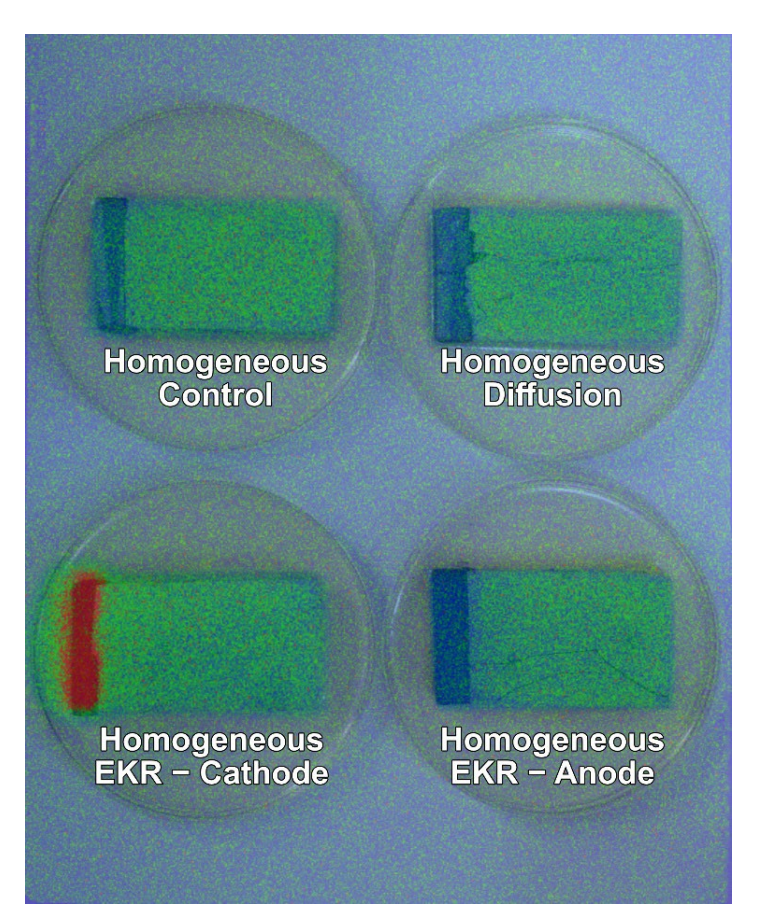
4.4.4 Autoradiography

Figure 4.5 shows autoradiography data of the cement section 6s overlain onto photos of their respective slices. Each core section has been orientated so the graphite electrode (centre of the core) is on the left-hand side and the edge (outside of the core) is on the right-hand side. Both the Homogeneous Set Control and Diffusion cores show an even distribution of activity throughout. The Homogeneous Set Cathode core has a horizontal activity gradient across the slice, with a relatively large presence of radionuclides in/on and surrounding the graphite electrode and a depleted zone near the outer edge of the cement. Green halo-ing is present around the electrode but is likely an artifact of shine from high-activity areas (red). The Homogeneous Set Anode core has a zone of depletion at the electrode but no area of enrichment.

All cores in the Soaking Set show high activities at, and proximal to, the outermost edge of the slice. Further into the samples, both the Control and Diffusion cores show a homogeneous distribution. The Cathode core has a minor increase in activity on, and immediately adjacent to,

the electrode, whereas the Anode core displays a minor radionuclide depletion in this area.

Both EKR core sections have low activities towards the middle of the slice.



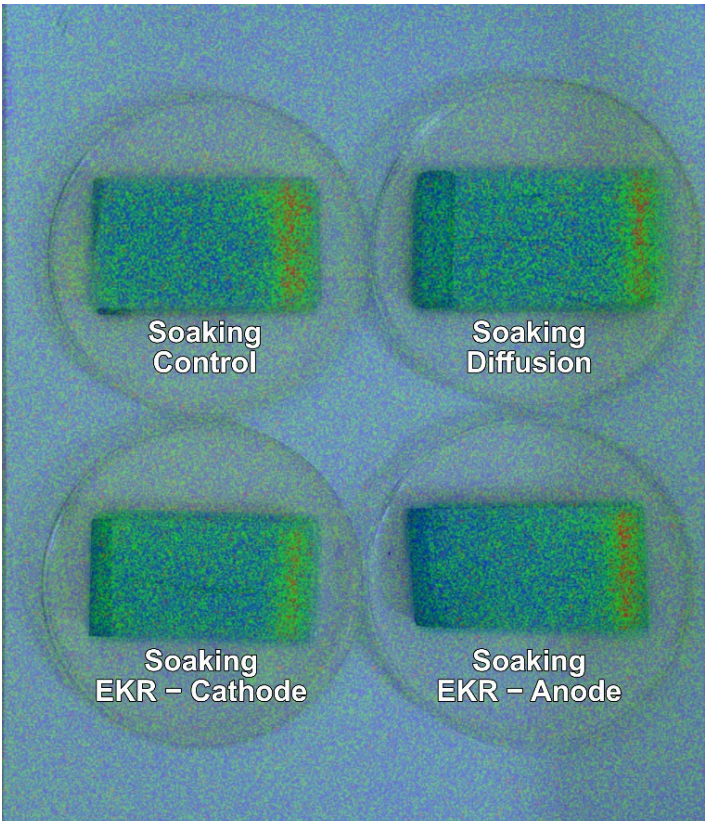


Figure 4.5 – Autoradiography for the Homogeneous Set (top) and Soaking Set (bottom) cores, after one week exposure to a tritium plate. Colour scale has minimum activity detected in blue and highest activity detected in red.

4.4.5 Discrete Radionuclide Analysis

4.4.5.1 H-3

The Homogeneous Set control core had an average H-3 activity 3.18 Bq/g, with all three measured cement sections within uncertainty of the mean (Figure 4.6). The diffusion core and both EKR cells showed the same trend of H-3 depletion in the core section containing the cement outer surface (core section 1) but no statistically significant change in radionuclide activity further into the core.

Radionuclide uptake into the Soaking Set cement averaged at 28 %. The control core showed a gradual decrease in H-3 activity from core section 1 (outermost section; 1.13 Bq/g) to section 5 (innermost; 0.27 Bq/g), with an overall average of 0.59 Bq/g (Figure 4.6). Similarly to the Homogeneous equivalents, diffusion and EKR cores showed the same trend of being within uncertainty of initial conditions in core sections 3 and 5 and with an activity decrease in core section 1. However, both treated cements had depletion in cement section 2, whereas the diffusion core did not.

4.4.5.2 Sr-90

Initial conditions in the Homogeneous Set control had core sections 1, 3, and 5 within uncertainty of the 0.39 Bq/g core average (Figure 4.6). This trend was mimicked by the other three cores. The diffusion electrolyte had detectable activities which, due to rounding, was determined as 0.00 Bq/g, with both treated cores at less than LOD of 0.00 Bq/g (Table B.1).

The Soaking Set had a collective average Sr-90 uptake of 28 % (Figure 4.6). The control core had 0.21 Bq/g present within cement section 1, but all other analysed core sections were found to have activities below LOD (0.02 Bq/g). The three cores exposed to electrolyte showed a similar trend, albeit with reduced core section 1 activities of 1.25-1.58 Bq/g. Only the diffusion electrolyte had Sr-90 above LOD (0.00 Bq/g), determined as 0.01 Bq/g (Table B.1).

Cement section 5 samples underwent acid digestion (as all cement samples did) followed by the fusion digest of filter paper residues, with both fractions recombined into a single sample for iron hydroxide precipitation. The Homogeneous Set samples showed no discernible activity increases compared to core section 3s (and, in fact, showed a slight decrease), supporting work by Hateley (2021) that double *aqua regia* digestion is sufficient for complete extraction of Sr-90.

4.4.5.3 I-129

All cores within the Homogeneous Set showed the same distribution of \sim 1.50 Bq/g of I-129 in cement sections 3 and 5 (Figure 4.6). The same was true for core section 1 in the control and

EKR cathode cements, although the diffusion and anode core sections had reduced activities to ~ 1.35 Bq/g. The diffusive and anode electrolytes also had similar, greater I-129 contents (0.01 Bq/g) compared to the cathode liquid, which, as a result of rounding, was reported as 0.00 Bq/g (Table B.1).

Average uptake into the Soaking Set cement was high, at 73 %. Starting activities comprised of $3.10 \, \text{Bq/g}$ in core section 1 and $\sim 0.05 \, \text{Bq/g}$ further into the core. The outermost core sections for the diffusion, cathode and anode cements showed a depletion to 2.73, 2.09, and $2.46 \, \text{Bq/g}$, respectively, yet cement sections $2-5 \, \text{did}$ not show any I-129 enrichment. Respective electrolyte values for these were 0.24, 0.04, and $0.07 \, \text{Bg/g}$ (Table B.1).

4.4.5.4 Cs-137

The Homogeneous Set contained consistent activities of ~ 0.45 Bq/g in all core sections (Figure 4.6). All but cement section 3 of the diffusion slice were within uncertainty of the control, which had an activity of 0.36 Bq/g. The cathode core having depletions within the outer sections (sections 1, 2, and 3 reduced to 0.17, 0.31, and 0.38 Bq/g, respectively) and enrichment close to the electrode (core section 5 increased to 0.91 Bq/g). Analysis of the electrode showed a portion of Cs-137 was present on or within the graphite, although, due to geometry calibration issues, quantification could not be performed. The Anode slice showed depletions in cement sections 1 and 5 (reduced to 0.29 and 0.12 Bq/g, respectively) but had no statistically significant migration from the middle sections. The diffusion and anode electrolytes had similar activities (0.21 and 0.19 Bq/g, respectively) whereas the cathode had lower values of 0.04 Bq/g (Table B.1).

Cs-137 had poor uptake in the Soaking Set cores, with an average of 5 % being retained. Only cement section 1 contained activities above the LOD (~ 0.02 Bq/g), measured at 0.07 Bq/g. Most values in the other cores were also below LOD, with only all core section 1s (diffusion, cathode, and anode at 0.02, 0.02, and 0.01 Bq/g, respectively), core section 5 for the cathode (0.03 Bq/g) and core section 2 for the anode (0.02 Bq/g) giving definitive values.

4.4.5.5 U-236

All four cores within the Homogeneous Set showed the same trend of 0.007 Bq/g present in cement sections 3 and 5, with the cathode core also being within uncertainty of the initial conditions in cement section 1 (0.008 Bq/g) but diffusion and anode slices having slight decreases (both 0.007 Bq/g) (Figure 4.6). Only the cathode electrolyte contained U-236 levels above the LOD, but due to rounding this was reported as 0.000 Bq/g (Table B.1).

U-236 uptake into the Soaking Set cores was high in all cores, averaging at 100 %. This was retained exclusively within cement section 1 of the control core, recording a value of 0.024 Bq/g,

whilst the other measured sections were determined as 0.000 Bq/g. Absence of the radionuclide in core sections 2-5 was also seen in the other Soaking Set, although cement section 1 values varied (diffusion, cathode, and anode, activities of 0.015, 0.016, and 0.006 Bq/g, respectively). Electrolytes were measured as 0.001, 0.002, and 0.001 Bq/g, respectively (Table B.1).

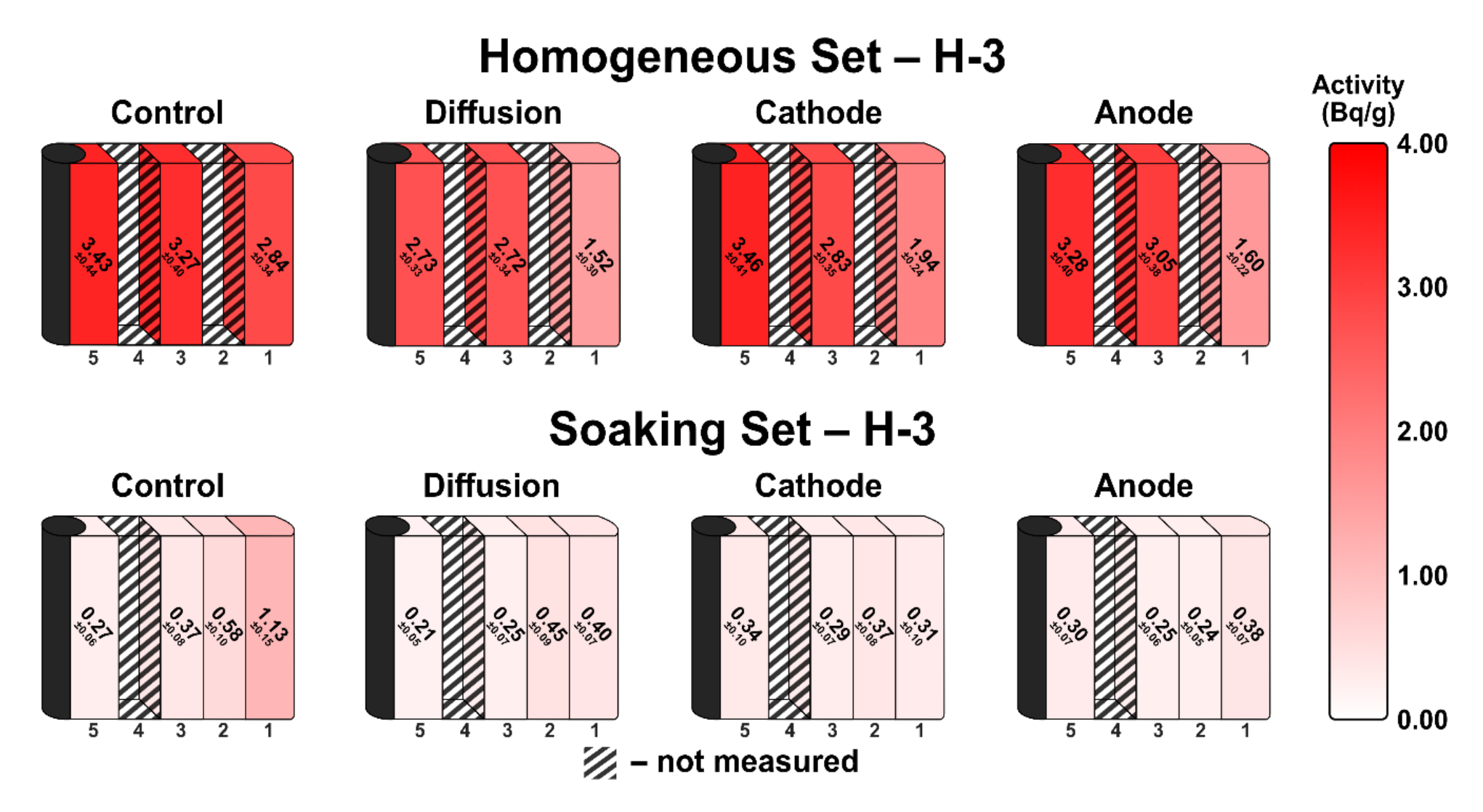


Figure 4.6 – activity concentrations present in each cement core section. Control cores describe the initial conditions, diffusion cores show passive radionuclide transportation, cathode cores display EKR treatment when the centre graphite electrode acted as the cathode, and anode cores show EKR treatment with the graphite being the anode. Cement section numbers are shown below each slice, with 1 being the outer core surface and 5 adjacent to the central graphite electrode. Uncertainties are quoted to 2σ. All radiometric measurements were single replicates, with error bars showing analytical uncertainties.

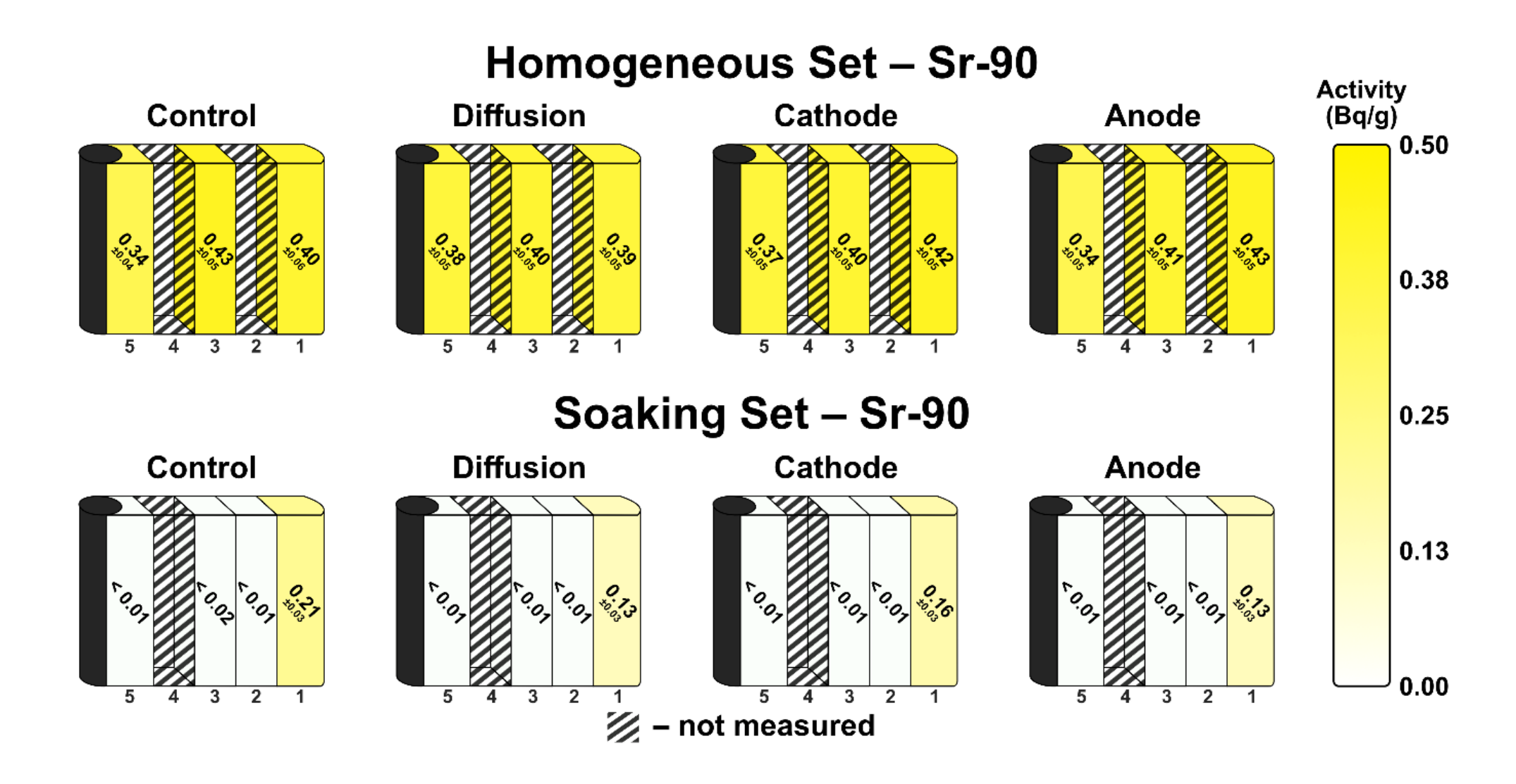


Figure 4.6 (Continued – Sr-90)

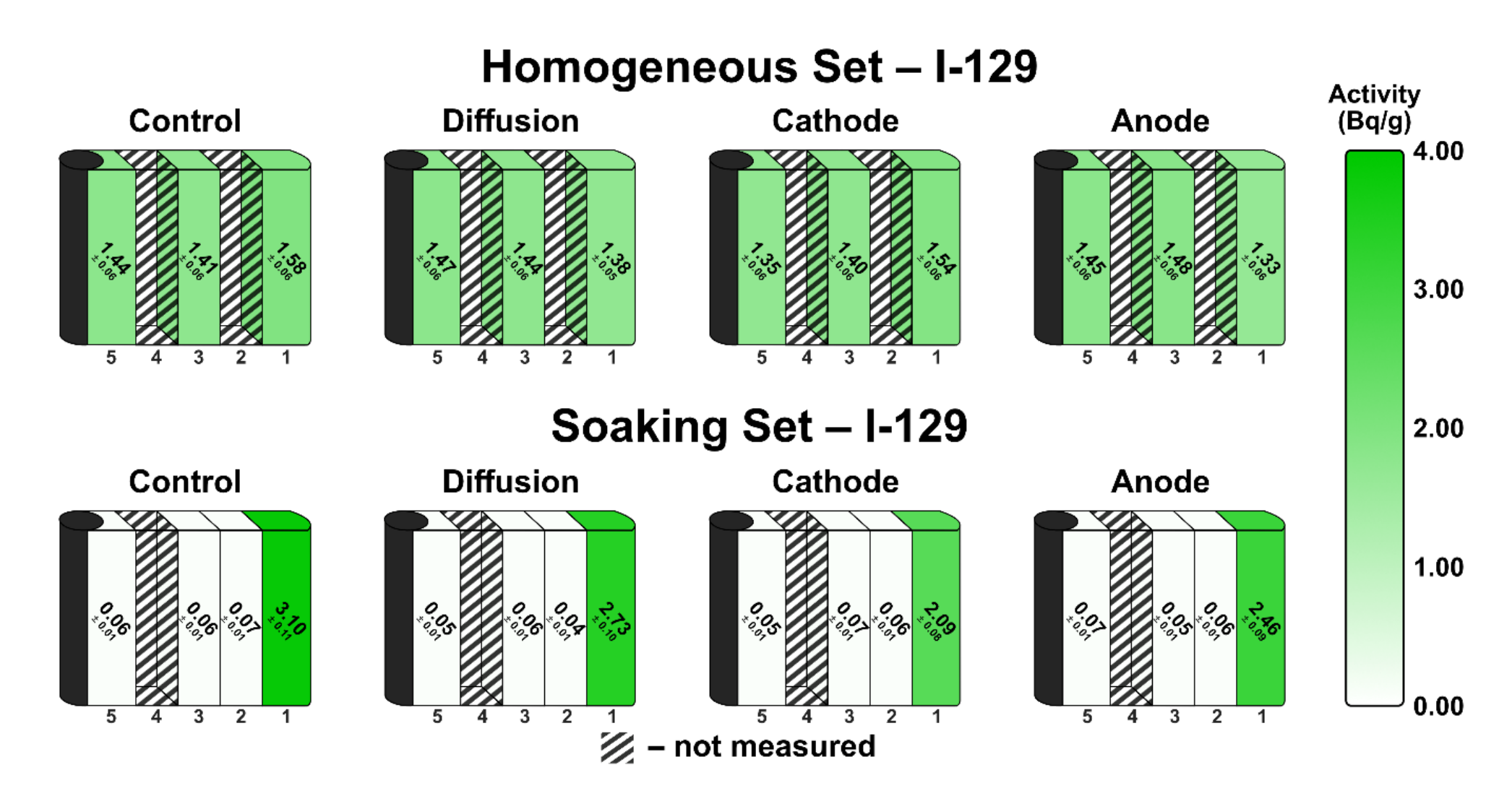


Figure 4.6 (Continued – I-129)

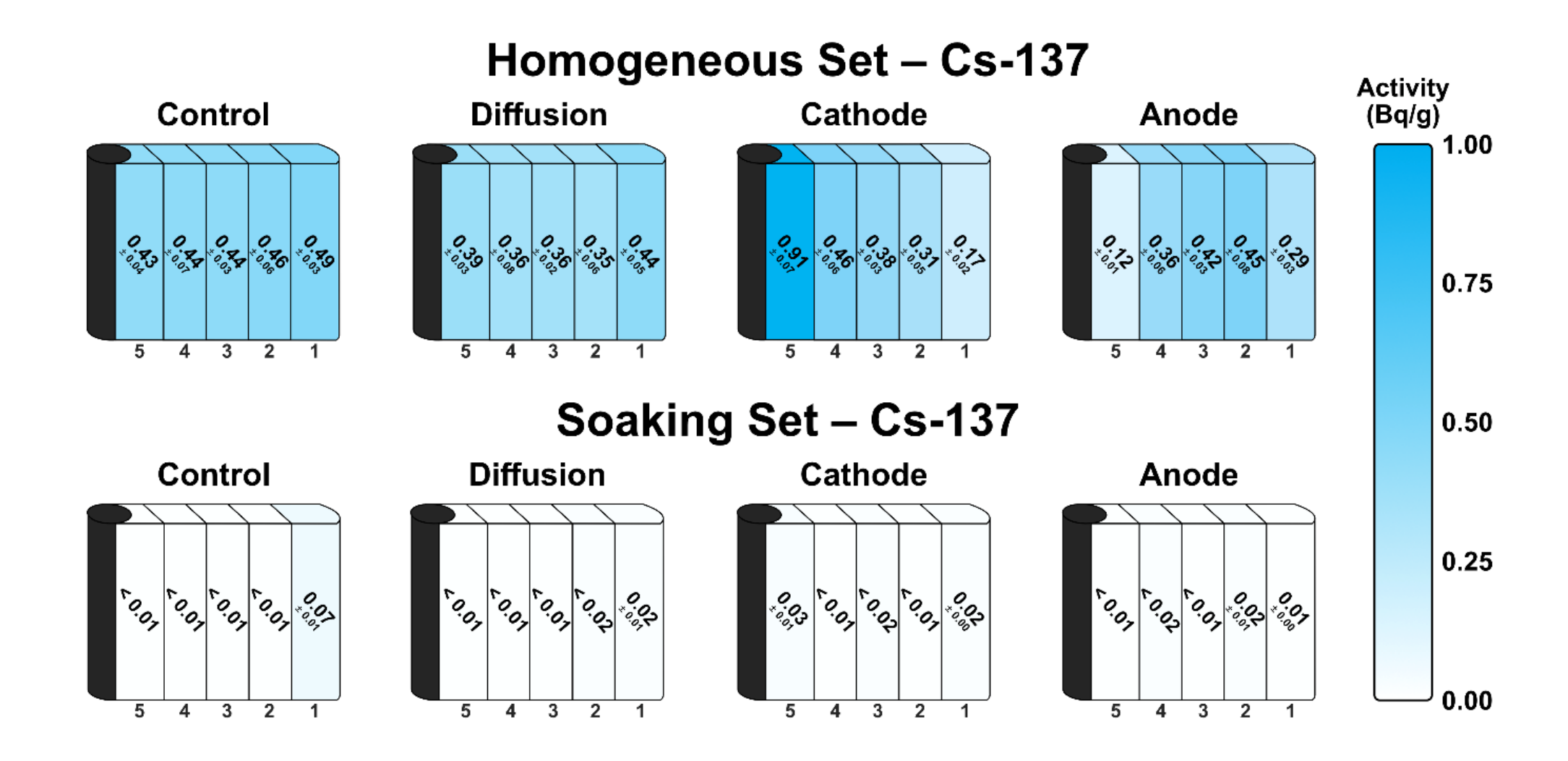


Figure 4.6 (Continued – Cs-137)

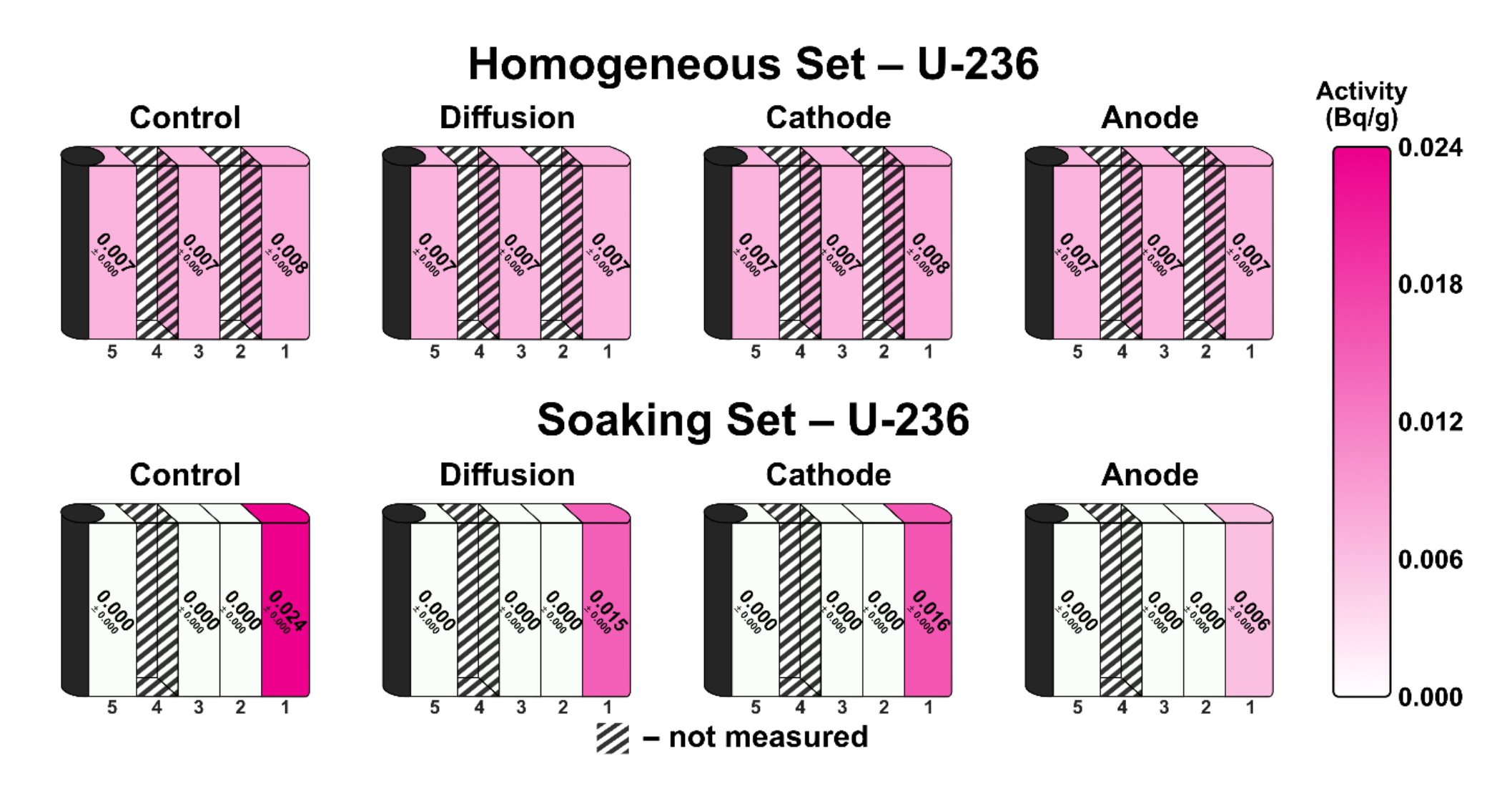


Figure 4.6 (Continued - U-236)

4.5 Discussion

4.5.1 Autoradiography

The Homogeneous Set control slice (*i.e.* without any electrokinetic treatment) had uniform activity distribution across the core section, suggesting that evenly distributed contamination through the cement was achieved. The activity abundance spike in or near the cathode core electrode, and depletion in the same region following EKR for the anode core suggests transportation of one or more positively charged radionuclides towards the cathode. Although the autoradiography plate was set up to maximise detection of DTMRs, the nature of higher energy beta and gamma radiation being more likely to deposit a detectable energy inside the film causes a bias towards these radionuclides being detected compared to lower energy or alpha radiation (Ang *et al.*, 2024). This, combined with the radionuclide's cationic migration behaviour, suggests that a significant proportion of the detected activity was from Cs-137. In addition, if naturally occurring radioactive material (NORM) had been mobilised then these may also contribute to the activity. K-40 would be a likely candidate for this as it was present in the fresh cement powder at 0.09 Bq/g and, once in solution, would likely display a similar migration behaviour to Cs-137 as both are group I alkali metals and have similar modelled aqueous behaviours, albeit in simplified systems to the cement cores (Takeno, 2005).

All Soaking Set core sections show the same general trend of highest activities found in proximity to the outer surface of the cores. This suggests the desired contamination profiles on the surface or near surface were achieved, although the exact distributions (e.g. a sharp activity drop with increasing depth into the core or a gradual decrease over ~ 1 cm) cannot be determined, as low levels of shine would mask the defining characteristics. The lack of higher activity areas (green and red) compared to the Homogeneous Set is likely the result of a lower radionuclide inventory, as discussed in Section 4.4.1. Cement sections further into the core show low levels of activity, which are likely from NORM due to the heterogeneity and 'patchy' nature of the distribution and the apparent lack of migration into the cement by the radionuclides of focus. The cathode and anode cores show a minor activity increase and decrease near their graphite electrode, respectively, which suggests migration of a positively charged ion or colloid, but these activity changes are not as clearly defined as those seen in the Homogeneous Set EKR slices. As with the Homogeneous Set, the radionuclide most likely to demonstrate this behaviour is Cs-137, with the potential of a minor NORM component also present. Only ~ 5 % of Cs-137 in the contamination solutions were transferred to the cores,

which would account for the much less definitive migration trends observed compared to those observed in the Homogeneous EKR cells.

4.5.2 Discrete Radionuclide Analysis

4.5.2.1 H-3

The lack of migration across core section 3s and 5s in the Homogeneous Set cement suggests a lack of detectable H-3 mobilisation over monthly timescales. As noted previously, H-3 immobilisation in concretes can be caused by isotopic exchange with stable H-1 nuclei, and adsorption to e.g. hydrated mineral phases (Furuichi et al., 2005; Takata et al., 2005). Whilst electroosmosis would be expected to transport tritiated water through the cement, the extent of isotope exchange and adsorption appear to mitigate this behaviour to below a detectable level. However, diffusion from each core section 1 into the respective electrolytes drastically reduces the likelihood of resorption as there are fewer exchange and sorption sites in the aqueous phase, explaining the decrease observed in the outermost fractions of cores. All three cores had broadly equal H-3 levels in the electrolyte (~ 1.5 Bq/g) suggesting transportation into the aqueous phase occurred because of diffusion instead of EKR. Use of a larger electrical current would enable a greater electroosmotic rate which could counter or enhance (depending on diffusion direction and electrode polarity) the rate of diffusion and extent of adsorption, but this would need to be balanced against the increased heat and H_2 generation at the cathode, potentially creating unwanted tritiated water vapour.

The same isotope exchange and adsorption mechanisms are likely present within the Soaking Set cements, although, as a result of the contamination mechanism, there may be a larger portion of tritiated water present in porewater (Eichholz *et al.*, 1989). This may explain why H-3 present in core sections 3-5 remained immobilised in all cores. Electromigration would drive water towards the cathodic region, but the lack of H-3 activity in proximity to the cathode core graphite suggests that little or no tritiated water has reached the electrode. Similarly, the anode core electrolyte had the same H-3 activity as those for the diffusion and cathode cores (\sim 0.6 Bq/g), despite the potential for the radionuclide to electroosmotically migrate towards the outer mesh. In both cases, a proportion of the radionuclide may have been lost through tritiated H₂ gas production resulting from electrolysis, but this was not measured and cannot be quantified with the data acquired.

Mass balance calculations show 20 % loss of tritium in the Homogeneous Set control core between the initiation of EKR and the completion of analysis, yet the diffusion, cathode and anode cores have ~ 8 % loss. The enhanced loss in the control core is likely due to its storage period in the freezer whilst the other cores were submerged in electrolyte. Tritium is known to

diffuse even when kept in sub-zero temperatures (Ramseier, 1967) and this passive migration would explain why the activity in core section 1 of the control core is lower than the activities deeper within the core. The ~8 % loss in the remaining Homogeneous Set cores was likely caused by evaporation and electrolysis during treatment as well as evaporation through friction with the saw blade during subsampling. The Soaking Set control core is estimated to have lost ~52 % of its theoretical activity, based on the H-3 reduction in the radionuclide bath before and after the cement core soaking, with the other cores having 42-50 % reductions. This suggests that H-3 freezer diffusion and evaporation with electrolysis had greater but similar effects on the tritium lost. Similar to the Homogeneous Set, evaporation is most likely to affect core section 1s more than cement sections 2-5 due to its much larger surface area, likely contributing to the activity reductions observed on the core outer edges.

4.5.2.2 Sr-90

The lack of Sr-90 migration in all Homogeneous Set cores correlates with previous work that indicates a high uptake into calcium-aluminium-hydrate (C-A-H) and, to a lesser extent, C-S-H phases (Atkins and Glasser, 1992; Wieland *et al.*, 2008). Previous work investigating Sr retention in cements showed evidence of remobilisation, thought to be caused by a combination of Ca substitution in C-S-H, and weakly bound Sr desorbing from C-S-H (Shiner *et al.*, 2022). However, this behaviour was not observed in the EKR work here, possibly due to differing levels of C-A-Hs in the OPC used.

Equal degrees of Sr-90 reduction for the Soaking Set diffusion core relative to the control suggests the presence of a phase that can be mobilised through diffusive processes alone. This phase is likely to be either weakly bound to C-S-H material or freely available in cement porewaters close to the core surface (Shiner *et al.*, 2022), with the first option more probable as no diffusion occurs into the core which suggests rapid resorption after mobilisation. Both EKR core section 1s had activity concentrations within uncertainty of the diffusion core, meaning treatment had little impact on the mobilised fraction. Further, the lack of Sr-90 accumulation next to the graphite electrode in both the cathode and anode cores suggests the mobile phase that Sr is strongly bound to either interacts with cement phases which stops migration into the core, or does not have an overall charge, and, thus, is not amenable to EKR.

4.5.2.3 I-129

Within the Homogeneous Set cores, all cement sections 3 and 5 display no signs of remobilisation. Batch sorption experiments have shown that I⁻, the likely species present in reducing, alkaline conditions (Takeno, 2005), can strongly sorb to Ca-Al(Fe) layered double hydroxide (AFm) phases within the OPC, as well as having weaker interactions with C-S-H and

Ettringite (Atkins and Glasser, 1992; Guo *et al.*, 2020; Nedyalkova *et al.*, 2022). The high degree of retention within anionic interstitial layers of AFm phases likely explains why no I-129 migration is observed within the core, even with EKR applied. However, core section 1s for the diffusion and anode cores show slightly reduced activities compared to the control, yet the cathode core does not, suggesting a minority fraction of I-129 was bound to a positively charged colloid instead. This phase was likely bound to the surface or near-surface of the core and had a high affinity for cement, explaining why increased activities within the cathode core are not observed.

The activity concentration decrease in the Soaking Set diffusion core section 1 in comparison to the control implies that ~ 10 % of I-129 is either weakly bound onto cement phases or is present within the pore water, allowing it to remobilise more easily compared to the Homogeneous Set. Of these options, weak interactions with cementitious material seems the more likely scenario as no statistically significant migration is seen in core section 2-5s, suggesting a form of retention that prevents diffusion further into the core. Both EKR cells show further reductions in core section 1 activities but no significant changes in cement sections 2-5, suggesting that both positively and negatively charged iodine species are present and EKR-amenable. The negative species is likely I⁻ and the positive is expected to be colloidal, as iodine is unlikely to form positive ionic species under expected Eh/pH conditions (Takeno, 2005). In either case, the lack of migration > 1 cm into the core suggests a high affinity for cementitious material, regardless of charge.

4.5.2.4 Cs-137

Despite seemingly little transport in the Homogeneous Set diffusion core compared to the control, EKR cells showed significant migration. In both treated cases, transportation occurred as a positively charged species, likely Cs⁺, which is consistent with predictions from Eh/pH diagrams for simplified aqueous systems (Takeno, 2005). Migration throughout the cathode core resulted in a doubling of Cs-137 activity in cement section 5, with radionuclide levels in the graphite bar demonstrating that remediation directly into the electrode may be a viable option, although future work is needed to confirm and optimise this. An approach such as this would benefit site operators, as removal of a sacrificial electrode may be an easier option for contaminant removal than migrating the radionuclide to a general area of the cell and consequently disposing of a larger volume of material. Core section 5 of the anode cell shows a 72 % reduction in Cs-137 levels, similar to the maximum removal efficiency obtained in previous EKR work by Parker et al. (2017). Interestingly, the contamination method used in the 2017 study was closer to that applied to the Soaking Set here, suggesting that Cs-137 retention mechanisms may be similar in both cases. This is consistent with Cs-137 uptake studies for

concrete that show the extent of sorption depends on the minerals present, likely making the aggregate added to OPC during creation the controlling factor in the radionuclide's retention (Kaminski *et al.*, 2019). However, solutions of Na⁺ or K⁺ can effectively desorb Cs⁺, which may explain why definitive migration is seen here. The same study also reported that greater desorption correlated well with a decrease in solution pH, suggesting that high alkalinities in these cores mitigated the effect of competing alkali metals. The pH of concrete porewaters typically decreases with age (Wan-Wendner, 2018), which could mean that EKR trials on authentic material may be even more effective.

Low Cs-137 uptakes into the Soaking Set cores make definitive interpretations difficult. However, similar radionuclide reductions in both the diffusion and EKR cores suggest the application of an electrical current was only a minor factor in Cs-137 mobility. However, enrichment around the cathodic cell graphite suggests migration as Cs⁺, similar to its Homogeneous Set counterpart, and that EKR has a noticeable impact on the remobilised fraction. Despite greater Cs retention occurring with increasing CaO: Al₂O₃ and CaO: SiO₂ ratios (Atkinson and Nickerson, 1984; Bagosi and Csetényi, 1998), Cs-137 adsorption sites within cements are limited, resulting in a significant proportion remaining in EKR-amenable porewaters (Hanna et al., 2011; Kaminski et al., 2016). EKR-treated concrete samples by Parker et al. (2017) underwent a similar contamination method to those here but generally had lower remobilisation efficiencies (60 % and 37 % with KCl addition to electrolyte, 19 % and 20 % without) than samples in this study (71 % and 86 % for cathode and anode cores, respectively). This may be explained by analysis on ~ 60-year-old storage pond concrete from the Hunterston-A nuclear site (Ayrshire, UK), which found evidence for artificially spiked stable Cs associating with the clay mineral vermiculite in aggregates rather than cementitious material (Bower et al., 2016). This association is caused by sequestration through ionic substitution into clay interstitial layers (Fuller et al., 2015; Livens and Baxter, 1988), which would reduce the potential efficacy of EKR. Experiments performed in this study did not have aggregate included, likely meaning the extent of Cs-137 remediation in in authentic material would be closer to results present by Parker et al. (2017).

4.5.2.5 U-236

Almost all Homogeneous Set core sections have a uniform nature, suggesting that U-236 is bound to phases that are not EKR-amenable. Further, although the diffusion and anode cores have a small decrease in cement section 1 values, a combination of initial U-236 activity concentrations being low, and the final electrolytes all containing < 0.000 Bq/g of the radionuclide suggest that core discrepancies are likely caused by minor heterogeneities in starting conditions rather than subsequent transportation. Modelling for concrete use as a

solidification matrix in reducing conditions (Eh < -450 mV, pH ~ 12) suggests that U(IV) is the species present, as UO_2 , but in more oxidising conditions (Eh -200 to -450 mV) either UO_2 or U(VI) uranophane ($Ca(UO_2)_2(SiO_3)_2(OH)_2 \cdot 5H_2O$) are predominant at pHs < 12, and U(VI) calcium uranium oxide hydrates ($Ca_2UO_5 \cdot xH_2O$) at pHs > 12 (Berner, 1992). In every case, these minerals are present in solid state within concretes, preventing U-236 migration from occurring.

Within the Soaking Set cores, $\sim 40\%$ of U-236 was retained as soluble phases, as shown by the decrease in diffusion core activity relative to the control. However, the lack of diffusion further into the core suggests the phases readily sorb to cementitious material and so are likely to be initially present within a few mm of the outer surface. Further activity reduction in the anode suggests the soluble phases are positively charged, which, if said species was prone to cement adsorption, would explain why similar core section 1 activities are observed for the diffusion and cathode cores. Eh/pH diagrams of simplified aqueous systems suggest that in more reducing conditions expected in fresh cements (Eh of < -400 mV, pH of 12) U(IV) will be the present species, either as solid UO₂ or aqueous U(OH)₄, and in more oxidising conditions expected in older cementitious material (Eh of > -400 mV, pH of 12) U(VI) will be the dominant form, as either UO₂(OH)₃- or UO₂(OH)₄²- (Takeno, 2005). However, none of these species are positively charged which indicates uranium migration was instead facilitated through electrophoresis of colloids, with further work required to understand the nature of these.

4.5.3 Radionuclide Comparison and Future Work

Cs-137 was the only radionuclide to show definitive migration in the Homogeneous Set (65 % activity decrease in cathode core section 1 compared to control core, and 72 % decrease in anode core section 5), with accumulation in the cathode core occurring both within and proximally to the graphite electrode. H-3 showed notable levels of mobilisation (32 % and 44 % core section 1 activity reduction, respectively), although, unlike Cs, the cause of transportation is unclear; diffusion is likely the primary driver, but processes such as isotopic exchange may have mitigated the impact of electroosmosis to such an extent that the difference between the diffusion and EKR cores is minimal. Sr-90 and U-236 exhibited no liberation, likely caused by retention within mineral phases instead of sorption with Cs-137 and H-3. I-129 appeared to show diffusive movement in the anode core (16 % activity reduction in cement section 1) but no mobilisation in the cathode core, making comparisons to other radionuclides inconclusive.

In the Soaking Set, both Cs-137 and U-236 showed significant migration in one EKR cell whilst the other had similar mobilisation levels as the diffusion core (for Cs -71 % activity reduction in cathode core section 1, with > 3x concentration increase in section 5; for U -75 % activity reduction in anode core section 1). This was likely caused by high resorption rates inhibiting

movement into the core and thus promoting transportation out into the electrolyte, although EKR appears to overcome this resorption in the case of Cs-137 as evidenced by radionuclide accumulation in the cathode core section 5. I-129 was the only radionuclide to show evidence of existing as both positively and negatively charged species that have high affinities to cement, as shown by both EKR cells having reduced activities compared to the diffusion core, yet neither showing signs of migration further into the cement. This may pose challenges for scaled-up EKR trials, as using an *in situ* electrode such as steel rebar within concrete would always result in a fraction of radioiodine being migrated further into the concrete. Therefore, a two-stage remedial process may be needed involving EKR followed by either scabbling the outer layer of concrete and reapplying EKR with a reversed polarity. Finally, H-3 and Sr-90 showed a lack of enhanced movement in EKR cells compared to the diffusion core. For H-3, this highlights that electroosmosis is not effective over the treatment period and may require EKR for several months to show definitive benefits, whilst Sr-90's existence in a neutrally charged phase makes it no longer EKR-amenable until desorption or mineral phase dissociation occurs.

Overall, Cs-137 was the most successfully remediated radionuclide, with its mobility expected from previous work (e.g. Frizon et al., 2005; Parker et al., 2017), whilst H-3, Sr-90, I-129 and U-236 generally showed a much lower or no degree of remobilisation. In the cases where radionuclides are expected to be primarily sequestered through sorption (e.g. Cs-137 in the Soaking Set), an increased voltage may allow the phases to mobilise and migrate towards the electrodes. Further, if the voltage is sufficient to cause initial desorption, it may also be able to negate any subsequent resorption as radionuclide are transported further into the cement, promoting accumulation in close proximity to the electrodes. However, if contaminants are present within key cement mineral phases (e.g. Sr-90 in the Homogeneous Set) then increased voltage is unlikely to improve remedial efficiency, as mineral breakdown or extensive ion exchange would be required to liberate the radionuclides. As such, future work is required on both better defining the exact phases the radionuclides are present in and determining if a minimum voltage required to mobilise these phases.

When considering all cores, the Soaking Set generally showed greater levels of radionuclide mobilisation, likely caused by weaker sorption mechanisms in comparison to the mineral incorporation that was expected to be more dominant in the Homogeneous Set. Greater extents of radionuclide migration broadly occurred when EKR polarity was arranged such that the direction of electromigration was out of the core rather than towards the centre of the cement. This suggests that, when the charge polarity was oriented correctly, EKR was generally capable of preventing diffusion out of the cores, but high resorption and reincorporation rates prevented transportation further into the cores. Greater voltages may be able to compensate for this phenomenon, but future work would be required to confirm this. In the context of field-scale

trials, EKR of concretes will likely be more successful when drawing radionuclides from the cementitious outer surface into an electrolyte, as retention will be minimised and therefore diffusive processes will assist in transporting contaminants into the solution. However, more work is needed to improve the remedial performance of radionuclides retained both within mineral phases and deeper within the cement, as bioshielding in nuclear reactors will have activation products at depths greater than a few mm.

The process of Soaking Set contamination involved introducing the radionuclide solution to dry cores with empty pores, unlike true nuclear storage ponds where years or decades of pore saturation with water can occur prior to contamination. As a result, hydraulic flow of contaminant solution within the Soaking Set cores may have caused deeper radionuclide penetration than that seen typically seen in storage ponds, where diffusion is likely the primary driving force for contamination. In addition, concrete properties such as porewater pH, buffering capacity and (Van Gerven et al., 2006; Wan-Wendner, 2018) change with age, meaning that experiments here, whilst robust proof-of-concept trials, do not necessarily reflect the conditions present in concretes that have been used for decades. Future work should focus on treating authentic material to better understand and optimise the efficacy of EKR in these conditions.

4.6 Conclusions

This paper has investigated the use of EKR for use on cement containing H-3, Sr-90, I-129, Cs-137 and U-236, with two separate contamination regimes involving either radionuclide inclusion during OPC curing (Homogeneous Set), or placement of the pre-set cement cores into contaminant baths (Soaking Set). Cs-137, an ETMR, was used as a comparator to previous studies, whilst the other radionuclides, classified as DTMRs, were trialled as proof-of-concepts for EKR in cements.

For the Homogeneous Set, Cs-137 was found to be much more susceptible to EKR migration (average activity reduction in cathode core section 1 and anode core section 5 of 69 %) than other radionuclides of focus. On average, 38 % of section 1 H-3 was mobilised through diffusion but was not transported by electroosmosis towards the cathode. Sr-90, I-129, and U-236 either remained bound to immobilised phases, interacted with neutrally charged colloids that could only diffuse, or bound to charged colloids that readily resorbed to cementitious phases which prevented electrophoresis. In the Soaking Set, Cs-137 and U-236 both showed evidence of migration (Cs-137 activity concentration more than tripled in cathode core section 5; 75 % U-236 activity concentration reduction in anode core section 1). A minority of both positively and negatively charged I-129 species appeared to exist, although their high affinity for cementitious

mineral phases prevents migration further into the cores, with and without EKR. H-3 and Sr-90 displayed movement caused diffusion, suggesting the mobile phases have a neutral charge but may still be amenable to electroosmosis.

Overall, mobilisation efficiencies are higher in the Soaking Set than the Homogeneous Set. This is likely due to sorption, which is the expected predominant mechanism in the Soaking Set, being more amenable to EKR than incorporation into mineral phases, the expected primary retention mechanism in the Homogeneous Set. As such, EKR shows more potential for effective *in situ* scaled-up remediation of surface contamination such as that found in nuclear storage pond concretes instead of cementitious material used in bioshielding. Despite this, Cs-137 migration directly into the cathode core graphite rod in the Homogeneous Set demonstrates that, with optimisation, the use of a sacrificial electrode that can retain radionuclides and be disposed of post-treatment would be the simplest and 'cleanest' application of EKR. However, the DTMRs focussed on here generally display much lower remedial efficacies, highlighting the need for better understanding of the liberation requirements for these in order to make sufficient remedial goals attainable.

4.7 References

Acar, Y.B., Gale, R.J., Alshawabkeh, A.N., Marks, R.E., Puppala, S., Bricka, M., Parker, R., 1995. Electrokinetic remediation: Basics and technology status. Journal of Hazardous Materials, Soil Remediation: Application of Innovative and Standard Technologies 40, 117–137. https://doi.org/10.1016/0304-3894(94)00066-P

Alonso, M.M., Suárez-Navarro, J.A., Pérez-Sanz, R., Gascó, C., Moreno de los Reyes, A.M., Lanzón, M., Blanco-Varela, M.T., Puertas, F., 2020. Data on natural radionuclide's activity concentration of cement-based materials. Data in Brief 33, 106488. https://doi.org/10.1016/j.dib.2020.106488

Ang, J.W.L., Bongrand, A., Duval, S., Donnard, J., Jolis, E.M., Utsunomiya, S., Minomo, K., Koivula, R., Siitari-Kauppi, M., Law, G.T.W., 2024. Detecting radioactive particles in complex environmental samples using real-time autoradiography. Sci Rep 14, 5413. https://doi.org/10.1038/s41598-024-52876-w

Asmussen, R.M., Turner, J., Chong, S., Riley, B.J., 2022. Review of recent developments in iodine wasteform production. Front Chem 10, 1043653. https://doi.org/10.3389/fchem.2022.1043653

Atkins, M., Glasser, F.P., 1992. Application of portland cement-based materials to radioactive waste immobilization. Waste Management, Cementitious Materials in Radioactive Waste Management 12, 105–131. https://doi.org/10.1016/0956-053X(92)90044-J

Atkinson, A., Nickerson, A.K., 1984. The diffusion of ions through water-saturated cement. J Mater Sci 19, 3068–3078. https://doi.org/10.1007/BF01026986

Bagosi, S., Csetényi, L.J., 1998. Caesium immobilisation in hydrated calcium-silicate-aluminate systems. Cement and Concrete Research 28, 1753–1759. https://doi.org/10.1016/S0008-8846(98)00163-X

Berner, U.R., 1992. Thermodynamic modelling of cement degradation: Impact of redox conditions on radionuclide release. Cement and Concrete Research, Special Double Issue Proceedings of Symposium D of the E-MRS Fall Meeting 1991 22, 465–475. https://doi.org/10.1016/0008-8846(92)90090-I

Bower, W.R., Morris, K., Mosselmans, J.F.W., Thompson, O.R., Banford, A.W., Law, K., Pattrick, R.A.D., 2016. Characterising legacy spent nuclear fuel pond materials using microfocus X-ray absorption spectroscopy. Journal of Hazardous Materials 317, 97–107. https://doi.org/10.1016/j.jhazmat.2016.05.037

Cao, Y., Zhou, L., Ren, H., Zou, H., 2022. Determination, Separation and Application of 137Cs: A Review. Int J Environ Res Public Health 19, 10183. https://doi.org/10.3390/ijerph191610183

Castellote, M., Andrade, C., Alonso, C., 2002. Nondestructive Decontamination of Mortar and Concrete by Electro-Kinetic Methods: Application to the Extraction of Radioactive Heavy Metals. Environ. Sci. Technol. 36, 2256–2261. https://doi.org/10.1021/es015683c

Croudace, I.W., Warwick, P.E., Greenwood, R.C., 2006. A novel approach for the rapid decomposition of Actinide[™] resin and its application to measurement of uranium and plutonium in natural waters. Analytica Chimica Acta 577, 111–118. https://doi.org/10.1016/j.aca.2006.06.012

Denman, A.E., 2023. Characterisation and Decontamination of Concrete and Plastic Infrastructure from the Hunterston A Spent Nuclear Fuel Storage Pond (PhD). University of Manchester, Manchester, UK.

DePaoli, D.W., Harris, M.T., Ally, M.R., Morgan, I.L., Cate, N., Ellis, M.E., Heath, K., Hovist, D.W., Kabalka, G.W., Anderson, C.L., Tang, C., 1996. Testing and Evaluation of Electrokinetic Decontamination of Concrete (No. DOE/ORO/2036). Oak Ridge National Laboratory, Oak Ridge, Tennessee.

Eichholz, G.G., 1988. Tritium penetration through concrete (No. E25- 626;). Atlanta, Georgia.

Eichholz, G.G., Park, W.J., Hazin, C.A., 1989. Tritium penetration through concrete. Waste Management 9, 27–36. https://doi.org/10.1016/0956-053X(89)90064-0

Frizon, F., Lorente, S., Auzuech, C., 2005. Nuclear decontamination of cementitious materials by electrokinetics: An experimental study. Cement and Concrete Research 35, 2018–2025. https://doi.org/10.1016/j.cemconres.2005.02.008

Fuller, A.J., Shaw, S., Ward, M.B., Haigh, S.J., Mosselmans, J.F.W., Peacock, C.L., Stackhouse, S., Dent, A.J., Trivedi, D., Burke, I.T., 2015. Caesium incorporation and retention in illite interlayers. Applied Clay Science 108, 128–134. https://doi.org/10.1016/j.clay.2015.02.008

Furcas, F.E., Lothenbach, B., Isgor, O.B., Mundra, S., Zhang, Z., Angst, U.M., 2022. Solubility and speciation of iron in cementitious systems. Cement and Concrete Research 151, 106620. https://doi.org/10.1016/j.cemconres.2021.106620

Furuichi, K., Takata, H., Katayama, K., Takeishi, T., Nishikawa, M., Hayashi, T., Kobayashi, K., Namba, H., 2005. Evaluation of tritium behavior in concrete, in: Journal of Nuclear Materials, Proceedings of the Twelfth International Conference on Fusion Reactor Materials (ICFRM-12). Presented at the International Conference on Fusion Reactor Materials, Santa Barbara, California, pp. 1243–1247. https://doi.org/10.1016/j.jnucmat.2007.03.227

Furuichi, K., Takata, H., Motoshima, T., Satake, S., Nishikawa, M., 2006. Study on behavior of tritium in concrete wall. Journal of Nuclear Materials 350, 246–253. https://doi.org/10.1016/j.jnucmat.2006.01.008

Glasser, F.P., Atkins, M., 1994. Cements in Radioactive Waste Disposal. MRS Bulletin 19, 33–38. https://doi.org/10.1557/S0883769400048673

Guo, B., Xiong, Y., Chen, W., Saslow, S.A., Kozai, N., Ohnuki, T., Dabo, I., Sasaki, K., 2020. Spectroscopic and first-principles investigations of iodine species incorporation into ettringite: Implications for iodine migration in cement waste forms. Journal of Hazardous Materials 389, 121880. https://doi.org/10.1016/j.jhazmat.2019.121880

Han, S., Hong, S., Nam, S., Kim, W.-S., Um, W., 2020. Decontamination of concrete waste from nuclear power plant decommissioning in South Korea. Annals of Nuclear Energy 149, 107795. https://doi.org/10.1016/j.anucene.2020.107795

Hanna, J.V., Aldridge, L.P., Vance, E.R., 2011. Cs Speciation in Cements. MRS Online Proceedings Library 663, 89. https://doi.org/10.1557/PROC-663-89

Harms, A., Gilligan, C., 2010. Development of a neutron-activated concrete powder reference material. Applied Radiation and Isotopes, Proceedings of the 17th International Conference on Radionuclide Metrology and its Applications (ICRM 2009) 68, 1471–1476. https://doi.org/10.1016/j.apradiso.2009.11.031

Hateley, A.H., 2021. Analysis of Expedited Chromatographic Separation Systems for Application to the Decommissioning of Nuclear Facilities (PhD). University of Southampton, Southampton, UK.

Hemming, S.D., Purkis, J.M., Warwick, P.E., Cundy, A.B., 2023. Current and emerging technologies for the remediation of difficult-to-measure radionuclides at nuclear sites. Environ. Sci.: Processes Impacts 25, 1909–1925. https://doi.org/10.1039/D3EM00190C

IAEA, 2025. IAEA Nuclear Data Services [WWW Document]. URL https://www-nds.iaea.org/ (accessed 1.13.25).

IAEA, 2015. Decommissioning of Pools in Nuclear Facilities (No. NW-T-2.6), IAEA Nuclear Energy Series. International Atomic Energy Agency, Vienna.

IAEA, 1998. Radiological Characterization of Shut Down Nuclear Reactors for Decommissioning Purposes (Technical Reports Series No. 389). International Atomic Energy Agency, Vienna.

Jackson, S.F., Monk, S.D., Riaz, Z., 2014. An investigation towards real time dose rate monitoring, and fuel rod detection in a First Generation Magnox Storage Pond (FGMSP). Applied Radiation and Isotopes 94, 254–259. https://doi.org/10.1016/j.apradiso.2014.08.019

Kaminski, M., Mertz, C., Ortega, L., Kivenas, N., 2016. Sorption of radionuclides to building materials and its removal using simple wash solutions. Journal of Environmental Chemical Engineering 4, 1514–1522. https://doi.org/10.1016/j.jece.2016.02.004

Kaminski, M.D., Mertz, C.J., Jerden, J., Kalensky, M., Kivenas, N., Magnuson, M., 2019. A case study of cesium sorption onto concrete materials and evaluation of wash agents: Implications for wide area recovery. J Environ Chem Eng 7, 10.1016/j.jece.2019.103140. https://doi.org/10.1016/j.jece.2019.103140

Kim, C., Choi, S., Shin, M., 2018. Editors' Choice—Review—Electro-Kinetic Decontamination of Radioactive Concrete Waste from Nuclear Power Plants. J. Electrochem. Soc. 165, E330. https://doi.org/10.1149/2.0281809jes

Kim, D.J., E. Warwick, P., Croudace, I.W., 2008. Tritium Speciation in Nuclear Reactor Bioshield Concrete and its Impact on Accurate Analysis. Anal. Chem. 80, 5476–5480. https://doi.org/10.1021/ac8002787

Kim, G.-N., Choi, W.-K., Lee, K.-W., 2010. Decontamination of radioactive concrete using electrokinetic technology. J Appl Electrochem 40, 1209–1216. https://doi.org/10.1007/s10800-010-0088-8

Kim, G.-N., Yang, B.-I., Choi, W.-K., Lee, K.-W., Hyeon, J.-H., 2009. Washing-Electrokinetic Decontamination For Concrete Contaminated With Cobalt and Cesium. Nuclear Engineering and Technology 41, 1079–1086. https://doi.org/10.5516/NET.2009.41.8.1079

Lee, E., 2019. Chapter 1 - Electrophoresis of a Single Rigid Particle, in: Lee, E. (Ed.), Interface Science and Technology, Theory of Electrophoresis and Diffusiophoresis of Highly Charged Colloidal Particles. Elsevier, pp. 3–45. https://doi.org/10.1016/B978-0-08-100865-2.00001-1

Lee, K.Y., Oh, M., Kim, J., Lee, E.H., Kim, I.S., Kim, K.W., Chung, D.Y., Seo, B.K., 2018. Trends in Technology Development for the Treatment of Radioactive Concrete Waste. Journal of Nuclear Fuel Cycle and Waste Technology 16, 93–105. https://doi.org/10.7733/jnfcwt.2018.16.1.93

Li, S.F.Y., Wu, Y.S., 2000. ELECTROPHORESIS | Capillary Electrophoresis, in: Wilson, I.D. (Ed.), Encyclopedia of Separation Science. Academic Press, Oxford, pp. 1176–1187. https://doi.org/10.1016/B0-12-226770-2/04321-0

Liu, Y., Gunten, H.R., 1988. Migration chemistry and behaviour of iodine relevant to geological disposal of radioactive wastes. A literature review with a compilation of sorption data. Paul Scherrer Institute, Wurenlingen, Switzerland.

Livens, F.R., Baxter, M.S., 1988. Chemical associations of artificial radionuclides in Cumbrian soils. Journal of Environmental Radioactivity 7, 75–86. https://doi.org/10.1016/0265-931X(88)90043-4

Ma, B., Fernandez-Martinez, A., Madé, B., Findling, N., Markelova, E., Salas-Colera, E., Maffeis, T.G.G., Lewis, A.R., Tisserand, D., Bureau, S., Charlet, L., 2018. XANES-Based Determination of Redox Potentials Imposed by Steel Corrosion Products in Cement-Based Media. Environ. Sci. Technol. 52, 11931–11940. https://doi.org/10.1021/acs.est.8b03236

Mahrous, S.S., Borai, E.H., Mansy, M.S., 2023. Polymeric gel for surface decontamination of long-lived gamma and beta-emitting radionuclides. Applied Radiation and Isotopes 197, 110834. https://doi.org/10.1016/j.apradiso.2023.110834

Min, B.-Y., Choi, W.-K., Lee, K.-W., 2010. Separation of clean aggregates from contaminated concrete waste by thermal and mechanical treatment. Annals of Nuclear Energy 37, 16–21. https://doi.org/10.1016/j.anucene.2009.10.010

NDA, 2023. 2022 UK Radioactive Waste Inventory. Nuclear Decommissioning Authority, Cumbria, UK.

NEA, 1999. Decontamination Techniques Used in Decommissioning Activities. Nuclear Energy Agency, Paris, France.

Nedyalkova, L., Tits, J., Renaudin, G., Wieland, E., Mäder, U., Lothenbach, B., 2022. Mechanisms and thermodynamic modelling of iodide sorption on AFm phases. Journal of Colloid and Interface Science 608, 683–691. https://doi.org/10.1016/j.jcis.2021.09.104

Nikolaev, A.N., Karlina, O.K., Yurchenko, A.Yu., Karlin, Yu.V., 2012. Assessment of 137Cs decontamination of concrete by the reagent method. At Energy 112, 57–62. https://doi.org/10.1007/s10512-012-9524-7

Pantelias, M., Volmert, B., 2015. Activation Neutronics for a Swiss Pressurized Water Reactor. Nuclear Technology 192, 278–285. https://doi.org/10.13182/NT15-13

Parker, A.J., Joyce, M.J., Boxall, C., 2017. Remediation of 137Cs contaminated concrete using electrokinetic phenomena and ionic salt washes in nuclear energy contexts. Journal of Hazardous Materials 340, 454–462. https://doi.org/10.1016/j.jhazmat.2017.07.007

PGE, 1995. Trojan Nuclear Plant Radiological Site Characterization Report Rev 0.1. Portland General Electric, Oregon, USA.

Popov, K., Glazkova, I., Yachmenev, V., Nikolayev, A., 2008. Electrokinetic remediation of concrete: Effect of chelating agents. Environmental Pollution, Chelating Agents in the Environment 153, 22–28. https://doi.org/10.1016/j.envpol.2008.01.014

Popov, K.I., Glaskova, I.V., Myagkov, S.V., Petrov, A.A., 2006. Removal of cesium from the porous surface via the electrokinetic method in the presence of a chelating agent. Colloid J 68, 743–748. https://doi.org/10.1134/S1061933X06060111

Purkis, J.M., Warwick, P.E., Graham, J., Hemming, S.D., Cundy, A.B., 2021. Towards the application of electrokinetic remediation for nuclear site decommissioning. Journal of Hazardous Materials 413, 125274. https://doi.org/10.1016/j.jhazmat.2021.125274

Ramseier, R.O., 1967. Self-Diffusion of Tritium in Natural and Synthetic Ice Monocrystals. Journal of Applied Physics 38, 2553–2556. https://doi.org/10.1063/1.1709948

Shiner, M.E., Klein-BenDavid, O., L'Hôpital, E., Dauzères, A., Neji, M., Teutsch, N., Peled, A., Bar-Nes, G., 2022. Retention of strontium in high- & low-pH cementitious matrices – OPC vs.

model systems. Cement and Concrete Research 152, 106659. https://doi.org/10.1016/j.cemconres.2021.106659

Takata, H., Motoshima, T., Satake, S., Nishikawa, M., 2005. Study of Tritium Behavior in Cement Paste. Fusion Science and Technology. https://doi.org/10.13182/FST05-A994

Takeno, N., 2005. Atlas of Eh-pH diagrams, Intercomparison of thermodynamic databases, Geological Survey of Japan Open File Report No.419 (Geological Survey of Japan Open File No. 419). National Institute of Advanced Industrial Science and Technology, Research Center for Deep Geological Environments, Tsukuba, Japan.

Van Gerven, T., Cornelis, G., Vandoren, E., Vandecasteele, C., Garrabrants, A.C., Sanchez, F., Kosson, D.S., 2006. Effects of progressive carbonation on heavy metal leaching from cement-bound waste. AIChE Journal 52, 826–837. https://doi.org/10.1002/aic.10662

Wan-Wendner, R., 2018. Aging concrete structures: a review of mechanics and concepts. Journal of Land Management, Food and Environment 69, 175–199. https://doi.org/10.2478/boku-2018-0015

Wattez, T., Duhart-Barone, A., Lorente, S., 2013. Modeling of Nuclear Species Diffusion Through Cement-Based Materials. Transp Porous Med 98, 699–712. https://doi.org/10.1007/s11242-013-0167-5

Wieland, E., Tits, J., Kunz, D., Dähn, R., 2008. Strontium Uptake by Cementitious Materials. Environ. Sci. Technol. 42, 403–409. https://doi.org/10.1021/es071227y

Yurchenko, A.Yu., Karlin, Yu.V., Nikolaev, A.N., Karlina, O.K., Barinov, A.S., 2009. Decontamination of radioactive concrete. At Energy 106, 225–230. https://doi.org/10.1007/s10512-009-9156-8

Chapter 5 Application of Electrokinetic Remediation for Clean-up of Medium- and Long-Lived Radionuclides in Coastal Sediments

Hemming, S. D., Ellis-Bone, C., Warwick, P. E., and Cundy, A. B.

Prepared for submission as a paper to Environmental Science and Technology.

Author contributions:

Hemming, S. D. – experimental design, data collection and processing, interpretation, manuscript writing

Cundy, A. B. – experimental design, core collection, data interpretation, manuscript editing

Warwick, P. E. – experimental design, core collection, data interpretation, manuscript editing

5.1 Introduction

Since 1952, the Sellafield nuclear facility (Cumbria, UK) has made authorised low-level radioactive discharges into the Irish Sea (Gray *et al.*, 1995; Kershaw *et al.*, 1992). Although the constituents of these discharges have varied over time depending on site operations and available technologies, radionuclides such as Tc-99, Cs-137, Np-237, Pu-239, Pu-240, and Am-241 dominated discharges for decades (BNFL, 1979-2005; Gray *et al.*, 1995; Sellafield Ltd., 2006-2021). Each of these radionuclides has a distinctive geochemical behaviour, exhibiting varying degrees of mobility once released into local marine systems (USEPA, 1999). Whilst more mobile radionuclides can readily disperse, those with high affinities for sediments can sorb onto suspended solids, be deposited in marine sedimentary sinks, and subsequently reworked by ocean currents back towards the UK coastline (Ray *et al.*, 2020).

One such affected area is the Ravenglass Saltmarsh; part of the Esk Estuary, it is a low-energy intertidal area located ~ 10 km southeast of Sellafield. Sediment within the saltmarsh originated predominantly from marine sources, with little fluvial deposition occurring from the Esk River (Halcrow, 2013). The sediment has a compositional gradient, with sandier material at the front and muddier material at the back, where the composition is approximately ~ 75 % silt, ~ 19 % clay and 7 % sand (Morris et al., 2000). Resuspended sediments containing Sellafield-derived radionuclides are transported from the Irish Sea and deposited in the saltmarsh, which has allowed material here to accumulate and retain a complete discharge history of the Sellafield site (Hunt and Kershaw, 1990; Marsden et al., 2006; Morris et al., 2000; Ray et al., 2020). This buildup over decades has created an unusual setting of aged radioactive material stored in a natural coastal environment (with e.g. Pu-241 activities up to 242,000 Bq/kg (Marsden et al., 2006) and Am-241 up to 29,000 Bq/kg (Morris et al., 2000)) which can be precisely linked to the site's annual discharges. However, recent work involving Diffusive Gradients in Thin Films (DGT) techniques and accelerator mass spectrometry (AMS) has identified ongoing actinide remobilisation from these marsh sediments (Chaplin et al., 2022), raising concerns about longterm stability and resilience of the site for radionuclide storage. This is exacerbated by the potential for enhanced erosion and sediment remobilisation due to more frequent and intense storms, as well as sea level rise (Balboni et al., 2022; Colombano et al., 2021; Temmerman et al., 2004).

No large-scale remediation attempts on the Ravenglass Saltmarsh have been undertaken. A report by Restoration Strategies for Radioactively Contaminated Sites and their Close surroundings (RESTRAT; 1999) evaluated the benefits of remediating the estuary, removing the contaminated material only, or monitoring the site without any remedial action. Soil washing and chemical solubilisation were considered for ex situ clean-up of material, but both were

deemed too expensive for use on the area. Although the report is somewhat dated and no more recent evaluations have been made for the area, this still highlights a need for development and assessment of more cost-effective remediation or risk management technologies which could be deployed as needed to minimise any enhanced future risk from "leave in place" strategies.

5.1.1 Electrokinetic remediation (EKR)

Electrokinetic remediation (EKR) can be a lower-cost and more sustainable remediation technology in comparison to traditional techniques (Purkis *et al.*, 2021b). The EKR process involves applying a direct current to a contaminated medium in order to mobilise and migrate pollutants to particular areas of the material (Figure 5.1). During treatment, three transport mechanisms can occur. First, electromigration is the movement of ions, with cations and anions travelling towards the oppositely charged electrode. Electrophoresis, a similar concept to electromigration, involves the transportation of charged colloids (typically 1 – 5000 nm in size (Lee, 2019)) within the material. Finally, electroosmosis describes the migration of water molecules, resulting in electrolysis that generates hydronium ions at the anode and hydroxide ions at the cathode. The charges of these will result in migration towards their respective electrodes, creating a pH gradient within the material over time.

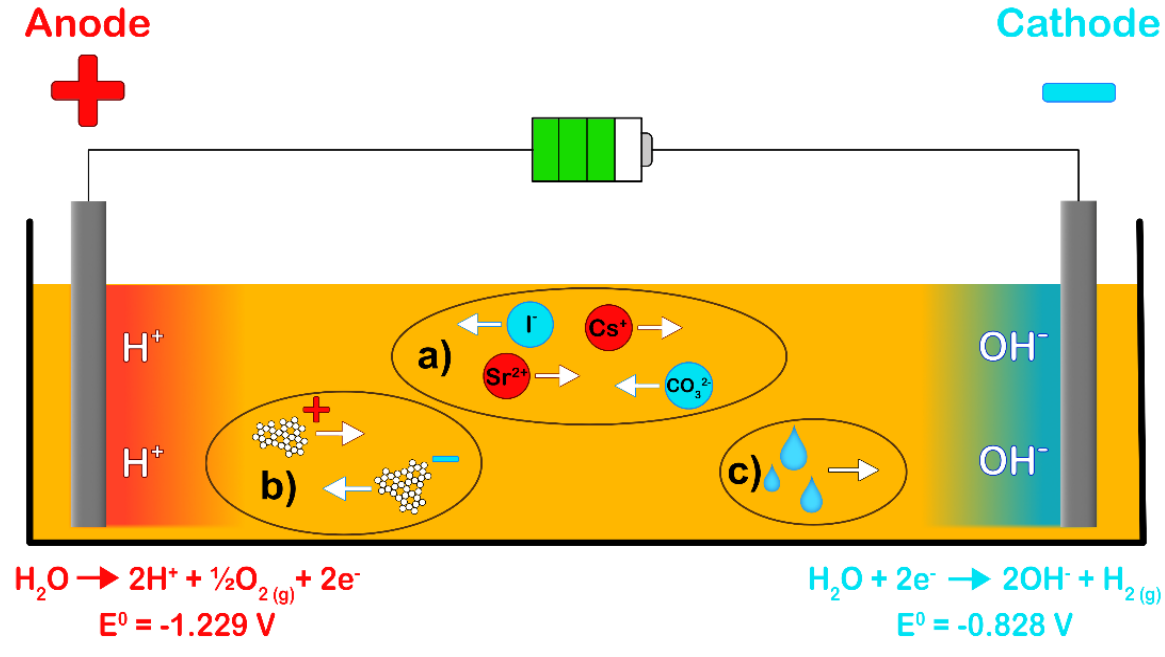


Figure 5.1 – Summary diagram of electrokinetic remediation, modified from (Purkis *et al.*, 2021b). a) – electromigration; b) – electrophoresis; c) – electroosmosis. Electrolysis also occurs which generates hydrogen cations at the anode and hydroxide ions at the cathode, creating a pH gradient over time.

Whilst EKR has been widely applied for remediating metals and organics in sediments in non-nuclear settings (e.g. Acar et al., 1995; Huang et al., 2012; Suied et al., 2018; Zhao et al., 2024), trials on radionuclides remain underdeveloped. Previous studies have focussed on soils found

at nuclear sites (see Purkis *et al.*, 2021b), with limited work performed on estuarine or coastal sediments (Cundy and Hopkinson, 2005). With many nuclear sites around the UK, and indeed globally, located on coastlines (Brown *et al.*, 2014; Grimston *et al.*, 2014; Kopytko and Perkins, 2011), developing cost-effective remediation approaches for these environments is becoming increasingly important. The well-characterised nature of radionuclides within the Ravenglass Saltmarsh makes this location the ideal setting for trialling new technologies.

This paper examines the application of EKR for remediating radiologically contaminated saltmarsh sediment. Cs-137, Pu-238, Pu-239+240, Pu-241, and Am-241 were selected due to their prominence in Sellafield marine discharges (BNFL, 1979-2005; Gray *et al.*, 1995; Sellafield Ltd., 2006-2021) and the Ravenglass Saltmarsh (*e.g.* Morris *et al.*, 2000; Ray *et al.*, 2020), as well as for having half-lives that span between decades and tens of thousands of years (IAEA, 2025; Table 4.1), and have undergone limited EKR trials in sediments. Separate experiments were performed with different electrolytes (Atlantic Seawater simulant and citric acid) to establish radionuclide remobilisation efficiency under different conditions and optimise the scaled-up remediation process in coastal sediments.

Radionuclide	Half-life [a]	Predominant oxidation state(s) in environmental conditions	K _d range in environmental conditions
Cs-137	30.08 years	(I) [b,c]	10 ³ – 10 ^{4 [h, i]}
Pu-238	87.7 years		
Pu-239	24110 years	(IV), (V) [d,e,f]	10 ⁴ – 10 ^{6 [i, j, k]}
Pu-240	6561 years	10 10	
Pu-241	14.4 years		
Am-241	432.6 years	(III) [g]	10 ⁴ - 10 ^{6 [d, i, j]}

Table 5.1 – Summary for radionuclides of focus. [a] – iaea.nds (2025); [b] – Baxter et al. (1979); [c] – McKinley et al. (1981); [d] – McMahon et al. (2000); [e] – Vives I Batlle et al. (2008); [f] – Ray et al. (2020); [g] – Morris et al. (2000); [h] – Hunt and Kershaw (1990); [i] – IAEA (2004); [i] – Marsden et al. (2006); [k] – McDonald et al. (2001).

5.2 Materials and Methods

5.2.1 Core Collection and Experimental Set Up

The 55-cm deep sediment core was collected from the Ravenglass Saltmarsh on 7/6/2021 (54°20'24.9"N, -3°24'12.8"E; Figure 5.2) and stored at 4°C until being cut in half. One half was

retained for stable element and radionuclide analysis, as the control core, whilst the other half was split again to make two quarter-section cores that were electrokinetically treated (Figure 5.3). The quarter-section cores were placed in separate plastic half-tubes that were then stuffed with lab roll for support, and graphite electrodes were inserted 2 cm and 45 cm from the upper surface of the core. Electrokinetic treatment was implemented for 45 days at 21.5 V (creating a 0.5 V/cm gradient; this is typically used to minimise soil heating and power consumption (e.g. Hahladakis et al., 2016; Kim et al., 2012; Purkis et al., 2021a)). Cling film was placed over the cores for the experimental duration (although temporarily moved for taking sediment pH samples) to minimise electrolyte evaporation due to fume cupboard air flow (Figure 5.3). Atlantic seawater simulant (General Purpose grade; Ocean Science International Ltd., Hampshire, UK) was used as an electrolyte for one quarter-section core, with 1.56 M (30 wt%) citric acid (Thermo Fisher Scientific International; Pennsylvania, USA) in Milli Q water used in the other. Atlantic Ocean simulant was chosen due to seawater's abundance at the site, and as a readily available higher ionic strength electrolyte that may enhance current flow, and hence electromigration process, in the cell. Citric acid was selected as it a naturally occurring organic acid that can complex with transition metals and actinides (Francis and Dodge, 2009) and has been successful at remobilising homogenised Pu-contaminated sediment in previous lab-scale EKR trials (Agnew et al., 2011). A secondary advantage of the molecule is its ability to biodegrade over days, weeks or months depending on soil conditions (Byrd et al., 2021; Francis et al., 1994; Wen et al., 2009), making it preferable for in situ trials in comparison to more traditional chelating agents such as ethylenediaminetetraacetic acid (EDTA) (Wen et al., 2009).

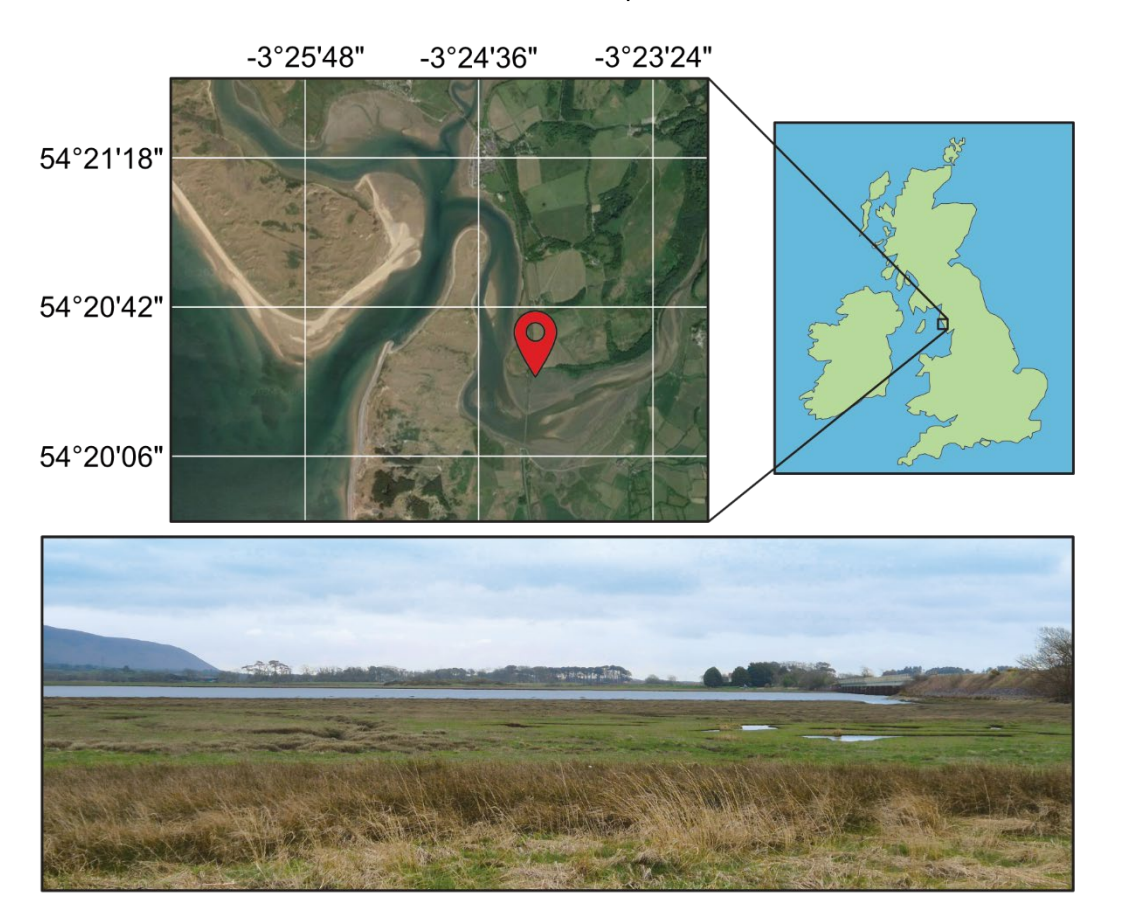


Figure 5.2 – Top: The Ravenglass Saltmarsh, Cumbria, UK, with the location of core sampling marked. Bottom: photo from the core sampling location. Satellite imagery from Google Maps (2025).

Throughout the experiment, dewatering was prevented by adding electrolyte to the anodic regions of both EKR cores. This was done by creating a cotton wool electrolyte 'bridge' (Figure 5.3) between a small electrolyte reservoir and the core. Liquids moved through capillary action from the reservoir into the cotton wool, and eventually onto the sediment, providing a successful pathway for continuous sediment rehydration. Core pHs were measured by taking \sim 1 g of sediment from either adjacent to the anode or cathode, or the centre point between the two electrodes, mixing the sediment in 2.5 mL of Milli Q, and using a HANNA HI98301 pH probe (uncertainty \pm 0.2) to record the value. This approach was a balance between using international standards for measuring soil pH (e.g. ASTM International, 2024; ISO, 2021) and removing as little sediment from the core as reasonably practicable. Measurements for pH were performed in both cores on days three and seven, and once a week thereafter.

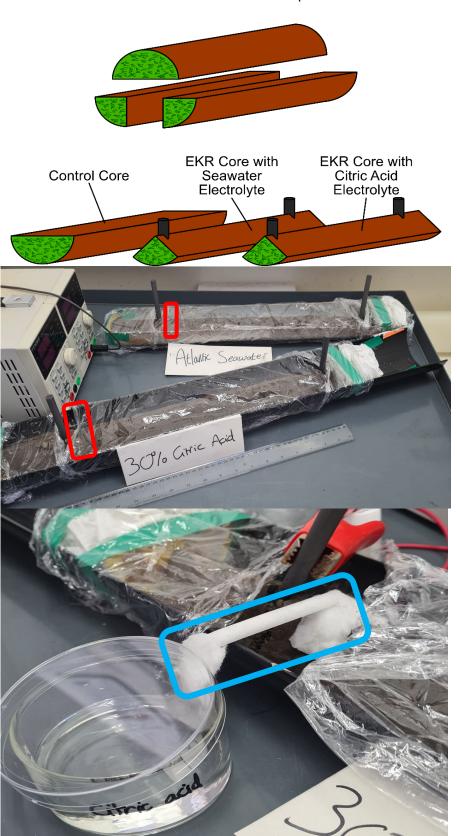


Figure 5.3 – Top - schematic showing how the collected core was divided up. Grey bars represent the location of graphite electrodes. Middle – photo of the experimental setup, with the locations of the electrolyte 'bridges' were placed marked in red. Bottom – photo of the citric acid core electrolyte 'bridge' (marked in blue). The system functioned by allowing electrolyte to move by capillary action from the reservoir, through the cotton wool, and onto the core. A transparent plastic tube was put around most of the cotton wool to minimise electrolyte evaporation and contamination.

5.2.2 Analysis

5.2.2.1 Reagents

For the following methods, all acids, ammonia solution, NH₄I, (NH₄)₂C₂O₄, polyethylene glycol 2000 (PEG-2000), and FeCl₃ were purchased from Thermo Fisher Scientific, 1x8 100-200 mesh anion exchange resin (Cl form) from TrisKem (Brittany, France), lithium metaborate flux for Fluxana (Bedburg-Hau, Germany), Pu-239 (used for quality control (QC) standards) from National Physical Laboratory and Pu-242 (used as a tracer for sample recovery) from AEA Technology (now Ricardo-AEA; Oxfordshire, UK).

5.2.2.2 X-ray Fluorescence (XRF)

Semi-quantitative distributions of over 20 elements within the sediment were obtained with an ITRAX micro-XRF core scanner (200 μ m step size, 15 count time, Mo anode X-ray tube, XRF conditions 30 kV, 30 mA) in accordance with the methods detailed by Croudace *et al.* (2006). In the case of the control core, this was performed before the experiments began, and in the cases of the seawater and citric acid cores, analyses were done after treatment.

5.2.2.3 Caesium-137 and Americium-241

After ITRAX scanning, each core was cut into 1-cm-thick sections perpendicular to core depth and freeze dried. The sections were then transferred to high density polyethylene (HDPE) vials and analysed in Canberra well-type hyper-pure germanium (HPGe) gamma-ray spectrometers (60-minute count times) to obtain Cs-137 and Am-241 activities, with spectra deconvolution performed in Fitzpeaks software (JF Computing, Stanton in the Vale, UK). All activities were decay corrected to the date of core collection. Samples were not made in replicate and so all uncertainties presented here are analytical and counting uncertainties.

5.2.2.4 Organic Matter and Carbonate Content

Loss on Ignition (LOI) was performed on 2 g of freeze-dried sediment per section. Samples were weighed, placed in a room-temperature furnace and ramped at 50 °C/hr to 450 °C, where they remained for four hours. These were then removed, cooled, and reweighed before being placed into a 450 °C furnace, ramped at 50 °C/hr to 950 °C, and remained there for four hours. Heating to 450 °C was performed to remove organic content and some water in clays, whilst heating to 950 °C removed carbonates (Heiri *et al.*, 2001; Rowell, 2014). Data are presented in Table C.1.

5.2.2.5 Plutonium

Methods have been previously published in Warwick et al. (1999) (Fe hydroxide precipitation) and Croudace et al. (1998) (fusion digest and ion chromatography for Pu separation) but are summarised here. Approximately 2 g of each sample underwent a metaborate fusion digest, HNO₃ dissolution and filtering, prior to being loaded onto a TrisKem anion exchange resin, washed with 45 mL 9 M HCl, 30 mL 8 M HNO₃, and 10 mL 9 M HCl, and eluted with 40 mL HCl with NH_4I to separate the Pu from other radionuclides (the use of a secondary column containing UTEVA resin and the use of 3 M HNO₃ in Croudace et al. (1998) was omitted here as this was for U retention which was not performed in this study). The final eluents were plated onto disks for Pu-238 and Pu-239+240 counted in EG&G ORTEC Octete PC alpha spectrometers (150,000-second count time) and analysed with MAESTRO software (Pu-239+240 is a single measurement as the alpha emission energies of both radionuclides are too similar to deconvolve into individual peaks). The disks were then acid stripped, and the radionuclides underwent an organic extraction before Pu-241 was measured on a WALLAC 1220 Quantulus™ Ultra low Level Liquid Scintillation Counter (4-hour count time) with WinQ software. All activities were decay corrected to the date of core collection. Samples were not made in replicate and so all uncertainties presented here are analytical and counting uncertainties.

5.3 Results and Discussion

5.3.1 Visual Observations

During treatment, a white solid gradually formed near the cathodic regions of both cores, due evaporation of electrolytes and precipitation of salts. Approximately two weeks into the experiments, yellow liquids started pooling at the bottom of both cores at an approximate rate of 1s-10s mL/day; the production of these occurred until the end of the experiments. The solutions contained small quantities of the radionuclides of focus, with the yellow colour likely produced by Fe chlorides (Table C.2; Purkis *et al.*, unpublished data). Drying was observed in the cathodic region of both cores starting at 3-4 weeks in, with the seawater core showing a larger extent of dewatering than the citric acid counterpart.

5.3.2 Current and pH Measurements

The seawater core recorded an initial current of 54 mA (Figure C.1) which stabilised at \sim 20 mA within the first three days. On day 12 an increase to 86 mA was recorded, with the current reaching > 100 mA for two days before gradually decreasing and stabilising at 14-20 mA. After, the cell generally maintained \sim 15 mA. The citric acid core showed the same initial trends as the

seawater, starting at 46 mA, peaking at 51.5 mA within the first few hours and then gradually decreasing. This decrease was exponential until the current was recorded as 0 mA on day 42 and remained constant until the end of the experiments. Current fluctuations are likely due to a dewatering and rewatering events, as periods of high electrolyte uptake correlated with greater current readings and yellow liquid generation.

All seawater core pH sampling points started with pH values of 6.5 (Figure C.2). By day three of electrokinetic treatment, a pH gradient had formed, with values of 12.2 at the cathode (~ 4 cm from core top), 7.4 in the centre (~ 19.5 cm from core top), and 1.4 (~ 43 cm from core top) at the anode. These values remained consistent until day 21, where the centre of the core dropped from neutral conditions to pH 2.9. Cathodic pHs of 12-13, and centre and anodic pHs of 2-3 remained until the end of the experiment.

Initial pHs in the citric acid core ranged from 6.3 to 6.9. A pH gradient formed within three days, although the centre point was within the acidic zone by this time (cathodic region: 10.7, centre point: 3.1, anodic zone: 1.4). For the remainder of the 45-day treatment period, the centre and anodic regions maintained pHs of 1.5 - 3.0. Within 21 days, the cathodic zone started becoming gradually more acidified, until 3.3 was measured at the end of treatment.

5.3.3 XRF

For the control core, XRF data for Mn, Fe, and S, normalised to total scatter (coherent + incoherent) for negating variations in composition and water content (Ge et al., 2005), alongside Si/Rb, S/Cl, Ca/Ti, and Zr/Rb data, are presented in Figure 5.4 (for all scanned elements see Figure C.3). The data presented are semi quantitative (elements were measured in counts but not converted to concentration) but reliably show elemental trends in the control and EKRtreated cores. Regarding seawater core data, it should be noted that lighter elements e.g. S, Cl, and Ca, have large abundance peaks relative to the other elements due to their presence within the electrolyte as well as the cores (OSIL, 2025). To summarise briefly, successful remediation of several elements can be seen in the seawater core including Ca, Mn, Ni, Zn, and I, all found at ~ 10-20 cm depth. However, approximate calculations based on the concentrations of Atlantic seawater simulant constituents (OSIL, 2025) and elemental abundance in Ravenglass sediments (Balboni et al., 2022; Warwick, 1999) suggest that notable quantities of S (~ 66 %), Cl (~ 85 %), Ca (~ 10-28 %), Br (~ 99 %), Rb (~ 34 %), Sr (~ 23-97 %) present in the post-treatment seawater core originate from the electrolyte instead of the sediment. These elements are more amenable to EKR as they are already in the aqueous phase and may consequently skew interpretations regarding treatment efficacy of material initially present in the core. All other elements in the electrolyte were found to only constitute < 5 % of their total mass in the core,

with many, including Fe and Mn, at levels < 0.01 %. Citric acid core ITRAX data show either full or partial remobilisation of elements such as Al, Ca, Mn, Fe, Sr, and Pb, with a variety of distributions throughout the cell.

5.3.3.1 Core Composition

Zr/Rb acts as a grain size indicator, as Rb strongly adsorbs to clays and Zr is incorporated into silts (Kylander *et al.*, 2011). Si/Rb is also included as, although the ratio is not commonly reported in XRF analysis due to detection issues with lighter elements (Davies *et al.*, 2015), Si represents sands and silicate material which makes Si/Rb act as an approximate analogue for sand to clay content. Both Zr/Rb and Si/Rb in the control core show a consistent ratio at depths > 2 cm, demonstrating a broadly uniform bulk sediment composition throughout the core (Figure 5.4).

5.3.3.2 Redox Sensitive Elements

Mn, Fe, and S can be used by microorganisms for anaerobic respiration (Froelich et al., 1979), making them useful for determining redox conditions within sediments. Control core Mn is concentrated within the top 10 cm (Figure 5.4), suggesting the transition zone in abundance represents reduction of insoluble Mn(IV) oxides to soluble Mn(II). This behaviour is not observed with Fe, which shows a slight, gradual increase in abundance with depth. This suggests that the majority of the core exists within suboxic conditions, specifically in a region where Mn(IV) can be reduced but not Fe(III) oxy(hydr)oxides (Froelich et al., 1979). Further, S/Cl ratios show changes in the biogenic S content, as lithogenic S/Cl are typically found at a near constant ratio (Thomson et al., 2006). Both S/Cl and S graphs show a broadly consistent trend with depth (with the exception of organic S at ~ 14 cm), with a minor increase in the bottom 5 cm. The lack of a large, sudden transition zone like that seen in the Mn profile suggests that the sulphate reduction zone has not been reached, further supporting the idea of suboxic sediment.

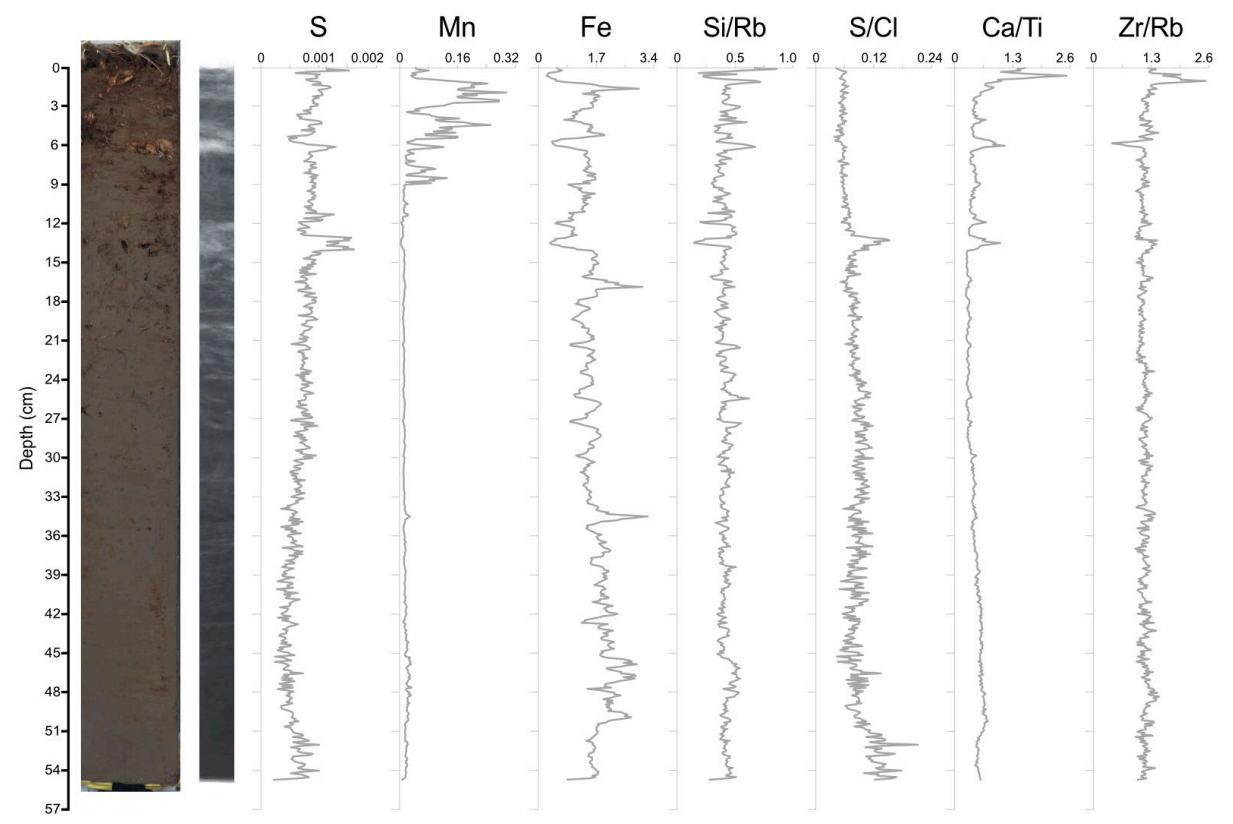


Figure 5.4 – Photo, radiograph, and μ -XRF data for key stable elements in the control core. S, Mn, and Fe graphs have been normalised to total scatter (coherent scatter + incoherent scatter).

5.3.4 Initial Radionuclide Distributions

The pre-treatment radionuclide profiles (Figure 5.5; tabled results in Table C.3) broadly match their respective Sellafield discharge histories, suggesting that the facility was the primary source for these as noted in previous work on the Esk estuary (e.g. Kershaw et al., 1990; Lucey et al., 2004; Marsden et al., 2006; Morris et al., 2000; Ray et al., 2020). The range of activities measured by previously published studies varies, which can be explained by spatial variations of radionuclide distribution present within the saltmarsh (Caborn et al., 2016; Horrill, 1984; Oh et al., 2009)

5.3.5 Defining Peaks of Elevated Radionuclide Activities

The distributions of elevated activities, referred to here as 'peaks', vary between radionuclides and, as such, a uniform procedure was created to consistently define the core depths containing these enriched zones. Full details are included in Table C.3 but are summarised here, with the final regions presented in Table 5.2. A 3-point moving average was applied to each dataset to smooth the profile, and the region of elevated activity was defined by the depth range containing values greater than 30 % of the core maximum. Moving averages have been used to identify peaks in previous work (e.g. Guo and Huan, 2023; Zhou et al., 2022) and an arbitrary 30 % threshold was chosen to maximise the number of data points in each peak for all

radionuclides whilst minimising the tailing included in the results. Whilst this 30 % value was chosen subjectively here to balance these factors consistently for all the profiles in this work, each radionuclide profile underwent the same process and so the discussion and conclusions drawn here are still valid. This smoothing process was only used for identifying regions of elevated activity and not for any subsequent analysis.

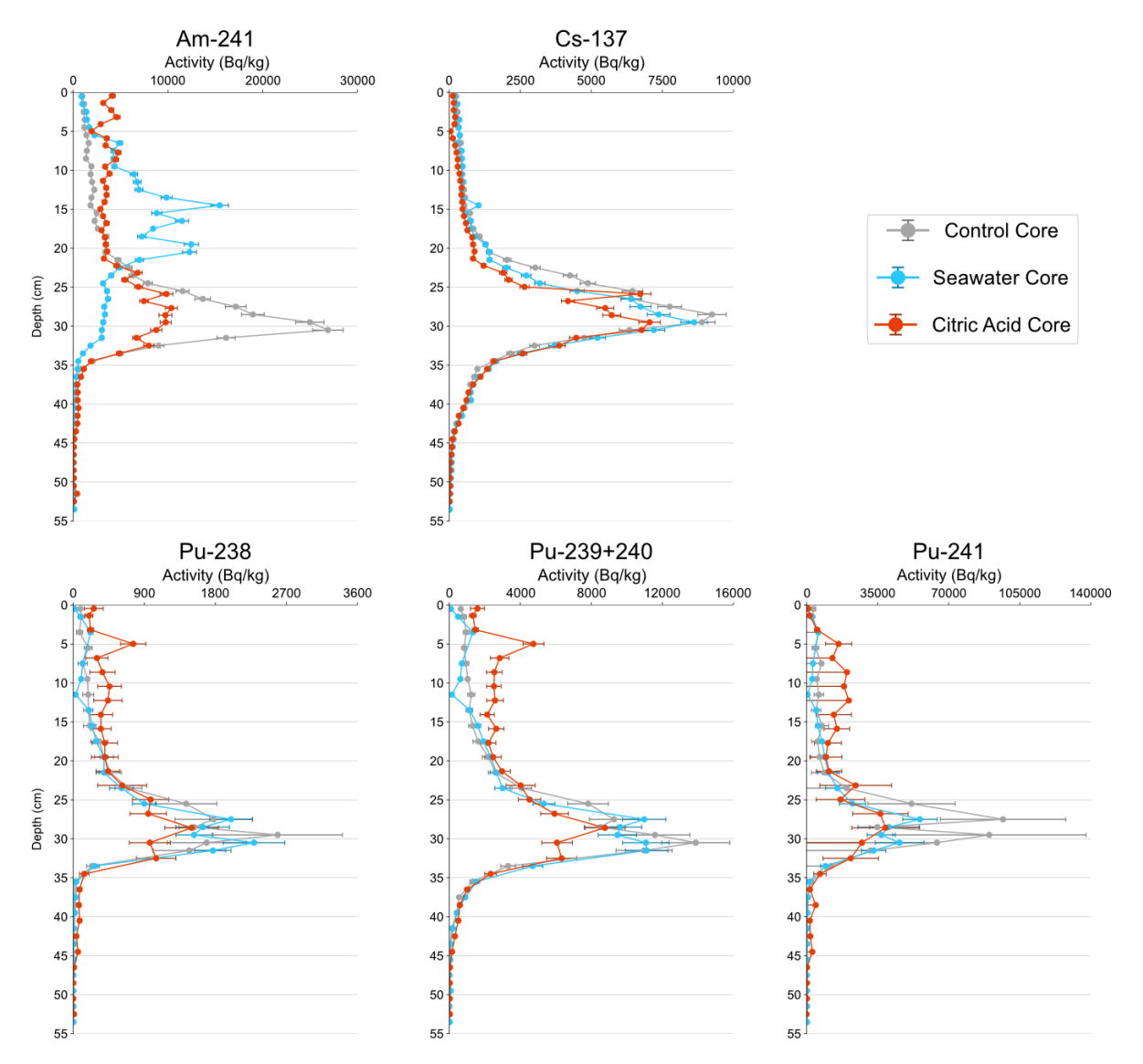


Figure 5.5 – Radionuclide distributions in the control core (grey), seawater core (blue) and citric acid core (orange). Uncertainties are quoted to 2σ . Data points without uncertainties are too small to be seen and those with an uncertainty bar in only one direction indicate the measured sample activity was less than the limit of detection. Samples were not made in replicate and so all uncertainties presented here are analytical and counting uncertainties.

5.3.6 Caesium-137

The majority of Cs-137 (half-life = 30.08 years (Table 4.1; IAEA, 2025)) in the control core is present in a large single subsurface maximum located at 22-33 cm depth (Figure 5.5; Table 5.2). A fraction of Cs released as Cs⁺ into marine environments will associate with fine particulate material, explaining the radionuclide's presence in the saltmarsh (ATSDR, 2004; Cornell, 1992;

USEPA, 1999). K_d s for Cs in sediments are estimated at 10^3 - 10^4 mL/g (Hunt and Kershaw, 1990; IAEA, 2004), with ~ 10 % of Sellafield's discharged Cs-137 estimated to have been stripped from seawater by clay mineral reactions (Jones *et al.*, 1999; Mackenzie and Scott, 1993). This immobilisation is driven by mineral surface sorption, cation exchange, and incorporation into the interstitial layers of mica-like clays such as illite (Cornell, 1992; Fuller *et al.*, 2015; USEPA, 1999).

Treatment with a seawater electrolyte retains the single peak, with a 11 ± 2 % reduction in the region of elevated activity, and a 500 Bq/kg increase in activity at 14-15 cm depth. The citric acid treated sediment also retains the single control core peak, with a 26 ± 2 % remobilisation, in addition to a minor depletion at 4-9 cm and no areas of enrichment throughout. The radionuclide's predominant immobility is likely caused by Cs's affinity for absorption onto and into clay minerals (Fuller et al., 2015; Livens and Baxter, 1988). Over years and decades in the saltmarsh, most Cs migrates into thermodynamically favourable interstitial layers within illites, making it difficult for EKR to remobilise. The greater Cs remobilisation in the citric acid core is unlikely to be caused by direct leaching of the radionuclide, as the organic molecule alone has previously shown minimal impact on Cs desorption from clays (Hazotte et al., 2016; USEPA, 1999). This is supported by sequential extraction by Ray et al. (2020) on Ravenglass Saltmarsh material, where only 1-22 % of Cs-137 was readily available or exchangeable with Mg²⁺. The available and exchangeable fractions will consists of weakly sorbed Cs on the clay mineral edges, as well as onto Fe/Mn oxy(hydr)oxides and organic matter (e.g. Ferris et al., 2000; Sawhney, 1972). Instead, the excess of protons dissociated from citric acid molecules may have entered interstitial clay layers during treatment and prevented subsequent Cs-137 resorption back into the minerals. Time-dependant radionuclide remobility has been observed in experimental data, with lab-scale EKR studies finding significant remobilisation if Cs is introduced to sediment immediately before a current application and a reduced efficacy when Cs is left for days/ weeks before treatment (Buehler et al., 1994; Purkis et al., 2021a; Putra et al., 2022). This trend was not observed in scaled-up trials on contaminated soils from around the Korean Atomic Energy Research Institute (KAERI), where Cs-137 removal efficiencies with a nitric acid electrolyte were ~ 57-94 % (Kim et al., 2010, 2009). However, the sandy, terrestrial sediment had a low proportion of silt- and clay-sized material, making the results less comparable to the complex coastal conditions with varying grain sizes present in this study. In addition, homogenisation of material prior to EKR would be counterintuitive for settings such as the Ravenglass Saltmarsh, where the majority of Cs-137 is present in a ~ 10 cm band within the sediment and, as such, mixing would increase volumes of higher-level contamination needing to be remediated.

Despite a low extent of remobility, Cs-137 enrichment in the seawater core at 14-15 cm coincides with ITRAX concentration spikes in several elements (e.g. Ca, Fe, Mn, Y, rare earth elements; see Figure C.3). This suggests precipitation of Cs⁺ alongside these nuclides, likely due to a pH change generated by the cathodic alkaline front, although further work is needed to determine phases the radionuclide is associated with. Yellow liquid produced by both cores during EKR contained low activities of Cs-137 (Table C.2), supporting solid phase data suggesting minor Cs remobilisation. However, a comparison on activity concentrations between the control core and post-treatment seawater core (including the yellow liquid; Table C.4) show a 96.4 ± 1.9 % radionuclide retention. This first possible explanation for this is by Cs migration into the graphite electrode, which has been shown to be possible (Chapter 4) but is not likely here due to potential precipitation in alkaline conditions present. Instead, the discrepancy is more likely caused by either an incorrect estimation on the volume of yellow liquid produced or the ~ 10 mL sample of yellow liquid collected for analysis was not representative of the 100s-1000s mL generated during treatment. The citric acid core shows an incomplete Cs-137 mass balance even with the yellow liquid accounted for, although the loss is greater than in the seawater core (80.0 ±1.6 %; Table C.4). In addition, the yellow liquid Cs-137 activity in the citric acid core is lower than its seawater counterpart, and there is no corresponding area of enrichment within the citric acid profile to account for this. These points contradict sediment data showing greater remobilisation in the citric acid core, with the most likely reason for this being (in the absence of sediment data suggesting successful migration adjacent to and into the electrode) being more Cs-137 was remobilised by the yellow liquid than that shown by the ~ 10 mL sample collected at the start of its formation. Whilst the misapproximation of yellow liquid generated may also be a contributing factor, the extent of unaccounted-for activity is too great to be solely explained by this. This would likely have been caused by the electrolyte gradually neutralising the cathodic alkaline front, preventing Cs precipitation and instead causing escape through the yellow liquid, assuming the hydraulic conductivity is greater than the rate of electromigration. This loss would need to be investigated before being deployed at larger scales, as the uncontrolled movement of the radionuclide could pose risks to the surrounding area if performed in situ. Anomalous Cs-137 activities in the citric acid material at 4-9 cm depth and 25-26 cm depth can be explained by lateral variations in the clay proportions between cores, which will alter the extent of Cs adsorption and desorption.

5.3.7 Plutonium

Despite large uncertainty values, Pu-238 (half-life = 87.7 years) and Pu-239+240 (Pu-239 half-life = 24110 years; half-life = 6561 years) (Table 4.1; IAEA, 2025) show a similar initial distribution of a single region of elevated activity at \sim 23-33 cm (Figure 5.5; Table 5.2). Pu-241 (half-life = 14.4)

years, (Table 4.1; IAEA, 2025)) data are more erratic as many samples were close to or below the limit of detection (LOD), but the same general trend of a single peak between \sim 25 cm and \sim 33 cm can be seen, with a sharp dip in activity at 28-29 cm depth. Understanding Pu behaviour in natural environments can be a challenge due to its possible speciation as Pu(III), (IV), (V), or (VI), although the (IV) and (V) are the dominant oxidation states in seawater (McMahon et al., 2000; Ray et al., 2020; Vives I Batlle et al., 2008). Reduced Pu(III) and Pu(IV) will rapidly associate with sediments and colloids in oceans whereas oxidised Pu(V) and Pu(VI) is more soluble and likely to be transported with water currents (McMahon et al., 2000; Nelson and Lovett, 1978; Vives I Batlle et al., 2008). It is thought that > 90 % of Pu in the Irish Sea is associated with sediment as Pu(IV) (Mackenzie and Scott, 1993), with the rest remaining in the water column as Pu(V/VI) dioxo-cations (e.g. PuO₂⁺ and PuO₂²⁺) (MacKenzie et al., 1999). Within sediments, Pu has been found to react with a range of minerals such as quartz, calcite, clays, and Fe/ Mn oxy(hydr)oxides (Begg et al., 2013; Keeney-kennicutt and Morse, 1985; Lu et al., 2003; Powell et al., 2005). Mineral surfaces, in addition to micro-organisms, can also mediate the reduction of Pu(V) to Pu(IV) (Powell et al., 2005; Renshaw et al., 2009; Zavarin et al., 2012). Work by Balboni et al. (2022) has shown that Pu in the Ravenglass Saltmarsh becomes recalcitrant to desorption with age due to stabilisation onto sediments and organic matter. As a result of the aforementioned factors as well as variables including the quantity of complexing agents present and the form of Pu that entered the environment (ATSDR, 2010), Pu has a Kd range of 104-106 (IAEA, 2004; Marsden et al., 2006; McDonald et al., 2001).

Only minor changes occur with the distributions of Pu isotopes when treated with seawater. The depths containing elevated activities do not change and, as such, remobilisation of Pu-238, Pu-239+240 and Pu-241 in these areas were determined as $4 \pm 13\%$, $8 \pm 7\%$, and $14 \pm 36\%$, respectively. Regions of depletion for all Pu isotopes are seen at 9-12 cm and areas of minor enrichment are observed for Pu-238 and Pu-239+240 at 3-4 cm. The seawater core 5-6 cm sample was not analysed due to a lack of sediment remaining for analysis. Treatment with citric acid shows a greater depletion of elevated Pu levels, resulting in remobilisation extents of 37 ± 14 % for Pu-238, 37 ± 7 % for Pu-239+240 and 50 ± 43 % for Pu-241. Enriched areas are observed at 0-15 cm for Pu-238 and Pu-239+240, with notable peaks forming for both at 5-6 cm depth. Due to large uncertainty values, the same trends cannot be seen for Pu-241. Whilst seawatertreated Pu-238 and Pu-239+240 show similar distributions, Pu-238 values in the region of elevated activity are within uncertainty both before and after EKR whereas Pu-239+240 values at ~ 25, ~ 27, and ~ 31 cm show a slight decreases post-treatment. Limited remobilisation of total Pu is expected as only a small proportion of the radionuclide was found to be readily exchangeable in Ravenglass Saltmarsh sediments (e.g. McDonald et al., 2001; Ray et al., 2020). This small electromigrated fraction appear to have moved towards the cathode, suggesting a

speciation of positively-charged Pu ions and/or colloids (Agnew et al., 2011). Modelled Eh/pH diagrams suggest that under acidic conditions created by the pH gradient, cationic Pu could exist as Pu(V)O₂⁺, Pu(IV)O₂ or Pu(III) (Takeno, 2005), of which only PuO₂⁺ and Pu(III) are charged. Migration may have been instigated by at least one of either direct remobilisation of the radionuclide or by minor dissolution of Fe oxyhydroxide phases that Pu has been shown to have an affinity for (e.g. Eilbeck and Learmonth, 1999; Powell et al., 2005; Sanchez et al., 1985). Fe mobilisation has been shown to occur during EKR (Cundy and Hopkinson, 2005), and the element was found in high concentrations in yellow liquid produced by both cores during treatment (Table C.2). Towards the top of the core, a depletion of Pu-238 and Pu-239+240 at 9-12 cm, as well as an enrichment at 3-4 cm, can also be seen. Models for Eh/pH diagrams suggest the Pu present in alkaline conditions, implied from early pH measurements during EKR (Figure C.2), a white precipitate on the core, and an XRF Ca spike (interpreted as CaCO₃) at 12-18 cm depth, would likely form uncharged $Pu(IV)O_2$ (Takeno, 2005) which would not electromigrate. As such, mobilisation at this depth likely only occurred in colloidal form. The area of enrichment coincides with a large spike in Mn concentration, although XRF measurements in this area failed quality control validity checks due to the core surface having been degraded by EKR and so cannot be confirmed as genuine. As such, post-EKR Pu may be associated with Mn phases, but further work would be needed to confirm this. The uncertainty of Pu-241 remobilisation is much larger in comparison to the lighter isotopes, making a definitive profile difficult to resolve. However, it is likely to display the same trend of little to no migration as EKR does not discriminate between isotopes, meaning that if Pu-238 and Pu-239+240 do not remobilise then Pu-241 will be similarly immobile. Mass balances for Pu-238 and Pu-241 between the control core and the treated seawater core are within uncertainty (92.8 \pm 9.9 % and 100.8 \pm 37.4 %, respectively; Table C.4) but Pu-239+240 shows a slightly decrease in total activity (89.4 \pm 5.3 %). Since the lattermost of these has the smallest uncertainty of the three values and all Pu isotopes are expected to behave similarly, it is likely that all isotopes have lost a small proportion of their starting values. This missing fraction may be located inside the cathode, as the Pu-239+240 enrichment zone is in proximity to the graphite, or may have been contained within the yellow liquid lost from the core during the later stages of treatment, and was consequently not accounted for. If the latter option is true, further investigations would be required on how to retain this fraction and avoid loss into the wider environment if deployed in situ. Results for the solid phase (sediment) here are similar to those found by Cundy and Hopkinson (2005) when treating Ravenglass sediment with a seawater electrolyte, with no significant Pu remobilisation. Even with a higher voltage gradient used here (0.5 V/cm compared to ~ 0.1 V/cm), the radionuclide showed little mobility which suggests much greater voltages may be required in order to obtain satisfactory remediation levels.

Similar behaviours between Pu-238 and Pu-239+240 are seen in the citric acid core, with both showing significant remobilisation within the peak area and enrichment within the top ~ 15 cm. The peak at 5-6 cm is likely caused by the cathodic alkaline zone, resulting in precipitation of Pu. ITRAX data at this depth failed quality control validation checks due to a void in the sediment, making interpretations of post-deposition Pu associations inconclusive. The same distribution is likely present for Pu-241 since EKR does not discriminate between isotopes but, due to most samples being close to or at the limits of detection, these are masked by the erratic profile. Migration of Pu-238 and 239+240 occurred towards the cathode, implying movement in colloidal and/or cationic forms (Abdel-Fattah et al., 2013; Agnew et al., 2011). Similarly to the seawater core, cationic Pu would likely exist as Pu(V) or Pu(IV) (McMahon et al., 2000; Takeno, 2005), and may have migrated through both direct remobilisation of the radionuclide or dissolution of the Fe phases that Pu was associated with (Powell et al., 2005; Sanchez et al., 1985). However, this contradicts Pu-citrate equilibrium data (albeit in simplified systems in comparison to the sediment here) (e.g. NEA, 2005; Tanaka et al., 2009), and previous EKR work that observed the radionuclide migrating towards the anode when treated with citric acid (Agnew et al., 2011) likely as a negatively-charged Pu-citrate complex. This may be caused by citrate ions preventing positively-charged Pu from resorbing onto otherwise available phases (Lucey et al., 2007, 2004), allowing migration to within proximity of the cathode. Inhibiting this resorption when leaching Pu associated with acid-soluble and reducible phases in Ravenglass Saltmarsh sediments can cause significant increases in total extraction (~ 50 % with citric acid present (Lucey et al., 2007), in comparison to ~ 5 % through conventional Tessier sequential extraction techniques (e.g. McDonald et al., 2001; Ray et al., 2020)). The remaining Pu fraction remained immobilised in organic or mineral phases (Lucey et al., 2007, 2004; Ray et al., 2020). Previous pilot EKR on aged soils at the Atomic Weapons Establishment Aldermaston site (Berkshire, UK) showed a lesser degree of Pu remobilisation with a citric acid electrolyte (Agnew et al., 2011). A notable proportion of Pu was remobilised towards the anode, leaving ~ 16 % of starting material below the 1700 Bq/kg activity threshold and reclassifying it as non-radioactive. However, the concentration of citric acid used was much lower than the study present here (0.04 M compared to 1.56 M) which may explain the difference in remediation efficiencies. Conditions within the terrestrial sediment will differ from those observed in more complex, dynamic systems, such as coastlines. In addition, Pu present in the Ravenglass Saltmarsh is primarily concentrated within a ~ 10 cm band (Marsden et al., 2006; McDonald et al., 2001; Ray et al., 2020), meaning that sediment homogenisation pre-EKR would increase the starting volumes of higher-level contamination. When comparing Pu mass balance between the control core and post-treatment citric acid core, a much greater loss of all isotopes is seen compared to the seawater core (79.2 \pm 9.6 %, 77.4 \pm 4.7 %, and 71.1 \pm 32.9 % for Pu-238, Pu-239+240, and Pu-241, respectively; Table C.4). Whilst it is possible the unaccounted-for fraction would be

present in one or both of the electrodes, the lack of Pu activity immediately adjacent to the graphite locations suggests this is unlikely. Instead, loss into the yellow liquid, after the portion that was later analysed had been taken, is more plausible. Pu present in the fluid may be present as neutrally-charged colloids, which would explain why some of the element appeared to undergo electrophoresis/electromigration as expected, whilst a minor component did not. The notable proportions unaccounted for require further work to understand why they are less amenable to EKR and how to retain them within proximity of the electrode(s).

5.3.8 Americium-241

Initial Am-241 (half-life = 432.6 years (Table 4.1; IAEA, 2025)) distribution closely mimics that of Cs-137, with a large, single peak at 24-33 cm depth containing much of the total activity (Figure 5.5; Table 5.2). Am-241 is commonly found as Am(III) under environmental conditions (Morris *et al.*, 2000). In seawater, the radionuclide will rapidly hydrolyse to Am(OH)₃, Am(OH)₂⁺, and Am(OH)²⁺ (Choppin, 2007), allowing it to readily complex with humates and sorb to suspended sediments and colloids that eventually settle out (Choppin, 2007; MacKenzie *et al.*, 1994; McMahon *et al.*, 2000). Consequently, Am is predominantly immobilised in soils and sediments (ATSDR, 2004), with most Sellafield-derived Am-241 in the Irish Sea thought to now be in its (III) oxidation state and associated with fine-grained material (MacKenzie *et al.*, 1999). The range of reported K_d s for Am are 10^4 - 10^6 mL/g (IAEA, 2004; Marsden *et al.*, 2006; McMahon *et al.*, 2000), with the lower of these values measured in lower salinity and lower pH conditions.

The seawater-treated core shows both migration and broadening of the initial Am-241 peak. Remobilisation extent is determined as 81 ± 3 %, with the new area of enrichment located at 6-24 cm. At depths where the initial peak was observed, Am-241 activities plateau at ~ 3000 Bq/kg. Despite the migration of the radionuclide peak, activities present within the ~ 4 cm closest to the cathode remained broadly consistent before and after EKR. For the citric acid core, the region of elevated activity has remained at its initial depth, albeit with a 49 ± 3 % reduction in activity. An area of enrichment is seen at 0-17 cm, forming a plateau of ~ 3000-5000 Bq/kg. Remobilisation of Am-241 within the seawater core towards the cathode implies the presence of positively charged ions and/or colloids. Based upon modelled Eh/pH diagrams, albeit for simplified systems compared to this sediment, cationic Am would likely exist as Am(III) in acidic to neutral conditions, with the potential of Am(OH)²⁺ species also present at pH ~ 7 (Takeno, 2005). However, the area of elevated activity in the seawater core correlates with both the location of the predominant ITRAX Ca spike, and visual observations of a white precipitate formation on the core surface after EKR. This suggests Am adsorption onto CaCO3 that precipitated due to the cathodic alkaline front, consistent with previous work showing Am's high affinities for the mineral phase (Higgo and Rees, 1986; Shanbhag and Morse, 1982).

Further, a spike in Mn abundance at 12-14 cm coincides with the upper region of elevated Am activities, potentially aiding immobilisation through adsorption onto Mn oxides (Means et al., 1978). Sequential extractions for Am in Ravenglass sediments suggest that the majority is associated with oxidisable sulphides and organic material, although the proportions can be variable e.g. 58-87 % (sulphides, organics, and inorganic oxides) measured by McDonald et al. (2001) and 14-77 % (sulphides and organics) recorded by Ray et al. (2020). Since the sediments collected did not show evidence of extensive sulphate reduction or secondary sulphide precipitation (see Section 5.3.3.2), it is most likely that Am was associated with organic phases. Despite this, S measurements for the seawater core correlate well with the Ca profile, suggesting that Am may have bound to S minerals once immobilised. The minority of Am remaining in the initial area of elevated activity is likely associated with refractory phases that were not remobilised in the experiments. Previous EKR work with Am is limited but Cundy and Hopkinson (2005) found no significant movement of the radionuclide when treating Ravenglass sediment using a seawater electrolyte. However, the ~ 0.1 V/cm voltage gradient applied in the 2005 study was lower than the 0.5 V/cm used here, suggesting there is a threshold gradient at which certain Am phases are remobilised. Control core and post-EKR seawater core mass balance (including Am-241 found in the yellow liquid, scaled to the approximate volume generated over the treatment period) shows a minor loss of Am-241 (89.8 ± 2.0 %; Table C.4) which, whilst possibly associated with migration into the cathode (although unlikely due to limited evidence of migration adjacent to the cathode), is likely explained by either an incorrect approximation of the yellow liquid generated or varying rates of loss into the yellow liquid over time. As the analysed yellow liquid was only collected when the fluid was first observed, if Am-241 loss from the core via this pathway did not happen at a constant rate then this would explain the inconsistency in activity. Additional work into how to retain the unaccounted-for fraction is needed to optimise the overall efficacy in scaled-up trials.

In the citric acid core, significant Am migration towards the cathode also occurred likely as Am(III) ions (Takeno, 2005) or in colloidal form. In the presence of citric acid, negatively-charged Am-citrate would be the expected species created (USEPA, 1999), but no such area of elevated activity near the anode was present. Since negatively-charged Am-citrates are preferentially produced over their positively-charged counterparts (USEPA, 1999), migration of the radionuclide by citric acid seems unlikely. Further, although Am(III) can be generated in acidic conditions it would still retain its high affinity for sediments, limiting its migration distance. As such, the predominant phase for the radionuclide is likely association with positively-charge colloids. The region of Am enrichment in the top ~ 15 cm of the core coincides with an increased abundance of Fe (Figure 5.4), making it the likely sorption site for the radionuclide. In addition, the neutralised alkaline front in the cathodic region, caused by the citric acid

electrolyte, promotes migration closer towards the cathode, as precipitation due to increasing pH is negated. The majority of migrated Am likely originated in association with organic material, as shown by sequential extraction studies on Irish Sea and Ravenglass Saltmarsh sediments, with only a small proportion bound to readily exchangeable sites (McDonald et al., 2001; Ray et al., 2020). The decrease in radionuclide activities at ~ 5 cm relative to the control core coincided with a visual observation of plant material in the core at the same depth, likely being the cause the Am abundance decrease. An activity mass balance between the control core a treated citric acid core (including the yellow liquid) highlights a loss of the starting Am-241 inventory (79.1 ± 1.6 % recovery from citric acid core; Table C.4). Whilst the location(s) of this fraction are unknown, it is likely to be found in either or both of the graphite cathode, evidenced by elevated activities around the electrode location, or in the yellow liquid that was generated after the analysed sample was collected. If present in the cathode, the Am-241 is likely bound to a positively-charged colloid, whereas in the yellow solution the colloid polarity is unknown, although a neutral charge would explain why some of the radionuclide was able to successfully migrate whilst a minority component was purged from the core. This process must be better understood before in situ trials would be performed, as unmanaged radionuclide remobilisation could pose issues for the surrounding environment.

Radionuclide	Depth of 'region of elevated activity' (cm)	Core section	Remobilisation across entire region of elevated activity (%)
Cs-137	22-33	Seawater	11 ± 2
		Citric acid	26 ± 2
Pu-238	23-33	Seawater	4 ± 13
		Citric acid	37 ± 14
Pu-239	23-33	Seawater	8 ± 7
		Citric acid	37 ± 7
Pu-241	24-32	Seawater	14 ± 36
		Citric acid	50 ± 43
Am-241	24-33	Seawater	81 ± 3
		Citric acid	49 ± 3

Table 5.2 – Summary table for definition and range of radionuclide regions of elevated activity, and extent of radionuclide remobilisation for each core. Uncertainties are quoted to 2σ . Samples were not made in replicate and so all uncertainties presented here are analytical and counting uncertainties.

5.3.9 Electrolyte Comparison and Upscaling Requirements

Citric acid was the more effective electrolyte for both Cs-137 and Pu (Table 5.2), which is consistent with previous usage for remobilising these metals (e.g. Agnew et al., 2011; Kim et al., 2010, 2009). Whilst the presence of citrate ions may not have directly resulted in electromigration of either radionuclide, a combination of hydrogen cation incorporation into clays preventing Cs resorption and citrate complexation with Pu promoted a significant reduction in activities within the region of elevated activities. In contrast, the combination of seawater electrolyte constituents, and 0.5 V/cm EKR were not sufficient for extraction of radionuclides from strong binding sites such as interstitial clay layers, and organic complexes and colloids. However, a seawater electrolyte was superior for Am remobilisation compared to citric acid. Although not fully constrained, complexation or substitution between dissolved ions in seawater and colloidal material appears the most likely mechanism for Am transport. The radionuclide's strong post-treatment association with Ca, interpreted as CaCO3, in the seawater core suggests that precipitation only occurred due to a change in pH and that buffering of the alkaline zone could allow Am to migrate adjacent to the cathode. However, whilst citric acid was generally the superior electrolyte to seawater for remobilisation, it caused ~ 10 % greater loss in core radionuclide inventories compared to its seawater counterpart. Whilst this is likely a result of either only analysing the initial fraction of yellow liquid produced and scaling the measured activities to the total approximated yellow liquid generated, which introduces a number of assumptions, this requires further investigation before the technology can be applied in situ at site scales to prevent risk of radionuclide loss into the environment. If this issue cannot be resolved then citric acid usage may be limited to ex situ trials only, where the electrolyte can be contained and collected post-treatment.

Whilst both Am and Pu were similar in levels of remobilisation and distribution post-citric-acid treatment (Table 5.2), use of a seawater electrolyte resulted in very different behaviours. This would suggest that Am and Pu were associated with different phases, likely because of differing oxidation states (Am(III) vs Pu(IV) or Pu(V)), with Am-bound material being amenable to electrophoresis and Pu phases being immobile Pu(IV).

The 0.5 V/cm voltage gradient used in this study was selected as a realistic lower bound for field-scale EKR trials. With this setup, Am-241 has shown the greatest potential for remediation in these dynamic coastal sediments. The radionuclide's remobilisation with a seawater electrolyte shows promise as the lack of additional chemicals required during field deployment will be advantageous for operators globally and streamline project timescales. In addition, the possibility for Am migration immediately adjacent to the cathode if the alkaline front is buffered would make removal of contaminated material quicker and easier, further improving the appeal

of EKR. Treatment with citric acid is a better compromise for simultaneous remediation of Am and Pu and offers the benefit of neutralising any alkaline zones, enhancing migration distances. However, this would reduce the efficiency of Am remediation, and further work is needed to identify the location of the unaccounted-for radionuclide inventories and prevent their loss from the solid phase, enhance the overall proportion of actinide remobilised, and promote subsequent immobilisation in a single peak near the cathode instead of a diffuse area of enrichment over ~ 15 cm. One possible way to progress the lattermost two points would be by using greater voltages, although the high affinities for sediments are likely to remain the primary factor in Am and Pu mobilities. Whilst Cs remobilisation was the least effective of the radionuclides tested and increased voltages are only likely to mobilise ions close to clay mineral edges. This may mean that electrolytes chosen specifically to target Cs-137 may be required e.g. those with high concentrations of K⁺ as they may substitute with Cs in the interstitial layers (Lammers et al., 2017; Ritchie and McHenry, 1990) although work by Purkis et al. (2021a) indicates that electrolytes with < 1000 ppm KCl are not sufficient for this exchange to take place in organic-rich sediments. However, addition of electrolyte prior to EKR may increase the rate of substitution and therefore final remediation efficiency.

To the authors' knowledge, this study is the first to show significant Am remobility in aged sediments. Historically high discharge activities into oceans from nuclear sites (e.g. BNFL, 1979-2005; GRNC, 1999; IAEA, 2015), long half-lives of Am-241 (433 years) and Am-243 (7364 years) (IAEA, 2025), and large contribution to long-term dose rates on account of its beta decay to Pu-241 (IAEA, 2025; Ray et al., 2020), make it a radionuclide of focus for coastline remediation. Notable remobilisation efficiencies, particularly in cheap and abundant electrolytes such as seawater, show the potential for effective treatment of sediments, even at low voltages that are more cost-effective and sustainable than conventional remediation techniques (Purkis et al., 2021b). Additional work is required to remobilise the residual fractions of the peaks, however. Am shares similar chemical properties and sediment partition behaviours with Cm, another actinide produced in the nuclear fuel cycle (BNFL, 1979-2005; Posey, 1973; Wang et al., 2022). Work here therefore highlights the potential for effective Cm clean-up with EKR, although further work is needed to confirm this. This study also demonstrates the trade-off between targeting an increased remobilisation of a single radionuclide (e.g. Am-241 with seawater electrolyte) and the lower remediation potential of simultaneous clean-up of multiple nuclides (e.g. Am-241, Pu, and Cs-137 with citric acid electrolyte). With each contaminated site across the world having its own unique characteristics, challenges, and decontamination thresholds, giving remediation workers the flexibility to prioritise single or multiple radionuclides is a useful tool for mitigating the legacy of nuclear in coastal environments.

Acknowledgements

The authors would like to thank the BOSCORF team at the National Oceanography Centre Southampton for access to and assistance with the XRF data collection, GAU-Radioanalytical, University of Southampton for their assistance and advice with radionuclide analysis, and the NNUF-EXACT facility (grant number EP/T011548/1) for use of laboratory facilities.

Acknowledgements also go to the TRANSCEND Consortium (grant number: EP/S01019X/1) for their support throughout the project. The authors would also like to thank Mark Taylor and Phoebe Hudson for advice on data analysis and manipulation, as well as Dr. Jamie Purkis and Dr. Sarah Lu for useful discussions.

Funding

Funding for the project was provided by the National Environmental Research Council through the INSPIRE DTP (grant number: NE/S007210/1).

Notes

The authors declare no competing financial interest.

5.4 References

Abdel-Fattah, A.I., Zhou, D., Boukhalfa, H., Tarimala, S., Ware, S.D., Keller, A.A., 2013. Dispersion Stability and Electrokinetic Properties of Intrinsic Plutonium Colloids: Implications for Subsurface Transport. Environ. Sci. Technol. 47, 5626–5634. https://doi.org/10.1021/es304729d

Acar, Y.B., Gale, R.J., Alshawabkeh, A.N., Marks, R.E., Puppala, S., Bricka, M., Parker, R., 1995. Electrokinetic remediation: Basics and technology status. Journal of Hazardous Materials, Soil Remediation: Application of Innovative and Standard Technologies 40, 117–137. https://doi.org/10.1016/0304-3894(94)00066-P

Agnew, K., Cundy, A.B., Hopkinson, L., Croudace, I.W., Warwick, P.E., Purdie, P., 2011. Electrokinetic remediation of plutonium-contaminated nuclear site wastes: Results from a pilot-scale on-site trial. Journal of Hazardous Materials 186, 1405–1414. https://doi.org/10.1016/j.jhazmat.2010.12.016

ASTM International, 2024. Standard Test Methods for pH of Soils.

https://doi.org/10.1520/D4972-19

ATSDR, 2010. Toxicological Profile for Plutonium. Agency for Toxic Substances and Disease Registry, Atlanta, Georgia.

ATSDR, 2004. Toxicological Profile for Americium. Agency for Toxic Substances and Disease Registry, Atlanta, Georgia.

Balboni, E., Merino, N., Begg, J.D., Samperton, K.M., Zengotita, F.E., Law, G.T.W., Kersting, A.B., Zavarin, M., 2022. Plutonium mobilization from contaminated estuarine sediments, Esk Estuary (UK). Chemosphere 308, 136240. https://doi.org/10.1016/j.chemosphere.2022.136240

Begg, J.D., Zavarin, M., Zhao, P., Tumey, S.J., Powell, B., Kersting, A.B., 2013. Pu(V) and Pu(IV) Sorption to Montmorillonite. Environ. Sci. Technol. 47, 5146–5153. https://doi.org/10.1021/es305257s

BNFL, 1979. Annual Discharge Monitoring Reports 1979-2005. British Nuclear Fuels Ltd. (BNFL)/ Sellafield Ltd.

Brown, S., Hanson, S., Nicholls, R.J., 2014. Implications of sea-level rise and extreme events around Europe: a review of coastal energy infrastructure. Climatic Change 122, 81–95. https://doi.org/10.1007/s10584-013-0996-9

Buehler, M.F., Surma, J.E., Virden, J.W., 1994. In situ soil remediation using electrokinetics. Presented at the 33rd hanford Symposium on Helath and the Environment, Richland, Washington.

Byrd, N., Lloyd, J.R., Small, J.S., Taylor, F., Bagshaw, H., Boothman, C., Morris, K., 2021.

Microbial Degradation of Citric Acid in Low Level Radioactive Waste Disposal: Impact on
Biomineralization Reactions. Front. Microbiol. 12. https://doi.org/10.3389/fmicb.2021.565855

Caborn, J.A., Howard, B.J., Blowers, P., Wright, S.M., 2016. Spatial trends on an ungrazed West Cumbrian saltmarsh of surface contamination by selected radionuclides over a 25 year period. Journal of Environmental Radioactivity 151, 94–104.

https://doi.org/10.1016/j.jenvrad.2015.09.011

Chaplin, J.D., Christl, M., Cundy, A.B., Warwick, P.E., Reading, D.G., Bochud, F., Froidevaux, P., 2022. Bioavailable actinide fluxes to the Irish Sea from Sellafield-labelled sediments. Water Research 221, 118838. https://doi.org/10.1016/j.watres.2022.118838

Choppin, G.R., 2007. Actinide speciation in the environment. J Radioanal Nucl Chem 273, 695–703. https://doi.org/10.1007/s10967-007-0933-3

Colombano, D.D., Litvin, S.Y., Ziegler, S.L., Alford, S.B., Baker, R., Barbeau, M.A., Cebrián, J., Connolly, R.M., Currin, C.A., Deegan, L.A., Lesser, J.S., Martin, C.W., McDonald, A.E., McLuckie, C., Morrison, B.H., Pahl, J.W., Risse, L.M., Smith, J.A.M., Staver, L.W., Turner, R.E., Waltham, N.J., 2021. Climate Change Implications for Tidal Marshes and Food Web Linkages to Estuarine and Coastal Nekton. Estuaries and Coasts 44, 1637–1648. https://doi.org/10.1007/s12237-020-00891-1

Cornell, R.M., 1992. Adsorption Behaviour of Cesium on Marl. Clay Minerals 27, 363–371. https://doi.org/10.1180/claymin.1992.027.3.09

Croudace, I., Warwick, P., Taylor, R., Dee, S., 1998. Rapid procedure for plutonium and uranium determination in soils using a borate fusion followed by ion-exchange and extraction chromatography. Analytica Chimica Acta 371, 217–225. https://doi.org/10.1016/S0003-2670(98)00353-5

Croudace, I.W., Rindby, A., Rothwell, R.G., 2006. ITRAX: description and evaluation of a new multi-function X-ray core scanner. Geological Society, London, Special Publications 267, 51–63. https://doi.org/10.1144/GSL.SP.2006.267.01.04

Cundy, A.B., Hopkinson, L., 2005. Electrokinetic iron pan generation in unconsolidated sediments: implications for contaminated land remediation and soil engineering. Applied Geochemistry 20, 841–848. https://doi.org/10.1016/j.apgeochem.2004.11.014

Davies, S.J., Lamb, H.F., Roberts, S.J., 2015. Micro-XRF Core Scanning in Palaeolimnology: Recent Developments, in: Croudace, I.W., Rothwell, R.G. (Eds.), Micro-XRF Studies of Sediment Cores: Applications of a Non-Destructive Tool for the Environmental Sciences, Developments in Paleoenvironmental Research. Springer Netherlands, Dordrecht, pp. 189–226. https://doi.org/10.1007/978-94-017-9849-5_7

Eilbeck, A.B., Learmonth, P.E., 1999. An Experiment into the Application of Electrokinetic Remediation to Contaminated Sellafield Soils (No. RDR 1707). British Nuclear Fuels Ltd., Sellafield, UK.

Ferris, F.G., Hallberg, R.O., Lyvén, B., Pedersen, K., 2000. Retention of strontium, cesium, lead and uranium by bacterial iron oxides from a subterranean environment. Applied Geochemistry 15, 1035–1042. https://doi.org/10.1016/S0883-2927(99)00093-1

Francis, A.J., Dodge, C.J., 2009. Microbial Transformation of Actinides and Other Radionuclides. Presented at the Proceedings of the DAE-BRNS symposium on nuclear and radiochemistry, Brookhaven National Laboratory, Mumbia, India.

Francis, A.J., Dodge, C.J., Chatterjee, S.D., Landrey, M.F., 1994. Citrate Biodegradation (No. BNL-60830). Brookhaven National Laboratory, New York.

Froelich, P.N., Klinkhammer, G.P., Bender, M.L., Luedtke, N.A., Heath, G.R., Cullen, D., Dauphin, P., Hammond, D., Hartman, B., Maynard, V., 1979. Early oxidation of organic matter in pelagic sediments of the eastern equatorial Atlantic: suboxic diagenesis. Geochimica et Cosmochimica Acta 43, 1075–1090. https://doi.org/10.1016/0016-7037(79)90095-4

Fuller, A.J., Shaw, S., Ward, M.B., Haigh, S.J., Mosselmans, J.F.W., Peacock, C.L., Stackhouse, S., Dent, A.J., Trivedi, D., Burke, I.T., 2015. Caesium incorporation and retention in illite interlayers. Applied Clay Science 108, 128–134. https://doi.org/10.1016/j.clay.2015.02.008

Ge, L., Lai, W., Lin, Y., 2005. Influence of and correction for moisture in rocks, soils and sediments on in situ XRF analysis. X-Ray Spectrometry 34, 28–34. https://doi.org/10.1002/xrs.782

Google LLC, 2025. Google Maps. URL https://www.google.co.uk/maps/@54.340246,-3.403555,5113m/ (accessed 28.11.24).

Gray, J., Jones, S.R., Smith, A.D., 1995. Discharges to the environment from the Sellafield site, 1951-1992. J. Radiol. Prot. 15. https://doi.org/10.1088/0952-4746/15/2/001

Grimston, M., Nuttall, W.J., Vaughan, G., 2014. The siting of UK nuclear reactors. J. Radiol. Prot. 34, R1. https://doi.org/10.1088/0952-4746/34/2/R1

GRNC, 1999. Annual Environmental Monitoring Reports - La Hague.

Guo, J., Huan, T., 2023. Mechanistic Understanding of the Discrepancies between Common Peak Picking Algorithms in Liquid Chromatography–Mass Spectrometry-Based Metabolomics. Anal. Chem. 95, 5894–5902. https://doi.org/10.1021/acs.analchem.2c04887

Hahladakis, J.N., Latsos, A., Gidarakos, E., 2016. Performance of electroremediation in real contaminated sediments using a big cell, periodic voltage and innovative surfactants. Journal of Hazardous Materials 320, 376–385. https://doi.org/10.1016/j.jhazmat.2016.08.003

Halcrow, 2013. Ravenglass Estuary Complex, North West Estuaries Processes Reports. Halcrow Group Ltd., York.

Hazotte, A.A., Peron, O., Abdelouas, A., Montavon, G., Lebeau, T., 2016. Microbial mobilization of cesium from illite: The role of organic acids and siderophores. Chemical Geology 428, 8–14. https://doi.org/10.1016/j.chemgeo.2016.02.024

Heiri, O., Lotter, A.F., Lemcke, G., 2001. Loss on ignition as a method for estimating organic and carbonate content in sediments: reproducibility and comparability of results. Journal of Paleolimnology 25, 101–110. https://doi.org/10.1023/A:1008119611481

Higgo, J.W., Rees, V.C., 1986. Adsorption of Actinides by Marine Sediments: Effect of the Sediment/Seawater Ratio on the Measured Distribution Ratio. Environmental Science & Technology 20, 483–490.

Horrill, A.D., 1984. Radionuclide levels and distribution in grazed saltmarsh in West Cumbria. Environmental Pollution Series B, Chemical and Physical 8, 265–280. https://doi.org/10.1016/0143-148X(84)90027-2

Huang, D., Xu, Q., Cheng, J., Lu, X., Zhang, H., 2012. Electrokinetic Remediation and Its Combined Technologies for Removal of Organic Pollutants from Contaminated Soils. International Journal of Electrochemical Science 7, 4528–4544. https://doi.org/10.1016/S1452-3981(23)19558-7

Hunt, G.J., Kershaw, P.J., 1990. Remobilisation of artificial radionuclides from the sediment of the Irish Sea. Journal of Radiological Protection 10. https://doi.org/10.1088/0952-4746/10/2/009

IAEA, 2025. IAEA Nuclear Data Services. URL https://www-nds.iaea.org/ (accessed 13.1.25).

IAEA, 2015. Annex IV of Technical Volume 4 Radioactivity in the Marine Environment Arising From Releases Following the Fukushima Daiichi Accidient (Technical Volume 4), The Fukushima Daiichi Accident. International Atomic Energy Agency, Vienna.

IAEA, 2004. Sediment Distribution Coefficients and Concentration Factors for Biota in the Marine Environment (No. 422), Technical Reports Series. International Atomic Energy Agency, Vienna.

ISO, 2021. ISO 10390:2021 Soil, treated biowaste and sludge – Determination of pH.

Jones, D.G., Roberts, P.D., Strutt, M.H., Higgo, J.J., Davis, J.R., 1999. Distribution of 137Cs and inventories of 238Pu, 239/240Pu, 241Am and 137Cs in Irish Sea intertidal sediments. Journal of Environmental Radioactivity 44, 159–189. https://doi.org/10.1016/S0265-931X(98)00133-7

Keeney-kennicutt, W.L., Morse, J.W., 1985. The redox chemistry of Pu(V)O2+ interaction with common mineral surfaces in dilute solutions and seawater. Geochimica et Cosmochimica Acta 49, 2577–2588. https://doi.org/10.1016/0016-7037(85)90127-9

Kershaw, P.J., Pentreath, R.J., Woodhead, D.S., Hunt, G.J., 1992. A Review of Radioactivity in the Irish Sea (No. MAFF-AEMR-32), Aquatic Environment Monitoring Report. Ministry of Agriculture, Fisheries and Food, United Kingdom.

Kershaw, P.J., Woodhead, D.S., Malcolm, S.J., Allington, D.J., Lovett, M.B., 1990. A sediment history of sellafield discharges. Journal of Environmental Radioactivity 12, 201–241. https://doi.org/10.1016/0265-931X(90)90024-P

Kim, G.-N., Choi, W.-K., Lee, K.-W., 2010. Decontamination of radioactive concrete using electrokinetic technology. J Appl Electrochem 40, 1209–1216. https://doi.org/10.1007/s10800-010-0088-8

Kim, G.-N., Yang, B.-I., Choi, W.-K., Lee, K.-W., Hyeon, J.-H., 2009. Washing-Electrokinetic Decontamination For Concrete Contaminated With Cobalt and Cesium. Nuclear Engineering and Technology 41, 1079–1086. https://doi.org/10.5516/NET.2009.41.8.1079

Kim, W.-S., Park, G.-Y., Kim, D.-H., Jung, H.-B., Ko, S.-H., Baek, K., 2012. In situ field scale electrokinetic remediation of multi-metals contaminated paddy soil: Influence of electrode configuration. Electrochimica Acta, EREM 2011 + ISEE'Cap 2011 + EMRS 2011 86, 89–95. https://doi.org/10.1016/j.electacta.2012.02.078

Kopytko, N., Perkins, J., 2011. Climate change, nuclear power, and the adaptation–mitigation dilemma. Energy Policy 39, 318–333. https://doi.org/10.1016/j.enpol.2010.09.046

Kylander, M.E., Ampel, L., Wohlfarth, B., Veres, D., 2011. High-resolution X-ray fluorescence core scanning analysis of Les Echets (France) sedimentary sequence: new insights from chemical proxies. Journal of Quaternary Science 26, 109–117. https://doi.org/10.1002/jqs.1438

Lammers, L.N., Bourg, I.C., Okumura, M., Kolluri, K., Sposito, G., Machida, M., 2017. Molecular dynamics simulations of cesium adsorption on illite nanoparticles. Journal of Colloid and Interface Science 490, 608–620. https://doi.org/10.1016/j.jcis.2016.11.084

Lee, E., 2019. Chapter 1 - Electrophoresis of a Single Rigid Particle, in: Lee, E. (Ed.), Interface Science and Technology, Theory of Electrophoresis and Diffusiophoresis of Highly Charged Colloidal Particles. Elsevier, pp. 3–45. https://doi.org/10.1016/B978-0-08-100865-2.00001-1

Livens, F.R., Baxter, M.S., 1988. Chemical associations of artificial radionuclides in Cumbrian soils. Journal of Environmental Radioactivity 7, 75–86. https://doi.org/10.1016/0265-931X(88)90043-4

Lu, N., Reimus, P.W., Parker, G.R., Conca, J.L., Triay, I.R., 2003. Sorption kinetics and impact of temperature, ionic strength and colloid concentration on the adsorption of plutonium-239 by

inorganic colloids. Radiochimica Acta 91, 713–720. https://doi.org/10.1524/ract.91.12.713.23422

Lucey, J.A., Gouzy, A., Boust, D., Vintró, L.L., Bowden, L., Finegan, P.P., Kershaw, P.J., Mitchell, P.I., 2004. Geochemical fractionation of plutonium in anoxic Irish Sea sediments using an optimised sequential extraction protocol. Applied Radiation and Isotopes, Proceedings of the 14th International Conference on Radionuclide Metrology and its Applications, ICRM 2003 60, 379–385. https://doi.org/10.1016/j.apradiso.2003.11.045

Lucey, J.A., Vintró, L.L., Boust, D., Mitchell, P.I., Gouzy, A., Bowden, L., 2007. A novel approach to the sequential extraction of plutonium from oxic and anoxic sediment using sodium citrate to inhibit post-extraction resorption. Journal of Environmental Radioactivity 93, 63–73. https://doi.org/10.1016/j.jenvrad.2006.11.004

MacKenzie, A.B., Cook, G.T., McDonald, P., 1999. Radionuclide distributions and particle size associations in Irish Sea surface sediments: implications for actinide dispersion. Journal of Environmental Radioactivity 44, 275–296. https://doi.org/10.1016/S0265-931X(98)00137-4

Mackenzie, A.B., Scott, R.D., 1993. Sellafield waste radionuclides in Irish sea intertidal and salt marsh sediments. Environ Geochem Health 15, 173–184. https://doi.org/10.1007/BF02627835

MacKenzie, A.B., Scott, R.D., Allan, R.L., Ben Shaban, Y.A., Cook, G.T., Pulford, I.D., 1994. Sediment radionuclide profiles: Implications for mechanisms of Sellafield waste dispersal in the Irish Sea. Journal of Environmental Radioactivity 23, 39–69. https://doi.org/10.1016/0265-931X(94)90504-5

Marsden, O.J., Abrahamsen, L., Bryan, N.D., Philip Day, J., Keith Fifield, L., Gent, C., Goodall, P.S., Morris, K., Livens, F.R., 2006. Transport and accumulation of actinide elements in the near-shore environment: field and modelling studies. Sedimentology 53, 237–248. https://doi.org/10.1111/j.1365-3091.2005.00761.x

McDonald, P., Vives i Batlle, J., Bousher, A., Whittall, A., Chambers, N., 2001. The availability of plutonium and americium in Irish Sea sediments for re-dissolution. Science of The Total Environment 267, 109–123. https://doi.org/10.1016/S0048-9697(00)00771-3

McMahon, C.A., León Vintró, L., Mitchell, P.I., Dahlgaard, H., 2000. Oxidation-state distribution of plutonium in surface and subsurface waters at Thule, northwest Greenland. Applied Radiation and Isotopes 52, 697–703. https://doi.org/10.1016/S0969-8043(99)00232-8

Means, J.L., Crerar, D.A., Borcsik, M.P., Duguid, J.O., 1978. Adsorption of Co and selected actinides by Mn and Fe oxides in soils and sediments. Geochimica et Cosmochimica Acta 42, 1763–1773. https://doi.org/10.1016/0016-7037(78)90233-8

Morris, K., Butterworth, J.C., Livens, F.R., 2000. Evidence for the Remobilization of Sellafield Waste Radionuclides in an Intertidal Salt Marsh, West Cumbria, U.K. Estuarine, Coastal and Shelf Science 51, 613–625. https://doi.org/10.1006/ecss.2000.0705

NEA, 2005. Chemical Thermodynamics of Compounds and Complexes of U, Np, Pu, Am, Tc, Se, Ni and Zr with Selected Organic Ligands, 1st ed, Chemical Thermodynamics. OECD-NEA, Paris, France.

Nelson, D.M., Lovett, M.B., 1978. Oxidation state of plutonium in the Irish Sea. Nature 276, 599–601. https://doi.org/10.1038/276599a0

Oh, J.-S., Warwick, P.E., Croudace, I.W., 2009. Spatial distribution of 241Am, 137Cs, 238Pu, 239,240Pu and 241Pu over 17 year periods in the Ravenglass saltmarsh, Cumbria, UK. Applied Radiation and Isotopes, 6th International Conference on Isotopes 67, 1484–1492. https://doi.org/10.1016/j.apradiso.2009.02.048

OSIL, 2025. Ocean Scientific International Ltd. URL https://osil.com/ (accessed 1.1.25).

Posey, J.C., 1973. Curium-244 isotopic power fuel: chemical recovery from commercial power reactor fuels (No. CONF-730602-1). Oak Ridge National Laboratory, Oak Ridge, Tennessee.

Powell, B.A., Fjeld, R.A., Kaplan, D.I., Coates, J.T., Serkiz, S.M., 2005. Pu(V)O2+ Adsorption and Reduction by Synthetic Hematite and Goethite. Environ. Sci. Technol. 39, 2107–2114. https://doi.org/10.1021/es0487168

Purkis, J.M., Tucknott, A., Croudace, I.W., Warwick, P.E., Cundy, A.B., 2021a. Enhanced electrokinetic remediation of nuclear fission products in organic-rich soils. Applied Geochemistry 125, 104826. https://doi.org/10.1016/j.apgeochem.2020.104826

Purkis, J.M., Warwick, P.E., Graham, J., Hemming, S.D., Cundy, A.B., 2021b. Towards the application of electrokinetic remediation for nuclear site decommissioning. Journal of Hazardous Materials 413, 125274. https://doi.org/10.1016/j.jhazmat.2021.125274

Putra, R.S., Jannah, N.Z., Amalia, A.I., 2022. Removal of caesium by soil electrokinetic remediation on the effect of acetic acid and carbonate salt as electrolyte. AIP Conference Proceedings 2645, 030018. https://doi.org/10.1063/5.0112696

Ray, D., Leary, P., Livens, F., Gray, N., Morris, K., Law, K.A., Fuller, A.J., Abrahamsen-Mills, L., Howe, J., Tierney, K., Muir, G., Law, G.T.W., 2020. Controls on anthropogenic radionuclide distribution in the Sellafield-impacted Eastern Irish Sea. Science of The Total Environment 743, 140765. https://doi.org/10.1016/j.scitotenv.2020.140765

Renshaw, J.C., Law, N., Geissler, A., Livens, F.R., Lloyd, J.R., 2009. Impact of the Fe(III)-reducing bacteria Geobacter sulfurreducens and Shewanella oneidensis on the speciation of plutonium. Biogeochemistry 94, 191–196. https://doi.org/10.1007/s10533-009-9318-8

RESTRAT, 1999. Ravenglass Estuary: Basic Characteristics and Evaluation of Restoration Options (No. RESTRAT-WP 1.4).

Ritchie, J.C., McHenry, J.R., 1990. Application of Radioactive Fallout Cesium-137 for Measuring Soil Erosion and Sediment Accumulation Rates and Patterns: A Review. Journal of Environmental Quality 19, 215–233. https://doi.org/10.2134/jeq1990.00472425001900020006x

Rowell, D.L., 2014. Soil Science: Methods & Applications. Routledge, London. https://doi.org/10.4324/9781315844855

Sanchez, A.L., Murray, J.W., Sibley, T.H., 1985. The adsorption of plutonium IV and V on goethite. Geochimica et Cosmochimica Acta 49, 2297–2307. https://doi.org/10.1016/0016-7037(85)90230-3

Sawhney, B.L., 1972. Selective Sorption and Fixation of Cations by Clay Minerals: A Review. Clays Clay Miner. 20, 93–100. https://doi.org/10.1346/CCMN.1972.0200208

Sellafield Ltd., 2006. Annual Discharge Monitoring Reports 2006-2021. Sellafield Ltd.

Shanbhag, P.M., Morse, J.W., 1982. Americium interaction with calcite and aragonite surfaces in seawater. Geochimica et Cosmochimica Acta 46, 241–246. https://doi.org/10.1016/0016-7037(82)90251-4

Suied, A.A., Tajudin, S.A.A., Zakaria, M.N., Madun, A., 2018. Potential Electrokinetic Remediation Technologies of Laboratory Scale into Field Application- Methodology Overview. J. Phys.: Conf. Ser. 995, 012083. https://doi.org/10.1088/1742-6596/995/1/012083

Takeno, N., 2005. Atlas of Eh-pH diagrams, Intercomparison of thermodynamic databases, Geological Survey of Japan Open File Report No.419 (Geological Survey of Japan Open File No. 419). National Institute of Advanced Industrial Science and Technology, Research Center for Deep Geological Environments, Tsukuba, Japan.

Tanaka, K., Suzuki, Y., Ohnuki, T., 2009. Sorption and Oxidation of Tetravalent Plutonium on Mn Oxide in the Presence of Citric Acid. Chemistry Letters 38, 1032–1033. https://doi.org/10.1246/cl.2009.1032

Temmerman, S., Govers, G., Wartel, S., Meire, P., 2004. Modelling estuarine variations in tidal marsh sedimentation: response to changing sea level and suspended sediment concentrations. Marine Geology 212, 1–19. https://doi.org/10.1016/j.margeo.2004.10.021

Thomson, J., Croudace, I.W., Rothwell, R.G., 2006. A geochemical application of the ITRAX scanner to a sediment core containing eastern Mediterranean sapropel units. Geological Society, London, Special Publications 267, 65–77.

https://doi.org/10.1144/GSL.SP.2006.267.01.05

USEPA, 1999. Understanding variation in partition co-efficient Kd values. Volume II: review of geochemistry and available Kd values for cadmium, cesium, chromium, lead, plutonium, radon, strontium, thorium, tritium and uranium (No. EPA402- R-99– 004B). U. S. Environmental Protection Agency, Washington D.C.

Vives I Batlle, J., Bryan, S., McDonald, P., 2008. A process-based model for the partitioning of soluble, suspended particulate and bed sediment fractions of plutonium and caesium in the eastern Irish Sea. J Environ Radioact 99, 62–80. https://doi.org/10.1016/j.jenvrad.2007.06.012

Wang, Z., Dong, X., Yan, Q., Chen, J., Xu, C., 2022. Separation of Americium from Curium through Oxidation State Control with Record Efficiency. Anal. Chem. 94, 7743–7746. https://doi.org/10.1021/acs.analchem.2c01492

Warwick, P.E., 1999. The determination of pure beta-emitters and their behaviour in a salt-marsh environment (Doctoral Thesis). University of Southampton, Southampton, UK.

Warwick, P.E., Croudace, I.W., Dale, A.A., 1999. An optimised and robust method for the determination of uranium and plutonium in aqueous samples. Applied Radiation and Isotopes 50, 579–583. https://doi.org/10.1016/S0969-8043(98)00064-5

Wen, J., Stacey, S.P., McLaughlin, M.J., Kirby, J.K., 2009. Biodegradation of rhamnolipid, EDTA and citric acid in cadmium and zinc contaminated soils. Soil Biology and Biochemistry 41, 2214–2221. https://doi.org/10.1016/j.soilbio.2009.08.006

Zavarin, M., Powell, B.A., Bourbin, M., Zhao, P., Kersting, A.B., 2012. Np(V) and Pu(V) Ion Exchange and Surface-Mediated Reduction Mechanisms on Montmorillonite. Environ. Sci. Technol. 46, 2692–2698. https://doi.org/10.1021/es203505g

Zhao, M., Zhang, Z., Ma, D., Sun, Z., Hu, J., Gong, Z., Song, C., 2024. Energy-efficient three-dimensional electrokinetic remediation of Cr-contaminated sites using particle electrodes with synergistic effects of oxidation and adsorption. Journal of Environmental Chemical Engineering 12, 114148. https://doi.org/10.1016/j.jece.2024.114148

Zhou, Y., Ma, J., Li, F., Chen, B., Xian, T., Wei, X., 2022. An Improved Algorithm for Peak Detection Based on Weighted Continuous Wavelet Transform. IEEE Access 10, 118779–118788. https://doi.org/10.1109/ACCESS.2022.3220640

Chapter 6 Remediation of Tc-99 in Legacy Coastal Sediments Through the use of Electrokinetic Remediation

Hemming, S. D., Warwick, P. E., and Cundy, A. B.

Prepared for submission as a paper to Science of the Total Environment.

Author contributions:

Hemming, S. D. – experimental design, data collection and processing, interpretation, manuscript writing

Cundy, A. B. – experimental design, core collection, data interpretation, manuscript editing

Warwick, P. E. – experimental design, core collection, data interpretation, manuscript editing

6.1 Introduction

Waste effluents are an inevitable consequence of activities at nuclear sites, often being released into fluvial or marine environments through authorised discharges (e.g. ORR, 2024; OSPAR, 2024). The Sellafield facility (Cumbria, UK) has discharged low-activity liquid wastes into the Irish Sea since 1952, containing radionuclides including H-3, Sr-90, Tc-99, Cs-137, U-238, Pu-239, and Am-241 (BNFL, 1979-2005; Gray et al., 1995; Kershaw et al., 1992; Sellafield Ltd., 2006-2021). Whilst the geochemical behaviour of some of these radionuclides will result in their dispersal at sea (USEPA, 1999), those with higher affinities for sediments can interact with suspended solids in the water column, initially settling on the sea bed and eventually becoming transported back towards the coastline by ocean currents (Ray et al., 2020).

One region of known radionuclide accumulation is the Ravenglass Saltmarsh ((Hunt and Kershaw, 1990; Lucey et al., 2004; Morris et al., 2000; Ray et al., 2020); location shown in Figure 6.1), located ~ 10 km southeast of the Sellafield site and within the Esk Estuary. A sediment grain size gradient exists across the saltmarsh, with sandier material near the river and finer grained deposits at the rear, creating an average composition of silt (~75 %), clay (~19 %), and sand (~7%) (Morris et al., 2000). A minority of the sediment inventory originates from the Esk river, with the rest transported in from marine environments (Halcrow, 2013). Particle-bound radionuclides derived from Sellafield have been carried and deposited into the saltmarsh by ocean sediments for decades, allowing areas with continuous sediment accumulation to capture and preserve a complete Sellafield discharge history (Hunt and Kershaw, 1990; Morris et al., 2000; Warwick, 1999). However, recent work has identified radionuclide remobilisation from within the marsh (Chaplin et al., 2022), raising concerns about the timescale of retention for not insignificant quantities of radionuclides currently sequestered within the Saltmarsh e.g. up to 30,000 Bq/kg for both Cs-137 and Am-241 (Marsden et al., 2006; Morris et al., 2000). Given the range of radionuclides present in the marsh, it offers an ideal "test bed" for the assessment of remediation approaches for radioactively contaminated organic-rich fine sediments.

This paper investigates the use of emerging decontamination technique electrokinetic remediation (EKR) for the remobilisation of Tc-99 in aged, coastal sediment. The radionuclide was selected due to its long half-life, historical abundance in Sellafield discharges (BNFL, 1979-2005; Sellafield Ltd., 2006-2021) and contemporary inventory in the Ravenglass Saltmarsh (Morris et al., 2000; Ray et al., 2020). Despite this, little work has been performed on Tc-99 due to its difficult-to-measure nature and analytical complications regrading a suitable chemical tracer. Treatment with both seawater and citric acid electrolytes has been performed to understand and optimise the conditions required for optimal Tc-99 remediation.

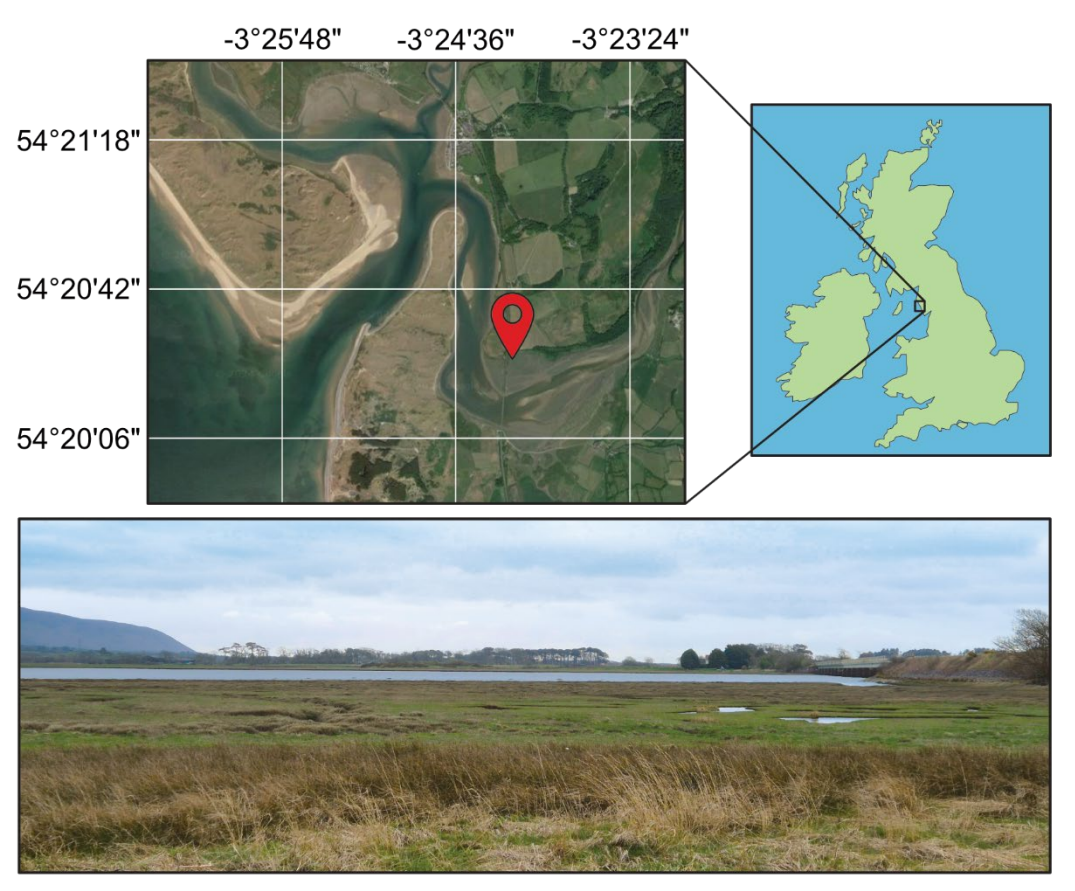


Figure 6.1 – Map of the Esk Estuary and Ravenglass Saltmarsh. Location of core sampling is marked in red. Satellite imagery from Google Maps (2025).

6.1.1 Tc-99

6.1.1.1 Environmental Geochemistry

Tc-99 (half-life = 211,100 years (IAEA, 2025)) is a difficult-to-measure radionuclide (defined by gamma emission energy during decay of < 100 keV (Hemming *et al.*, 2023)) that predominantly exists in (VII) and (IV) oxidation states in environmental settings (Lindahl *et al.*, 2003; Wildung *et al.*, 1979). The primary Tc species present in oxygenated seawater is Tc(VII)O₄, a soluble and highly mobile compound due to its repulsion away from negatively charge sediment particles (CEFAS, 2004; Kaplan and Jeffrey, 1998; Lindahl *et al.*, 2003). Quantification of particle mobility can be determined through the use of partition coefficients (K_d; Equation 5.1), which shows whether a species has a higher affinity a solid phase (K_d > 1 mL/g) or the surrounding liquid phases (K_d < 1 mL/g) (for more detail see Hemming *et al.*, 2023).

$$K_d = \frac{\text{radionuclide on adsorbent at equilibrium (mg/g)}}{\text{radionuclide in solution at equilibrium (mg/mL)}}$$
(5.1)

For TcO_4 discharged into the Irish Sea, the K_d has been estimated as up to 10 mL/g (Fowler et al., 1983; Kershaw et al., 1992), showing a slight preference for particulates whilst still able to migrate large distances without interaction with sediment. However, when exposed to more reducing conditions (electric potential (Eh) of ~ 0.0 V at Atlantic Seawater pH of ~ 8 (Kerr et al.,

2023; Takeno, 2005)) the radionuclide is converted to its (IV) oxidation state, either precipitating as hydrated TcO_2 or Tc sulphides, co-precipitating with metallic sulphides, or associating with carbonate or organic material (Burke *et al.*, 2010; CEFAS, 2004; Keith-Roach *et al.*, 2003). The greater particle affinity of reduced Tc(IV) produces K_d s of 10^2 - 10^3 in seawaters both close to Sellafield (CEFAS, 2004) as well as an averaged value for ocean margins (IAEA, 2004). Chemical reduction of the radionuclide can also occur through in contact with Fe and Mn minerals, causing subsequent adsorption to their surfaces, as well as through microbial processes (Abdelouas *et al.*, 2005; Burke *et al.*, 2010; Peretyazhko *et al.*, 2008). As such, it is estimated that ~ 20 % of discharged Tc-99 from Sellafield has been retained by Irish Sea sediments (Finegan *et al.*, 2009), with a proportion of that subsequently being reworked and deposited back onto the Cumbrian coastline (Morris *et al.*, 2000).

6.1.1.2 Analytical Complexities

Despite the potential health hazards Tc poses, it is much less studied in natural systems compared to Cs-137 (Morris et al., 2000) for two main reasons. The first is that the absence of high-energy gamma emissions during radioactive decay of its key environmentally-relevant isotopes make non-destructive analysis problematic, instead requiring chemical separation from the initial matrix before quantification can be accurately performed. This can be expensive, require specialist laboratory equipment, and take days or weeks to receive the final activities, in comparison to a high-energy gamma emitter e.g. Cs-137 which can have accurate measurements in situ within minutes to hours (Caesium-137 and Americium-241). The second major issue is the chemical tracer used to determine yield recovery post-separation-chemistry. Typically, a different isotope of the same element would be used but because no stable Tc nuclide exists naturally, a range of options have previously been previously considered (Shi et al., 2012; Warwick, 1999; Wigley, 2000), summarised in Table 6.1.

Tracer	Half-life	Advantages	Disadvantages
	[a]		
Tc-95m	61 days	Identical chemistry to Tc-	Short half-life, separate measurement to Tc-
		99 ^[b, c]	99 required, decay product interferes with
			Tc-99 LSC peak ^[b, c]
Tc-97	4.2x10 ⁶	Can be measured	Difficult to acquire, expensive, interferes
	years	simultaneously with Tc-99	with Tc-99 LSC peak ^[c, d, e]
		by ICP-MS, identical	
		chemistry to Tc-99 ^[c, d, e]	

Tc-97m	91 days	Identical chemistry to Tc- 99 ^[c, f]	Short half-life, separate measurement technique to Tc-99 required, decay product interferes with Tc-99 LSC peak, low-energy, low intensity gamma emission ^[c, f]
Tc-99m	6 hours	Easier to acquire than other Tc isotopes, identical chemistry to Tc-99 [c.g]	Very short half-life, separate measurement technique to Tc-99 required, Tc-99 can only be measured after all Tc-99m has decayed (~ 1 week) [c, g]
Re	N/A	Stable isotopes, easy to acquire, can be measured simultaneously with Tc-99 by ICP-MS [c, h, i]	Differing chemistry to Tc ^[c, h]

Table 6.1 – Summary of chemical tracers that can be used for Tc-99 analysis. [a] – IAEA (2025); ^[b] – Golchert and Sedlet (1969); ^[c] – Shi *et al.* (2012); ^[d] – Beals (1996); ^[e] – Beals and Hayes (1995); ^[g] – Chen *et al.* (1994); ^[h] – Butterworth *et al.* (1995) ^[i] – Morris *et al.* (2000). LSC = liquid scintillation countingConventional analysis uses Tc-99m as a tracer (e.g. Ray, 2018; Warwick, 1999; Wigley *et al.*, 1999)due to its identical behaviour to Tc-99 and relative ease of acquisition through facilities such as medical physics departments at hospitals. However, despite some concerns over its similar but not identical chemistry, previous studies have had success using Re as a tracer (e.g. CEFAS, 2004; Morris *et al.*, 2000), offering a longer analytical timeframe and reduced radiological risk to laboratory staff.

6.1.2 Electrokinetic Remediation (EKR)

Electrokinetic remediation (EKR) is an emerging technology for clean-up of contaminated soils, sediments, and other materials that could offer a more sustainable and lower-cost alternative to traditional techniques (Purkis *et al.*, 2021b). The process operates by applying a direct current to a contaminated medium, inducing the mobilisation and migration of hazardous chemicals to designated areas within the material (Figure 6.2). Three primary transport mechanisms drive this process:

- Electromigration movement of ions, with cations and anions migrating towards their respective oppositely charged electrode.
- Electrophoresis similar to electromigration, involves transportation of charged colloidal particles (typically 1–5000 nm in size (Lee, 2019)).
- Electroosmosis the migration of water molecules towards the cathode.

Electrolysis of water molecules at the anode generates hydronium ions at the anode and hydroxide ions at the cathode, which, due to their respective charges, electromigrate which gradually creates a pH gradient across the cell. In non-nuclear settings, EKR is used commonly in remediation of heavy metals using electromigration (e.g. Wang et al., 2021) and well as for dewatering with electroosmosis (e.g. Raats et al., 2002). However, its application on radionuclides, particularly on realistic or real-world environmental waste materials is comparatively limited.

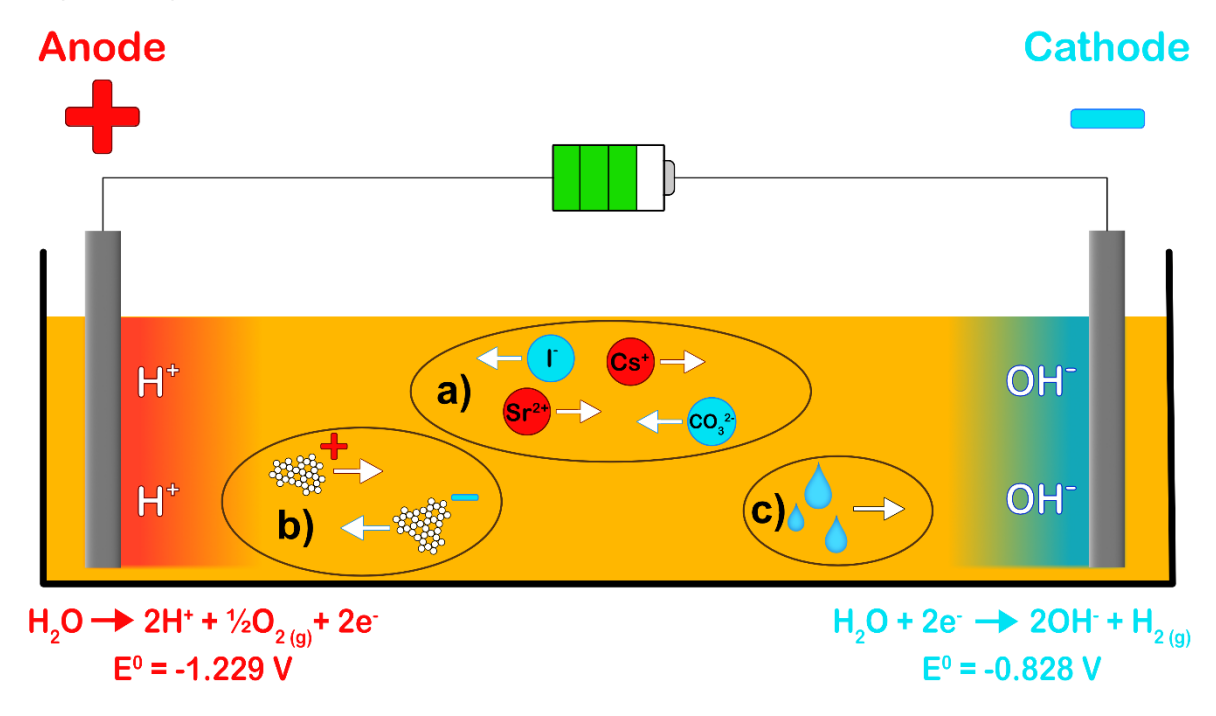


Figure 6.2 – Schematic for the principles of electrokinetic remediation. A= electromigration, B = electrophoresis, C = electroosmosis. Modified from (Purkis *et al.*, 2021b).

Only one previous study could be found for EKR use with Tc-99, which looked at the metastable form of the radionuclide (half-life = 6 hours (IAEA, 2025)) in phaeozem soils contaminated with organic compounds originally used for liquid scintillation counting (Valdovinos *et al.*, 2016). Whilst results show a high degree of remediation (61 % of total Tc-99m present at anode after 4 hours), the authors conclude that the radionuclide species that migrated to the anode was $Tc(VII)O_4$, identical to the form introduced prior to EKR switch-on. The soil used was contaminated in the 1970s and 1980s but had been kept in containers before treatment, making the results less valid for aged sediment in uncontrolled natural environments where Tc(VII) would migrate in porewater or seawater, only being immobilised by reduction to Tc(IV). Further, the short half-life of Tc-99m restricts the duration of the experiment, and, hence, the conclusions that can be drawn about EKR efficacy on aged sediments.

6.2 Methods

6.2.1 Materials and Apparatus Setup

A 55-cm sediment core was collected from the Ravenglass Saltmarsh (54°20'24.9"N -3°24'12.8"E) on 7th June 2021 using a PVC coring tube, and was stored at 4°C for further processing. The core was cut vertically, with one half retained as a control for both stable element and radionuclide analyses, and the other half further divided into two quarter-section cores for electrokinetic treatment (Figure 6.3). Each quarter-section was placed into a separate plastic half-tube, with each end stuffed with lab roll to support the sediment, and graphite electrodes inserted ~ 2 cm and ~ 45 cm from the top of the core. Electrokinetic treatment then was conducted over 45 days at a constant voltage of 21.5 V, creating a 0.5 V/cm gradient. This gradient was chosen to minimise soil heating and power consumption, consistent with established methodologies (e.g. Hahladakis et al., 2016; Kim et al., 2012; Purkis et al., 2021a). To prevent excessive dewatering from fume cupboard air flow, cling film was placed over the cores for the experimental duration and only removed temporarily when sediment pH samples were taken. Atlantic seawater simulant (Ocean Science International Ltd.; Hampshire, UK) was used as the electrolyte in one quarter-section core, with 30 wt% citric acid (Thermo Scientific; Oxford, UK) in Milli-Q water applied in the other. Seawater was selected due to its abundance at the site as well as its high ionic strength, which can enhance current flow and aid electromigration within the cell. Citric acid was chosen as it is a naturally occurring organic acid capable of forming complexes with transition metals and actinides (Francis and Dodge, 2009) and has demonstrated previous efficacy in remobilising plutonium from sediment in laboratoryscale EKR studies (Agnew et al., 2011). The molecule may be more effective at liberating Tc compared to traditional chelating agents such as ethylenediaminetetraacetic acid (EDTA) and diethylenetriaminepentaacetic acid (DTPA), as these have been found ineffective at destabilising the radionuclide either when complexed with organic matter or as precipitates (Stalmans et al., 1986). Additionally, citric acid's biodegradability over time, ranging from days to months depending on soil conditions (Byrd et al., 2021; Francis et al., 1994; Wen et al., 2009), makes it a more environmentally favourable option compared to traditional chelating agents such as more persistent EDTA (Wen et al., 2009).

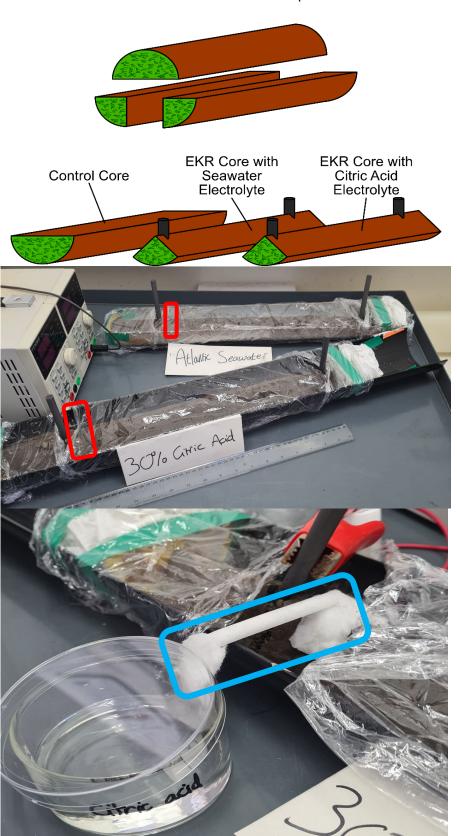


Figure 6.3 – Top – schematic of the divided sediment core, with the grey bars indicating the position of the electrodes. Middle – photo of the experimental setup, with the positions of the electrolyte 'bridges' indicated in red. Bottom – photo of the citric acid core electrolyte 'bridge' (highlighted in blue). The system operated by drawing electrolyte from the reservoir, through the cotton wool, and onto the core. To reduce evaporation and contamination, the majority of cotton wool was enclosed within a transparent plastic tube.

Throughout core treatment, electrolyte was periodically replenished in the anodic regions of the material using a 'bridge' to prevent excessive dewatering (Figure 6.3). pH measurements were

taken by extracting ~ 1 g of sediment adjacent to the anode, cathode, and midpoint between the electrodes. Sediment samples were mixed with 2.5 mL of Milli-Q water, and pH values were measured using a HANNA HI98301 pH probe (uncertainty ±0.2). This protocol balanced international standards for soil pH measurement (e.g. ASTM International, 2024; ISO, 2021) with the need to minimise sediment removal. pH measurements were recorded on days three and seven, and weekly thereafter for both cores.

6.2.2 Analysis

6.2.2.1 X-ray Fluorescence (XRF)

Semi-quantitative elemental distributions for over 20 elements within the sediment were obtained using an ITRAX micro-XRF core scanner at the National Oceanography Centre Southampton's BOSCORF facility, operated with a 200 µm step size, 15-second count time, and a Mo-anode X-ray tube under conditions of 30 kV and 30 mA. The methodology followed the protocols outlined by Croudace *et al.* (2006). For the control core, scanning was conducted prior to the commencement of experiments, whereas the seawater and citric acid-treated cores were analysed post-treatment.

6.2.2.2 Tc-99

After XRF analysis, the cores were sliced into 1-cm thick sections and freeze dried prior to Tc-99 analysis. All sections were analysed using a stable Re tracer (chosen over other Tc isotopes for ease of handling and lower cost; see Section 6.1.1.2 for more details), with 13 samples from the control core being repeated using the more conventional approach with Tc-99m tracer.

6.2.2.2.1 Reagents

All acids and ammonia, as well as FeCl₃ and xylene were purchased from Fisher Scientific (now Thermo Fisher Scientific; Pennsylvania, USA), and Re, Rh, Fe and Mn solutions from Agilent Technologies (California, USA). Trioctylamine (TOA) was procured from Sigma-Aldrich (Massachusetts, USA), Gold Star scintillation cocktail from HIDEX (Turku, Finland), and 1x8 100-200 mesh anion exchange resin (Cl form) from Eichrom Technologies (Illinois, USA). Ground state Tc-99 was sourced from Amersham (now GE Healthcare; Chicago, USA); supplied as NH₄TcO₄) and Tc-99m acquired from Southampton General Hospital (Southampton, UK; supplied as NaTcO₄).

6.2.2.2.2 Quantification Using Tc-99m Tracer

The methodology used was performed in accordance with Wigley et al. (1999) and is summarised here, with deviations from the original method described. Per sample, 2 g of freezedried sediment and ~80 MBq of Tc-99m were placed in a beaker and wetted with ammonia, before being warmed on a hotplate to dryness. The beakers were then heated in a furnace to 550 °C, cooled and acid leached in 30 mL of HNO₃ on a 125 °C hotplate for two hours. The solutions and residues were transferred to centrifuge tubes, where FeCl₃ was added, the solution neutralised with ammonia until a reddish-brown precipitate formed, and centrifuged. The aqueous phase was then washed through a Whatman® 1 filter paper and loaded onto a column containing TrisKem anion exchange resin, preconditioned with 10 mL of Milli Q water. The column was then washed with 10 mL Milli Q and 10 mL 1.2 M HCl before being eluted with concentrated HNO₃ into glass scintillation vials. The solutions were evaporated to dryness and redissolved in H₂SO₄ before undergoing a solvent extraction with 5 % TOA in xylene. Resultant organic phases were mixed with scintillation cocktail in high density polyethylene (HDPE) vials and counted on a HIDEX AMG gamma spectrometer (10-minute count times) and analysed with HidexAMG software to determine the Tc-99m yield. After being left for nine days to allow for complete decay of Tc-99m, the samples were then counted in a Wallac 1220 Quantulus Ultra Low Level Liquid Scintillation Counter (LSC; 4-hour count times) using WinQ software. Samples were not made in replicate and so all uncertainties presented here are analytical and counting uncertainties.

Tc-99m decays to ground state Tc-99, meaning the tracer contributes to the overall activity in each sample. However, due to the large difference in half-life, 80 MBq of Tc-99m decays to 0.26 Bq of Tc-99. During sample Tc-99m spiking, an equal volume of tracer was placed in a vial (with 5 mL TOA in xylene and 15 mL Gold Star to matrix match it to the final samples) to act as a reference material for 100 % yield recovery. A week post-gamma spectrometry counting, to allow time for full Tc-99m decay, the vial was counted in the LSC to determine the activity of daughter Tc-99 created. This value was then subtracted from all sample activities.

6.2.2.2.3 Quantification Using Stable Re Tracer

The method used for quantification with Re tracer is largely similar to that used with a Tc-99m tracer but is still described here in full. 0.1 mg of 10 ppm Re, 2 g of freeze-dried sediment and 25 mL of 8 M HNO $_3$ were added to a beaker and left on a 100 °C hotplate for two hours. After, the solutions and solids were poured into centrifuge tubes, along with 0.5 mL of 10 mg/mL FeCl $_3$ and 2 x 5 mL Milli Q washings from the beaker. Ammonia was then added to the tubes until a reddish-brown precipitate formed, left to cool, and centrifuged (4500 RPM for 4 minutes).

Meanwhile, 0.7×5 cm columns of TrisKem anion exchange resin (Cl form) with Whatman® 1 filter papers in the funnels were preconditioned with 10 mL Milli Q water and loaded with the centrifuge tube supernatants. Columns were then washed with 10 mL Milli Q, had filter papers removed, and washed with 10 mL of 1.2 M HCl. Tc and Re were eluted into HDPE scintillation vials with 20 mL concentrated HNO $_3$ and evaporated to dryness on a 70 °C hotplate. The samples were then redissolved in 4 mL of 2.5 % HNO $_3$ containing 5 ppb Rh (used as an internal standard).

Analysis of both sediment samples and the yellow liquid produced during EKR (see Section 6.3.1) were performed on an Agilent 8800 ICP-QQQ inductively coupled plasma mass spectrometer (ICP-MS) (samples with no gas mode, yellow liquid in He mode introduced at 4.3 mL/min), MS/MS both set at mass to charge ratio (m/z) = 99, sample input ~ 0.3 mL/min, 5 ppb Rh as the internal standard; reference solutions = 0-600 ppt Tc, 0-25 ppb Re, 0-20 ppb Mn and 0-20 ppb Fe, each in 2.5 % HNO₃ with 5 ppb Rh) and processed using MassHunter software. ICP-MS samples were single replicates derived from an average of ten measurements per isotope, with uncertainties accounting for analytical uncertainties and the standard deviation of the ten measurements. Tc-99 and Re Calibration standards were run at the beginning of each batch to allow for full concentration quantification. ICP-MS measurements of Tc-99 can have interferences from both Ru-99 and Mo-98 (forming MoH⁺, where molecular m/z = 99). Whilst Tc purification was performed by column separation, instrument counts per second (CPS) values for the radionuclide were expected to be low in the samples, meaning that even trace amounts of relatively more abundant Mo and Re could provide inaccurate measurements. As such, test solutions of Mo and Ru were run through the instrument to determine the ratios between Mo-98 and MoH⁺ (molecular mass of 99), and Ru-101 and Ru-99. Mo was found to cause minimal interference at the m/z = 99 (47 CPS at m/z = 99 with 2.07×10^7 CPS at m/z = 98) and Ru-99 was detectable at ratios consistent with naturally occurring Ru (e.g. 4.78x10⁶ CPS at m/z = 99 with 6.55x106 CPS at m/z = 101; this gives experimentally derived Ru-99/Ru-101 ratio of 0.7296, comparable to the natural isotopic abundance ratio of 0.7479). As a result, no Mo corrections were performed and Ru corrections to the Tc CPS were calculated through equation 5.1:

Which, using the experimentally derived Ru-99/Ru-101 CPS ratio of 0.7296, gives equation 5.2:

Corrected Tc99 CPS = raw Tc99 CPS -
$$(Ru101 CPS * 0.7296)$$
 (5.2)

After, CPS values were drift corrected using the Rh-103 internal standard and concentrations were determined, all using MassHunter 4.6 (version C.01.06, build 621.2) offline analysis. Post-corrections, the Tc-99 CPS, and therefore concentration, in the blank sample produced in each

batch were \sim 0, indicating that these were the only major interferences present. After all corrections had been applied, the final Tc-99 activities were determined from the concentrations by equation 5.3:

$$A = \frac{c * N_A * ln(2)}{T_{0.5} * RAM}$$
 (5.3)

Where A is the activity in Bq/kg, c is the Tc-99 concentration in g/g, N_A is Avogadro's number (6.022x10²³), $T_{0.5}$ is the half-life of Tc-99 (6.66x10¹² seconds), and RAM is the relative atomic mass of Tc-99.

6.2.2.2.4 Defining Regions of Elevated Activity

To ensure consistency when defining elevated radionuclide levels, also referred to as 'peaks' with work presented in Chapter 5, a uniform procedure was applied. A full explanation is provided in the Table C.5 but summarised here. A 5-point moving average was used on the dataset, smoothing the distribution profile, with the region of elevated activity determined by activities greater than 30 % of the maximum smoothed value. Whilst a moving average has been used in peak analysis before (e.g. Guo and Huan, 2023; Zhou et al., 2022), the 30 % threshold was an arbitrary value chosen to balance the removal of region tails and areas at background activities within the cores, whilst including as many data points in each elevated region as possible. Since all cores underwent the same process for defining peaks, the analysis and conclusions derived from these experiments are valid, despite the 30 % cut-off being subjective to these data. The smoothing process was only used to identify regions of elevated activity and was discarded before any further analysis was performed.

6.3 Results

6.3.1 Visual EKR Observations

Approximately two weeks into EKR treatment, yellow liquids started pooling under both cores with a production rate of approximately 1s-10s mL per day. This continued until the end of treatment, although the volumes varied throughout the duration. Analyses of the liquids is provided in Table 6.2. Drying in the cathodic regions became apparent after 3–4 weeks, with the seawater core exhibiting more extensive dewatering compared to the citric acid core. Throughout treatment, a white solid progressively accumulated near the cathodic regions of both cores, resulting from electrolyte evaporation and salt precipitation.

Radionuclide/ stable element detected	Units	Yellow liquid from seawater core	Yellow liquid from citric acid core
Tc-99	Bq/kg	3.7 ± 1.1	< 0.12
Mn-55 (stable)	ppm	128 ± 0.4	47 ± 0.3
Fe-56 (stable)	ppm	5260 ± 10	4281 ± 10
Fe-57 (stable)	ppm	5175 ± 26	4106 ± 37

Table 6.2 – Summary of the yellow liquids produced from the EKR cores during treatment. All isotopes listed in this table were analysed by ICP-MS, following the same procedure used for Tc as described by Purkis $et\,al.$ (2021a). Uncertainties are quoted to 2σ . All radiometric measurements were single replicates and so uncertainties presented here are analytical and counting uncertainties, whereas ICP-MS samples were single replicates derived from an average of ten measurements per isotope, with uncertainties accounting for analytical uncertainties and the standard deviation of the ten measurements.

6.3.2 XRF Analysis

XRF data have been previously presented in Section 5.3.3 but are included here for completeness. Graphs for the control core distributions of Mn, Fe, and S, which have been normalised to total scatter (coherent + incoherent) to correct for variations in sediment composition and water content (Ge et al., 2005), in addition to Si/Rb, S/Cl, Ca/Ti, and Zr/Rb ratios, are presented in Figure 6.4 (data for all scanned elements across all three cores can be found in Figure C.3). While the measurements are semi-quantitative (measured in counts but not determined as concentrations), they effectively illustrate elemental trends in each core. For the seawater-treated core, lighter elements such as S, Cl, and Ca exhibited greater abundance peaks compared to other nuclides due to their presence in both the electrolyte as well as the sediment. Clear migration of several elements was observed in both cores (Figure C.3). The seawater-treated core demonstrated remobilisation of nuclides including Ca, Mn, Ni, Zn, Sr, and I, primarily concentrated at depths of approximately 10–20 cm. However, it should be noted that calculations based on the compositions of Atlantic seawater simulant (OSIL, 2025) and Ravenglass sediments (Balboni et al., 2022; Warwick, 1999) suggest a sizable fraction of S (~ 66 %), Cl (~ 85 %), Ca (~ 10–28 %), Br (~ 99 %), Rb (~ 34 %), and Sr (~ 23–97 %) in the post-treatment seawater core originated from the electrolyte rather than the sediment. As these elements are already in the aqueous phase, they are more susceptible to mobilisation during EKR, potentially distorting conclusions drawn on treatment effectiveness. All other electrolyte-derived elements accounted for less than 5 % of their total post-treatment core mass, with several, such as Fe and Mn, present at trace levels below 0.01 %. The citric acid-treated core also exhibited full or partial remobilisation of elements such as Al, Ca, Mn, Fe, Sr, and Pb, with varying distributions throughout the treatment cell.

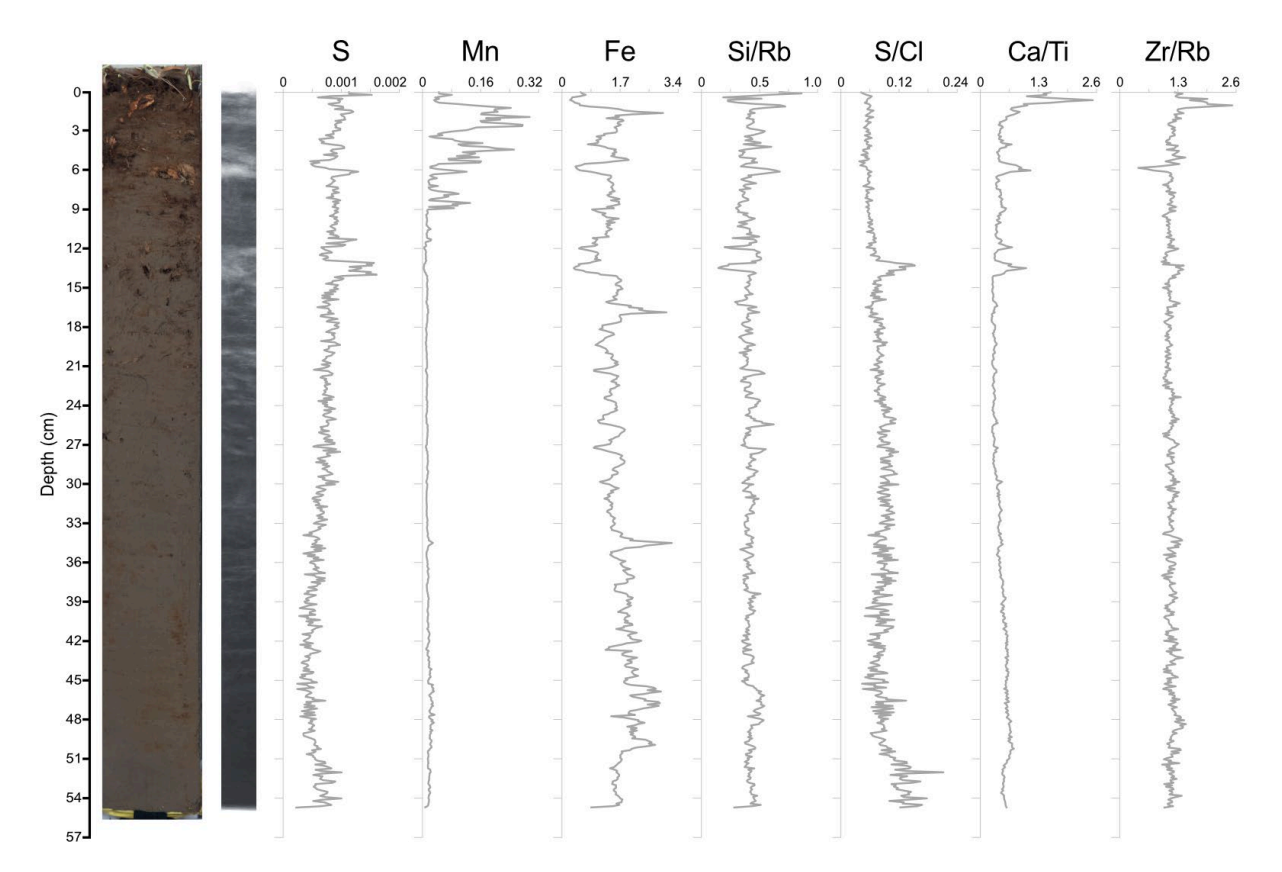


Figure 6.4 – Photograph, radiograph, and elemental and ratioed XRF data for key nuclides (XRF) in the control core. XRF results are semi quantitative, meaning that only relative changes across a profile should be interpreted and not comparisons of absolute values between cores. For all data collected across all three cores, see Figure C.3.

6.3.3 Tc-99m and Re Tracer Comparison

Full details of comparison activities are listed in Table C.6 but are summarised here. Both tracers show the same general distribution profiles, with areas of elevated activity at 14-15 cm and 27-28 cm depth. The 99m profile has a larger upper peak, also encompassing the 12-13 cm sample as well as 14-15 cm, whereas much lower activities are observed at 12-13 cm in the Re distribution. The Re sample activities are generally 50-80 % the value of Tc-99m values, although eight of the 13 samples have measurements within 2σ uncertainty of each other and 11 of the 13 with 3σ .

99m Tracer and Re Tracer

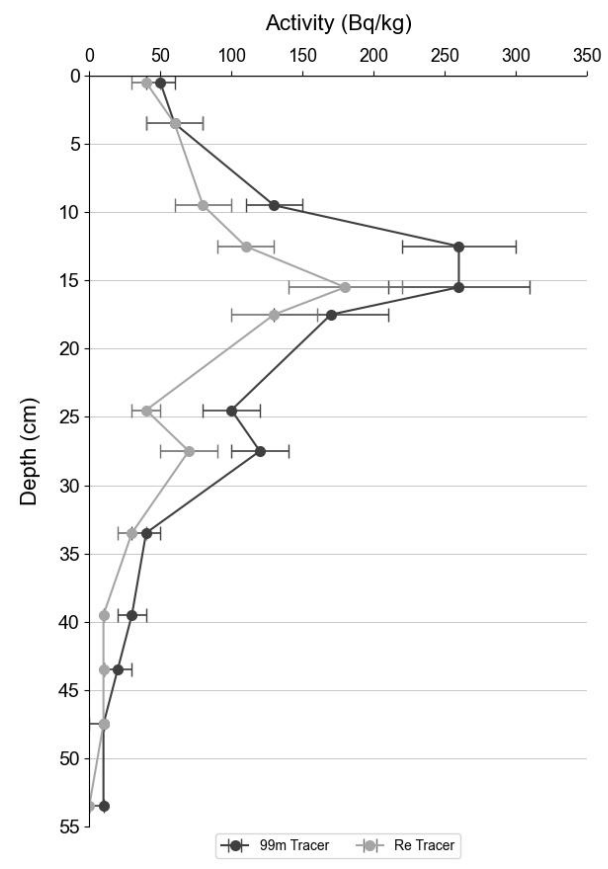


Figure 6.5 – Sediment Tc-99 activities when using Re (light grey) and Tc-99m (dark grey) tracers. Uncertainties are quoted to 2σ . All radiometric measurements were single replicates, with error bars showing analytical uncertainties, and ICP-MS samples were single replicates derived from an average of ten measurements per isotope, with error bars accounting for analytical uncertainties and the standard deviation of the ten measurements.

6.3.4 Sediment Core Tc Distributions

Whilst large uncertainties in the control core make the profile somewhat erratic, three 'peaks' of elevated activity are defined as described in Section 6.2.2.2.4. Peaks A, B, and C are located at 1-6, 7-24 and 25-30 cm, respectively. Peak B is asymmetrical, tailing towards shallower core depths, whilst smaller peaks A and C appear symmetrical. The profile is broadly consistent with the Sellafield discharge history (BNFL, 1979-2005; Sellafield Ltd., 2006-2021), albeit with differences resulting from sediment of different ages mixing offshore before being deposited on the coastline. Previous studies also show similar trends (e.g. Lucey et al., 2004; Ray et al., 2020; Wigley et al., 1999), albeit with differing activity ranges caused by spatial variation of radionuclides in the saltmarsh (Caborn et al., 2016; Horrill, 1984), further indicating that Sellafield is the primary source of Tc found in the core analysed here. There does not appear to be any evidence of post-depositional Tc movement unlike that suggested in some previous studies (Ray, 2018; Wigley et al., 1999), although the offshore sediment mixing and analysis resolution used here may have masked minor changes in distribution.

EKR with seawater electrolyte shows a distinct decrease in activity in the top \sim 12 cm of the core, with values remaining within uncertainty of the control core at depths $> \sim$ 15 cm. As such, the extent of remobilisation for peaks A, B, and C is 81 ± 36 %, 25 ± 11 %, and 22 ± 33 %, respectively, although no areas of Tc-99 enrichment were observed. Treatment with a citric acid electrolyte showed activity reductions across the entire core whilst still maintaining the general control core profile, with peaks A, B, and C remobilisations determined as 70 ± 35 %, 45 ± 10 %, and 66 ± 32 %, respectively. No regions of Tc enrichment were found across the core.

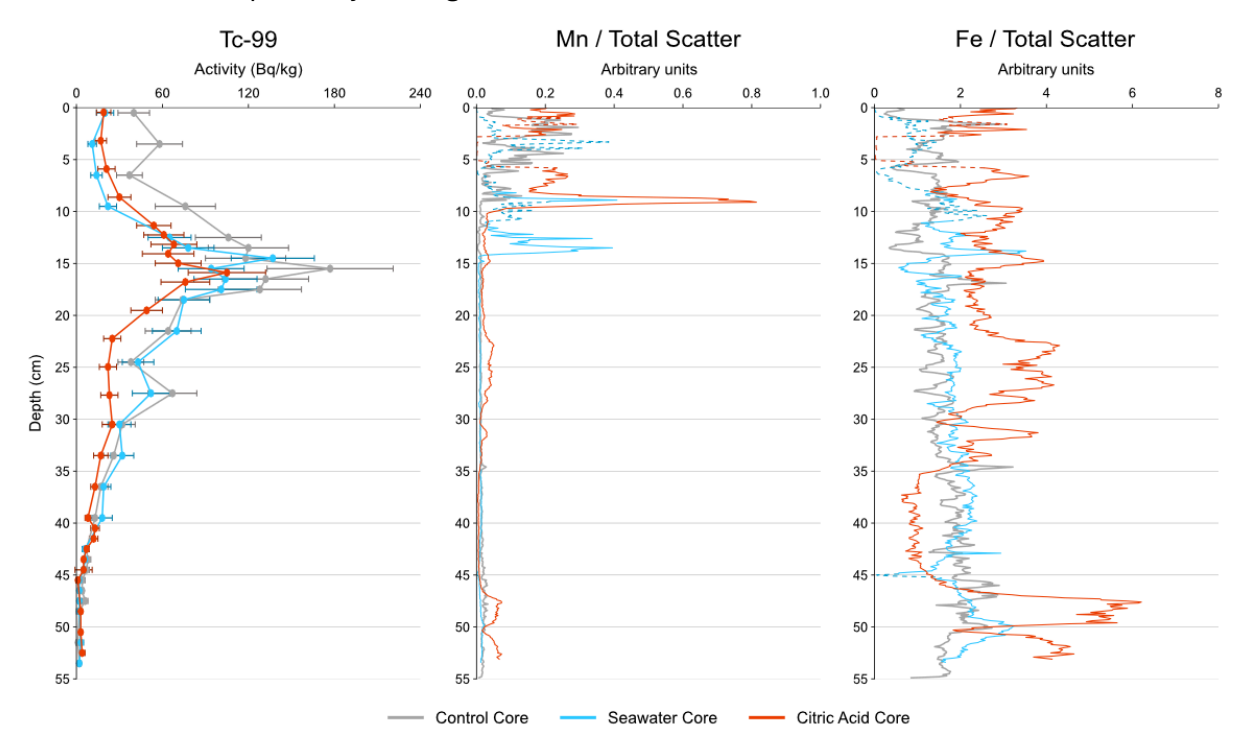


Figure 6.6 – Quantitative Tc data and semi-quantitative XRF Mn and Fe measurements (normalised to total scatter) for the control (grey), seawater (blue), and citric acid (orange) cores. For the Mn and Fe plots, dashed lines show XRF values that did not pass quality control checks but have been included to show possible areas of elemental remobilisation. Radiometric uncertainties are quoted to 2σ .

Peak number	Depth of 'region of elevated activity' (cm)	Core section	Proportion of Tc-99 in peak remobilised (%)
А	1-6	Seawater	81 ± 36
		Citric acid	70 ± 35
В	7-24	Seawater	25 ± 11
		Citric acid	45 ± 10
С	25-30	Seawater	22 ± 33
	20 00	Citric acid	66 ± 32

Table 6.3 – Summary table for the extent of remobilisation in each of the three 'peaks' containing elevated levels of Tc-99 activity. Uncertainties are quoted to 2σ . Samples were not made in replicate and so all uncertainties presented here are analytical and counting uncertainties.

6.4 Discussion

6.4.1 Visual EKR Observations

The yellow liquids observed in both cores are likely derived from their respective electrolytes, which served as the primary source of fluid within the systems. Dissolution of various chemicals, including Tc-99, into the electrolytes likely contributed to the composition of the liquid. The high concentrations of Fe (Table 6.2) are presumed to be responsible for the yellow colouration.

6.4.2 Tc-99m and Re Tracer Comparison

Despite the majority of measurement sets being within uncertainty, samples with Re tracer have consistently lower activities than with a Tc-99m tracer, suggesting preferential retention of Re over Tc during at least one stage in the separation chemistry. Whilst no studies into preferential Tc and Re retention could be found, 1x8 resin used here has similar exchange sites to the Eichrom TEVA resin, with the main difference between the two being the 1x8 having the adsorption sites bound to a solid phase instead of retained in TEVA's liquid phase (which is, in turn, bound through hydrophobic interactions to a stationary phase) (Snow et al., 2017). Previous work by Butterworth et al. (1995) showed that Tc is preferentially retained over Re by TEVA when eluting in 20 mL of 10 M HNO₃ (\sim 85 % of Tc present in eluent vs. \sim 96 % of Re). Whilst the HNO₃ concentration used by Butterworth et al. is lower than that used in this study (~ 16 M), the discrepancy in nuclide retention is likely to have still been present in the 1x8 resin elution which would result in an artificially high Tc recovery. When using the 85 % to 96 % Tc to Re ratio as the basis for a Re recovery correction factor of 0.89, the number of control core Re and Tc-99m tracer measurements that are within uncertainty increases to 11 out of 13. Butterworth et al. show that 30 mL column elutions would be sufficient to strip equal proportions of Tc and Re from the column, alleviating the problem. As such, the method should be adjusted to minimise uncertainty in future work.

Despite this consistent reduction in Tc-99 activity with the Re tracer compared to the Tc-99m equivalent, the overall trends of both profiles are very similar. This suggests that, even without a correction factor applied, values obtained using the Re tracer method are still comparable relative to each other. Since the evaluation of EKR is dependent on relative sample differences

before and after treatment, absolute values are not required and so conclusions drawn for EKR efficacy of Tc remobilisation are still valid.

6.4.3 Sediment Core Tc Distributions

The proportion of seawater-treated Tc-99 remobilised in each peak appears to decrease with depth, resulting from significant Tc liberation at depths < ~ 9 cm (that is, peak A and the upper region of peak B). This correlates with changes in Mn distribution, which migrated towards the anode and precipitated at ~ 14 cm (Figure 6.6). Any Tc associated with this phase would have been mobilised when Mn electromigrated, leaving recalcitrant fractions (e.g. Tc associated with insoluble organic material (Wigley, 2000)) in place. Eh/pH diagrams for Mn, although modelled for simplified systems compared to these sediments, suggest Mn(OH)₃-can form at pHs > ~ 12 (Takeno, 2005) – conditions that were observed adjacent to the cathode, within peak A, during EKR (Figure C.3). As anions migrated away from the cathode and the accompanying alkaline front, sediment pH would have decreased and caused Mn to precipitate, possibly as pyrolusite (MnO_2) (Takeno, 2005). This ~ 14 cm depth abundance spike is also seen with Tc which may indicate Tc adsorption onto Mn (Abdellah et al., 2020; Szlamkowicz et al., 2023). Further, although the exact species has not been identified, XRF data also show the radionuclide present at the same depths as a Ca enrichment, which has been interpreted as CaCO3 due to the radionuclide's observed association with the mineral (Keith-Roach et al., 2003; Wigley, 2000) and Mn's ability to co-precipitate to form MnCO₃ (Wartel et al., 1990). The reduced remobility of peak B (7-24 cm depth range) compared to peak A, and the absence of statistically significant depletion in peak C (25-30 cm depth range) can also be explained by the lack of Mn at > 9cm, indicating that these minerals were the only Tc phase in the sediment that was significantly mobilised by EKR. The activity reduction in peak A (81 %) is particularly high in comparison to previous modified Tessier sequential extraction data in sediment from, or proximal to, the Ravenglass Saltmarsh (EKR-amenable phases, i.e. leachable and exchangeable, contribute < 10 % of total Tc at shallow core depths (Keith-Roach et al., 2003; Wigley, 2000)), whilst peaks B (25 %) and C (no statistically significant Tc-99 depletion) are much lower (leachable and exchangeable phases at ~ 20 cm depth when excluding (~ 60 %) and including (~ 75 %) the acidsoluble phase (Wigley, 2000)). These variations are likely the result of spacial heterogeneity of sediment composition within the saltmarsh, particularly for Mn mineral content, showing the variable nature of the environmental setting. Finally, mobilised Tc identified in the yellow liquid is likely to be a very minor component of the total sediment core inventory, as a radionuclide mass balance between the control and seawater cores (once corrected to be the same volume of material; the control core is ~ 3x heavier than the seawater core) are within uncertainty of each other (93.3 ± 8.6 % of control core activity measured in seawater core, excluding yellow

liquid activities; Table C.4), suggesting no statistically significant activity was been lost during treatment. This also indicates the 3.7 Bq/kg of Tc-99 present in the liquid is likely the maximum activity concentration created throughout treatment rather than an average.

When treated with citric acid, the top 9 cm of sediment, which includes peak A and the upper region of peak B, showed a significant reduction of both Tc-99 and Mn (Figure 6.6). This may have been caused by mobilisation of Mn as Mn(OH)₃ in alkaline conditions (Takeno, 2005) or by dissolution and citrate complexation (Matzapetakis et al., 2000; Wall et al., 2013) after the alkaline front had been neutralised. Further work is needed to understand which mechanism occurred in this setting. In either case, the introduction of citrate ions would stabilise and mobilise the radionuclide only in its reduced (IV) oxidation state (Wall et al., 2013), with Tc(VII)O₄ being repelled from the negatively charged carboxylic acid binding sites (Kaplan and Jeffrey, 1998). Tc(IV) citrate complexes have been reported to form in laboratory experiments from radionuclide desorption off calcareous, sandy loam from the Hanford site (Washington, USA), although evidence for this was tenuous as only one trial, which used the highest concentrations Tc-99 (1x10-6 mol/dm3; 63 Bq/mL) and citric acid (0.01 mol/dm3; 0.2 wt%) in the study, showed a definitive decrease in sorption (Franz et al., 1982). However, the concentration of citric acid is much lower than that used in this study (30 wt%), which may have enhanced mobilisation of the smaller Tc-99 inventory (average control core Tc-99 activity of 51 Bq/kg) compared to the Hanford trials. More-compelling evidence from the same study showed minimal resorption of Tc(IV) citrate onto the sediment, resulting in a Kd of 0.026, suggesting that once Tc in the core was mobilised it likely remained in the aqueous phase. Total activity reduction for peaks B and C show a definitive decrease in activity compared to the control core, although large uncertainties for the latter make precise quantification difficult. These depletions are likely caused through Mn mobilisation at 0-2 cm depth and clay desorption at ~ 20-30 cm depth (Russell and Speiser, 1980; Wall et al., 2013). The latter has been suggested as the following mechanisms were considered unlikely at this depth range: Fe mobilisation (XRF data showed depletion at 35-45 cm and accumulation at ~ 35 cm which was not observed by Tc) and desorption as weakly bound ions or colloids (similar mobility at this depth would have also been seen in the seawater core, but was not). Minor remobilisation from clay minerals at depths outside the ~ 20-30 cm region may have occurred but have been masked by large uncertainty values. When comparing peak remobilisation to sequential extraction of Esk Estuary sediment, all peaks differ from what would be expected (peaks A, B, and C – 81 %, 45 %, and 66 %, respectively vs ~ 25 % at 0 cm depth and ~ 78 % at 18 cm for Wigley et al. (2000)), which demonstrates the spacial and temporal variation across the saltmarsh. However, despite large regions of Tc depletion in the core, no zone of enrichment was observed. Tc mass balance discrepancies between the control and citric acid cores suggest the remobilised fraction was no

longer present in the solid material post-treatment (59.4 ± 5.2 % of control core activity measured in citric acid core, excluding yellow liquid activities; Table C.4). The absent fraction may have been located in the yellow liquid created during treatment or inside the electrode(s), with the latter seeming less likely as there is no evidence of accumulation around either graphite rod. Whilst an incorrect approximation of the yellow liquid volume produced during the experiment may have contributed, the large proportion of activity unaccounted for makes it unlikely for it to be the sole factor in this discrepancy. ICP-MS analysis of the yellow liquid was attempted but Tc-99 was not been detected (Table 6.2) due to LOD effects resulting from the dilutions required to analyse the sample. Radionuclide retention in the aqueous phase is supported by previous trials using Hanford sediment, which showed minimal resorption of Tc(IV) citrate after complexation (Franz et al., 1982). As such, the mass balance was not possible to complete. This has serious implications for scaled-up in situ trials, as, if the unaccounted-for fraction has been remobilised but not retained, a significant proportion of Tc would be lost into the surrounding environment. Future work must either determine the location of this portion or how to facilitate migration and precipitation in proximity to the electrodes only.

6.4.4 Comparison Between Electrolytes and Future Work

For all three Tc-99 activity peaks present in the sediment core, the extent of remobilisation with seawater and citric acid were within uncertainty of each other. However, when comparing activities at specific depths, particularly at 20-30 cm, citric acid sediment often contained a lower activity than in the seawater core, indicating a more efficient liberation overall. For contamination in the upper 10 cm, both electrolytes showed a similar degree of remobility. Contrastingly, for material exposed to redox conditions capable of reducing Mn(IV) to Mn(II) (> 10 cm in this core), citric acid is the preferred electrolyte, with higher concentrations of the acid potentially increasing the extent of Tc desorption, and, hence, remobilisation efficiency (Franz et al., 1982). However, the ~40 % Tc-99 inventory unaccounted for after the citric acid setup requires further investigation before larger-scale trials can be performed, as this may indicate a notable extent of uncontrolled transportation. If this fraction is found in the yellow liquid, the electrolyte may have to be limited to ex situ applications only, where the liquid can be contained and collected post-treatment to avoid any risk of environmental contamination. In addition, future work should also address the immobile component in both cores, which is likely caused by association with insoluble organic matter that EKR is ineffective at migrating unless the insoluble material is first oxidised. As such, EKR shows promise for being a viable remediation technique for fine-grained higher salinity sediments (e.g. coastal, estuarine, and marine

sediments), but further work is needed to (re-)examine possible electrolytes for optimised, controlled Tc extraction.

6.5 Conclusions

This paper evaluated the first use of EKR as a potential remediation technique for Tc-99 decontamination in authentically contaminated coastal sediments, with seawater and citric acid electrolytes applied and compared. Tc analysis using Re and more conventional Tc-99m tracers were compared, with the Re tracer generally producing activities 50-80 % of the corresponding Tc-99m values. Of the 13 samples analysed with both tracers, eight had pairs that were within uncertainty of each other.

Three areas of elevated Tc activities were identified in the sediment core, referred to as 'peaks'. EKR treatment using a seawater electrolyte resulted in 81 %, 25 % and no statistically significant remobilisation for peaks A, B, and C, respectively. Areas of Tc depletion in peak A and the upper region of peak B correlate with regions of Mn migration, suggesting the radionuclide was initially associated with this transition metal before its dissolution. Both Tc and Mn are enriched at \sim 14 cm depth in the core, coinciding with less alkaline conditions and a spike in Ca abundance, suggesting co-precipitation or adsorption onto CaCO₃ caused subsequent immobility. Treatment with the citric acid electrolyte showed Tc-99 remobilisations of 70 %, 45 %, and no statistically significant movement for peaks A, B, and C, respectively. Radionuclide depletion coincides with migration of Mn in the upper region of the core, with both elements having likely complexed with citrate ligands. Remobilisation in the lower region of peak B and below (20-30 cm) is likely caused by Tc desorbing off clay minerals and complexing with citrate ligands. However, no regions of Tc enrichment were observed; the radionuclide most likely remained in the electrolyte as reduced Tc(IV) citrate complexes, but further work is needed to confirm this.

Overall, EKR with seawater and citric acid shows the potential to remobilise Tc-99 that has been immobilised in sediment for years and decades, although the depth at which remediation is required will have repercussions on the electrolyte used. If Tc contamination is present in sub-oxic conditions in sediments, either electrolyte would be capable of achieving similar clean-up efficiencies. However, in deeper, more reducing environments, especially those with higher clay contents, citric acid is the superior electrolyte, improving decontamination rates and making remediation projects more viable. Next steps should look at addressing the unaccounted-for Tc-99 activity in the citric acid core, to verify whether the electrolyte is suitable for use *in situ* applications or *ex situ* only, optimising the concentration of citric acid used, and identifying any alternative or complementary electrolytes that could be used to extract Tc bound to oxidisable organic matter.

6.6 Acknowledgements

The authors extend their gratitude to BOSCORF team at the National Oceanography Centre Southampton for access to and assistance with the XRF data collection, the GAU-Radioanalytical team at the University of Southampton for their valuable assistance and advice on radionuclide analysis, and to the NNUF-EXACT facility (grant number EP/T011548/1) for providing access to laboratory facilities. Appreciation is also expressed to the TRANSCEND Consortium (grant number EP/S01019X/1) for their ongoing support throughout the project. The authors would like to thank Mark Taylor and Phoebe Hudson for their assistance with data analysis and manipulation, as well as Dr. Jamie Purkis and Dr. Sarah Lu for their insightful discussions.

6.7 References

Abdellah, W.M., El-Ahwany, H.I., El-Sheikh, R., 2020. Removal of Technetium (99Tc) from Aqueous Waste by Manganese Oxide Nanoparticles Loaded into Activated Carbon. Journal of Analytical Sciences, Methods and Instrumentation 10, 12–35. https://doi.org/10.4236/jasmi.2020.101002

Abdelouas, A., Grambow, B., Fattahi, M., Andrès, Y., Leclerc-Cessac, E., 2005. Microbial reduction of 99Tc in organic matter-rich soils. Science of The Total Environment 336, 255–268. https://doi.org/10.1016/j.scitotenv.2004.06.005

Agnew, K., Cundy, A.B., Hopkinson, L., Croudace, I.W., Warwick, P.E., Purdie, P., 2011. Electrokinetic remediation of plutonium-contaminated nuclear site wastes: Results from a pilot-scale on-site trial. Journal of Hazardous Materials 186, 1405–1414. https://doi.org/10.1016/j.jhazmat.2010.12.016

ASTM International, 2024. Standard Test Methods for pH of Soils. https://doi.org/10.1520/D4972-19

Balboni, E., Merino, N., Begg, J.D., Samperton, K.M., Zengotita, F.E., Law, G.T.W., Kersting, A.B., Zavarin, M., 2022. Plutonium mobilization from contaminated estuarine sediments, Esk Estuary (UK). Chemosphere 308, 136240. https://doi.org/10.1016/j.chemosphere.2022.136240

Beals, D.M., 1996. Determination of Technetium-99 in Aqueous Samples by Isotope Dilution Inductively Coupled Plasma Mass Spectrometry. Journal of Radioanalytical and Nuclear Chemistry, Articles 204, 253–263.

Beals, D.M., Hayes, D.W., 1995. Technetium-99, iodine-129 and tritium in the waters of the Savannah River Site. Science of The Total Environment, Environmental Radiochemical Analysis 173–174, 101–115. https://doi.org/10.1016/0048-9697(95)04769-7

BNFL, 1979. Annual Discharge Monitoring Reports 1979-2005. British Nuclear Fuels Ltd. (BNFL)/ Sellafield Ltd.

Burke, I.T., Livens, F.R., Lloyd, J.R., Brown, A.P., Law, G.T.W., McBeth, J.M., Ellis, B.L., Lawson, R.S., Morris, K., 2010. The fate of technetium in reduced estuarine sediments: Combining direct and indirect analyses. Applied Geochemistry 25, 233–241. https://doi.org/10.1016/j.apgeochem.2009.11.008

Butterworth, J.C., Livens, F.R., Makinson, P.R., 1995. Development of a method for the determination of low levels of technetium-99. Science of The Total Environment, Environmental Radiochemical Analysis 173–174, 293–300. https://doi.org/10.1016/0048-9697(95)04774-3

Byrd, N., Lloyd, J.R., Small, J.S., Taylor, F., Bagshaw, H., Boothman, C., Morris, K., 2021.

Microbial Degradation of Citric Acid in Low Level Radioactive Waste Disposal: Impact on
Biomineralization Reactions. Front. Microbiol. 12. https://doi.org/10.3389/fmicb.2021.565855

Caborn, J.A., Howard, B.J., Blowers, P., Wright, S.M., 2016. Spatial trends on an ungrazed West Cumbrian saltmarsh of surface contamination by selected radionuclides over a 25 year period. Journal of Environmental Radioactivity 151, 94–104.

https://doi.org/10.1016/j.jenvrad.2015.09.011

CEFAS, 2004. Accumulation and remobilisation of 99Tc in eastern Irish Sea sediments (Environmental Report No. RL 01/04). Centre of Environment Fisheries and Aquaculture Science, Lowestoft, UK.

Chaplin, J.D., Christl, M., Cundy, A.B., Warwick, P.E., Reading, D.G., Bochud, F., Froidevaux, P., 2022. Bioavailable actinide fluxes to the Irish Sea from Sellafield-labelled sediments. Water Research 221, 118838. https://doi.org/10.1016/j.watres.2022.118838

Chen, Q., Dahlgaard, H., Nielsen, S.P., 1994. Determination of 99Tc in sea water at ultra low levels. Analytica Chimica Acta 285, 177–180. https://doi.org/10.1016/0003-2670(94)85021-6

Croudace, I.W., Rindby, A., Rothwell, R.G., 2006. ITRAX: description and evaluation of a new multi-function X-ray core scanner. Geological Society, London, Special Publications 267, 51–63. https://doi.org/10.1144/GSL.SP.2006.267.01.04

Finegan, P., Vintró, L.L., Mitchell, P.I., Boust, D., Gouzy, A., Kershaw, P.J., Lucey, J.A., 2009. Accumulation, solid partitioning and remobilisation of 99Tc in subtidal and intertidal sediments

in the Irish Sea. Continental Shelf Research, Special issue in honour of Michael Collins 29, 1995–2010. https://doi.org/10.1016/j.csr.2009.02.005

Fowler, S.W., Aston, S.R., Benayoun, G., Parsi, P., 1983. Bioavailability of technetium from artificially labelled north-east atlantic deep-sea sediments. Marine Environmental Research 8, 87–100. https://doi.org/10.1016/0141-1136(83)90029-6

Francis, A.J., Dodge, C.J., 2009. Microbial Transformation of Actinides and Other Radionuclides. Presented at the Proceedings of the DAE-BRNS symposium on nuclear and radiochemistry, Brookhaven National Laboratory, Mumbia, India.

Francis, A.J., Dodge, C.J., Chatterjee, S.D., Landrey, M.F., 1994. Citrate Biodegradation (No. BNL-60830). Brookhaven National Laboratory, New York.

Franz, J.A., Martin, L.Y., Wiggins, D.J., 1982. Behavior of Reduced 99Tc and 99Tc Organic Complexes on Hanford Soil (No. PNL-4178). Pacific Northwest Lab., Richland, Washington.

Golchert, N.W., Sedlet, Jacob., 1969. Radiochemical determination of technetium-99 in environmental water samples. Anal. Chem. 41, 669–671. https://doi.org/10.1021/ac60273a021

Google LLC, 2025. Google Maps. URL https://www.google.co.uk/maps/@54.340246,-3.403555,5113m/ (accessed 28.11.24).

Gray, J., Jones, S.R., Smith, A.D., 1995. Discharges to the environment from the Sellafield site, 1951-1992. J. Radiol. Prot. 15. https://doi.org/10.1088/0952-4746/15/2/001

Guo, J., Huan, T., 2023. Mechanistic Understanding of the Discrepancies between Common Peak Picking Algorithms in Liquid Chromatography–Mass Spectrometry-Based Metabolomics. Anal. Chem. 95, 5894–5902. https://doi.org/10.1021/acs.analchem.2c04887

Hahladakis, J.N., Latsos, A., Gidarakos, E., 2016. Performance of electroremediation in real contaminated sediments using a big cell, periodic voltage and innovative surfactants. Journal of Hazardous Materials 320, 376–385. https://doi.org/10.1016/j.jhazmat.2016.08.003

Halcrow, 2013. Ravenglass Estuary Complex, North West Estuaries Processes Reports. Halcrow Group Ltd., York.

Hemming, S.D., Purkis, J.M., Warwick, P.E., Cundy, A.B., 2023. Current and emerging technologies for the remediation of difficult-to-measure radionuclides at nuclear sites. Environ. Sci.: Processes Impacts 25, 1909–1925. https://doi.org/10.1039/D3EM00190C

Horrill, A.D., 1984. Radionuclide levels and distribution in grazed saltmarsh in West Cumbria. Environmental Pollution Series B, Chemical and Physical 8, 265–280. https://doi.org/10.1016/0143-148X(84)90027-2

Hunt, G.J., Kershaw, P.J., 1990. Remobilisation of artificial radionuclides from the sediment of the Irish Sea. Journal of Radiological Protection 10. https://doi.org/10.1088/0952-4746/10/2/009

IAEA, 2025. IAEA Nuclear Data Services. URL https://www-nds.iaea.org/ (accessed 13.1.25).

IAEA, 2004. Sediment Distribution Coefficients and Concentration Factors for Biota in the Marine Environment (No. 422), Technical Reports Series. International Atomic Energy Agency, Vienna.

ISO, 2021. ISO 10390:2021 Soil, treated biowaste and sludge – Determination of pH.

Kaplan, D.I., Jeffrey, R., 1998. Pertechnetate Exclusion from Sediments. Radiochimica Acta 81, 117–124. https://doi.org/10.1524/ract.1998.81.2.117

Keith-Roach, M.J., Morris, K., Dahlgaard, H., 2003. An investigation into technetium binding in sediments. Marine Chemistry 81, 149–162. https://doi.org/10.1016/S0304-4203(03)00014-8

Kerr, D.E., Grey, A., Kelleher, B.P., 2023. Organic alkalinity dynamics in Irish coastal waters: Case study Rogerstown Estuary. Marine Chemistry 254, 104272.

https://doi.org/10.1016/j.marchem.2023.104272

Kershaw, P.J., Pentreath, R.J., Woodhead, D.S., Hunt, G.J., 1992. A Review of Radioactivity in the Irish Sea (No. MAFF-AEMR-32), Aquatic Environment Monitoring Report. Ministry of Agriculture, Fisheries and Food, United Kingdom.

Kim, W.-S., Park, G.-Y., Kim, D.-H., Jung, H.-B., Ko, S.-H., Baek, K., 2012. In situ field scale electrokinetic remediation of multi-metals contaminated paddy soil: Influence of electrode configuration. Electrochimica Acta, EREM 2011 + ISEE'Cap 2011 + EMRS 2011 86, 89–95. https://doi.org/10.1016/j.electacta.2012.02.078

Lee, E., 2019. Chapter 1 - Electrophoresis of a Single Rigid Particle, in: Lee, E. (Ed.), Interface Science and Technology, Theory of Electrophoresis and Diffusiophoresis of Highly Charged Colloidal Particles. Elsevier, pp. 3–45. https://doi.org/10.1016/B978-0-08-100865-2.00001-1

Lindahl, P., Ellmark, C., Gäfvert, T., Mattsson, S., Roos, P., Holm, E., Erlandsson, B., 2003. Long-term study of 99Tc in the marine environment on the Swedish west coast. Journal of Environmental Radioactivity 67, 145–156. https://doi.org/10.1016/S0265-931X(02)00176-5

Lucey, J.A., Gouzy, A., Boust, D., Vintró, L.L., Bowden, L., Finegan, P.P., Kershaw, P.J., Mitchell, P.I., 2004. Geochemical fractionation of plutonium in anoxic Irish Sea sediments using an optimised sequential extraction protocol. Applied Radiation and Isotopes, Proceedings of the 14th International Conference on Radionuclide Metrology and its Applications, ICRM 2003 60, 379–385. https://doi.org/10.1016/j.apradiso.2003.11.045

Marsden, O.J., Abrahamsen, L., Bryan, N.D., Philip Day, J., Keith Fifield, L., Gent, C., Goodall, P.S., Morris, K., Livens, F.R., 2006. Transport and accumulation of actinide elements in the near-shore environment: field and modelling studies. Sedimentology 53, 237–248. https://doi.org/10.1111/j.1365-3091.2005.00761.x

Matzapetakis, M., Karligiano, N., Bino, A., Dakanali, M., Raptopoulou, C.P., Tangoulis, V., Terzis, A., Giapintzakis, J., Salifoglou, A., 2000. Manganese Citrate Chemistry: Syntheses, Spectroscopic Studies, and Structural Characterizations of Novel Mononuclear, Water-Soluble Manganese Citrate Complexes. Inorg. Chem. 39, 4044–4051. https://doi.org/10.1021/ic9912631

Morris, K., Butterworth, J.C., Livens, F.R., 2000. Evidence for the Remobilization of Sellafield Waste Radionuclides in an Intertidal Salt Marsh, West Cumbria, U.K. Estuarine, Coastal and Shelf Science 51, 613–625. https://doi.org/10.1006/ecss.2000.0705

ORR, 2024. Oak Ridge Reservation Annual Site Environmental Report 2023 (No. DOE-SC-OSO/RM_ASER-2024-02), Annual Site Environmental Reports. Oak Ridge Reservation, Oak Ridge, Tennessee.

OSIL, 2025. Ocean Scientific International Ltd. URL https://osil.com/ (accessed 1.1.25).

OSPAR, 2024. Annual Report and Assessment of Discharges of Liquid Discharges from Nuclear Installations in 2022, Radioactive Substances. Convention for the Protection of the Marine Environment of the North-East Atlantic.

Peretyazhko, T., Zachara, J.M., Heald, S.M., Jeon, B.-H., Kukkadapu, R.K., Liu, C., Moore, D., Resch, C.T., 2008. Heterogeneous reduction of Tc(VII) by Fe(II) at the solid–water interface.

Geochimica et Cosmochimica Acta 72, 1521–1539. https://doi.org/10.1016/j.gca.2008.01.004

Purkis, J.M., Tucknott, A., Croudace, I.W., Warwick, P.E., Cundy, A.B., 2021a. Enhanced electrokinetic remediation of nuclear fission products in organic-rich soils. Applied Geochemistry 125, 104826. https://doi.org/10.1016/j.apgeochem.2020.104826

Purkis, J.M., Warwick, P.E., Graham, J., Hemming, S.D., Cundy, A.B., 2021b. Towards the application of electrokinetic remediation for nuclear site decommissioning. Journal of Hazardous Materials 413, 125274. https://doi.org/10.1016/j.jhazmat.2021.125274

Raats, M.H.M., van Diemen, A.J.G., Lavèn, J., Stein, H.N., 2002. Full scale electrokinetic dewatering of waste sludge. Colloids and Surfaces A: Physicochemical and Engineering Aspects 210, 231–241. https://doi.org/10.1016/S0927-7757(02)00380-1

Ray, D., 2018. Controls on Radionuclide Behaviour in the Sellafield-Impacted Eastern Irish Sea (PhD). University of Manchester, Manchester.

Ray, D., Leary, P., Livens, F., Gray, N., Morris, K., Law, K.A., Fuller, A.J., Abrahamsen-Mills, L., Howe, J., Tierney, K., Muir, G., Law, G.T.W., 2020. Controls on anthropogenic radionuclide distribution in the Sellafield-impacted Eastern Irish Sea. Science of The Total Environment 743, 140765. https://doi.org/10.1016/j.scitotenv.2020.140765

Russell, C.D., Speiser, A.G., 1980. Complexes of Technetium with Hydroxycarboxylic Acids: Gluconic, Glucoheptonic, Tartaric, and Citric. Journal of Nuclear Medicine 21, 1086–1090.

Sellafield Ltd., 2006. Annual Discharge Monitoring Reports 2006-2021. Sellafield Ltd.

Shi, K., Hou, X., Roos, P., Wu, W., 2012. Determination of technetium-99 in environmental samples: A review. Analytica Chimica Acta 709, 1–20. https://doi.org/10.1016/j.aca.2011.10.020

Snow, M.S., Finck, M.R., Carney, K.P., Morrison, S.S., 2017. Extraction chromatographic separations of tantalum and tungsten from hafnium and complex matrix constituents. Journal of Chromatography A 1484, 1–6. https://doi.org/10.1016/j.chroma.2017.01.019

Stalmans, M., Maes, A., Cremers, A., 1986. Role of Organic Matter as a Geochemical Sink for Technetium in Soils and Sediments, in: Desmet, G., Myttenaere, C. (Eds.), Technetium in the Environment. Springer Netherlands, Dordrecht, pp. 91–113. https://doi.org/10.1007/978-94-009-4189-2_9

Szlamkowicz, I., Stanberry, J., Lugo, K., Murphy, Z., Ruiz Garcia, M., Hunley, L., Qafoku, N.P., Anagnostopoulos, V., 2023. Role of Manganese Oxides in Controlling Subsurface Metals and Radionuclides Mobility: A Review. ACS Earth Space Chem. 7, 1–10. https://doi.org/10.1021/acsearthspacechem.2c00113

Takeno, N., 2005. Atlas of Eh-pH diagrams, Intercomparison of thermodynamic databases, Geological Survey of Japan Open File Report No.419 (Geological Survey of Japan Open File No. 419). National Institute of Advanced Industrial Science and Technology, Research Center for Deep Geological Environments, Tsukuba, Japan.

USEPA, 1999. Understanding variation in partition co-efficient Kd values. Volume II: review of geochemistry and available Kd values for cadmium, cesium, chromium, lead, plutonium, radon,

strontium, thorium, tritium and uranium (No. EPA402- R-99– 004B). U. S. Environmental Protection Agency, Washington D.C.

Valdovinos, V., Monroy-Guzmán, F., Bustos, E., 2016. Electrokinetic removal of radionuclides contained in scintillation liquids absorbed in soil type Phaeozem. Journal of Environmental Radioactivity 162–163, 80–86. https://doi.org/10.1016/j.jenvrad.2016.05.017

Wall, N.A., Karunathilake, N., Dong, W., 2013. Interactions of Tc(IV) with citrate in NaCl media. Radiochimica Acta 101, 111–116. https://doi.org/10.1524/ract.2013.2001

Wang, Y., Han, Z., Li, A., Cui, C., 2021. Enhanced electrokinetic remediation of heavy metals contaminated soil by biodegradable complexing agents. Environmental Pollution 283, 117111. https://doi.org/10.1016/j.envpol.2021.117111

Wartel, M., Skiker, M., Auger, Y., Boughriet, A., 1990. Interaction of manganese(II) with carbonates in seawater: Assessment of the solubility product of MnCO3 and Mn distribution coefficient between the liquid phase and CaCO3 Particles. Marine Chemistry 29, 99–117. https://doi.org/10.1016/0304-4203(90)90008-Z

Warwick, P.E., 1999. The determination of pure beta-emitters and their behaviour in a salt-marsh environment (Doctoral Thesis). University of Southampton, Southampton, UK.

Wen, J., Stacey, S.P., McLaughlin, M.J., Kirby, J.K., 2009. Biodegradation of rhamnolipid, EDTA and citric acid in cadmium and zinc contaminated soils. Soil Biology and Biochemistry 41, 2214–2221. https://doi.org/10.1016/j.soilbio.2009.08.006

Wigley, F., 2000. Mechanisms for accumulation and migration of technetium-99 in saltmarsh sediments (Doctoral Thesis). University of Southampton, Southampton, UK.

Wigley, F., Warwick, P.E., Croudace, I.W., Caborn, J., Sanchez, A.L., 1999. Optimised method for the routine determination of Technetium-99 in environmental samples by liquid scintillation counting. Analytica Chimica Acta 380, 73–82. https://doi.org/10.1016/S0003-2670(98)00676-X

Wildung, R.E., McFadden, K.M., Garland, T.R., 1979. Technetium Sources and Behavior in the Environment. Journal of Environmental Quality 8, 156–161. https://doi.org/10.2134/jeq1979.00472425000800020004x

Zhou, Y., Ma, J., Li, F., Chen, B., Xian, T., Wei, X., 2022. An Improved Algorithm for Peak Detection Based on Weighted Continuous Wavelet Transform. IEEE Access 10, 118779–118788. https://doi.org/10.1109/ACCESS.2022.3220640

Chapter 7 Conclusions and Future Work

7.1 Overall Conclusions

Within environmental material (i.e. groundwaters and sediments) EKR shows promise for being a useful remediation technique (thesis objectives 1 and 3; Section 1.4). When radionuclides are introduced to a material shortly before EKR application, mobilisation of through electromigration appears to be effective. This was seen with Sr-90 and Tc-99, although their migration rates differed which highlights the need for radionuclide-specific remediation time periods. Electroosmosis for H-3 was also evident, but the much slower transportation rate compared to Sr-90 and Tc-99 further showed that remediating multiple radionuclides simultaneously will require an approach of 'remediation is only as fast as your slowest responding contaminant' during remedial projects. EKR also showed applicability on aged sediment containing radionuclides that are much more resistant to mobilisation. Whilst Pu and Tc-99 required chelating agents to enhance their mobility, Am-241 was more efficiently migrated using a seawater electrolyte which would minimise the hazards to operators associated with handling acidic electrolytes during scaled-up EKR use at nuclear sites. However, the citric acid appeared to leave notable proportions of these radionuclides unaccounted for, likely lost through a discharge of yellow liquid from the sediment during treatment, meaning further work is needed to understand and this movement and prevent future losses from the aqueous phase. Cs-137 showed little remobility in the sediment, suggesting that higher voltages may be required to overcome the energy barrier retaining the radionuclide in clay minerals. Further, comparison between saltmarsh sediment here and work by Purkis et al. (2021a) on fresh, artificially contaminated, organic-rich sediment confirms the suggestion by the authors that with increased time between Cs-137 release into the subsurface and the application of EKR determines the extent at which the radionuclide is remediated. Based on results from spiked groundwater (chapter 3) and legacy sediment (chapter 6) contamination, the same is true for Tc-99 and likely other radionuclides as well.

EKR work on cementitious material was comparatively less successful (thesis objective 2; Section 1.4). Whilst Cs-137 shows clear mobility in the cement cores that were mixed with radionuclides to create a uniform contaminant distribution (referred to as the Homogeneous Set), cores that were cured and subsequently soaked in a radionuclide bath (referred to as the Soaking Set) had low Cs-137 uptakes, making the extent of remediation that would occur with greater uptakes difficult to accurately quantify. H-3 in both sets of cores only shows diffusion out into the electrolyte, implying that either electroosmosis is not occurring or that diffusion is the dominant transportation process. Both I-129 and U-236 show tentative evidence for remobilisation in the Homogeneous Set, with the former also showing limited electromigration in the Soaking Set and the latter demonstrating a more significant transportation. Sr-90 showed

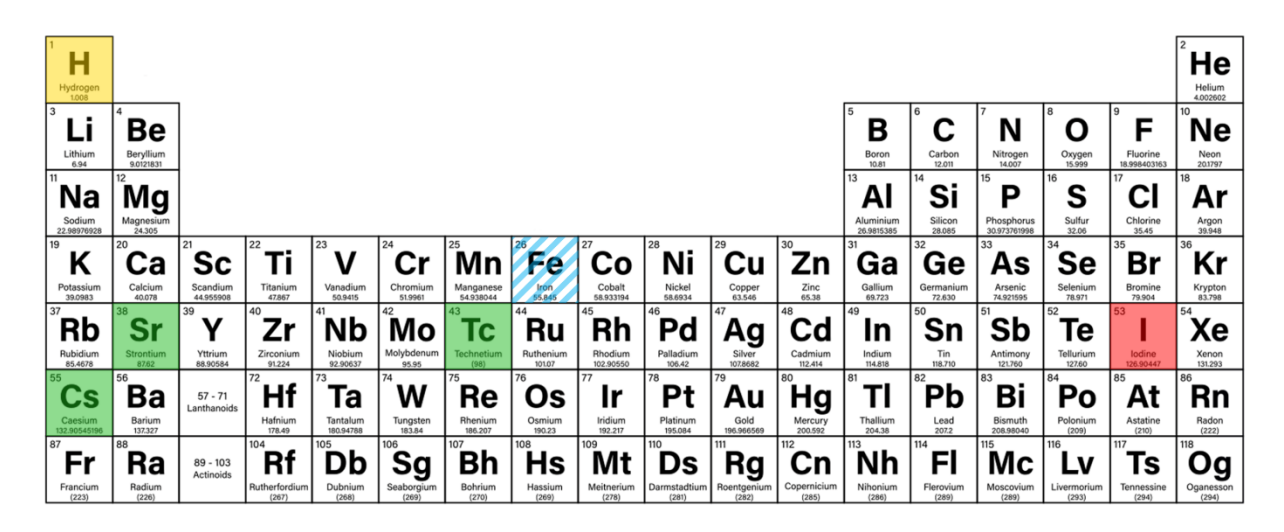
no mobilisation in the Homogeneous Set and limited movement in the Soaking Set. Overall, none of the DTMRs used in the experiment were as mobile as Cs-137, likely due to Cs having few retention sites within or onto the cementitious phases present (in the absence of aggregate material). However, all but H-3 showed some degree of EKR efficacy in the Soaking Set, whilst migration in the Homogeneous Set was much more limited.

When considering all the experiments performed here, EKR at a more sustainable 0.5 V/cm voltage gradient has been more successful at remediating radionuclides in environmental settings than cementitious settings. DTMRs in groundwaters and sediments generally showed reasonable extents and rates of migration. A trade-off when applying EKR exists between sustainability (using as lower voltage gradient as possible) and remediation speed and efficiency (using higher voltages for quicker results and enabling more radionuclides to overcome the energy barriers that cause their retention). With groundwaters and, to a reasonable extent, sediments, 0.5 V/cm can achieve significant migration and subsequent accumulation in particular areas of the cell. Mobilisation rates for the groundwater experiments indicate that lower voltages could be used for Tc-99, although this was performed in ideal conditions and may not apply in scaled-up trials. In contrast, Comparatively, most of the radionuclides examined for the Soaking Set of the cements project are likely to require higher voltages to promote significant desorption and the Homogeneous Set will probably require an even larger voltage gradient, if the radionuclides can be mobilised at all from their mineralphase incorporated state. Whilst the cements work was performed with an alkaline electrolyte, which was likely to promote more radionuclide precipitation compared to neutral or acidic conditions, these conditions were chosen to reflect conditions found in in situ remediation of storage pond concrete.

7.2 Contributions to EKR Knowledge

Figure 7.1 shows a summary of experimental results in this thesis. A range of chemical elements have been remobilised through EKR, with the most success coming from Sr-90 and Tc-99 (groundwaters; Chapter 3), Cs-137 (cements; Chapter 4), and Am-241 (sediments; Chapter 5). H-3 has only shown notable movement in the proof-of-concept groundwater work and no evidence of electroosmosis in cements, making results about scale up work inconclusive. Similarly, both U and Pu have had one experiment show limited mobility (Homogeneous Set in cements and citric acid core in the sediments, respectively) and another show minimal mobility (Soaking Set in the cement sand the seawater core in the sediments, respectively). Iodine showed little or no enhanced remobilisation with EKR for all cement trials. Figure 7.1 also shows elements relevant to the nuclear sector which may be amenable to EKR (shown with blue

stripes). Eu and Cm can have similar chemistries to Am, albeit in simplified aqueous systems (Takeno, 2005), meaning that both may be susceptible to EKR treatment in sediments as well as other media. In addition, XRF data from the Ravenglass sediment core showed migration of some stable Fe and a significant proportion of stable Ni. This suggests activation products Fe-55 and Ni-63, with the latter meeting the DTMR definition defined in Section 1.2.1, may also be amenable to EKR in sediments. These were historically discharged from the Sellafield site (BNFL, 1979-2005; Sellafield Ltd., 2006-2021) and so are likely present in the core, raising opportunities for definitive efficiencies to be determined.



La Lanthanum	Cerium		Nd	Promethium	Sm Samarium	Europium	Gd Gadolinium	7b	Dy Dysprosium 162,500	Ho Holmium 164,93033	Erbium 167,259	Tm Thulium 168,93422	Yb Ytterbium	Lutetium
⁸⁹ Ac	⁵Th	⁹¹ Pa	92 U	Np	Pu Pu	95 Am	Č m	97 Bk	°Cf	⁹⁹ Es	Fm	Md	No	Lr
Actinium (227)	Thorium 232.0377	Protactinium 231.03588	Uranium 238.02891	Neptunium (237)	Plutonium (244)	Americium (243)	Curium (247)	Berkelium (247)	Californium (251)	Einsteinium (252)	Fermium (257)	Mendelevium (258)	Nobelium (259)	Lawrencium (266)

Figure 7.1 – periodic table showing EKR amenability based on work presented within this thesis. Green shading shows high amenability in at least one contaminated material, yellow shows either notable but minor results in one chapter or mixed results across multiple chapters, red shows low affinities for EKR-induced mobilisation, and blue stripes shows nuclear-sector-relevant elements that may be susceptible to EKR based on the results here.

When reflecting on previous EKR literature and the developments resulting from the work in this thesis, updates have been made to the EKR amenability schematic (pre-thesis work – section 1.3.2 and Figure 1.3; post-thesis work - Figure 7.2). Whilst only one previous Tc-99 trial has been performed (Valdovinos *et al.*, 2016), clear success in groundwater and, to a lesser extent, sediment core mobilisation have caused an upgrade from yellow to green. No previous work has looked specifically at the use of EKR for Am-241, although Agnew *et al.* (2011) showed a significant reduction in gross alpha measurements of both Pu and Am in aged sediments, and so the radionuclide remains yellow despite notable remobilisation of both legacy contaminated sediment cores in Chapter 5. In addition, due to the relatively low extent of Pu mobilisation in the sediments, this radionuclide has remained as yellow. Tritium has been upgraded from red to yellow as electroosmosis in the groundwaters work showed promise at proof-of-concept stage for its susceptibility to EKR, but more work is required to see if similar success can be repeated

at larger scales. Cs and U have remained green due to their catalogue of previous EKR success, and Sr has remained yellow as its slow (but definitive) migration speeds in groundwaters and minimal mobilisation in cements have not been sufficient to support previous finding of significant remediation (e.g. DePaoli et al., 1996; Purkis et al., 2021a). The only downgrade was for iodine due to its poor remediation in cements, resulting in a change from dashed yellow (only proven to work on a stable nuclide) to red (more work on radionuclides is needed). However, H-3 and Sr-90 also showed low removal efficiencies in the cements work but higher mobilities in groundwater trials, meaning that I-129 remediation in other settings may be possible. Further, evidence of stable iodine migration in the Ravenglass sediment core (Figure C.3) suggests that EKR in environmental scenarios may be much more effective with I-129.

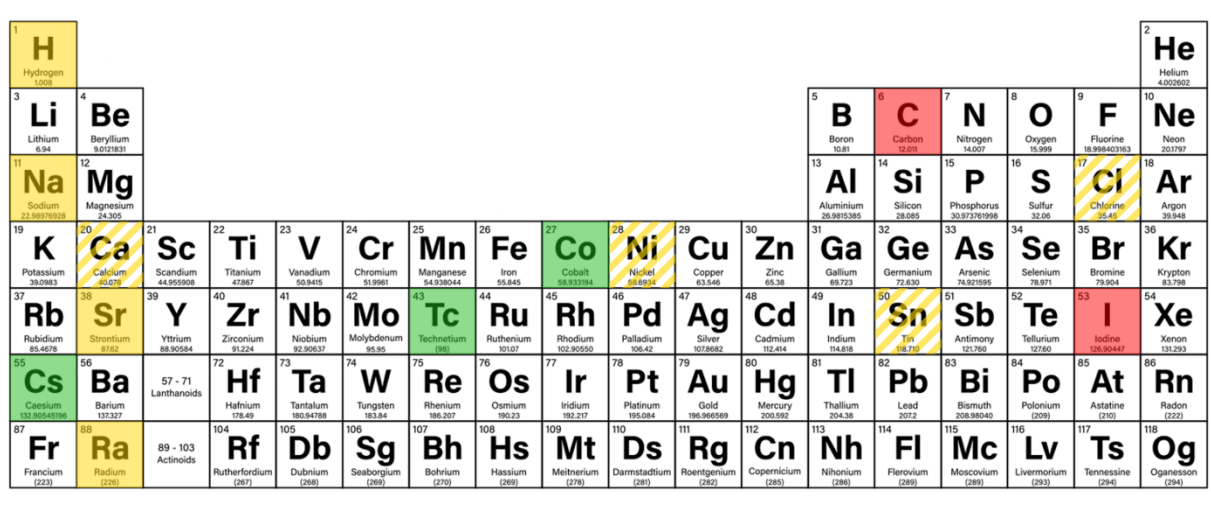




Figure 7.2 – Periodic table showing the state of progress since 2009 for EKR on elements with isotopes commonly found at nuclear sites (excluding those with half-lives of < 1 year; Purkis et al. (2021b)), with work from this thesis included. Green shading shows elements that have demonstrated EKR-amenability in multiple studies, solid yellow shows limited work, striped yellow shows work has only been performed of stable isotopes, and red shows further work is needed.

7.3 Future Work

Three main avenues exist for future EKR work focussing on radionuclide contamination in nuclear decommissioning and remediation contexts – improving the efficiency of bench-scale remedial trials and upscaling the volume of treated material for both *ex situ* and *in situ* trials. The key factor for the first target is determining the optimal voltage gradient for each radionuclide in a given material, as this will minimise the electricity use and make the process as sustainable as possible under the pre-determined conditions. For potential future nuclear site deployment, the ability to approximate the minimum voltage required for a remedial project

would be useful for allowing site operators to balance financial budgets against program timescale deadlines. This is important as increased voltages result in quicker and more efficient EKR but at the expense of a larger cost. Current lab-scale work could also be improved by minimising the distance from the electrodes at which different radionuclides precipitate. A good case study for this is Am-241 in the Ravenglass sediment core when treated with seawater (Figure 5.5), which precipitated 10-25 cm away from the cathode likely due to alkaline conditions. This scenario could potentially occur with many cations in EKR systems due to hydroxide ion production at the cathode generating alkaline conditions. Neutralisation of the alkaline front through the addition of a weak acid would negate this effect, in addition to enhancing radionuclide remobilisation through acid dissolution, and promote consistent remediation to a known point in the contaminated material instead of over a broad area. This would ensure that subsequent removal or immobilisation of the contaminated media encapsulated as much radionuclide activity as possible and leaving the remaining material as clean as possible. Repeating the experiments described in this thesis with either the same radionuclides or those with potential for EKR susceptibility (Section 7.2; Figure 7.1) without the presence of a pH gradient may greatly assist the predictability of eventual contaminant immobilisation region.

The second option for future work involves *ex situ* pilot field-scale trial with isotopes that have shown promise in bench-scale work. As EKR experiments undertaken as part of this thesis generally showed better removal efficiencies when using environmental material, this is likely the most suitable media for starting larger, more systematic remediation. Previous work by Agnew *et al.* (2011) used a containment (overpack) skip in order to conduct metre-scale work on Pu- and Am-contaminated soil, allowing treatment of ~ 4 tonnes of material at once. This approach should be repeated with other radionuclides in similar conditions to compare which contaminants are the most amenable to EKR at this scale (via batch treatment approaches) and optimise the conditions needed for effective remediation. Demonstrating the scalable nature to site operators is important, as frequent replacement of material for treatment could be a large drain in financial budgets due to the number of operators required and the time required to swap batches of material. Instead, larger volumes of material replaced less frequently could be more cost effective over longer periods of time.

Alternatively, treatment of *in situ* material would be an effective way of promoting EKR. Demonstrating the technology's capability is key for nuclear sector uptake, with the best way to achieve this being to show real-world efficacy on heterogeneous material without the need for prior extraction or sample preparation. This work would start over scales of ~ 1 m, similarly to previous studies (see Section 1.3.2), but should aim to expand up to several metres in order to demonstrate its applicability for larger sources and volumes of contamination. When increasing

the volumes of material treated, the voltage required, and therefore the electricity cost, could increase by a up to a cubic factor, making the knowledge of minimal voltage gradients required especially important. Future in situ EKR remediation projects may be more viable by having multiple smaller, adjacent cells running simultaneously to be more cost effective whilst covering the same volume of material. EKR also offers the possibility of performing effective remedial work around already-present infrastructure, potentially allowing routine operations in the contaminated area to continue unaffected during treatment. As well as uses in isolation, the technology could also enhance removal efficiencies of other techniques such as permeable reactive barriers (PRBs), with EKR used to draw radionuclides into the barrier where they can be sequestered. Alternatively, contaminant migration and precipitation onto in situ barriers created within the material, such as Fe barriers generated through dissolution of the steel anode(s) during EKR (known as ferric iron remediation and stabilisation – FIRS (Cundy and Hopkinson, 2005)) would allow retention of radionuclides whilst requiring minimal disruption to infrastructure and personnel (Purkis et al., 2023). With these exploration of these pathways for future work and continued academic and industry support, EKR can become a key remedial tool for successful completion of future nuclear site remediation and decommissioning challenges.

7.4 References

Agnew, K., Cundy, A.B., Hopkinson, L., Croudace, I.W., Warwick, P.E., Purdie, P., 2011. Electrokinetic remediation of plutonium-contaminated nuclear site wastes: Results from a pilot-scale on-site trial. Journal of Hazardous Materials 186, 1405–1414. https://doi.org/10.1016/j.jhazmat.2010.12.016

BNFL, 1979. Annual Discharge Monitoring Reports 1979-2005. British Nuclear Fuels Ltd. (BNFL)/ Sellafield Ltd.

Cundy, A.B., Hopkinson, L., 2005. Electrokinetic iron pan generation in unconsolidated sediments: implications for contaminated land remediation and soil engineering. Applied Geochemistry 20, 841–848. https://doi.org/10.1016/j.apgeochem.2004.11.014

DePaoli, D.W., Harris, M.T., Ally, M.R., Morgan, I.L., Cate, N., Ellis, M.E., Heath, K., Hovist, D.W., Kabalka, G.W., Anderson, C.L., Tang, C., 1996. Testing and Evaluation of Electrokinetic Decontamination of Concrete (No. DOE/ORO/2036). Oak Ridge National Laboratory, Oak Ridge, Tennessee.

Purkis, Burrell, F., Brydie, J.R., Graham, J., Hopkinson, L., Cundy, A.B., 2023. Electrokinetic generation of iron-rich barriers in soils: realising the potential for nuclear site management and

Chapter 7

decommissioning. Environmental Science: Advances 2, 652–662. https://doi.org/10.1039/D2VA00308B

Purkis, J.M., Tucknott, A., Croudace, I.W., Warwick, P.E., Cundy, A.B., 2021a. Enhanced electrokinetic remediation of nuclear fission products in organic-rich soils. Applied Geochemistry 125, 104826. https://doi.org/10.1016/j.apgeochem.2020.104826

Purkis, J.M., Warwick, P.E., Graham, J., Hemming, S.D., Cundy, A.B., 2021b. Towards the application of electrokinetic remediation for nuclear site decommissioning. Journal of Hazardous Materials 413, 125274. https://doi.org/10.1016/j.jhazmat.2021.125274

Sellafield Ltd., 2006. Annual Discharge Monitoring Reports 2006-2021. Sellafield Ltd.

Takeno, N., 2005. Atlas of Eh-pH diagrams, Intercomparison of thermodynamic databases, Geological Survey of Japan Open File Report No.419 (Geological Survey of Japan Open File No. 419). National Institute of Advanced Industrial Science and Technology, Research Center for Deep Geological Environments, Tsukuba, Japan.

Valdovinos, V., Monroy-Guzmán, F., Bustos, E., 2016. Electrokinetic removal of radionuclides contained in scintillation liquids absorbed in soil type Phaeozem. Journal of Environmental Radioactivity 162–163, 80–86. https://doi.org/10.1016/j.jenvrad.2016.05.017

Appendix A

Supporting Information for Chapter 3

Sellafield Groundwater Simulant	Mass used per litre of Milli Q water
Constituent	
MgSO ₄	50 mg
KHCO₃	11 mg
CaCl ₂	95 mg
NaHCO ₃	94 mg
Ca(NO ₃) ₂	37 mg
SrCl ₂ .6H ₂ O	34 mg
0.1 M HCl	6 mL

Table A.1– Sellafield groundwater simulant (SGWS) recipe.

A.1 Radionuclide Solution Preparation

The volume for Sr-85 and Tc-99 solutions were made to be 0.1 g per silicone tube/ recovery standard. However, due to the activity of the H-3 source available and the low limits of detection possible with liquid scintillation counting (LSC), it was decided that 0.07 g (200 Bq) would be used instead. This was seen as an acceptable compromise to introducing a similar volume of solution as with Sr-85 and Tc-99 without using excess H-3 or requiring source dilution. As the source was tritiated water, no pH adjustments needed to be made before addition to the experiments.

The initial Sr-85 source was dissolved in 0.1 M HCl, meaning 0.1 mL of the radionuclide would greatly affect the pH of \sim 4.5 mL of SGWS used in each experiment. As such, 4000 Bq of Sr-85 (1000 Bq per experiment and 1000 Bq remainder kept as a 100 % recovery reference for gamma spectrometry counting) was evaporated and redissolved in 0.4 g of 0.01 M HCl, giving it a final pH of 3 and therefore causing a much smaller impact on the starting experimental conditions. This decayed over a few days, making the starting activities for the experiments < 1000 Bq.

Tc-99 was stored in water, meaning no pH adjust had to be made prior to the experimental start time. An aliquot of the source was taken and diluted to create 0.4 g solution containing 18 Bq Tc (4.5 Bq per silicone tube, with the final 4.5 Bq fraction retained as a 100 % recovery reference for LSC counting).

A.2 Preliminary Experiments with Stable Sr and Re

A.2.1 Introduction

Initial proof-of-concept experiments were carried out over 54 hours to determine the EKR efficacy for stable Sr and Re (as analogues for Sr-90 and Tc-99, respectively) through 3-dimensional trials containing simulated groundwaters in authentic Sellafield subsurface material. Trials were performed in six plastic boxes that contained one of three sediment configurations: sand only, as a simplified recreation of the Sellafield subsurface, homogeneous sand (80 %) and clay (20 %) mix, as a more accurate representation of true Sellafield sediments, and sand with two biochar barriers, to imitate a combined remedial approach of EKR and permeable reactive barriers (PRBs). Biochar was selected as it deemed a more environmentally friendly alternative to peat compost (Steiner and Harttung, 2014), organic material known to adsorb Sr and Re (e.g. Jang et al., 2018; Zinicovscaia et al., 2021), If successful, the combination of EKR-induced migration into a biochar PRB could be an effective pairing for containing and retaining radionuclides.

A.2.2 Methods

Sediment configurations were created in plastic boxes (22 x 10 x 7 cm, L x W x H), henceforth referred to as cells, creating six cells with three different scenarios (Figure A.1). One of each configuration had EKR applied, whilst the remaining cells were diffusion-only cells. Plastic perforated tubes were burrowed into the sediment at the centre of the cells and at both ends, creating water sampling wells. Each cell was saturated with ~ 200 mL of Sellafield groundwater simulant (SGWS; recipe in Table A.1) and graphite electrodes placed in perforated tubes at either end of each EKR cell. Initial pH and SGWS samples were taken before 15 g of contaminant solution, containing 1000 ppm Sr and Re, were introduced to the centre wells. Sampling periods were at five minutes, two hours, seven hours, 30 hours, and 54 hours post-addition of Sr and Re contaminant solution. Cells were left without coverings during the experimental run time to allow evaporation to occur, creating more authentic Sellafield conditions and also avoiding build-up of H₂ and O₂ gases generated at the electrodes. As a result, SGWS was added each morning to compensate for the extensive evaporation that occurred overnight. After collection, SGWS samples were filtered through 20 µm filters, diluted using 2.5 % HNO₃ in Milli Q water (MQ) and analysed in an Agilent 8800 Triple Quadrupole ICP-MS, following the method outlined in Purkis et al. (2021).

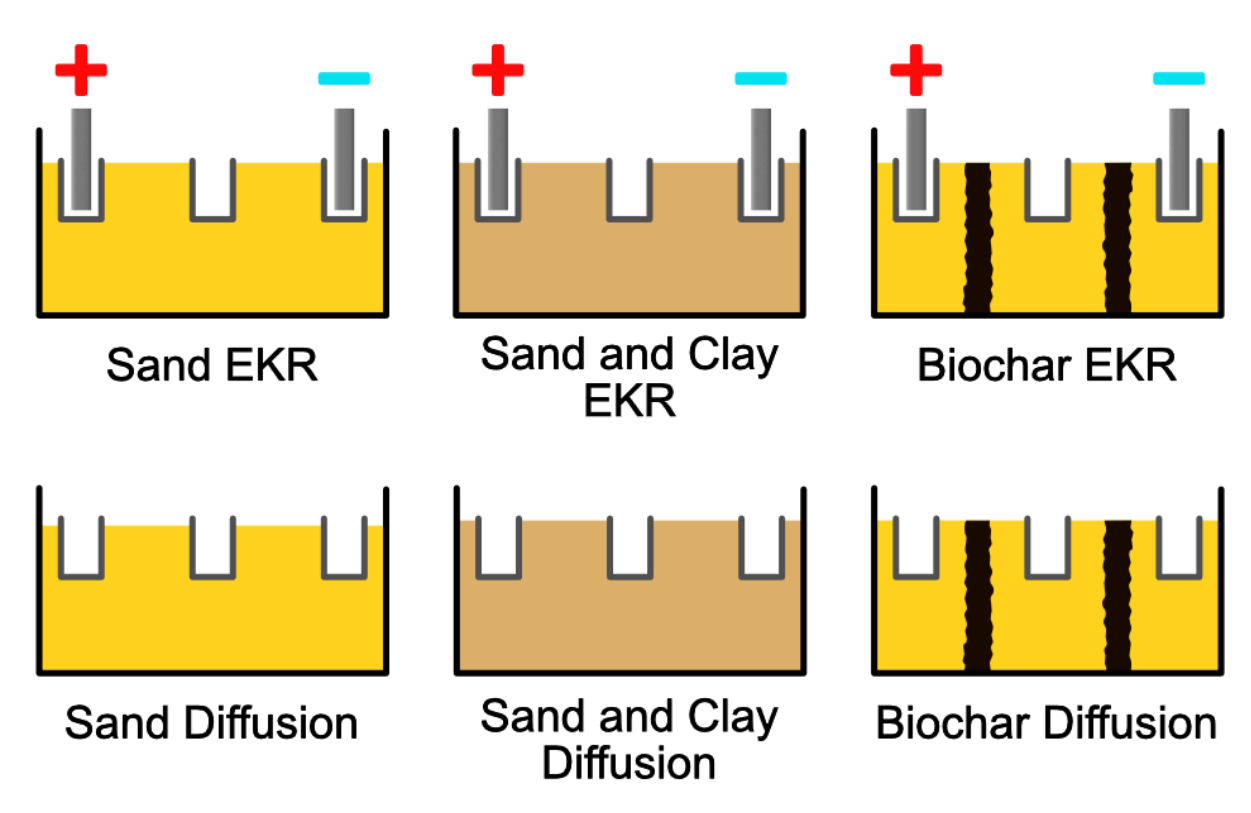


Figure A.1 – Schematic for the groundwater experiment setups, with the abbreviations used.

A.2.3 Results

A.2.3.1 Cell pHs

Each EKR cell established a pH gradient within 2-4 hours of treatment initiation (Figure A.2). Starting pHs across all cells were between 6.4 and 7.6, with all three EKR cathodic and anodic regions maintaining pHs of ~ 11 and ~ 3 , respectively after 4 hours of treatment. In contrast, after an initial equilibration period of ~ 2 hours, each control cell maintained a pH of ~ 6 for treatment duration.

A.2.3.2 Sr and Re Concentrations

Pre-contamination background concentrations for Sr and Re in the middle wells were found to be < 1 ppm. Across all cells, the middle well concentrations of both contaminants five minutes after contaminant solution addition were $\sim 600\text{-}700$ ppm before decreasing gradually over the following 54-hour period. In each of the three setups, the rate of concentration decrease in the EKR cells was faster than in the control counterparts. Consequently, the final Sr and Re concentrations in the EKR middle wells were $\sim 10 \%$ lower than in the diffusion equivalents (Figure A.3; Table A.2), although only the treated sand-only cell had concentrations decrease close to background levels with 54 hours.

Appendix A

Generally, edge wells experienced Sr and Re increases to 2-9 ppm within two hours of contaminant addition and would gradually decrease towards background levels over the experimental period. However, exceptions to this were observed, particularly in the diffusion cells, where concentrations would fluctuate at one time period before returning to earlier behaviour. After treatment, no Sr concentration increases were observed in any of the edge wells, whereas the sand-only and sand with clay EKR setups displayed elevated Re levels of 5 ppm and 49 ppm, respectively.

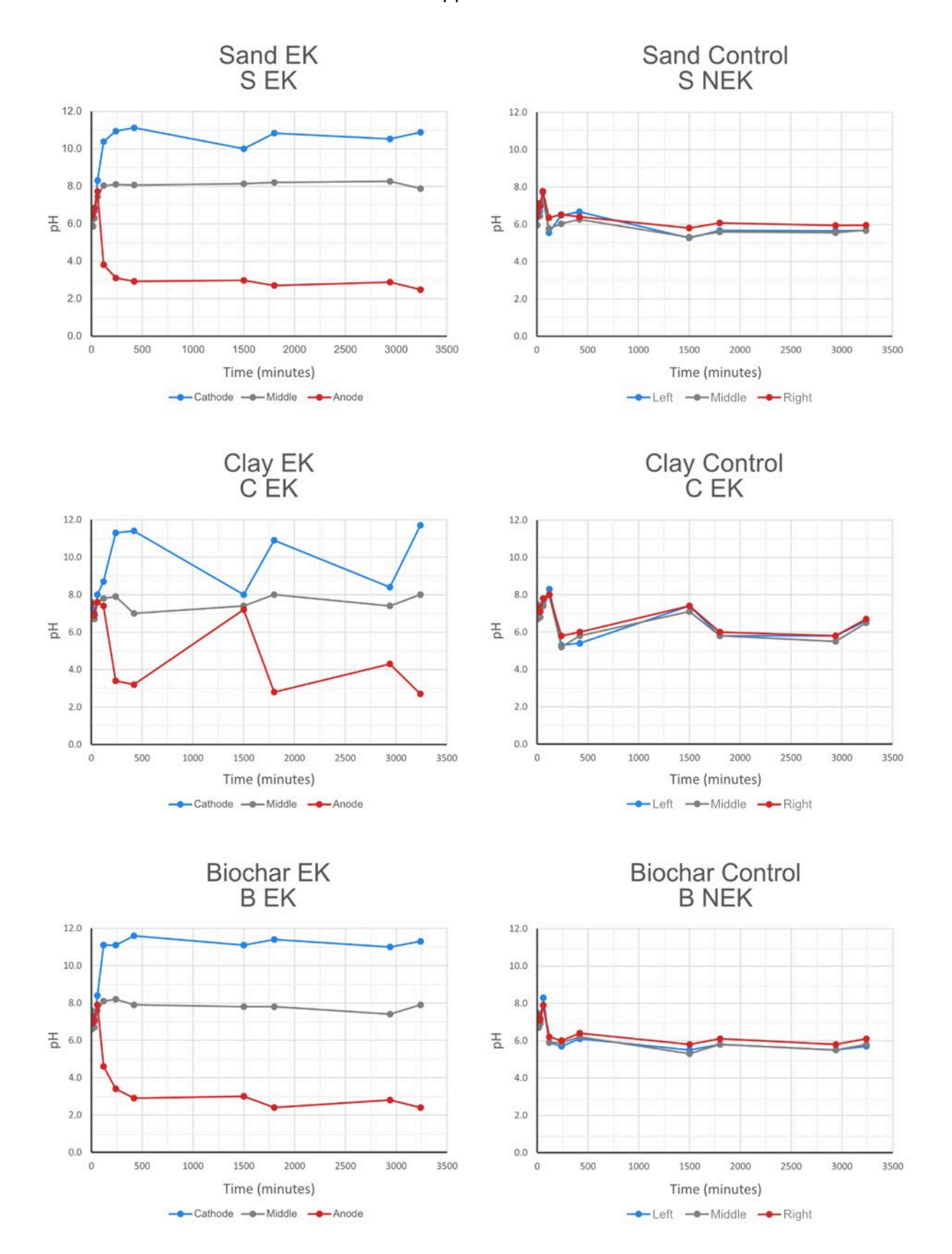


Figure A.2 – Groundwater pH graphs from each cell throughout the experiment

Concentration Reductions in Centre Wells

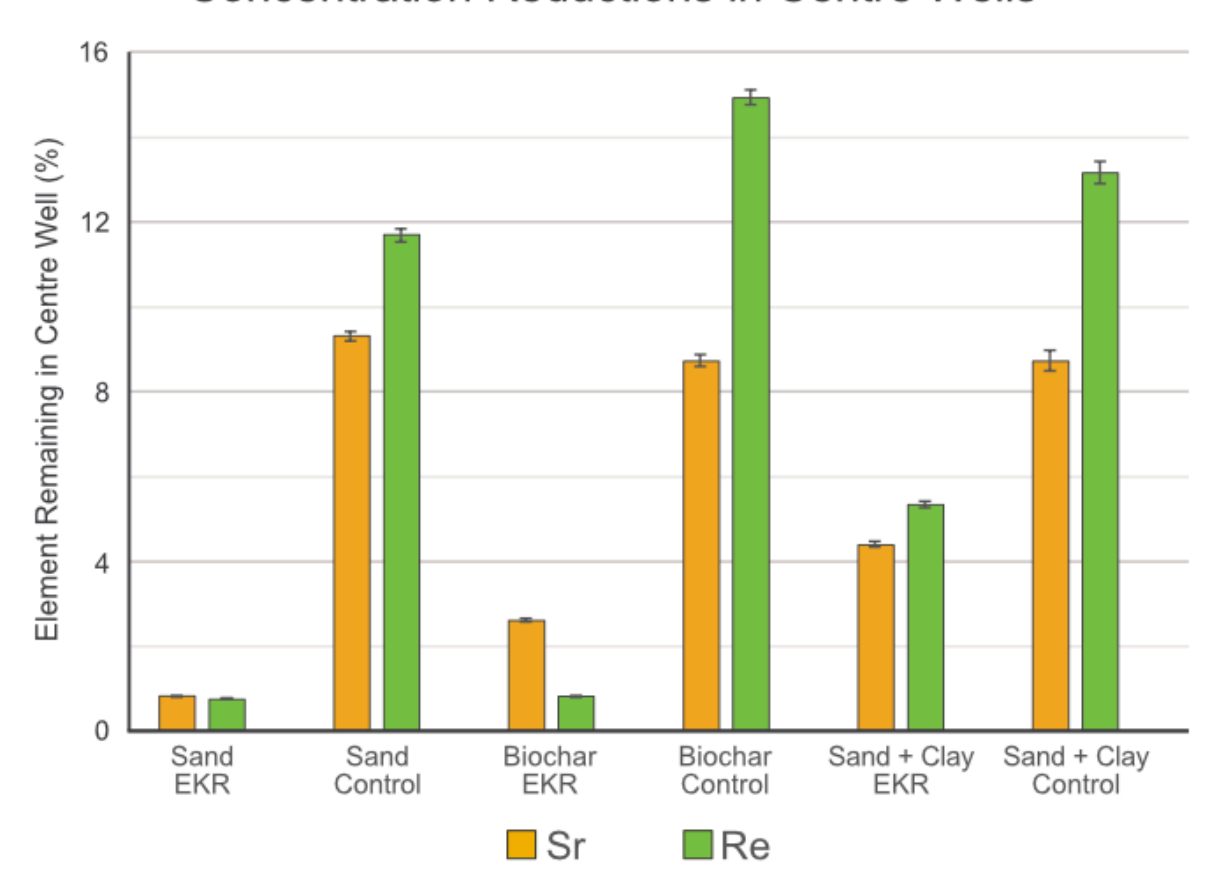


Figure A.3 – Reduction in Sr and Re concentration within the centre wells of each cell. Bars without uncertainties are too small to see.

Cell	Increased Sr reduction in EKR centre well relative to diffusion cell centre well (%)	Increased Re reduction in EKR centre well relative to diffusion cell centre well (%)
Sand	8.5 ± 0.1	11.0 ± 0.2
Sand with clay	6.2 ± 0.1	14.2 ± 0.2
Biochar	4.4 ± 0.2	7.9 ± 0.3

Table A.2 – Summary showing improvement in Sr and Re removal from the centre wells of EKR cells compared to diffusion cells.

A.2.4 Discussion

The \sim 10 % greater average in Sr and Re reduction for each EKR cell compared to the diffusion-only counterparts (Figure A.3) suggests that EKR can migrate Sr and Re away from the cell centres more efficiently than with diffusion alone. Increased Re abundances in the sand and sand with clay anode wells suggests the element's existence of a negatively charged species, likely ReO_4 as predicted by Eh/pH models for simplified systems (Takeno, 2005). However,

whilst the sand-only and sand with clay EKR cells showed some Re migration, the lack of Sr in the majority of edge wells was unexpected considering the large decreases in nuclide concentrations in the centre wells. If Sr and Re had completely diffused into the ~ 200 mL of SGWS then all wells would be expected to have concentrations of ~70 ppm, significantly greater than the 1 ppm frequently measured at the edge wells of all cells. Low permeabilities within the sediments may have prevented water and ionic flow, but this would not explain why the sand with clay EKR cell, which were expected to have a lower permeability of all three setups, had the greatest Re accumulation at the anode of all cells despite also having the highest Re concentration remaining in the centre well after 54 hours. Further, this hypothesis also does not explain anomalies observed in the edge wells, where Sr and Re concentrations would fluctuate before dropping to background levels after. Instead, it is much more likely that significant evaporation each night, caused by the cells being operated in a fume cupboard, and the subsequent daily ~50 mL SGWS addition to the edge wells each morning repeatedly washed Sr and Re back towards the cell centres. A revised experimental setup that removed the complexities introduced by evaporation and rehydration of the cell should be devised in order to accurately assess EKR as a viable option for groundwater remediation.

A.2.5 Conclusions

Proof-of-concept groundwater remedial trials for Sr and Re were performed using authentic Sellafield sediment and simulated groundwater, with three different cell setups used. Overall, EKR enhanced contaminant migration away from the centre wells, where the contaminant solution was added, but evidence of transportation to the electrode was absent in the case of Sr and somewhat tentative for Re, given the apparent decreases in the concentration of both radionuclides compared to the ~70 ppm expected if complete diffusion had occurred. This was likely caused by the extreme fluctuation in water levels during the experiment caused by evaporation from fume cupboard air flow, and subsequent addition of SGWS washing contaminants away from the cell edges. As such, simplified two-dimension trials should be attempted to ascertain EKR efficacy with these contaminants before larger three-dimensional cells are repeated.

A.2.6 References

Jang, J., Miran, W., Divine, S.D., Nawaz, M., Shahzad, A., Woo, S.H., Lee, D.S., 2018. Rice straw-based biochar beads for the removal of radioactive strontium from aqueous solution. Science of The Total Environment 615, 698–707. https://doi.org/10.1016/j.scitotenv.2017.10.023

Appendix A

Purkis, J.M., Tucknott, A., Croudace, I.W., Warwick, P.E., Cundy, A.B., 2021. Enhanced electrokinetic remediation of nuclear fission products in organic-rich soils. Applied Geochemistry 125, 104826. https://doi.org/10.1016/j.apgeochem.2020.104826

Steiner, C., Harttung, T., 2014. Biochar as a growing media additive and peat substitute. Solid Earth 5, 995–999. https://doi.org/10.5194/se-5-995-2014

Takeno, N., 2005. Atlas of Eh-pH diagrams, Intercomparison of thermodynamic databases, Geological Survey of Japan Open File Report No.419 (Geological Survey of Japan Open File No. 419). National Institute of Advanced Industrial Science and Technology, Research Center for Deep Geological Environments, Tsukuba, Japan.

Zinicovscaia, I., Yushin, N., Grozdov, D., Vergel, K., Nekhoroshkov, P., Rodlovskaya, E., 2021. Treatment of Rhenium-Containing Effluents Using Environmentally Friendly Sorbent, Saccharomyces cerevisiae Biomass. Materials 14, 4763. https://doi.org/10.3390/ma14164763

Experiment	Aqueous												11-12	13-14	Aqueous
Description	(start)	0-1 cm	1-2 cm	2-3 cm	3-4 cm	4-5 cm	5-6 cm	6-7 cm	7-8 cm	8-9 cm	9-10 cm	10-11 cm	cm	cm	(End)
H-3 Diffusion	63.29 +/-	12.33 +/-	6.94 +/-	5.57	3.24 +/-	3.49 +/-	2.11	1.15 +/-	0.76 +/-	0.36 +/-	0.29 +/-	0.18 +/-	0.12 +/-	0.08 +/-	0.09 +/-
	4.37	1.64	0.93	+/-	0.45	0.48	+/-	0.17	0.12	0.07	0.04	0.03	0.02	0.02	0.02
				0.75			0.30								
H-3 0.5 V/cm	19.04 +/-	7.01 +/-	10.16	11.28	10.97	10.17	9.89	6.07 +/-	6.18 +/-	3.88 +/-	1.87 +/-	1.29 +/-	0.93 +/-	0.55 +/-	0.62 +/-
	1.27	0.93	+/- 1.33	+/-	+/- 1.44	+/- 1.33	+/-	0.81	0.82	0.52	0.25	0.17	0.13	0.08	0.09
				1.48			1.30								
Sr-85	53.73 +/-	0.00 +/-	0.00 +/-	38.75	5.61 +/-	0.77 +/-	0.71	0.41 +/-	0.02 +/-	< 0.01	< 0.01	< 0.01	< 0.01	< 0.01	< 0.01
Diffusion	2.19	0.00	0.00	+/-	0.24	0.04	+/-	0.03	0.00						
				1.58			0.04								
Sr-85 0.5	13.69 +/-	21.66 +/-	32.76	27.21	4.55 +/-	0.08 +/-	0.05	< 0.01	< 0.01	< 0.01	< 0.01	< 0.01	< 0.01	< 0.01	< 0.01
V/cm	0.53	0.83	+/- 1.25	+/-	0.19	0.01	+/-								
				1.04			0.01								
Sr-85 1 V/cm	0.99 +/-	1.72 +/-	1.57 +/-	5.38	4.71 +/-	10.79	31.74	29.74 +/-	12.51	0.82 +/-	0.01 +/-	< 0.01	< 0.01	< 0.01	< 0.01
	0.05	0.07	0.07	+/-	0.18	+/- 0.40	+/-	1.09	+/- 0.47	0.04	0.00				
				0.21			1.16								

Tc-99	35.21 +/-	17.03 +/-	11.26	11.14	7.14 +/-	7.6 +/-	2.58	2.67 +/-	0.9 +/-	1.81 +/-	1.36 +/-	0.09 +/-	0.4 +/-	0.36 +/-	0.44 +/-
Diffusion	3.89	4.76	+/- 2.03	+/-	1.36	2.31	+/-	1.05	0.29	0.74	0.36	0.34	0.22	0.39	0.23
				3.23			0.64								
Tc-99 0.5	< 0.01	Not	< 0.01	< 0.01	< 0.01	Not	< 0.01	< 0.01	< 0.01	1.29 +/-	< 0.01	4.17 +/-	10.3 +/-	42.99	10.52 +/-
V/cm		measured				measure				0.96		1.70	2.30	+/-	2.34
						d								12.67	
Tc-99 1 V/cm	0.66 +/-	1.06 +/-	< 0.01	< 0.01	< 0.01	Not	< 0.01	Not	< 0.01	1.90 +/-	1.85 +/-	Not	4.58 +/-	5.01 +/-	23.43 +/-
	0.30	0.73				measure		measured		0.92	0.56	measured	0.99	1.7	4.05
						d									

Table A.3 – Percentage of total recovered activities present in each tubing section of every experiment performed in Chapter 3. Summarised results can be found in Figure 3.4. Uncertainties are quoted to 2σ.

Appendix B

Supporting Information for Chapter 4

B.1 Analytical Methods

For all radionuclide analysis, each cement section was first ground into a powder using an agate mortar and pestle, and subsamples from these were taken for analytical preparation.

B.1.1 H-3 and I-129

The following paragraph describes the method used for the cement samples only. Cement samples were loaded into a RADDEC Pyrolyser-6 $Trio^{TM}$. The Pyrolyser was set to run for 5.5 hours, with the sample zone ramping from 50 °C to 900 °C and catalyst zone maintaining 800 °C throughout. Air was selected as the flow-through gas, with volatile radionuclides collected in 20 mL solution of 6 mmol Na_2CO_3 .

Of this, 8 mL was mixed with 12 mL of Gold Star™ cocktail for direct counting of I-129 in a Wallac 1220 Quantulus™ Ultra Low Level Liquid Scintillation Counter (2-hour count times) and analysed with WinQ software. The remaining 12 mL was placed in a distillation rig to allow the tritiated water to evaporate and recondense, consequently separating it from the I-129. Finally, 8 mL of the recondensed fraction was mixed with 12 mL of Gold Star™ cocktail and counted in a Wallac 1220 Quantulus™ Ultra Low Level Liquid Scintillation Counter (2-hour count times) and analysed with LSC+ software (Raddec; Romsey, UK).

The following paragraph describes the procedure undergone by electrolyte and soaking solution samples only. TrisKem Cl-Resin^{M} was loaded with 2 x 50 mg of AgNO₃, and left in darkness overnight. The following day, the column was washed with 2 x 5 mL of Milli Q. Load solutions were prepared by adding \sim 4.8 mg of stable I^{T} carrier to each \sim 45 mL of sample, followed by enough 2 M $\mathrm{H}_2\mathrm{SO}_4$ to obtain a pH of 5-6. These were loaded onto the columns, washed with 2 x 5 mL of Milli Q and then 2 x 5 mL of 1 M NaOH.

I-129 was eluted with 5 mL of freshly prepared 0.35 M Na₂S. A 0.1 mL aliquot of eluent was taken, transferred into a centrifuge tube, and diluted to 5 mL for stable iodine recovery analysis by ion chromatography. The remaining solution had 0.5 mL of 2 M Na₂SO₃ added and then mixed with 14.5 mL of Gold Star™ LSC cocktail before being counted in a Wallac 1220 Quantulus™ Ultra Low Level Liquid Scintillation Counter.

B.1.2 Sr-90, Cs-137, and U-236

As Sr-90, Cs-137, and U-236 analysis were performed sequentially, cement samples were placed in beakers and spiked with 50 mg of Sr-85 and 50 mg of U-232. Beakers then had 30 g of *aqua regia*

added and were left on a hotplate at 95 °C for three hours. The contents of each were then poured into centrifuge tubes and centrifuged at 4000 rpm for four minutes. The supernatant was decanted, replaced with 30 g of fresh *aqua regia*, and left on a hotplate overnight at 85 °C. The supernatant was decanted and combined with the first digest, before being evaporated down to ~ 20 g. Cement residues in the tubes were individually gravity filtered to ensure all digest was collected. The final samples were counted in a well-type HPGe gamma spectrometers (3-hour count times for samples above limit of detection (LOD), 12-hour times for samples close to, or below, LOD) and analysed with Fitzpeaks software (JF Computing, Stanton in the Vale, UK).

The filtered cement residues for Section 5 samples later underwent fusion digestion to confirm that acid digestion was sufficient for extracting all radionuclides of focus. For this, Section 5 residues and filter papers were ignited at 450 °C overnight and then transferred into graphite crucibles. Li metaborate was added to the crucibles at a 5:1 metaborate: residue ratio. Samples were then fused at 1100 °C for 45 minutes before being quenched in water. This liquid was decanted and replaced with 50 mL of 8 M HNO₃ and left to dissolve on a magnetic stirrer/hotplate at 80 °C overnight. The resultant solutions were combined with the original *aqua regia* digests and recounted in HPGe gamma spectrometers.

B.1.3 Sr-90 and U-236 (Continued)

After Cs-137 counting, the digests were made to pH < 4 using concentrated HNO₃, with 2 mg of stable $SrCl_2 \cdot 6H_2O$ and 10 mg of $FeCl_3$ added to each to act as carriers. Bromocresol green indicator was introduced, along with enough concentrated ammonia to create a pH of >4 and form Fe precipitates. After the precipitates had coalesced and cooled, samples were centrifuged at 4000 RPM for four minutes. The Sr fractions (supernatant) were decanted, leaving the U fractions (precipitate).

B.1.3.1 Sr-90 Purification

The following paragraph describes the method used for the cement samples only. Sr supernatants was evaporated to dryness before being redissolved in 5 mL of concentrated HNO $_3$ and 5 mL of concentrated HCl. The solutions were then diluted to 50 mL with Milli Q water, before 50 mL of 4 % ammonium oxalate and 5 drops of bromocresol green were added. Concentrated ammonia was introduced dropwise until the solutions changed from a yellow to blue colour (pH 4-5). The mixtures were warmed to allow the precipitate to coagulate and settle. A further 2 drops of 4 % ammonium oxalate were added to ensure no further precipitation occurred – if more precipitate formed then additional 4 % ammonium oxalate was added until no more solid was produced. The solutions were then passed through a cellulose nitrate filter. Filtrates were washed

with 20 mL of Milli Q before being ignited in a furnace overnight at 450°C. Residues were left to cool and then dissolved in 5 mL of 8 M HNO $_3$. These were loaded onto a TrisKem Sr Resin[™] (100 – 150 µm particle size) column, before 3 x 5 mL 8 M HNO $_3$ washing were performed. The time of the final HNO $_3$ washings were recorded as these were the point of Y-90 separation and was used when decay correcting final sample activities. The Sr was eluted using 2 x 5 mL of Milli Q water. The chemical recovery was determined through Hidex AMG gamma spectrometry of Sr-85 (2-hour count times), whilst Cerenkov counting in a Wallac 1220 Quantulus[™] Ultra Low Level Liquid Scintillation Counter determined the Sr-90 activity (2-hour count times).

The following paragraph describes the procedure undergone by electrolyte and soaking solution samples only. The Sr solutions were evaporated to dryness and then had 3 mL of concentrated HCl and 1 mL of concentrated HNO₃ added to them. After an additional evaporation to dryness, addition of 3 mL of concentrated HCl and 1 mL of concentrated HNO₃, and final evaporation to dryness, the residues were dissolved in 5 mL of 8 M HNO₃. Subsequent filtering through cellulose nitrate filters, Sr columns, and gamma spectrometry and liquid scintillation counting were performed identically to the method described above for cement samples.

B.1.3.2 U-236 Purification and Electrodeposition

The U-containing residues were dissolved in 5 mL of concentrated HNO $_3$, before 15 mL of 8 M HNO $_3$ was added. These were loaded onto TrisKem UTEVA columns (100 – 150 μ m particle size), followed by TrisKem anion exchange columns (Cl-form; 100 – 200 μ m particle size). After a 40 mL 8 M HNO $_3$ washing, the anion columns were removed and 20 mL of 6 M HCl was put through the UTEVA column. The U was then eluted using 30 mL 0.02 M HNO $_3$. The eluents had 1 mL of 1 % Na $_2$ SO $_4$ added before being evaporated to dryness. The samples were then dissolved in 1 mL of 1.2 M HCl and gently warmed, before the addition of 5 mL of 4 % ammonium oxalate. These underwent electrodeposition onto stainless steel discs for 1.5 hours and then had 5 drops of concentrated ammonia was added. The discs were counted via EG&G ORTEC Octete PC alpha spectrometer.

Electrokinetic Cells' Current Over Time

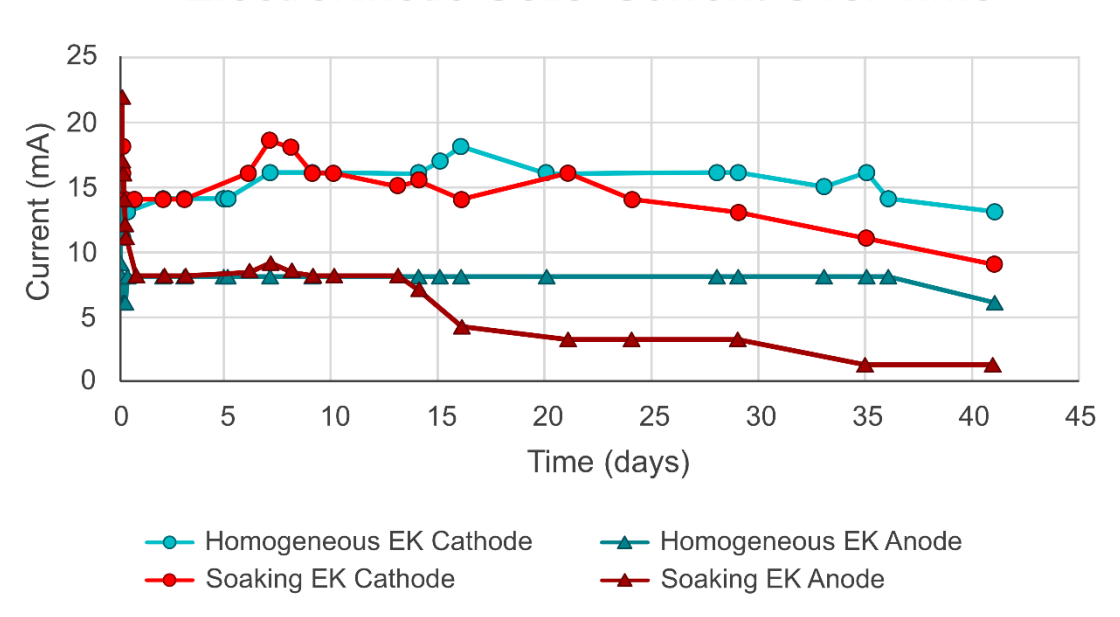


Figure B.1 – Electrical current recorded over the duration of the experiment.

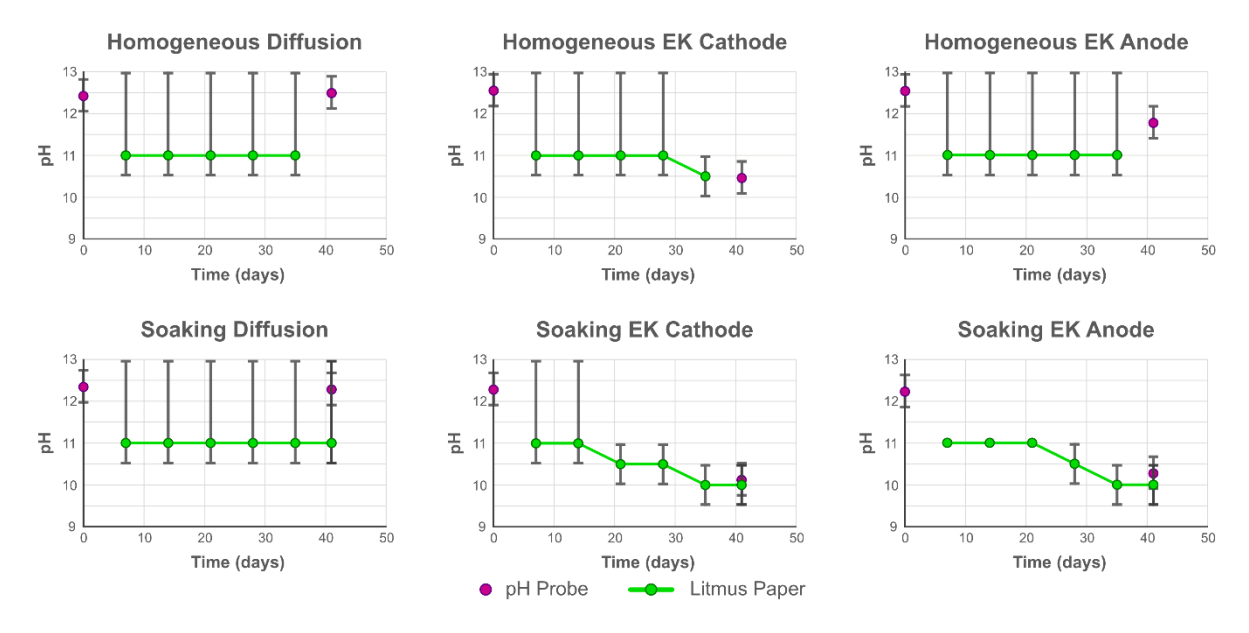


Figure B.2 – pH data recorded over the duration of the experiment. Data measured with a HANNA pH probe (uncertainty \pm 0.2) is shown with a purple dot and values recorded through indicator paper are shown in green (\pm 0.5). The pH probe measured up to a maximum pH of 14, whereas the indicator paper measured pH up to 11, meaning any value of 11 has a lower bound of \sim 10.5 and no upper bound.

Appendix B

Electrolyte	H-3 (Bq/g)	Sr-90 (Bq/g)	I-129 (Bq/g)	Cs-137 (Bq/g)	U-236 (Bq/g)
Homogeneous	1.67 ± 0.02	< 0.01	< 0.01	0.21 ± 0.01	< 0.001
Diffusion					
Homogeneous	1.52 ± 0.02	< 0.01	< 0.01	0.04 ± 0.00	< 0.001
Cathode					
Homogeneous	1.45 ± 0.02	< 0.01	< 0.01	0.19 ± 0.01	< 0.001
Anode					
Soaking	0.76 ± 0.03	< 0.01	0.24 ± 0.01	0.04 ± 0.00	< 0.001
Diffusion					
Soaking	0.65 ± 0.03	< 0.01	0.04 ± 0.00	0.07 ± 0.00	0.002 ± 0.000
Cathode					
Soaking	0.59 ± 0.03	< 0.01	0.07 ± 0.00	0.04 ± 0.00	0.001 ±0.000
Anode					

Table B.1 – Radionuclide activities found in the electrolyte after diffusion or EKR.

Supporting Information for Chapters 5 and 6

Section	Control core		Seawater c	ore	Citric acid core	9
	LOI 450°C	LOI 950°C	LOI 450°C	LOI 950°C	LOI 450°C	LOI 950°C
	(wt%)	(wt%)	(wt%)	(wt%)	(wt%)	(wt%)
0-1	16.60	4.06	*	*	*	*
1-2	17.66	3.33	8.13	10.94	25.82	28.47
3-4	22.79	3.39	9.50	5.50	*	*
5-6	14.84	3.02	8.42	5.53	48.92	19.29
7-8	13.06	2.74	*	*	49.58	3.42
9-10	12.58	2.64	*	*	52.73	2.62
11-12	12.08	5.94	*	*	51.42	2.20
13-14	11.42	2.76	12.86	4.17	49.29	2.25
15-16	10.19	2.71	13.31	3.59	44.04	2.34
17-18	10.26	2.51	13.22	3.40	41.42	4.65
19-20	10.02	2.81	12.91	3.69	40.67	5.85
21-22	7.92	2.57	12.22	4.25	43.09	2.30
23-24	8.60	2.52	9.66	2.81	41.41	5.78
25-26	7.80	2.57	10.23	2.67	43.14	2.37
27-28	6.90	2.73	8.78	2.64	40.08	2.41
28-29	6.97	3.28	9.41	3.48	Not performed	Not performed
29-30	7.66	2.71	8.21	2.61	36.79	2.45
30-31	7.40	3.21	8.41	3.12	Not performed	Not performed
31-32	7.39	3.17	8.05	2.68	37.33	2.55
33-34	6.66	2.84	7.70	2.86	32.93	2.35
35-36	7.44	3.08	7.48	2.41	34.36	2.47
37-38	6.52	2.96	7.51	2.58	25.06	9.60
39-40	6.28	2.85	7.21	2.78	30.25	2.05

41-42	6.00	3.05	6.89	2.52	30.59	1.80
43-44	6.14	2.94	7.32	2.99	27.92	1.68
45-46	5.97	2.67	8.07	4.20	26.13	1.77
47-48	5.89	2.54	5.98	2.88	27.91	5.75
49-50	5.47	2.77	7.48	2.74	26.95	1.94
51-52	6.06	2.85	6.96	3.87	25.08	1.77
53-54	6.11	2.74	8.59	3.10	25.99	2.00
55-56	-	-	-	-	26.78	2.37

Table C.1 – Loss on ignition (LOI) data for freeze-dried sediment sections. Asterisks denote samples that did not have LOIs determined due to samples at adjacent depths melting at 950°C and fusing to the crucibles.

Radionuclide/ stable element detected	Units	Yellow liquid from seawater core	Yellow liquid from citric acid core
Tc-99	Bq/kg	3.7 ± 1.1	< 0.12
Cs-137	Bq/kg	3.9 +/- 0.9	1.1 +/- 0.5
Pu-238	Bq/kg	0.9 +/- 0.2	0.8 +/- 0.2
Pu-239+240	Bq/kg	9.8 +/- 1.1	22 +/- 2.3
Pu-241	Bq/kg	17 +/- 7.5	21 +/- 7.9
Am-241	Bq/kg	129 +/- 0.5	4.8 +/- 0.6
Mn-55 (stable)	ppm	128 +/- 0.4	47 +/- 0.3
Fe-56 (stable)	ppm	5260 +/- 10	4281 +/- 10
Fe-57 (stable)	ppm	5175 +/- 26	4106 +/- 37

Table C.2 – Radiometric and selected stable element analysis of yellow liquids produced from the seawater and citric acid cores during EKR. Stable element quantification was performed with ICP-MS using the method used in (Purkis et al., 2021) with the following modifications: Hefilled reaction cell (introduced at 4.3 mL/min); sample input = \sim 0.3 mL/min; 5 ppb Rh was used as the internal standard; reference solutions = 0-20 ppb Mn and 0-20 ppb Fe, both in 2.5 % HNO₃ with 5 ppb Rh.

Control	Cs-137	Pu-238	Pu-239+240	Pu-241	Am-241	Tc-99
Core	(Bq/kg)	(Bq/kg)	(Bq/kg) *	(Bq/kg)	(Bq/kg)	(Bq/kg)
Depth						
(cm)						
-0.5	245 +/- 26	90 +/- 22	653 +/- 83	3360 +/- 1205	957 +/- 63	40 +/- 11
-1.5	291 +/- 35	97 +/- 44	816 +/- 153	< 2925	1137 +/- 75	-
-2.5	303 +/- 26	-	-	-	1100 +/- 71	-
-3.5	316 +/- 30	81 +/- 42	953 +/- 155	< 5851	1224 +/- 82	58 +/- 16
-4.5	319 +/- 36	-	-	-	1169 +/- 78	-
-5.5	371 +/- 29	191 +/- 54	839 +/- 134	4316 +/- 1616	1392 +/- 89	-
-6.5	406 +/- 32	-	-	-	1625 +/- 110	37 +/- 9
-7.5	383 +/- 36	117 +/- 59	942 +/- 172	< 7364	1444 +/- 92	-
-8.5	394 +/- 31	-	-	-	1350 +/- 85	-
-9.5	459 +/- 39	179 +/- 21	1037 +/- 109	4976 +/- 473	1916 +/- 120	76 +/- 21
-10.5	456 +/- 44	-	-	-	1826 +/- 120	-
-11.5	495 +/- 37	186 +/- 67	1235 +/- 199	6030 +/- 2317	1986 +/- 130	-
-12.5	518 +/- 40	-	-	-	2217 +/- 140	106 +/- 23
-13.5	564 +/- 45	186 +/- 64	1133 +/- 188	4715 +/- 2360	1926 +/- 120	120 +/- 28
-14.5	528 +/- 36	-	-	-	1816 +/- 120	118 +/- 28
-15.5	731 +/- 49	209 +/- 82	1325 +/- 229	7621 +/- 3253	2478 +/- 161	177 +/- 44
-16.5	727 +/- 51	-	-	-	2247 +/- 140	132 +/- 30
-17.5	850 +/- 55	331 +/- 111	1625 +/- 280	5444 +/- 2978	2588 +/- 161	128 +/- 29
-18.5	1072 +/- 70	-	-	-	3531 +/- 221	74 +/- 19
-19.5	1277 +/- 85	395 +/- 120	2212 +/- 339	6363 +/- 4300	3411 +/- 211	-
-20.5	1405 +/- 81	-	-	-	3371 +/- 211	-
-21.5	2042 +/- 126	472 +/- 140	2599 +/- 403	8668 +/- 6248	4715 +/- 291	64 +/- 16

-22.5	3026 +/- 168	-	-	-	5859 +/- 361	-
-23.5	4251 +/- 241	699 +/- 170	4082 +/- 556	< 19757	6270 +/- 381	-
-24.5	4879 +/- 272	-	-	-	7875 +/- 472	38 +/- 9
-25.5	6450 +/- 356	1431 +/- 385	7820 +/- 1150	51717 +/- 21467	11537 +/- 692	-
-26.5	6387 +/- 346	-	-	-	13674 +/- 823	-
-27.5	7758 +/- 419	1783 +/- 492	9268 +/- 1381	96762 +/- 30894	17155 +/- 1104	67 +/- 17
-28.5	9245 +/-	1534 +/- 189	8532 +/- 927	34869 +/- 3812	18960 +/- 1204	-
-29.5	8889 +/- 471	2589 +/- 824	11579 +/- 1974	89994 +/- 47655	24980 +/- 1505	-
-30.5	6345 +/- 346	1694 +/- 499	13880 +/- 1921	< 64208	26886 +/- 1605	32 +/- 9
-31.5	4753 +/- 262	1474 +/- 459	10969 +/- 1585	< 31492	16131 +/- 973	-
-32.5	3005 +/- 168	-	-	-	9019 +/- 542	-
-33.5	2157 +/- 126	241 +/- 73	3316 +/- 421	< 11991	4976 +/- 301	26 +/- 7
-34.5	1537 +/- 93	-	-	-	2067 +/- 130	-
-35.5	990 +/- 59	< 15	1331 +/- 170	< 2158	741 +/- 48	-
-36.5	881 +/- 55	-	-	-	391 +/- 20	17 +/- 5
-37.5	736 +/- 53	12 +/- 5	564 +/- 68	< 466	219 +/- 21	-
-38.5	755 +/- 47	-	-	-	214 +/- 18	-
-39.5	609 +/- 41	8 +/- 3	416 +/- 49	< 249	136 +/- 13	13 +/- 4

-40.5	536 +/- 42	-	-	-	84 +/- 23	-
-41.5	445 +/- 32	7 +/- 3	154 +/- 20	< 237	107 +/- 12	-
-42.5	286 +/- 23	-	-	-	91 +/- 11	7 +/- 2
-43.5	203 +/- 18	5 +/- 2	50 +/- 8	< 232	79 +/- 9	8 +/- 2
-44.5	164 +/- 21	-	-	-	47 +/- 9	7 +/- 2
-45.5	116 +/- 14	4 +/- 1	25 +/- 4	99 +/- 65	43 +/- 7	4 +/- 2
-46.5	67 +/- 9	-	-	-	27 +/- 6	4 +/- 1
-47.5	53 +/- 12	2 +/- 1	10 +/- 2	< 63	20 +/- 7	6 +/- 2
-48.5	43 +/- 8	-	-	-	20 +/- 6	2 +/- 2
-49.5	30 +/- 7	2 +/- 1	12 +/- 2	< 210	16 +/- 5	-
-50.5	19 +/- 8	-	-	-	< 14	-
-51.5	11 +/- 4	< 2	7 +/- 1	< 188	< 9	1 +/- 1
-52.5	< 12	-	-	-	< 11	-
-53.5	12 +/- 6	2 +/- 1	12 +/- 2	54 +/- 29	20 +/- 6	2 +/- 1
Seawater	Cs-137	Pu-238	Pu-239+240	Pu-241	Am-241	Tc-99
Core	(Bq/kg)	(Bq/kg)	(Bq/kg) *	(Bq/kg)	(Bq/kg)	(Bq/kg)
Depth						
(cm)						
-0.5	198 +/- 32	20 +/- 3	102 +/- 12	452 +/- 89	879 +/- 63	20 +/- 6
-1.5	285 +/- 28	88 +/- 12	503 +/- 55	2410 +/- 351	962 +/- 65	-
-2.5	211 +/- 43	-	-	-	1395 +/- 100	-
-3.5	362 +/- 31	218 +/- 26	1331 +/- 140	5663 +/- 598	1447 +/- 94	11 +/- 3
-4.5	344 +/- 47	-	-	-	1695 +/- 120	-
-5.5	375 +/- 42	#N/A	#N/A	#N/A	2247 +/- 150	-
-6.5	287 +/- 51	-	-	-	4896 +/- 311	14 +/- 4
-7.5	437 +/- 37	119 +/- 14	708 +/- 74	3149 +/- 310	4233 +/- 261	-
	i .	i .	1	1	1	1

-15.5 558 +/- 38 241 +/- 29 1607 +/- 169 5571 +/- 599 8808 +/- 532 94 +/- 23 -16.5 762 +/- 53 11477 +/- 692 104 +/- 2: -17.5 751 +/- 53 289 +/- 35 1935 +/- 204 7516 +/- 829 8427 +/- 51 101 +/- 2: -18.5 913 +/- 58 7243 +/- 441 75 +/- 18 -19.5 1267 +/- 80 391 +/- 47 2331 +/- 247 8887 +/- 979 12460 +/- 75220.5 1411 +/- 95 12269 +/- 74221.5 1424 +/- 83 387 +/- 97 2663 +/- 349 10770 +/- 5291 6992 +/- 421 70 +/- 17 -22.5 2010 +/ 4855 +/- 30123.5 2712 +/- 615 +/- 148 2997 +/- 427 15141 +/- 5784 4003 +/- 251 - 168 -24.5 3193 +/ 3150 +/- 201 43 +/- 11 -25.5 4502 +/- 251 903 +/- 152 5330 +/- 621 22619 +/- 6496 3571 +/- 22126.5 6408 +/- 356 3682 +/- 23127.5 6732 +/- 1997 +/- 10982 +/- 55829 +/- 8493 3270 +/- 201 52 +/- 13 -28.5 7371 +/- 1637 +/- 9632 +/- 1214 40483 +/- 3351 +/- 211 -							
-10.5	-8.5	446 +/- 42	-	-	-	4284 +/- 271	-
-11.5	-9.5	470 +/- 38	99 +/- 12	632 +/- 66	2726 +/- 276	4344 +/- 271	22 +/- 6
-12.5	-10.5	428 +/- 36	-	-	-	6410 +/- 391	-
-13.5	-11.5	478 +/- 43	27 +/- 5	149 +/- 18	482 +/- 163	6752 +/- 411	-
-14.5	-12.5	440 +/- 30	-	-	-	6942 +/- 421	65 +/- 15
-15.5	-13.5	480 +/- 34	199 +/- 24	1161 +/- 122	4768 +/- 507	9851 +/- 592	78 +/- 18
-16.5	-14.5	1025 +/- 70	-	-	-	15459 +/- 933	137 +/- 29
-17.5	-15.5	558 +/- 38	241 +/- 29	1607 +/- 169	5571 +/- 599	8808 +/- 532	94 +/- 23
-18.5 913 +/- 58 7243 +/- 441 75 +/- 18 -19.5 1267 +/- 80 391 +/- 47 2331 +/- 247 8887 +/- 979 12460 +/- 75220.5 1411 +/- 95 12269 +/- 74221.5 1424 +/- 83 387 +/- 97 2663 +/- 349 10770 +/- 5291 6992 +/- 421 70 +/- 17 -22.5 2010 +/ 4855 +/- 30123.5 2712 +/- 615 +/- 148 2997 +/- 427 15141 +/- 5784 4003 +/- 25124.5 3193 +/ 3150 +/- 201 43 +/- 11 -25.5 4502 +/- 903 +/- 152 5330 +/- 621 22619 +/- 6496 3571 +/- 22126.5 6408 +/- 356 3682 +/- 23127.5 6732 +/- 1997 +/- 10982 +/- 55829 +/- 8493 3270 +/- 201 52 +/- 13 -28.5 7371 +/- 1637 +/- 9632 +/- 1214 40483 +/- 3351 +/- 211 -	-16.5	762 +/- 53	-	-	-	11477 +/- 692	104 +/- 22
-19.5	-17.5	751 +/- 53	289 +/- 35	1935 +/- 204	7516 +/- 829	8427 +/- 51	101 +/- 25
-20.5	-18.5	913 +/- 58	-	-	-	7243 +/- 441	75 +/- 18
-21.5	-19.5	1267 +/- 80	391 +/- 47	2331 +/- 247	8887 +/- 979	12460 +/- 752	-
-22.5	-20.5	1411 +/- 95	-	-	-	12269 +/- 742	-
-23.5	-21.5	1424 +/- 83	387 +/- 97	2663 +/- 349	10770 +/- 5291	6992 +/- 421	70 +/- 17
-23.5	-22.5	2010 +/-	-	-	-	4855 +/- 301	-
168 -24.5 3193 +/- 178 3150 +/- 201 43 +/- 11 -25.5 4502 +/- 251 903 +/- 152 5330 +/- 621 22619 +/- 6496 3571 +/- 221 3682 +/- 231 3682 +/- 231 3682 +/- 231 - 356 3682 +/- 231 - 3682 +/- 231		126					
-24.5 3193 +/- 178 3150 +/- 201 43 +/- 11 -25.5 4502 +/- 903 +/- 152 5330 +/- 621 22619 +/- 6496 3571 +/- 221 - 251 -26.5 6408 +/- 356 3682 +/- 231 - 356 -27.5 6732 +/- 1997 +/- 10982 +/- 55829 +/- 8493 3270 +/- 201 52 +/- 13 366 274 1217 - 3351 +/- 211 -	-23.5		615 +/- 148	2997 +/- 427	15141 +/- 5784	4003 +/- 251	-
178		168					
-25.5	-24.5	3193 +/-	-	-	-	3150 +/- 201	43 +/- 11
251		178					
-26.5 6408 +/- - - 3682 +/- 231 -	-25.5	4502 +/-	903 +/- 152	5330 +/- 621	22619 +/- 6496	3571 +/- 221	-
356 10982 +/- 55829 +/- 8493 3270 +/- 201 52 +/- 13 366 274 1217 55829 +/- 8493 3270 +/- 201 52 +/- 13 -28.5 7371 +/- 1637 +/- 9632 +/- 1214 40483 +/- 3351 +/- 211 -		251					
-27.5 6732 +/- 1997 +/- 10982 +/- 55829 +/- 8493 3270 +/- 201 52 +/- 13 366 274 1217 55829 +/- 8493 3270 +/- 201 52 +/- 13 -28.5 7371 +/- 1637 +/- 9632 +/- 1214 40483 +/- 3351 +/- 211 -	-26.5	6408 +/-	-	-	-	3682 +/- 231	-
366 274 1217		356					
-28.5 7371 +/- 1637 +/- 9632 +/- 1214 40483 +/- 3351 +/- 211 -	-27.5	6732 +/-	1997 +/-	10982 +/-	55829 +/- 8493	3270 +/- 201	52 +/- 13
		366	274	1217			
	-28.5	7371 +/-	1637 +/-	9632 +/- 1214	40483 +/-	3351 +/- 211	-
398 344 15182		398	344		15182		

-29.5	8617 +/-	1525 +/-	9474 +/- 1081	36790 +/- 6939	3170 +/- 201	
-29.3	471	231	3474 +/- 1001	30790 +7- 0939	3170 +/- 201	
	4/1	231				
-30.5	7203 +/-	2286 +/-	11067 +/-	45785 +/-	3020 +/- 191	30 +/- 8
	387	386	1306	11980		
-31.5	5225 +/-	1771 +/-	11123 +/-	33051 +/- 5996	3010 +/- 191	-
	283	234	1204			
-32.5	3706 +/-	-	-	-	1826 +/- 120	-
	209					
-33.5	2544 +/-	270 +/- 62	4703 +/- 565	9265 +/- 2370	1027 +/- 66	32 +/- 8
	147					
-34.5	1647 +/- 93	-	-	-	534 +/- 36	-
-35.5	1391 +/- 84	41 +/- 14	1529 +/- 177	< 1265	453 +/- 33	-
-36.5	1023 +/- 66	-	-	-	319 +/- 24	19 +/- 5
-37.5	848 +/- 54	31 +/- 10	900 +/- 103	699 +/- 415	273 +/- 21	-
-38.5	747 +/- 47	-	-	-	265 +/- 21	-
-39.5	766 +/- 53	24 +/- 8	429 +/- 54	< 477	191 +/- 17	18 +/- 7
-40.5	502 +/- 34	-	-	-	133 +/- 12	-
-41.5	448 +/- 35	13 +/- 5	206 +/- 27	< 258	158 +/- 15	-
-42.5	251 +/- 23	-	-	-	58 +/- 7	6 +/- 2
-43.5	161 +/- 16	6 +/- 2	70 +/- 9	94 +/- 78	52 +/- 6	6 +/- 2
-44.5	140 +/- 16	-	-	-	45 +/- 7	5 +/- 1
-45.5	120 +/- 17	6 +/- 1	64 +/- 8	155 +/- 54	31 +/- 7	2 +/- 1
-46.5	95 +/- 10	-	-	-	17 +/- 4	2 +/- 1
-47.5	88 +/- 12	3 +/- 1	24 +/- 3	56 +/- 29	18 +/- 5	2 +/- 1
-48.5	77 +/- 12	-	-	-	35 +/- 6	2 +/- 1
-49.5	61 +/- 8	4 +/- 1	86 +/- 10	69 +/- 58	38 +/- 6	-
-50.5	49 +/- 8	-	-	-	59 +/- 7	-
-51.5	37 +/- 8	2 +/- 1	13 +/- 3	< 150	81 +/- 10	3 +/- 2

-52.5	23 +/- 5	-	-	-	82 +/- 8	-
-53.5	24 +/- 6	4 +/- 2	34 +/- 7	< 186	106 +/- 12	2 +/- 1
Citric	Cs-137	Pu-238	Pu-239+240	Pu-241	Am-241	Tc-99
Acid	(Bq/kg)	(Bq/kg)	(Bq/kg) *	(Bq/kg)	(Bq/kg)	(Bq/kg)
Core						
Depth						
(cm)						
-0.45	126 +/- 26	263 +/- 117	1589 +/- 388	< 723	4133 +/- 301	19 +/- 5
-1.36	157 +/- 18	199 +/- 47	1327 +/- 189	1521 +/- 553	3170 +/- 201	-
-2.27	162 +/- 24	-	-	-	4013 +/- 251	-
-3.18	214 +/- 40	217 +/- 36	1473 +/- 168	5165 +/- 1174	4605 +/- 341	17 +/- 4
-4.08	186 +/- 16	-	-	-	2889 +/- 181	-
-4.99	53 +/- 7	756 +/- 161	4743 +/- 595	15774 +/- 6416	1936 +/- 120	-
-5.90	132 +/- 19	-	-	-	3541 +/- 221	21 +/- 6
-6.81	207 +/- 18	301 +/- 139	2837 +/- 519	< 12714	3421 +/- 211	-
-7.72	265 +/- 23	-	-	-	4745 +/- 291	-
-8.62	297 +/- 27	366 +/- 159	2535 +/- 441	< 19891	4474 +/- 321	30 +/- 8
-9.53	297 +/- 35	-	-	-	3371 +/- 221	-
-10.44	364 +/- 31	464 +/- 146	2524 +/- 406	< 18392	3832 +/- 241	-
-11.35	395 +/- 34	-	-	-	3140 +/- 231	54 +/- 12
-12.25	444 +/- 38	440 +/- 179	2577 +/- 465	< 20767	3481 +/- 221	61 +/- 14
-13.16	430 +/- 35	-	-	-	3521 +/- 221	68 +/- 16
-14.07	460 +/- 4	353 +/- 147	2142 +/- 403	13394 +/- 8721	3311 +/- 241	64 +/- 18
-14.98	471 +/- 35	-	-	-	2869 +/- 181	71 +/- 16
-15.88	520 +/- 38	350 +/- 130	2655 +/- 432	14909 +/- 6327	3150 +/- 201	105 +/- 27
-16.79	588 +/- 47	-	-	-	3521 +/- 261	76 +/- 17

	1	1	1	T	1	1
-17.70	643 +/- 42	404 +/- 162	2209 +/- 425	10501 +/- 6659	2990 +/- 191	-
-18.61	807 +/- 54	-	-	-	3341 +/- 211	-
-19.52	841 +/- 60	400 +/- 172	2469 +/- 462	9501 +/- 7867	3441 +/- 251	49 +/- 11
-20.42	888 +/- 57	-	-	-	3591 +/- 221	-
-21.33	836 +/- 51	437 +/- 152	2974 +/- 467	10996 +/- 6242	3240 +/- 201	-
-22.24	1212 +/- 79	-	-	-	4605 +/- 331	25 +/- 6
-23.15	1895 +/-	622 +/- 309	4021 +/- 819	24146 +/-	6812 +/- 482	-
	126			17686		
-24.05	2094 +/-	-	-	-	5447 +/- 331	-
	126					
-24.96	2649 +/-	982 +/- 227	4521 +/- 629	16669 +/-	6892 +/- 421	22 +/- 6
	157			11946		
-25.87	6722 +/-	-	-	-	9841 +/- 692	-
	377					
-26.78	4178 +/-	953 +/- 231	5925 +/- 777	36342 +/-	7464 +/- 451	-
	230			13670		
-27.68	5486 +/-	-	-	-	10363 +/- 632	23 +/- 6
	304					
-28.59	5717 +/-	1496 +/-	8769 +/- 1134	38858 +/-	9731 +/- 682	-
	325	336		16621		
-29.50	7046 +/-	-	-	-	9761 +/- 592	-
	377					
-30.50	6774 +/-	971 +/- 262	6066 +/- 860	< 27222	8768 +/- 612	25 +/- 7
	377					
-31.50	4471 +/-	-	-	-	6681 +/- 411	-
	241					
-32.50	3874 +/-	1053 +/-	6335 +/- 848	21749 +/-	7985 +/- 562	-
	220	251		13629		
-33.50	2586 +/-	-	-	-	4866 +/- 301	17 +/- 5
	147					

24.50	4504 . / 04	110 . / 61	2227 . / 220	CE04 - / 2000	1066 - / 120	
-34.50	1581 +/- 91	140 +/- 61	2327 +/- 328	6584 +/- 3060	1866 +/- 120	-
-35.50	1338 +/- 84	-	-	-	1116 +/- 81	-
-36.50	1096 +/- 65	82 +/- 31	1022 +/- 150	1643 +/- 1037	820 +/- 53	13 +/- 3
-37.50	837 +/- 52	-	-	-	444 +/- 32	-
-38.50	677 +/- 47	73 +/- 32	596 +/- 107	< 4480	471 +/- 37	-
-39.50	615 +/- 39	-	-	-	467 +/- 32	8 +/- 2
-40.50	502 +/- 34	81 +/- 25	512 +/- 81	< 1568	563 +/- 39	13 +/- 3
-41.50	341 +/- 27	-	-	-	460 +/- 36	12 +/- 3
-42.50	328 +/- 25	39 +/- 21	321 +/- 64	< 1793	436 +/- 31	7 +/- 2
-43.50	192 +/- 17	-	-	-	284 +/- 21	5 +/- 1
-44.50	122 +/- 14	< 61	163 +/- 53	< 2820	114 +/- 11	5 +/- 2
-45.50	90 +/- 97	-	-	-	57 +/- 7	1 +/- 1
-46.50	67 +/- 10	7 +/- 2	49 +/- 7	210 +/- 62	26 +/- 5	-
-47.50	43 +/- 6	-	-	-	24 +/- 5	-
-48.50	30 +/- 5	5 +/- 2	33 +/- 6	153 +/- 71	30 +/- 5	3 +/- 1
-49.50	31 +/- 7	-	-	-	58 +/- 8	-
-50.50	25 +/- 5	4 +/- 2	26 +/- 5	< 157	45 +/- 6	3 +/- 1
-51.50	19 +/- 5	-	-	-	410 +/- 6	-
-52.50	15 +/- 5	6 +/- 2	40 +/- 7	31 +/- 16	56 +/- 7	4 +/- 2
•	•			•		

Table C.3 – Activities for each section of all three cores, with the midpoint depths of the 1-cm-thick samples shown. All radionuclides are decay corrected to the date of core collection (06/07/2021) apart from Pu-239+240 as the proportion of each isotope, and therefore contribution to total activity, is unknown. However, because of their long half-lives (24110 years and 6561 years for Pu-239 and Pu-240, respectively (IAEA, 2025)) the extent of decay between collection and analysis will be negligible. Uncertainties are quoted to 2σ .

	Cs-137	Pu-238	Pu-239+240	Pu-241	Am-241	Tc-99
Average radionuclide activity in entire dried control core	1.7x10 ⁻³ +/-	2.9x10-4 +/-	1.9x10-3 +/-	6.3x10-3 +/-	4.0x10 ⁻³ +/-	2.1x10 ⁻⁵ +/-
sediment (Bq/kg)	2.3x10 ⁻⁵	2.6x10-5	8.6x10-5	2.3x10-3	6.5x10 ⁻⁵	1.3x10 ⁻⁶
Average radionuclide activity in entire dried seawater core	1.6x10 ⁻³ +/-	2.7x10 ⁻⁴ +/-	1.7x10 ⁻³ +/-	6.3x10 ⁻³ +/-	3.0x10 ⁻³ +/-	1.9x10 ⁻⁵ +/-
sediment (excluding yellow liquid) (Bq/kg)	2.2x10 ⁻⁵	1.5x10 ⁻⁵	5.9x10 ⁻⁵	5.34x10 ⁻⁴	3.6x10 ⁻⁵	1.3x10 ⁻⁶
Proportion of control core activity in treated seawater core (excluding yellow liquid) (%)	95.4 +/- 1.9	92.8 +/- 9.9	89.4 +/- 5.3	100.8 +/- 37.4	74.7 +/- 1.5	93.3 +/- 8.6
Is seawater core inventory (excluding yellow liquid) within uncertainty of control core inventory?	No	Yes	No	Yes	No	Yes
Average radionuclide activity in entire dried seawater core	1.6x10 ⁻³ +/-	2.7x10 ⁻⁴ +/-	1.7x10 ⁻³ +/-	6.3x10 ⁻³ +/-	3.6x10 ⁻³ +/-	3.6x10 ⁻⁵ +/-
sediment (including yellow liquid) (Bq/kg)	2.3x10 ⁻⁵	1.5x10 ⁻⁵	5.9x10 ⁻⁵	5.3x10 ⁻⁴	5.6x10 ⁻⁵	5.4x10 ⁻⁶
Proportion of control core activity in treated seawater core (including yellow liquid) (%)	96.4 +/- 1.9	92.8 +/- 9.9	89.4 +/- 5.3	100.8 +/- 37.4	89.8 +/- 2.0	176.4 +/- 28.6
Is seawater core inventory (including yellow liquid) within uncertainty of control core inventory?	No	Yes	No	Yes	No	No
Average radionuclide activity in entire dried citric acid core	1.4x10 ⁻³ +/-	2.3x10 ⁻⁴ +/-	1.4x10 ⁻³ +/-	4.5x10 ⁻³ +/-	3.1x10 ⁻³ +/-	1.2x10 ⁻⁵ +/-
sediment (excluding yellow liquid) (Bq/kg)	1.9x10 ⁻⁵	1.8x10 ⁻⁵	5.6x10 ⁻⁵	1.3x10 ⁻³	3.9x10 ⁻⁵	7.5x10 ⁻⁷
Proportion of control core activity in treated citric acid core (excluding yellow liquid) (%)	79.8 +/- 1.6	79.2 +/- 9.6	77.4 +/- 4.7	71.1 +/- 32.9	78.9 +/- 1.6	59.4 +/- 5.2

	Cs-137	Pu-238	Pu-239+240	Pu-241	Am-241	Tc-99
Is citric acid core inventory (excluding yellow liquid) within uncertainty of control core inventory?	No	No	No	Yes	No	No
Average radionuclide activity in entire dried citric acid core sediment (including yellow liquid) (Bq/kg)	1.4x10 ⁻³ +/- 1.9x10 ⁻⁵	2.3x10 ⁻⁴ +/- 1.8x10 ⁻⁵	1.4x10 ⁻³ +/- 5.6x10 ⁻⁵	4.5x10 ⁻³ +/- 1.3x10 ⁻³	3.1x10 ⁻³ +/- 3.9x10 ⁻⁵	1.2x10 ⁻⁵ +/- 7.5x10 ⁻⁷
Proportion of control core activity in treated citric acid core (including yellow liquid) (%)	80.0 +/- 1.6	79.2 +/- 9.6	77.4 +/- 4.7	71.1 +/- 32.9	79.1 +/- 1.6	59.4 +/- 5.2
Is citric acid core inventory (including yellow liquid) within uncertainty of control core inventory?	No	No	No	Yes	No	No

Table C.4 – Total Radionuclide inventories for each core, including activities present in the yellow liquid, and activity changed before and after EKR treatment. Uncertainties quoted to 2σ. N.B. for these calculations, it is assumed the activity in the measured yellow liquid sample is representative of all yellow liquid produced during the experiment.

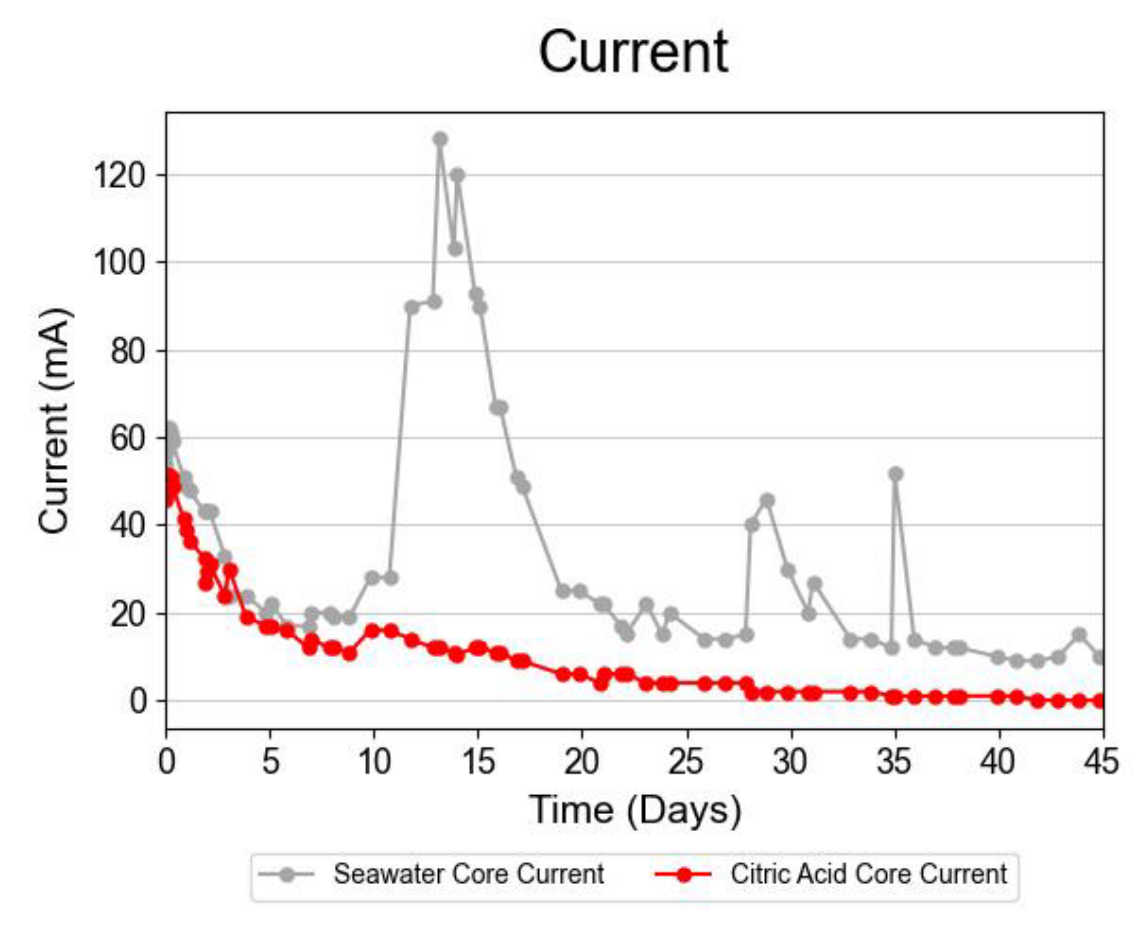


Figure C.1 – electrical current data recorded during EKR trials.

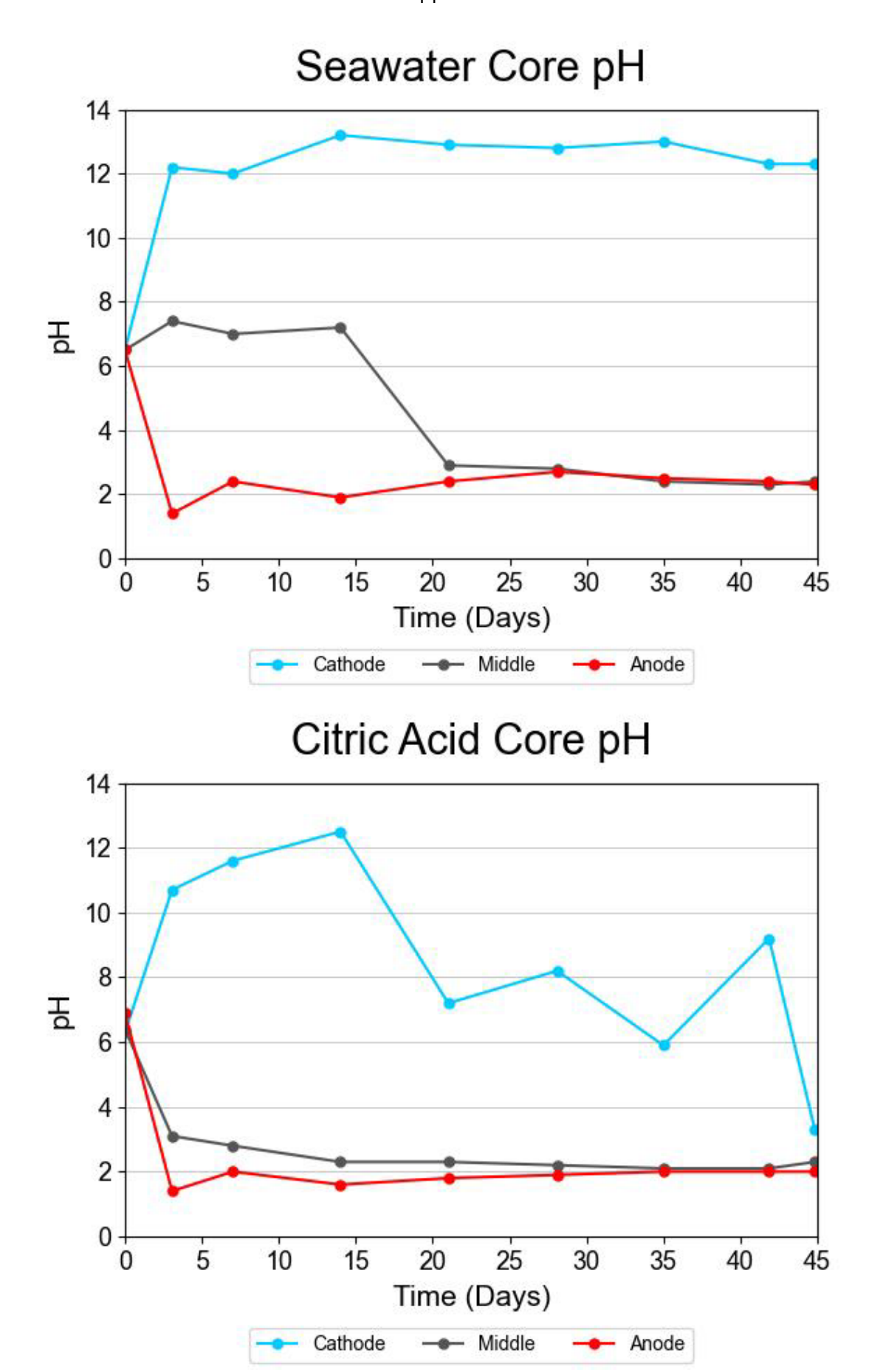


Figure C.2 – sediment and porewater pH data collected seawater core (top) and citric acid core (bottom) during experiments.

.

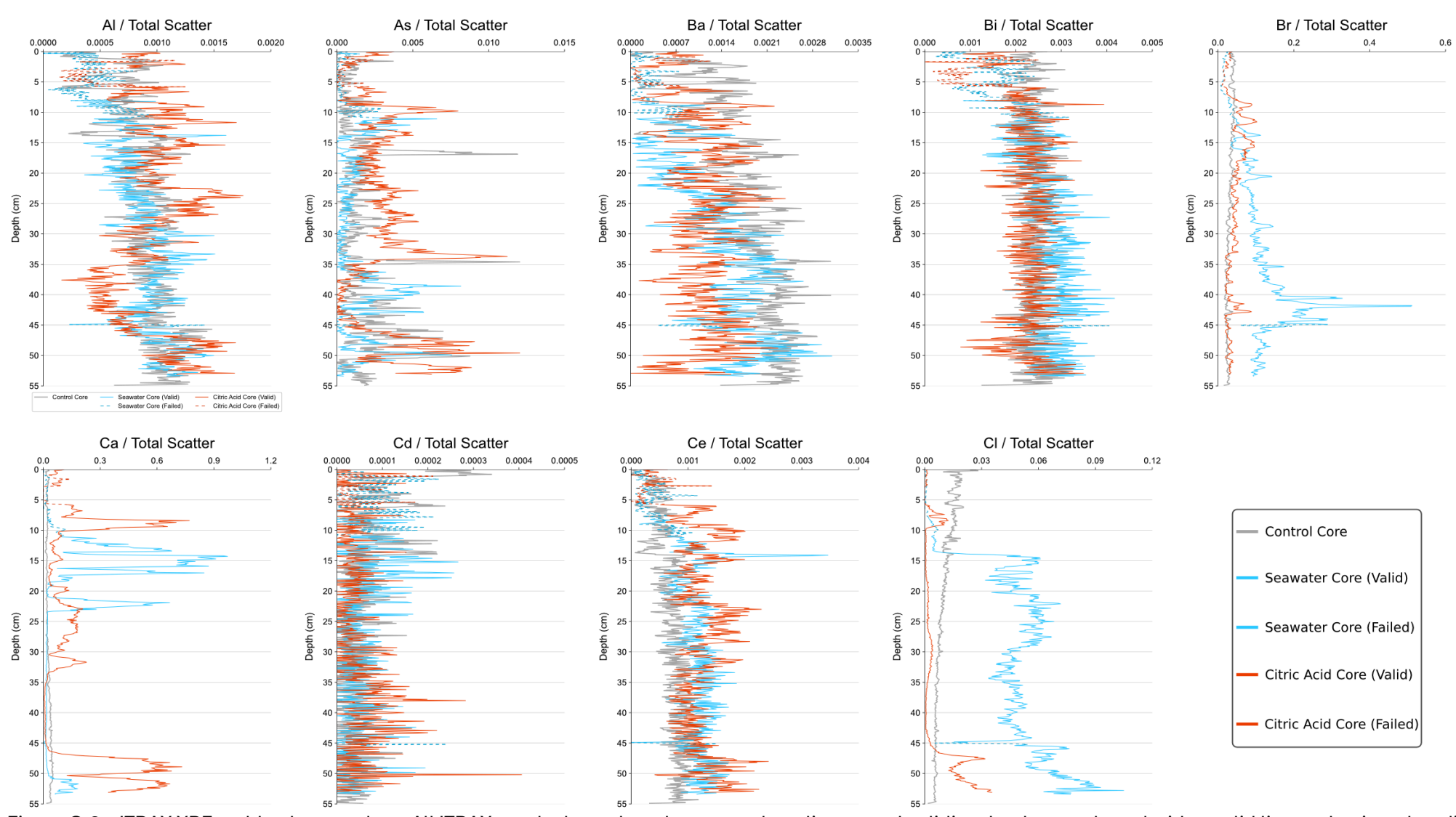
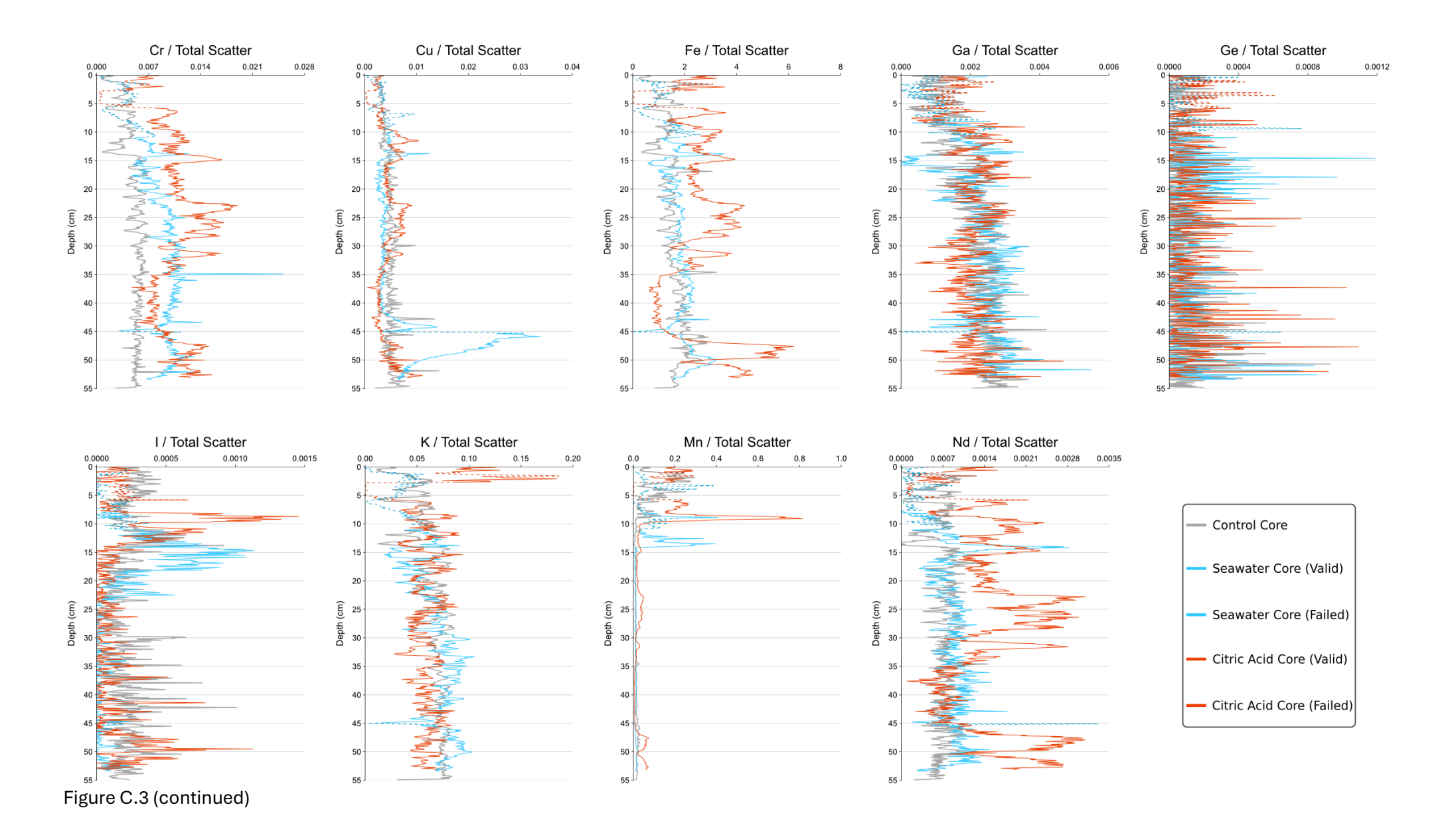


Figure C.3 – ITRAX XRF stable element data. All ITRAX graphs have data that passed quality control validity checks are plotted with a solid line and points that did not meet the criteria are marked with a dashed line. 'Invalid' data points have been included, as peaks and troughs may still indicate large increases or decreases in element concentrations, despite these variations not being quantifiable.



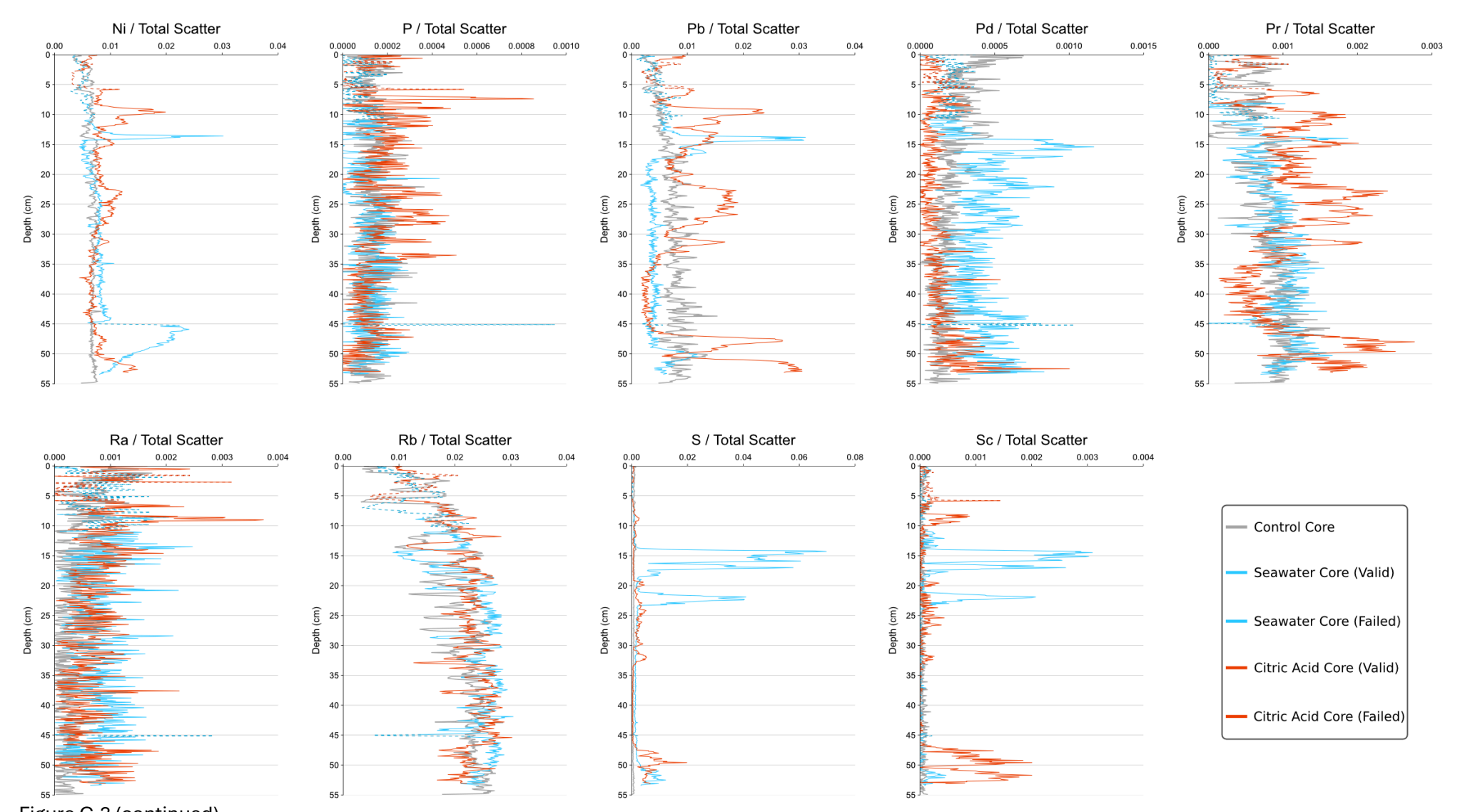
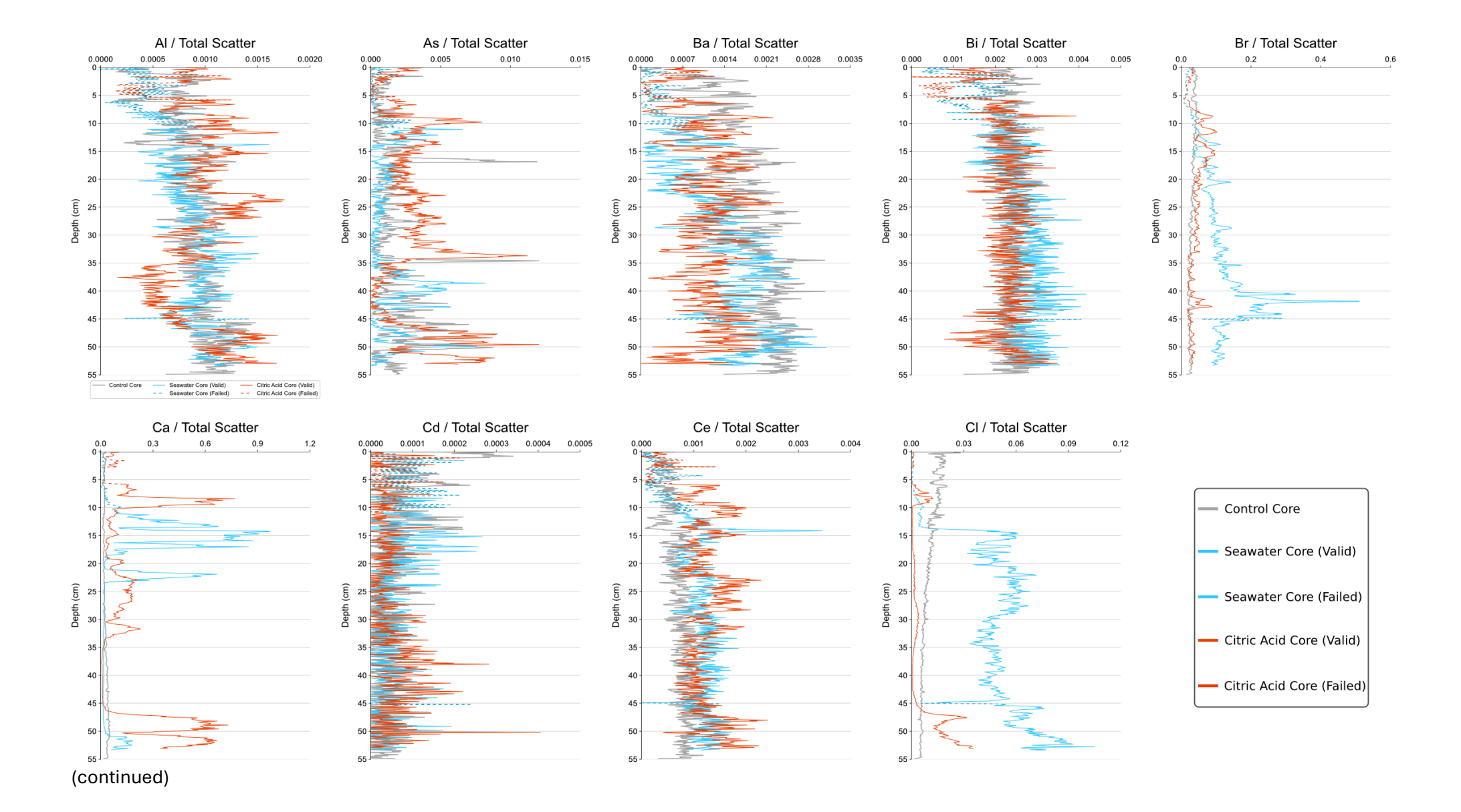


Figure C.3 (continued)

Appendix C



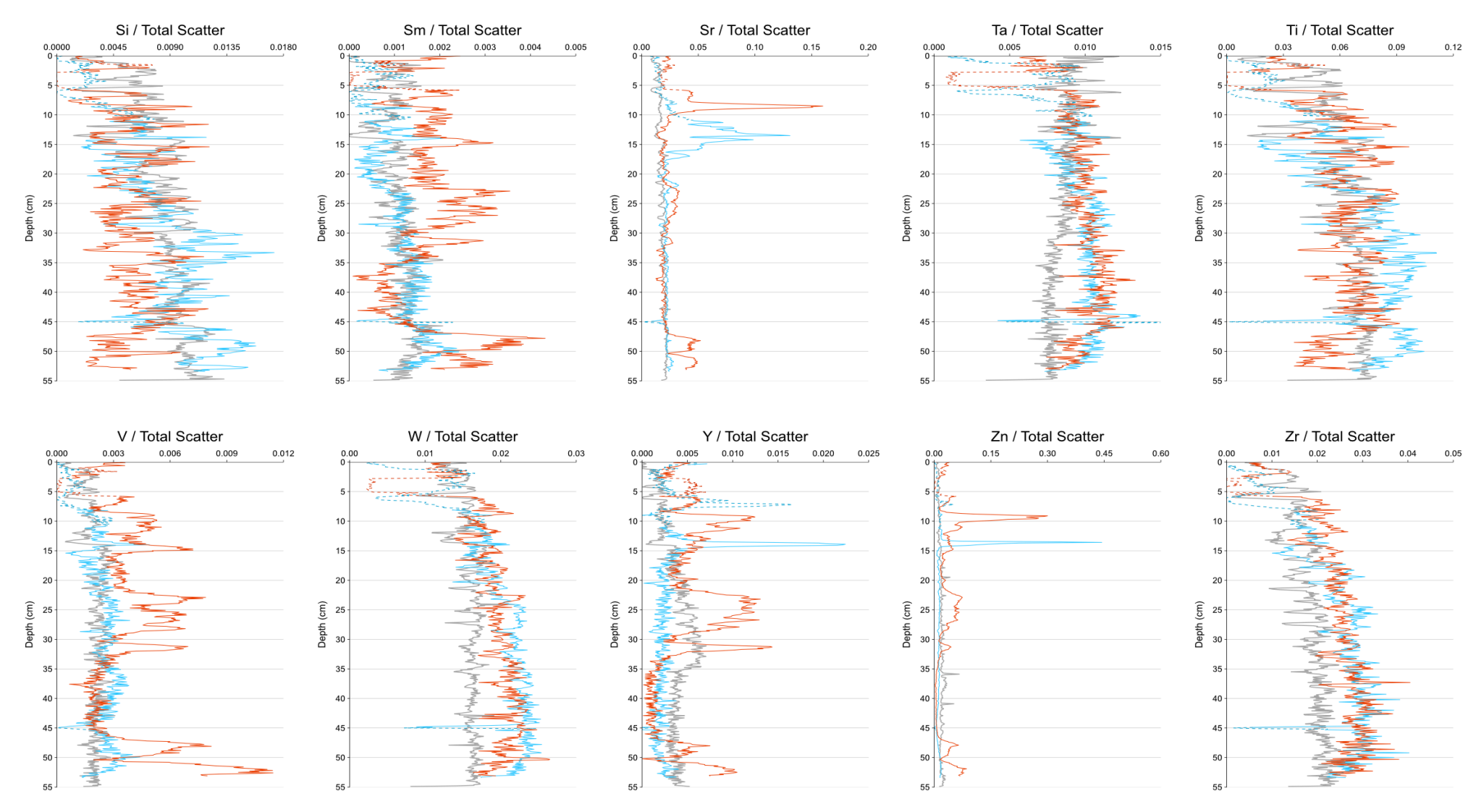


Figure C.3 (continued)

Appendix C

Radionuclide	Threshold defining 'region of elevated activity' (Bq/g)	Depth of 'region of elevated activity' (cm)			
Cs-137	2.6	22-33			
Pu-238	0.6	23-33			
Pu-239	3.7	23-33			
Pu-241	19.8	24-32			
Am-241	7.1	24-33			
Tc-99 peak A	0.04	1-6			
Tc-99 peak B	0.04	7-24			
Tc-99 peak C	0.04	25-30			

Table C.5 – Summary of the threshold definitions and depths of 'regions of elevated activity' for each radionuclide of focus. Multiple regions were found for Tc-99, described here as 'peaks' A, B, and C. Cs-137, Pu, and Am-241 data were initially smoothed by applying a 3-point moving average to every data point (except for the values at the top and bottom of the core, which could only have a 2-point moving average applied), whilst the Tc-99 graph had a 5-point moving average applied to all data points (except for the values at the top and bottom of the core, where 4- or 3-point moving averages were applied). A 3-point moving average was chosen to maintain the resolution of the data and avoid large discrepancies between the true and smoothed maximum values, whilst only performing 1 pass through minimised erratic "noisy" values in the data whilst preserving key traits in each distribution profile. A 5-point moving average for Tc-99 was selected to preserve the resolution of individual peaks, whilst still including multiple data points in each average. The moving-point average did not account for uncertainties. A threshold 'region of elevated activity' value was then calculated for each radionuclide as > 30 % of the maximum smoothed activity to exclude tails in all smoothed profiles whilst consistently including the majority of higher activity samples.

Control Core	Tc-99 activity using Re Tracer	Tc-99 activity using Tc-99m	Measurements within 2σ uncertainty	Measurements within 3σ uncertainty
Sample	(Bq/kg)	Tracer (Bq/kg)	of each other?	of each other?
0-1 cm	0.04 ± 0.01	0.05 ± 0.01	Yes	Yes
3-4 cm	0.06 ± 0.02	0.06 ± 0.02	Yes	Yes
9-10 cm	0.08 ± 0.02	0.13 ± 0.02	No	Yes
12-13 cm	0.11 ± 0.02	0.26 ± 0.04	No	No
15-16 cm	0.18 ± 0.04	0.26 ± 0.05	Yes	Yes
17-18 cm	0.13 ± 0.03	0.17 ± 0.04	Yes	Yes
24-25 cm	0.04 ± 0.01	0.10 ± 0.02	No	No
27-28 cm	0.07 ± 0.02	0.12 ± 0.02	No	Yes
33-34 cm	0.03 ± 0.01	0.04 ± 0.01	Yes	Yes
39-40 cm	0.01± 0.00	0.03 ± 0.01	No	Yes
43-44 cm	0.01 ± 0.00	0.02 ± 0.01	Yes	Yes
47-48 cm	0.01 ± 0.00	< LOD (0.01)	Yes	Yes
53-54 cm	0.00 ± 0.00	< LOD (0.01)	Yes	Yes

Table C.6 – Comparison between Tc-99 activities when using a Re and Tc-99m tracer. Of the 13 samples, eight had pairs of values within 2σ uncertainty of each other and 11 had pairs of values within 3σ .

C.1 References

Purkis, J.M., Tucknott, A., Croudace, I.W., Warwick, P.E., Cundy, A.B., 2021. Enhanced electrokinetic remediation of nuclear fission products in organic-rich soils. Applied Geochemistry 125, 104826. https://doi.org/10.1016/j.apgeochem.2020.104826

Appendix D

Towards the application of electrokinetic remediation for nuclear site decommissioning

Jamie M. Purkis, Phil E. Warwick, James Graham, **Shaun D. Hemming**, Andrew B. Cundy

Published in: Journal of Hazardous Materials 413, 125274 (2021)

ELSEVIER

Contents lists available at ScienceDirect

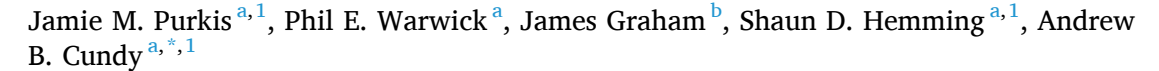
Journal of Hazardous Materials

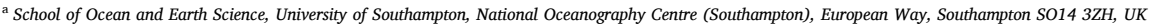
journal homepage: www.elsevier.com/locate/jhazmat



Review

Towards the application of electrokinetic remediation for nuclear site decommissioning





^b National Nuclear Laboratory, Sellafield, Cumbria CA20 1PG, UK

ARTICLE INFO

Editor: Dr. J. He

Keywords: Electrokinetic remediation Nuclear decommissioning Radioactive contamination Sustainable remediation

ABSTRACT

Contamination encountered on nuclear sites includes radionuclides as well as a range of non-radioactive cocontaminants, often in low-permeability substrates such as concretes or clays. However, many commercial remediation techniques are ineffective in these substrates. By contrast, electrokinetic remediation (EKR), where an electric current is applied to remove contaminants from the treated media, retains high removal efficiencies in low permeability substrates. Here, we evaluate recent developments in EKR for the removal of radionuclides in contaminated substrates, including caesium, uranium and others, and the current benefits and limitations of this technology. Further, we assess the present state of EKR for nuclear site applications using real-world examples, and outline key areas for future application.

1. Introduction

Anthropogenic radionuclide contamination arising from nuclear energy generation is a major land quality concern. Accordingly, many technologies exist for the remediation of contaminated materials and effluents at nuclear sites. These include bio- and phyto-remediation, thermal treatment, soil flushing, in-situ chemical oxidation (ISCO), ion exchange and excavation and encapsulation, among others (IAEA, 1999, 2004; US Environmental Protection Agency (EPA), 1996, 2007; TÜV SÜD – Nuclear Technologies Division and Office of Nuclear Regulation (ONR), 2020). Technologies that avoid physical removal of material (in-situ) offer significant benefits over ex-situ techniques, as in-situ approaches reduce the need to handle potentially contaminated materials meaning it is safer for workers. It also reduces the need to transport, store or dispose large quantities of materials, saving energy, waste disposal costs and reducing risk. These make in-situ technologies preferred on-site when safe and practical to do so. However, in-situ technologies must work effectively in a range of low- and high-permeability substrates (soils, sands, clays, etc.) as well as on or around infrastructure (pipework, plastics, concretes, steel, *etc.*). Many existing technologies struggle in low permeability substrates given limited water or reagent flow.

Electrokinetic remediation, EKR, is a technology with several potential advantages over established remediation methods. These include flexible set-up, low-energy requirements and, most importantly, an ability to work in low permeability substrates around (sub)surface infrastructure (Kornilovich et al., 2005). In contrast to soil flushing and similar techniques, EKR is effective in clays, silts and may be applied to varied tills, alluvial and lacustrine deposits, and loess, in addition to various process sludges and other materials. The wide ranging advantages of EKR techniques have driven a number of studies of EKR as a practical, on-site remediation technology including on active and legacy nuclear sites. Following an initial surge in papers in the late 1980s and early 1990s, (Ho et al., 1999) practical uptake of EKR as an "off-the-shelf' remediation technology has been limited however compared to other methods such as bioremediation, ISCO, etc. Research interest in EKR technologies has continued nonetheless (e.g. 123 papers were published in 2016, with "Electrokinetic remediation" either in the title

 $^{^{\}ast}$ Corresponding author.

E-mail address: A.Cundy@noc.soton.ac.uk (A.B. Cundy).

¹ ORCID IDs: Dr. Jamie M. Purkis (0000-0002-6387-1220), Shaun D. Hemming (0000-0001-5826-8710), Prof. Andrew B. Cundy (0000-0003-4368-2569).

or topic, as defined by Clarivate Analytics Web of Science platform). In addition, industry interest in EKR as an on-site and *in-situ* solution is re-emerging, and in the UK EKR is currently being examined as one of a range of technologies to address the UK's nuclear decommissioning legacy. This is under the UK-funded TRANSCEND project.²

1.1. Electrokinetic remediation, EKR

In EKR electrodes are implanted into a contaminated substrate and voltage applied. Under the effect of a low-energy direct current (DC) electric field, the movement of ions (electromigration), solid particulates (electrophoresis) and water (electro-osmosis) can be controlled and thus problem contaminants accumulated at desired points within a cell, usually around the electrodes. Water is also electrolysed within the cell with acid and alkaline fronts generated at the anode and cathode, respectively, shown in Fig. 1, below. For the treatment of radionuclides this normally involves electromigration to the electrode of opposing polarity; *e.g.*, Cs⁺ towards the cathode or ${\rm Tc^{VII}O_4^-}$ towards the anode. Where radionuclides are sorbed to the surfaces of soil particulates, the combined effect from the electric field and pH gradient can help mobilise them into pore water, ensuring EKR remains effective for the remediation of a variety of radionuclide contaminants (Kornilovich et al., 2005).

By driving contaminants out of solid wastes, EKR can be used to reduce the amount of solid material requiring disposal. Where liquid effluent generation is minimal, it may therefore be considered a *waste minimisation* technique. This aligns strongly with the preferred treatment routes outlined in the 'waste hierarchy' model of waste management, Fig. 2, which outlines the preferred treatment options for hazardous wastes. This approach is widely employed in the UK nuclear sector and is a fundamental precept in radioactive inventory management (ONR, 2015).

The simplicity and low power use of EKR systems also ensure that they can easily be combined with other techniques. This adaptability has resulted in several studies in which EKR is combined with bio- or phytoremediation (EKR-Bio or EKR-Phyto), nanoparticle delivery, dewatering, and others and there are a number of comprehensive reviews on the use of EKR for the remediation of organic (Cameselle and Gouveia, 2018; Pham and Sillanpää, 2015; Saini et al., 2020) and other (Reddy and Cameselle, 2009; Lima et al., 2017; Yang, 2019) pollutants. While EKR and electrochemical technologies for non-nuclear remediation schemes are a popular area of research, (Acar et al., 1995; López-Vizcaíno et al., 2016; Suied et al., 2018; Lacasa et al., 2019; Yeung and Gu, 2011; Kim et al., 2011a; Yeung, 2011) there remains a lack of detailed and critical research and technology overviews directed towards using EKR in full-scale, sustainable applications on nuclear sites. We are unaware of any comprehensive review of EKR literature devoted specifically to nuclear legacy and remediation issues since 2009 (Korolev, 2009). Recent years have also seen numerous advances in the application of sustainable remediation ("a remedy or combination of remedies whose net benefit on human health and the environment is maximised through the judicious use of limited resources") (Ellis and Hadley, 2009) approaches which despite the low energy, inexpensive and flexible nature of EKR equipment, has translated poorly into solutions at nuclear sites undergoing decommissioning. Given this knowledge gap we present this critical review on ongoing efforts and future directions for EKR for nuclear site remediation, applied sustainably.

1.2. Scope

While we aim to provide a comprehensive and accessible discussion of the current state of EKR technologies, we deliberately exclude detailed theoretical background on electrokinetic processes, which is sufficiently discussed elsewhere (Acar and Alshawabkeh, 1993). Our focus here is instead on three key questions, of more relevance to the application of EKR techniques than a re-examination of the first principles of EKR technology:

- 1. What developments have there been since 2009, the date of the last major review into EKR for nuclear sites, (Korolev, 2009) for specific problem radionuclides?
- 2. How has EKR been applied and what are the primary challenges at selected nuclear sites with international importance?
- 3. How can EKR best be applied to address these challenges, especially within emerging sustainable remediation frameworks?

We survey recent, nuclide-specific advances in EKR (Section 2) and give a detailed examination of site-specific challenges at three international installations (Section 3). Finally, we discuss how EKR may be adapted to address future key challenges at these and other sites, particularly under sustainable remediation "drivers" (Section 4). We also include our estimate of the technology readiness level (TRL) (De Rose et al., 2017) of EKR and other technologies, to reflect progress since 2009 towards large-scale implementation of this technology. Economic estimates are quoted in USD (\$), calculated using a GBP (£) to USD (\$) exchange rate of 1–1.3, and adjusted for inflation to 2019–2020 equivalent prices.

2. EKR developments since 2009 for specific problem radionuclides

Contaminated materials on nuclear sites contain a complex mix of fission and/or activation products along with other non-radioactive contaminants, and deciding targets for remediation can be challenging. Korolev has previously (Korolev, 2009) considered 'problem' radionuclides to include $^{90}\mathrm{Sr}$, $^{90}\mathrm{Y}$, $^{99}\mathrm{Tc}$, $^{137}\mathrm{Cs}$, $^{144}\mathrm{Ce}$, and actinides (U–Cm) for EKR at nuclear sites. Here, we refine this definition to include several 3d transition elements and lanthanides; Table 1. We also exclude radionuclides with short half-lives (t $_{1/2} < 1$ year), as these do not contribute significantly to long-term radioactive contamination of affected sites on the timescales of site-wide remediation schemes.

Significant developments in the EKR of uranium and, following the Fukushima-Daiichi nuclear power plant (FDNPP; Section 3.1) disaster and subsequent clean-up, radiocaesium have been reported since 2009. The surge in interest of radiocaesium remediation is particularly concentrated in Japan and South Korea, with a significant number of publications coming from these countries in recent years. We note also that ¹³⁷Cs is frequently examined in combination with ⁶⁰Co, an activation product of the neutron flux of stainless steel materials (e.g. pipework). It is a site-specific contaminant (e.g., Hanford site, USA; (Buehler et al., 1994) Winfrith, UK (Leonard et al., 1993)) with a short half-life (5.3 years) that is produced in reactor containment materials. It is not normally present in ground contamination and tends to decay by the time general site remediation schemes start.

2.1. Radionuclide-specific remediation: caesium

Caesium-137 is a medium-lived fission isotope (²³⁵U parent) with a half-life of 30.2 years and fission yield of *ca*. 6.3%, present in site wastes and from nuclear weapons testing, authorised nuclear facility discharges and major nuclear accidents. Construction waste-focused research in Korea has examined EKR applications for ¹³⁷Cs in artificially contaminated and crushed simulant TRIGA-reactor (TRIGA: training, research, isotopes, general atomics) concrete. For example, Kim et al. have

² The UK Government-funded TRANSCEND consortium (Transformative Science and Engineering for Nuclear Decommissioning, https://transcendconsortium.org/) is a £9.4 million (ca. \$12.2 million) research programme of 40 research projects across industry and academia to address some of the key challenges remaining in nuclear decommissioning and waste management.

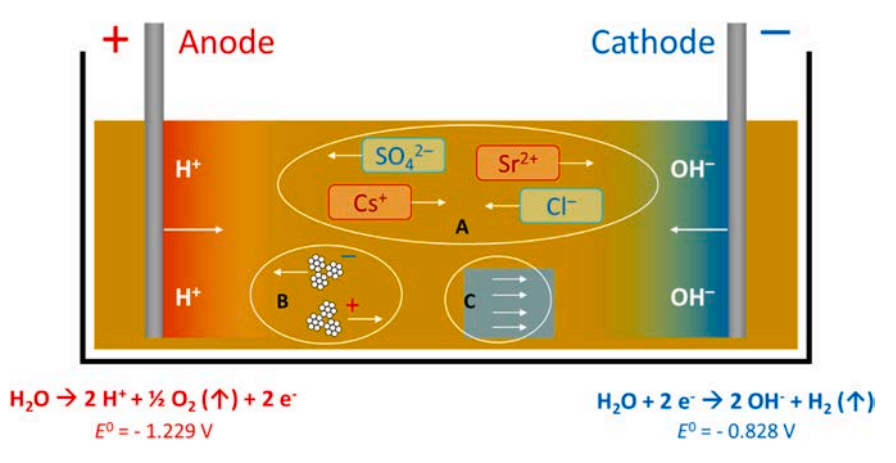


Fig. 1. EKR processes in a simplified cell, with pH fronts developing from the electrodes. **A**, electromigration of ions; **B**, electrophoresis of particulates (clays, *etc.*); **C**, electro-osmosis of (pore) water. Half-cell *E*⁰ values are *vs.* the standard hydrogen electrode, SHE.



Fig. 2. The waste hierarchy. "Prevent", that is preventing waste from being generated where possible, is the preferred approach to managing radioactive inventories. Disposal is the least preferred option after waste minimisation, reuse and recycling have been considered.

reported one system in which Cs removal efficiencies of above 50% were achieved over 15 days with a 4 V cm⁻¹ gradient using > 0.01 M (acetic) acid as an electrolyte. Removal efficiencies in their system increased dramatically from 55% in 0.1 M acetic acid in a static cell to > 99% in 0.01 M acetic acid with a flow-system and pre-treatment with 3 M hydrochloric acid (Ti cathode, dimensionally stable anode (DSA)). This highlights the effect that intelligent process design, specifically ex-situ pre-treatment, can have on EKR removal efficiency (Kim et al., 2009a). Further work by Kim et al. showed pre-treatment of the same TRIGA-simulant concrete with 3 M sulfuric acid increased removal efficiency of ¹³⁷Cs from 52% (no pre-treatment) to > 99% (with sulfuric acid pre-treatment), using 0.01 M nitric acid as the electrolyte (15 days) and Ti cathode and DSA anode. Importantly, the radionuclide activity concentration detected in the remediated concrete was below the 100 Bq kg-1 limit suggested 'safe' by the Korea Institute of Nuclear Safety. This enables these effluents to be disposed in municipal waste without further treatment, therefore aligning with the objectives of the waste hierarchy, Fig. 2 (Kim et al., 2010b). Effluent volumes were small (< 3 mL per gram of concrete remediated), and the effect of pre-treatment was to lower the pH of the concrete by partial dissolution/decomposition of the calcium carbonate.

However, removing one hazard (137 Cs) by introducing another (conc. acid) is clearly undesirable for on-site, *in-situ* remediation techniques, which are advantageous precisely because they are benign (Purkis et al., 2021). A key development, therefore, towards dealing with contaminated concrete safely and cheaply on-site came recently from Parker et al., on showing that simply washing 137 Cs-contaminated concretes with aqueous KCl (0.4 M) increases the removal efficiency threefold from 19 (no KCl) to *ca.* 60% upon EKR (cathode: steel, anode: DSA) (Parker et al., 2017). The setup used by Parker et al. is shown in

Table 1
Key radionuclides for EKR on nuclear sites. Half lives, decay modes, daughter products and fission yield data are compiled from Nuclear Data Services infor-

mation, hosted by the IAEA. ec is electron capture, RN is radionuclide. Where multiple decay modes are known (*e.g.* 36 Cl; 98% β^- [36 Ar], 2% β^+ [36 S]) only the predominant mode (β^-) is shown.

Radionuclides	Half-life/ y	Predominant decay mode [daughter created]	Comment
³ H	12.3	β ⁻ [³ He]	Neutron activation of ⁶ Li (and minor fission products); widespread contaminant
¹⁴ C	5730	β ⁻ [¹⁴ N]	Neutron activation of graphite or CO ₂ coolant, present in organic or inorganic form
³⁶ Cl	3.0×10^5	β ⁻ [³⁶ Ar]	Neutron activation of ³⁵ Cl (mineral salts, <i>etc.</i>) (Sheppard et al., 1996)
⁴¹ Ca	9.9×10^4	ec [⁴¹ K]	Neutron activation of ⁴⁰ Ca (cements, <i>etc.</i>) (Hou, 2005)
⁵⁵ Fe	2.7	ec [⁵⁵ Mn]	Neutron activation of steel
⁶⁰ Co	5.3	β ⁻ , γ [⁶⁰ Ni]	construction materials (Lin,
⁵⁹ Ni	7.6×10^4	ec [⁵⁹ Co]	1996)
⁶³ Ni	100	β ⁻ [⁶³ Cu]	
⁹⁰ Sr	28.9	β ⁻ [⁹⁰ Y]	Fission product (yield <i>ca</i> . 4.5%)
⁹⁹ Tc	2.1×10^{5}	β- [⁹⁹ Y]	Fission product (yield <i>ca</i> . 6.1%)
¹²⁵ Sb	2.8	β- [^{125m} Te]	Fission products
¹²⁶ Sn	$2.3 imes 10^5$	β- [^{126m} Sb]	F
¹²⁹ I	1.6×10^7	β ⁻ [¹³⁰ Xe]	
¹³⁷ Cs	30.2	β ⁻ [^{137m} Ba]	Fission product (yield <i>ca</i> . 6.3%)
152 _{Eu}	13.5	ec [¹⁵² Sm]	
¹⁵⁴ Eu	8.6	β^{-} [154Gd]	
¹⁵⁵ Eu	4.8	β^{-} [155Gd]	
²³¹ Pa	3.3×10^4	α [²²⁷ Ac]	Produced in fuel cycle
²³³ U	1.6×10^5	α [229 Th]	
²³⁴ U	2.5×10^5	α [²³⁰ Th]	
²³⁵ U	7.0×10^8	α [²³¹ Th]	
²³⁶ U	2.3×10^{7}	α [²³² Th]	
²³⁸ U	4.5×10^{9}	α [²³⁴ Th]	
²³⁶ Np	1.6×10^{5}	ec [²³⁶ U]	
²³⁷ Np	2.1×10^6	α [²³³ Pa]	
²³⁸ Pu	87.7	α [²³⁴ U]	
²³⁹ Pu	2.4×10^{4}	α [²³⁵ U]	
²⁴¹ Pu	14.3	β ⁻ [²⁴¹ Am]	
²⁴¹ Am	432.2	α [²³⁷ Np]	
²⁴⁴ Cm	18.1	α [²⁴⁰ Pu]	

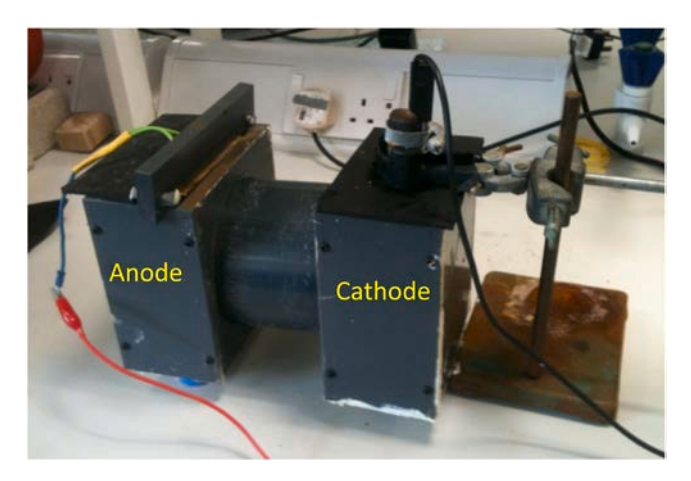


Fig. 3. EKR apparatus used by Parker et al. for remediation of 137 Cs-contaminated concrete. The anode is a platinum-titanium DSA, and cathode, right, is mild steel.

Fig. 3.

Enhancing EKR with a saline wash had been discussed previously (Reddy, 2013) but until 2017 not applied on concretes. In this case the high strength KCl wash ion-exchanges the entrained Cs^+ ions for aqueous K^+ ions, mobilising them and enhancing the EKR effectiveness relative to EKR alone (e.g. without a KCl wash). An important caveat to this, however, is that high concentrations of competing ions retained in waste effluents could significantly hinder subsequent ion exchange-based clean-up processes for effluent treatment. Further work may therefore be needed to identify how high ionic strength solutions could be employed without inhibiting subsequent steps in the remediation process.

Radiocaesium in other wasteforms is also accessible by EKR. Soils surrounding the Korean Atomic Energy Research Institute, KAERI, have been intensively studied by Kim et al. since 2009 (Kim et al., 2009b, 2010a). Sandstone is the primary rock type on which this and other Korean nuclear facilities are constructed, meaning EKR is effective in combination with pumping technologies. Indeed, a nitric acid electrolyte was most effective in the vertical EKR of ¹³⁷Cs⁺ contaminated (ca. 74–1643 Bq kg⁻¹), acidic (pH 5.6) simulant material over between 20 and 50 days (nitric or acetic acid electrolyte, Ti cathode, DSA anode) (Kim et al., 2009b). Removal efficiencies in the bespoke 10 L containment cell used ranged from ca. 57 to 94% depending on soil pre-treatment, electric current (< 20 mA cm⁻²) and particle size, with approximately 2.5 mL of waste effluent generated per gram of remediated soil (Kim et al., 2009b). Scaling this apparatus fivefold to 50 L (Fig. 4) resulted in no reduction in removal efficiency under nearly identical conditions (soil pH 6.4, 0.01 M nitric acid electrolyte, Ti cathode, DSA anode, 116–1186 Bq kg⁻¹, 55 days), although more waste effluent (ca. 5 mL g⁻¹) was generated (Kim et al., 2010a). Both techniques are amenable to electrodialysis with use of a selective ion-exchange membrane, resulting in $^{137}\mathrm{Cs}$ removal efficiencies of up to 98% (21 days EKR, 600 mA, < 5.2 V) (Kim et al., 2015b).

In addition to work on Cs-contaminated soils and concretes, Kim et al. have examined EKR on incinerated waste ash (134 Cs- and 137 Cs-contaminated) and demonstrated a 75% removal efficiency of 134 Cs and 137 Cs after 7 days of EKR on the bench-scale with prior washing using nitric acid (Kim et al., 2013a). Removal efficiency in this 200 L washing/EKR apparatus was as high as 94% after 10 days EKR, using a 2 M nitric acid electrolyte.

2.2. Radionuclide-specific remediation: uranium

The five major isotopes of uranium (233 U, 234 U, 235 U, 236 U and 238 U) have long half-lives ($\geq 10^5$ years; Table 1) with *in-vivo* toxicity being the

main hazard (Briner, 2010). Enriched uranium wastes have the added of being more radiotoxic. The remediation uranium-contaminated soils remains an active area of research (Gavrilescu et al., 2009) and since 2009 EKR has achieved significant attention, including from Kim et al. and researchers at KAERI. Unlike ¹³⁷Cs, however, uranium is redox active and often co-precipitates (with CaO) as cathode plate-coating metal oxides, such as UO₂. These solids reduce the effectiveness of EKR and lower the removal efficiency, hindering pilot-scale in-situ remediation efforts (Kim et al., 2011c). To address this Kim et al. used a metal oxide particulate filter (75 μ m) with pH control to successfully remediate a 50 L batch of contaminated (25-100 Bq g⁻¹ ²³⁸U), slightly acidic (pH 6.2) soil (0.01 M nitric acid electrolyte, 28 V electric field over 28-49 days, Ti cathode, DSA anode). Under these conditions > 99% of uranium contamination in the soil was removed. Adding sulfuric acid to these solutions further inhibited metal oxide formation, (Kim et al., 2014c) and aided recycling of contaminated electrolyte and uranium leachates (Kim et al., 2011b). Scaling the technology up from 50 to 800 L (Kim et al., 2015a) (Fig. 5) and even 1.2 tonne (Kim et al., 2016) mixing silos had little to no negative impact on the EKR removal efficiency of ²³⁸U. Removal efficiencies of ca. 94% (30 days EKR, 20 V system, water or nitric acid electrolyte, Ti cathodes, DSA anodes) and up to 83% (40 days EKR) were achieved for the 800 L and 1.2 tonne systems, respectively.

An emerging area of EKR research is uranium removal from concretes and other building aggregates and developing flowcharts for material processing. Kim et al. (2014b) have shown that remediating the floor of a former uranium processing facility (containing epoxy and urethane binders, cements, aggregate, etc.) can be enhanced by ball milling the material prior to treatment. Although EKR was not performed on these materials the authors suggested a process flowchart, hypothesising a 70% reduction in waste volumes compared to other techniques (Kim et al., 2013b) where EKR was applied in tandem with ex-situ milling. Yurchenko et al. have taken this one step further, by applying EKR to reinforced concrete (Fig. 6) from a uranium processing facility in Moscow, contaminated with ²³⁵U and ²³⁸U (Yurchenko et al., 2009).

Here, crushing of 98 kg of authentic concrete building materials (complete with reinforcing steel pins and other concrete building supports), washing (sodium carbonate electrolyte) and applying the EKR process (0.22 A cm⁻²) over 30 days resulted in activity dropping by 8.2 MBq in the remediated concrete, a reduction of 95%. Only small amounts of waste (3.5-3.8 mL effluent per g of remediated concrete) were generated, an important step towards potential scale-up and aligning with the waste hierarchy (Fig. 2). Gravels (> 10 mm) may also be treated by EKR. As 20-30% of soil surrounding the Korean KAERI facility is gravel (Park et al., 2015), Kim et al. (2014a) were motivated to remediate the ²³⁸U levels from ca. 10 Bq g⁻¹ to below 0.43 Bq g⁻¹, the disposal limit for landfill. Depending on particulate size, the authors proposed a processing flowchart including ball mill crushing or soil washing, followed by electrodialytic (pump) EKR on the resulting aggregates. Removal efficiencies after EKR for 20 days (20 V, 200 L reactor, nitric acid electrolyte) were as high as 83%, with an average of 37% depending on pre-treatment processing.

2.3. Radionuclide-specific remediation: other nuclides (99Tc, Eu, Pu, etc.)

Other, easier-to-detect radionuclides have also been targeted through EKR in recent years. For example, Agnew et al. demonstrated for the first time in 2011 the on-site EKR of Pu-contaminated soils at the Atomic Weapons Establishment (AWE) Aldermaston site in the UK (Agnew et al., 2011). This pilot study used a 10-electrode array (Fig. 7; 19.2 V, 30% citric acid electrolyte, steel electrodes) implanted into ca. 4 tonnes of soil and monitored the gross alpha activity (e.g. Pu and Am) after EKR for 60 days. The study showed ca. 60% of monitored soil could be reclassified to the level of 'exempt' waste, based on the exemption limit of < 0.4 Bq $\rm g^{-1}$ above background alpha and beta contamination

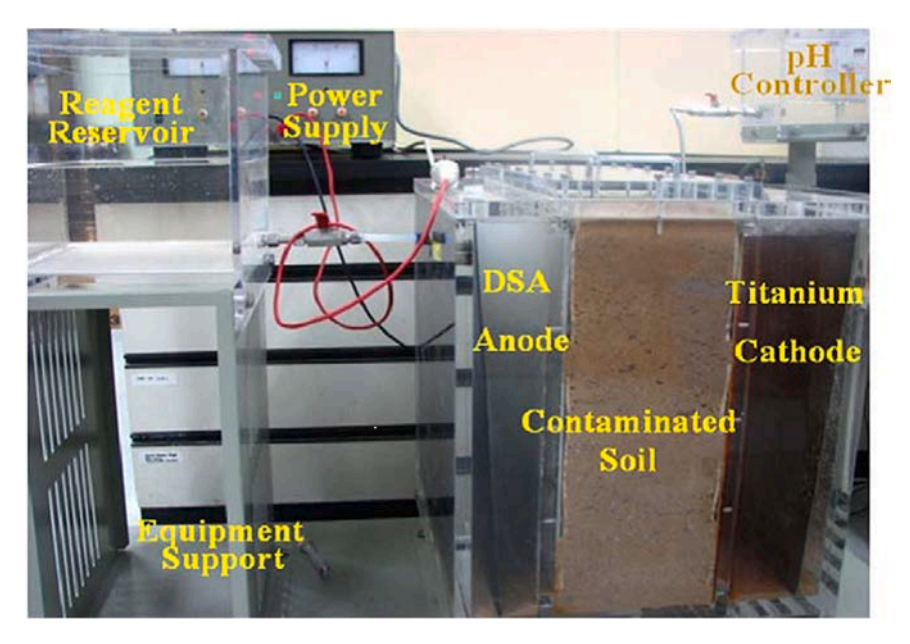


Fig. 4. The 50 L scaled set-up used by Kim et al. (2010a) used to assess the scalability of the EKR cell to simulate remediation of contaminated KAERI sandstone. DSA is dimensionally-stable anode.

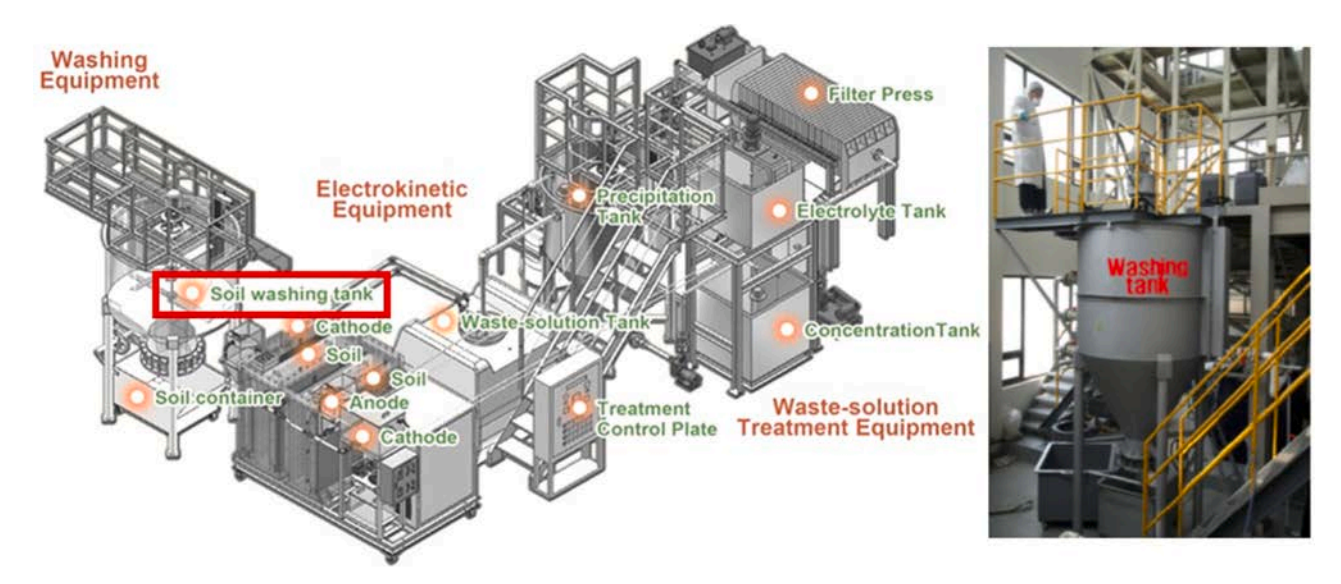


Fig. 5. Schematic of the set-up used by Kim et al. (2015a) on the 800 L scale EKR process on contaminated KAERI material, with washing drum highlighted on the right. The drum is several metres tall so is a significant improvement from laboratory scale.

relevant at the time of the study (Agnew et al., 2011; UK Government, 1993).

The estimated cost (2011) of remediating this waste was ca. \$2700 per m³ (2019 USD; £2054), less than ca. \$7830 per m³ (2019 USD; £6054) for conventional excavation and disposal ('dig and dump').

Irradiated nuclear material may also be remediated electrochemically (but not, specifically, electrokinetically), as demonstrated by Bespala et al. (2019) in the treatment of spent graphite from the Zheleznogorsk nuclear reactor in Russia. By using the contaminated graphite rods as electrodes, Bespala et al. demonstrated that applying an electric field of varying voltages (1–32 V) in nitric or sulfuric acid or DI water electrolytes removes ⁶⁰Co, ¹³⁷Cs, and ^{152/154}Eu from the electrodes. Potassium permanganate added to selected electrolyte baths also allowed complete dissolution of the graphite electrodes upon application of electric current.

Finally, Valdovonis et al. have shown that EKR of ²⁴Na and ^{99m}Tc (as

analogues for the longer lived isotopes ²²Na and ⁹⁹Tc, a difficult-to-measure, DTM, nuclide) is effective in either removing (²⁴Na⁺) or migrating and reducing (^{99m}Tc, as ^{99m}Tc^{VII}Ō4) present in Mexican phaeozemic (*cf.* mollisolic) (Food and Agricultural Organisation (FAO) of the United Nations (UN), 2015) soil in the presence of scintillation fluids. These fluids were adsorbed onto the soils during the 1970s and 80s as an interim storage method (Valdovinos et al., 2016). Removal efficiencies after 4 h were highest near the cathode (Ti rod) for ²⁴Na⁺ (*ca.* 72% from initial), and the anode (DSA) for ^{99m}TcŌ4; 61% removal from initial after 4 h EKR) with a *ca.* 32 V system.

2.4. Summary of EKR targets, efficiencies and parameters in post-2009 experiments

Summary data from these and the other experiments outlined here are given in Table 2, below.



Fig. 6. Examples of the concrete examined by Yurchenko et al. (2009) complete with reinforced steel pins used in construction. X-ray (Rietveld) analysis indicated α -quartz, orthoclase and plagioclase feldspar, calcite and boltwoodite – $H(K_1Na)(UO_2)(SiO_4)\cdot 1.5(H_2O)$ – phases in the concretes.

The removal efficiency of selected elements from a variety of wasteforms is high (often 90%+). Although many studies are limited to bench-scale, our review highlights that progress is being made towards scaling EKR for use on-site. Pilot-scale studies up to tonnes of material show little to no loss of EKR effectiveness and although the current state-of-the-art is *ex-situ*, demonstrating successful pilot-scale viability is vital to ensuring EKR can be used effectively on site.

3. EKR at nuclear sites of international importance

As noted, the wide scale deployment of EKR at complex nuclear sites, such as FDNPP (Japan), the Hanford site (US), and Sellafield (UK) is currently lacking. Contamination at these sites often exists for decades in many wasteforms, meaning remediating these sites is expensive, technologically difficult and hazardous. It is typically only governments that possess the resources and logistical ability to successfully remediate such sites, managed through governmental bodies and subsidiaries. These include the Nuclear Decommissioning Authority (NDA) in the UK, the US Department of Energy (DoE) and the Tokyo Electric Power Company (TEPCO) in Japan, and subsidiaries. As governments are ultimately responsible to taxpayers, remediation efforts are always high on the political agenda, providing substantial political and economic pressures to ensure remediation is both successful and cost effective. Here we outline three of the most challenging international nuclear

legacy sites, and our assessment of the opportunities and challenges that EKR schemes could face if applied (Fig. 8).

3.1. Fukushima-Daiichi Nuclear Power Plant (FDNPP) and exclusion zone, Japan

Following meltdown at the FDNPP, significant quantities (ca. 3.3 PBq) of 137 Cs and 90 Sr were released into the atmosphere. Much of this remains trapped within the 30 km exclusion zone, with a total decommissioning cost estimate (2016) of between \$50 and \$150 billion (Tasutaka and Naito, 2016).

The current remediation method, topsoil removal ('dig and dump') generates considerable soil (estimated 20 million m³ from 13,000 km² of land, 2019) (Evrard et al., 2019) waste which will need to be remediated if TEPCO and the Government of Japan are to fully implement their final disposal plan. Currently this involves constructing a permanent storage bunker within the Fukushima prefecture by 2045 but projections (2018) indicate this target will be missed without significantly enhanced volume reduction measures. Local opposition in all previously consulted sites has been also considerable and widespread, further complicating remediation efforts (Okumura et al., 2018).

There are two noteworthy areas of the Fukushima exclusion zone, an organic-rich, clayey-silt with significant vegetation (Kikuchi et al., 2015), and an alluvial Quaternary-era sand terrace. The clayey-silt contains significant amounts of phyllosilicate micas (such as high cation-exchange capacity illite and biotite) that retain entrained ¹³⁷Cs⁺ within clay matrices (Tanaka et al., 2018). Much of this contamination is concentrated in the top 5 cm of topsoil and is unaffected by rainwater flow (Tanaka et al., 2012), meaning soil flushing, ion exchange, and similar technologies are ineffective at remediating these; other remediation techniques must be applied. The second area, the Quaternary sandy terrace, underlies the FDNPP itself and contains significant groundwater contamination resulting from the core flushing immediately after containment failure. More than 1 million tonnes of this caesium and tritium contaminated waste water is currently stored at Fukushima (from the Advanced Liquid reProcessing System (ALPS) and Simplified Active water Retrieve and Recovery (SARRY) systems) in corrodible water storage tanks (Lehto et al., 2019). TEPCO estimates that at current rates tank space will be exhausted by the summer of 2022 and has contingencies to discharge contaminated liquid wastes into the Pacific Ocean.

To date, we are not aware of any successful, site-scale attempts to remediate either the soil or groundwater within the Fukushima exclusion zone. Although an "ice-wall" of frozen brine-saturated soil (estimated cost of \$350–400 million) was deployed to limit the flow and volume of contaminated groundwater, the success of the scheme is debatable and many international news agencies have carried articles

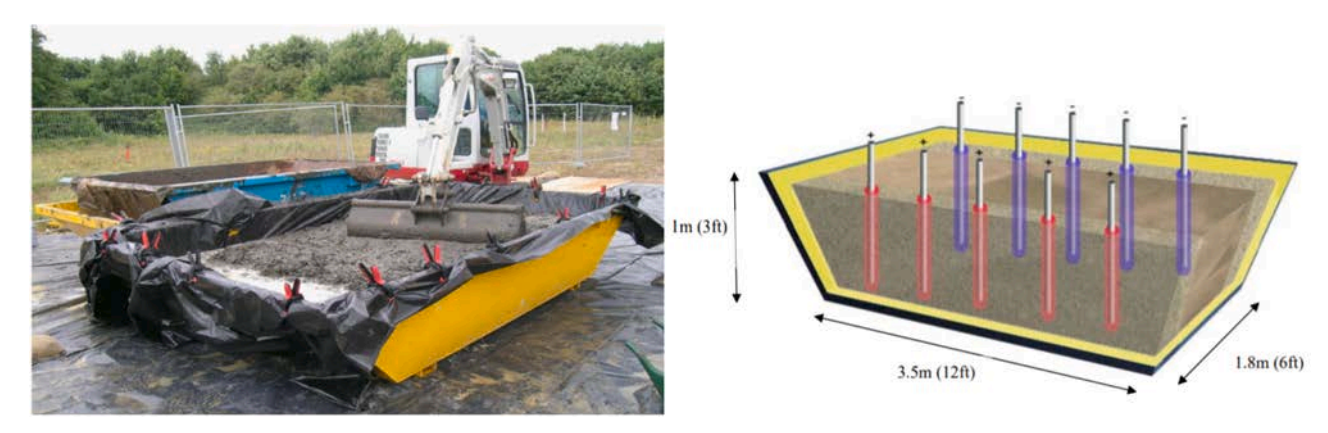


Fig. 7. Left, ex-situ processing of plutonium contaminated waste by Agnew et al. (2011) at the Atomic Weapons Establishment (AWE), UK, plus scale and electrode arrangement used on the right.

Table 2 Summary of EKR experiments described in Section 2. Multiple experiments are often reported in the same reference, and selected data refer to experiments with the highest quoted removal efficiency for a given element or radionuclide. Abbreviations: n.r. is not reported, conc. is concentration, aq. is aqueous, soln. is solution, and DSA is dimensionally-stable anode (two or more metal oxides (e.g., $Pt^{IV}O_2$ and $Ti^{IV}O_2$) grafted onto a corrosion-resistant mesh). Ultima Gold XR® is a branded reagent mixture commonly used in liquid scintillation counting analysis.

Elements or RNs	Wasteform	Voltage	Current	Electrode material	Time/ d	Highest quoted removal efficiency	Bench, intermediate, or pilot scale?	Electrolyte	Ref.
Cs, Co	crushed concrete	4 V cm ⁻¹	500 mA	cathode: Ti anode: DSA	15	99 + % for both	bench	Acetic acid (1 L, 0.01 M)	(Kim et al., 2009a)
⁶⁰ Co, ¹³⁷ Cs	crushed concrete	n.r	20 mA cm ⁻²	cathode: Ti anode: DSA	15	99.6% ¹³⁷ Cs 99.7% ⁶⁰ Co	bench	Nitric acid (0.01 M)	(Kim et al., 2010b)
¹³⁷ Cs	concrete	60 V	35 mA	cathode: steel anode: DSA	37.5	60%	bench	Aq. KCl (0.4 M)	(Parker et al., 2017)
⁶⁰ Co, ¹³⁷ Cs	washed soil	n.r.	20 mA cm ⁻²	cathode: Ti anode: DSA	50	99.9% ⁶⁰ Co 94.3% ¹³⁷ Cs	bench	Nitric and acetic acid	(Kim et al., 2009b)
⁶⁰ Co, ¹³⁷ Cs	washed soil	n.r.	15 mA cm ⁻²	cathode: Ti anode: DSA	55	95.8% (both)	intermediate (50 L)	Nitric acid (0.01 M)	(Kim et al., 2010a)
¹³⁷ Cs	washed soil	< 5.2 V	600 mA	n.r.	21	98.2%	bench	With ion exchange membrane	(Kim et al., 2015b)
¹³⁴ Cs, ¹³⁷ Cs	ash	10.5 V	2.2 A	n.r	7.2	74.7% ¹³⁴ Cs 75.5% ¹³⁷ Cs	bench	Nitric acid (2 M)	(Kim et al., 2013a)
		n.r	n.r.		10	94.0% ¹³⁴ Cs 93.9% ¹³⁷ Cs	intermediate (200 L)	Nitric acid (conc. n.r.)	
U	soil	28	15 mA cm ⁻²	cathode: Ti anode: DSA	49	99.0%	intermediate (50 L)	Nitric acid (0.01 M)	(Kim et al., 2011b)
^{238}U	washed soil	20	13 mA cm ⁻²	cathode: Ti anode: DSA	30	93.9%	pilot (800 L)	Nitric acid (3 M)	(Kim et al., 2015a)
U	washed soil	n.r.	18 mA cm ⁻²	cathode: Ti anode: DSA	40	83.3	pilot (1.2 tonnes)	Nitric acid (conc. n.r.)	(Kim et al., 2016)
U (various)	concrete	n.r.	0.22 A cm ⁻²	n.r.	30	n.r.	bench	Aq. Na ₂ CO ₃	(Yurchenko et al., 2009)
U	crushed gravel	20 V	200 A	n.r.	20	83%	intermediate (400 L)	Nitric acid (conc. n.r.)	(Kim et al., 2014a)
Pu, Am	soil	19.2	n.r.	steel	60	n.r.	pilot (4 tonnes)	Aq. citric acid (30% soln.)	(Agnew et al., 2011)
¹⁵² Eu, ¹⁵⁴ Eu (+ ⁶⁰ Co, ¹³⁷ Cs)	reactor graphite	31.8 (max.)	$< 0.3~{\rm A~cm}^{-}$	reactor graphite	n.r.	n.r.	bench	Mineral acids (< 8 M)	(Bespala et al., 2019)
²⁴ Na, ^{99 m} Tc	soil	n.r.	1 mA	cathode: Ti rod anode: DSA	0.17	71.8% ²⁴ Na 61.0% ^{99m} Tc	bench	1:1 Ultima Gold XR:water	(Valdovinos et al., 2016)

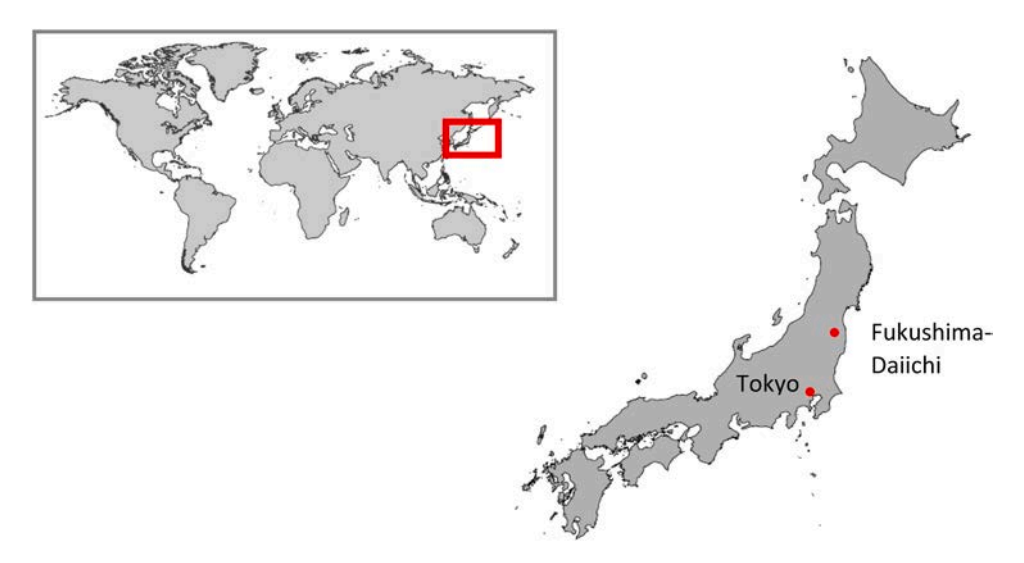


Fig. 8. Global and national location of the FDNPP in Eastern Japan. The figure omits the Okinawa Islands to the south of Kyushu.

questioning its effectiveness.³ EKR technology (EK fencing (López-Vizcaíno et al., 2017), EKF, where flow of contaminants is inhibited by application of electrodes, Fig. 9) has been proposed to limit the spread of groundwater (Lageman, 2014) or remediate contaminated seawater (Lageman, 2014), but we have not been able to find any primary literature to suggest these proposals were successful. Although small scale, limited evidence also exists suggesting that EKR of mountainous slopes contaminated with ¹³⁷Cs may be possible (Miura et al., 2015).

Any successful remediation technology must address several key challenges at Fukushima. It must be versatile, and work in both lowpermeability clays (e.g. forest soils), and higher permeability sandstone deposits (that underlie the FDNPP) (Gallardo and Marui, 2016). Techniques that work only in high-permeability substrates are not applicable for site-wide use. Secondly it must be cheap, and while EKR is often considered a low cost technique (Section 1.1), one of the key limitations of the EKF proposals by Lambda Consult are projected costs of \$47-64 million (£36-49 m) in capital outlays and \$2.8-5.6 million (£2.1–4.3 m) in annual running costs. Although a smaller pilot project (6 months, \$278k/£213k) was proposed we have been unable to confirm if this was funded. Thirdly, although much ¹³⁷Cs⁺ remains entrained within clay lattices (Fuller et al., 2015), clayer soils rich in organic carbon, such as those within the Fukushima exclusion zone, often contain significant micro-aggregated regions in which ¹³⁷Cs preferentially resides. Koarashi et al. (2018) have previously demonstrated that between 69% and 83% of ¹³⁷Cs⁺ in Fukushima soils resides in micro- or sand-sized-aggregate particulates, which have much higher extractability than clay regions.

Given the on-going and controversial plans currently being employed by TEPCO for FDNPP remediation, we suggest that EKR may be beneficial in targeted, small-scale testing in authentic contaminated Fukushima soils. We have begun to make progress towards this goal, with work in our laboratories showing significant Cs $^+$ mobilisation from a Fukushima simulant soil upon application of a low-energy EK field (Purkis et al., 2021). Here, we demonstrated removal efficiencies of 80 + % for Cs, over timescales of up to 45 days in cells with low power requirements (< 1 kWh and < 1 V cm $^{-1}$). We are also aware of work at the University of Leeds, UK and the Korean Advanced Institute of Science and Technology (KAIST), South Korea, to develop new materials to selectively extract entrained Cs $^+$ in clay interlayers such as those present at Fukushima (Harbottle and Hunter, 2019). These studies should highlight the likely efficacy of EKR to the FDNPP in more detail, and we eagerly anticipate such results.

3.2. Hanford Site, Washington, USA

The Hanford Site (Fig. 10) is the largest and oldest nuclear site in the US, having provided much of the plutonium enrichment capability for the USA during the 1940s and 1950s

The site has widespread contamination (60 Co, 90 Sr, 99 Tc, 129 I, 3 H, plus 106 Ru, 144 Ce, 147 Pm, various U and Pu isotopes and organics including CCl₄) (Peretyazhko et al., 2012; Qafoku et al., 2005), although wastewater tank leakages remain most pressing. This includes significant 137 Cs contamination in some areas greater than 4 kBq g $^{-1}$, Fig. 11

(Fredrickson et al., 2004; McKinley et al., 2001; Beavers et al., 2019). Remediation is extremely expensive, and recent estimates (2019) target a nuclear end-state of 2130 at a cost of between \$323 and \$677 billion (ca. £250 to £525 billion) (Department of Energy (DoE), 2019).

The surficial geology of the Hanford site is primarily unconsolidated, high-permeability sands and gravels (Department of Energy (DoE), 2010). This means that unlike the clayey soils surrounding the FDNPP, a range of remediation techniques have been tested or are currently applied on the Hanford site at varying scales (Nuclear Energy Agency (NEA), 2014). These include the injection of an apatite-rich barrier to limit ⁹⁰Sr influx into the Columbia River, (Vermeul et al., 2014) ongoing pump-and-treat systems, (Office of Environmental Management, Department of Energy (DoE), 2004; Brines et al., 2013) simple excavation (Department of Energy (DoE), 2013), and the bioremediation of residual organic contaminants in groundwater (Skeen et al., 1992; Office of Environmental Management, Department of Energy (DoE), 1999). EKR on the Hanford site has received less attention, although a small number of studies have examined EKR on Hanford-relevant materials to date.

In 1994, Buehler et al. artificially spiked authentic Hanford sediment with either a 1.85 MBq ^{137}Cs , or 0.74 MBq $^{137}\text{Cs}/1.85$ MBq ^{60}Co solution, and applied an EKR treatment whilst monitoring γ -activities over 200 h. Under a 200 V electric field (22.8 cm cell; 7 V cm $^{-1}$) (Buehler et al., 1994) both ^{137}Cs and ^{60}Co migrated a small but significant distance (10 cm) towards the cathode, leaving much of the soil radiometrically free of contamination. In 2015, Jung et al. illustrated (Fig. 12) that EKR on ^{133}Cs -contaminated Hanford site soil for 68 days can reduce the Cs concentration by up to 55%. Cs removal by EKR was more effective in silty-clayey fractions (average 51%) than sandy ones (average 38%), primarily from the cathodic region of the tested cell (Jung et al., 2015).

A key limitation with both of these studies is the size of the experiments; all cells were less than 25 cm in length. Owing to its comparative technological immaturity to other techniques, we suggest that the niche of EKR at Hanford is to supplement existing technologies. One example is the growth of the aforementioned apatite permeable reactive barriers (PRBs) (Vermeul et al., 2014), where apatite (calcium phosphate) precursors were injected into target sites along the Columbia Riverbank and ⁹⁰Sr measurements taken over time. EKR has been previously used to force-migrate and focus reactants into specific points along a remedial cell and we believe a similar approach could be of interest here, where existing injection methods prove ineffective (Faulkner et al., 2005). Calcium (Tanaka, 2018) (and by extension strontium) and phosphate (Lee et al., 2007) ions are known to be mobile in soils under the effect of an applied electric field, and with careful electrode placement the EKR-enhanced growth of in-situ generated PRBs into difficult-to-inject materials could be an interesting prospect to explore.

3.3. Sellafield, Cumbria, UK

The third of the selected international sites discussed here is the Sellafield industrial complex in NW England, UK, the largest nuclear complex in Europe (Sellafield Ltd., 2017). As much as 12 million m³ of soil may be radioactively contaminated, including 1600 m³ of highly hazardous intermediate-level waste (Sellafield Ltd., 2017). Significant contamination also resides in the site groundwater, which shows maximal activity concentrations of ¹³⁷Cs, ⁹⁰Sr and ⁹⁹Tc of 129, 84,000, and 71 Bq L⁻¹, respectively (Sellafield Ltd., 2016). These values are above or very close to World Health Organisation (WHO) guidelines for safe drinking water (10 Bq $\rm L^{-1}$ for ^{90}Sr and ^{137}Cs , and 100 Bq $\rm L^{-1}$ for ⁹⁹Tc) (World Health Organisation (WHO), 2011). Tritium is also a significant contaminant at the Sellafield site, with concentrations in analysed boreholes consistently above WHO guidelines (10,000 Bq L⁻¹). In some cases concentrations can exceed the guideline limit by a factor of over 25 (255,000 Bq L⁻¹) (World Health Organisation (WHO), 2011). We discuss these DTM radionuclides further in Section 5.

³ The "ice-wall" has been widely reported in international news and TEPCO documents. TEPCO retains updated information on the status of the scheme, see https://www.tepco.co.jp/en/decommision/planaction/landwardwall/index-e. html. International news agencies carrying the stories of interest regarding the status of the "ice-wall" scheme include Reuters (https://www.nytimes.com/2016/08/30/science/fukushima-daiichi-nuclear-plant-cleanup-ice-wall.html), the New York Times (https://www.nytimes.com/2016/08/30/science/fukushima-daiichi-nuclear-plant-cleanup-ice-wall.html) and the Japan Times (https://www.japantimes.co.jp/news/2016/07/20/national/first-tepco-admits-ice-wall-cant-stop-fukushima-no-1-groundwater/).

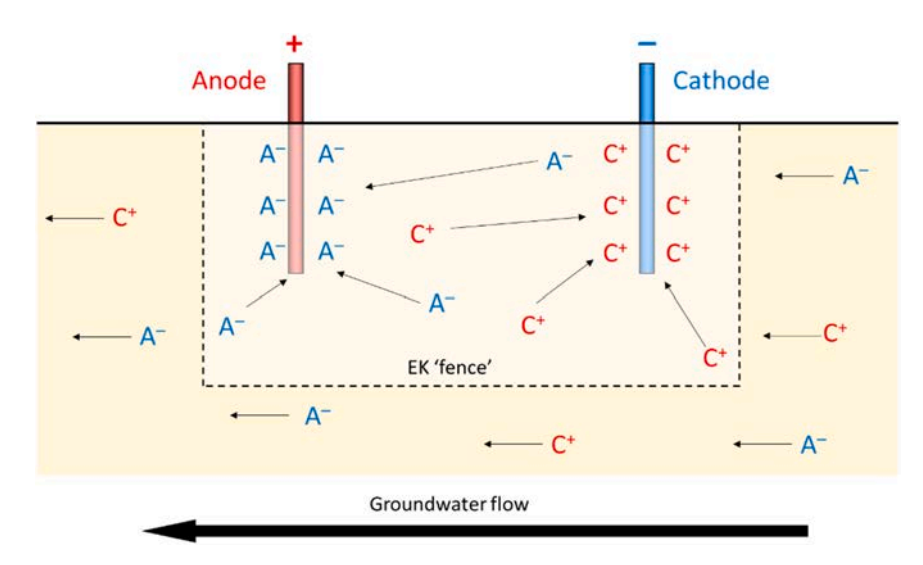


Fig. 9. Simplified schematic illustrating EK fencing, EKF. A⁻ and C⁺ are generic anions or cations, respectively.

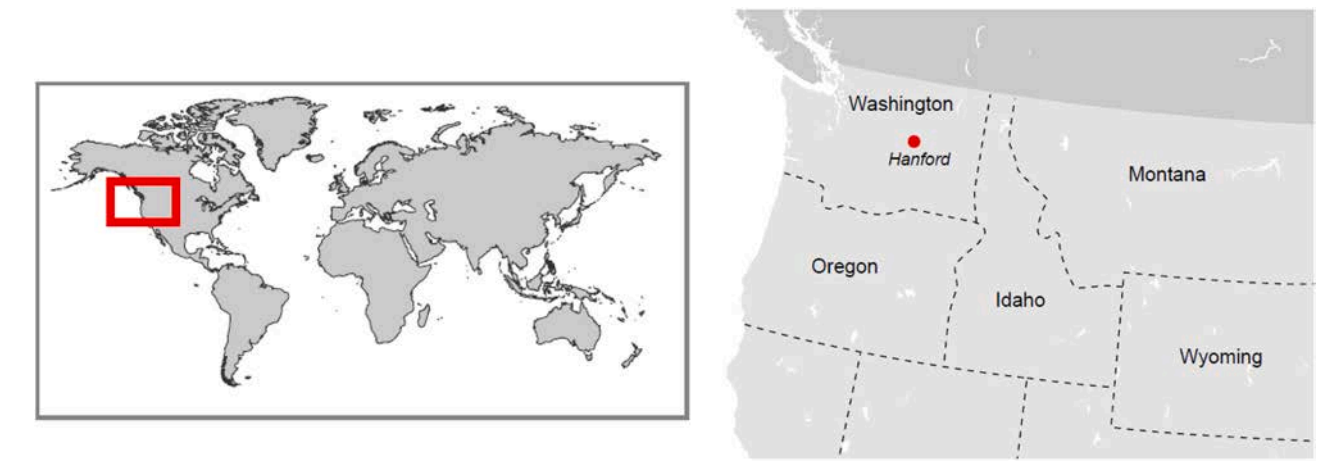


Fig. 10. Global and national location of the Hanford site, Washington state, USA.

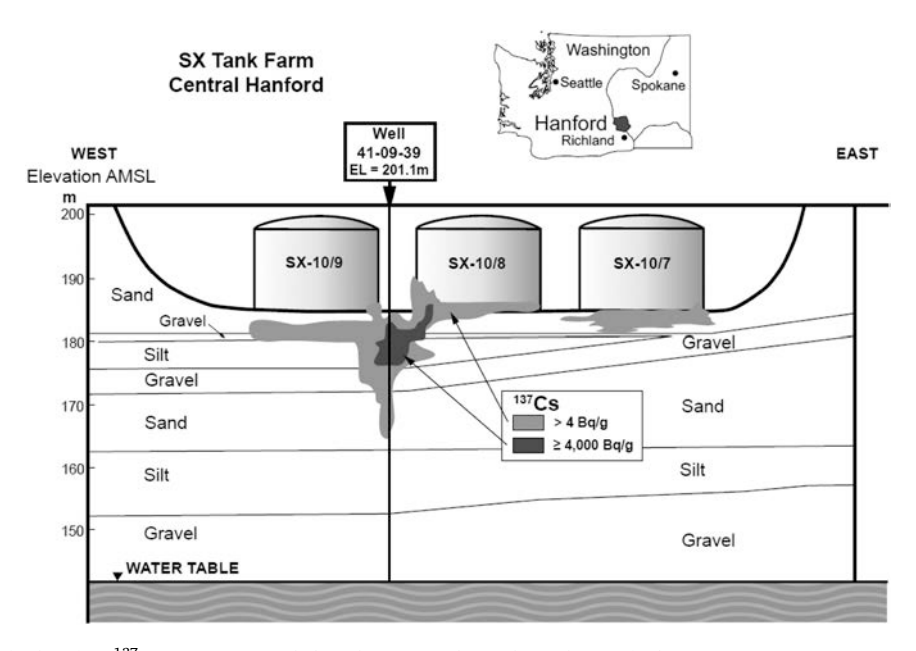
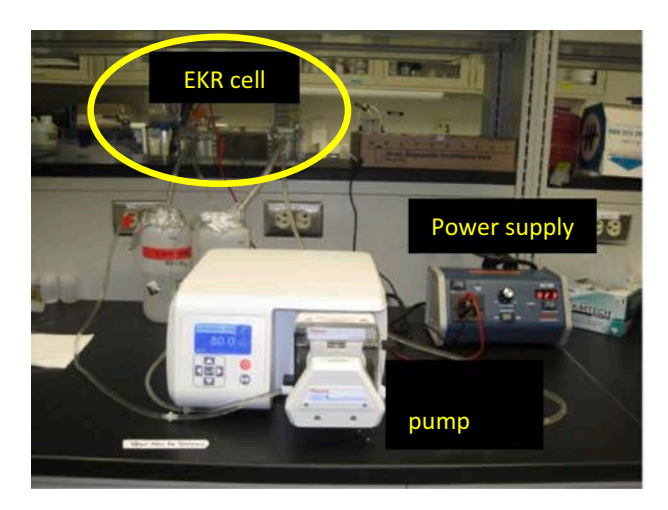


Fig. 11. Extent and levels of subsurface 137 Cs-contamination below three exemplar tanks at the Hanford site. The figure is redrawn from McKinley et al. (2001).



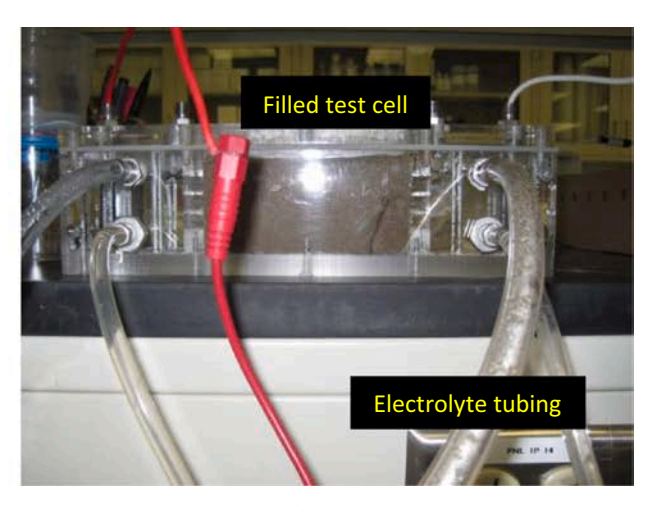


Fig. 12. Left, the set-up used by Jung et al. (2015), and right, magnified view of the clear Perspex® container (width = 25 cm) used for the EKR experiments.

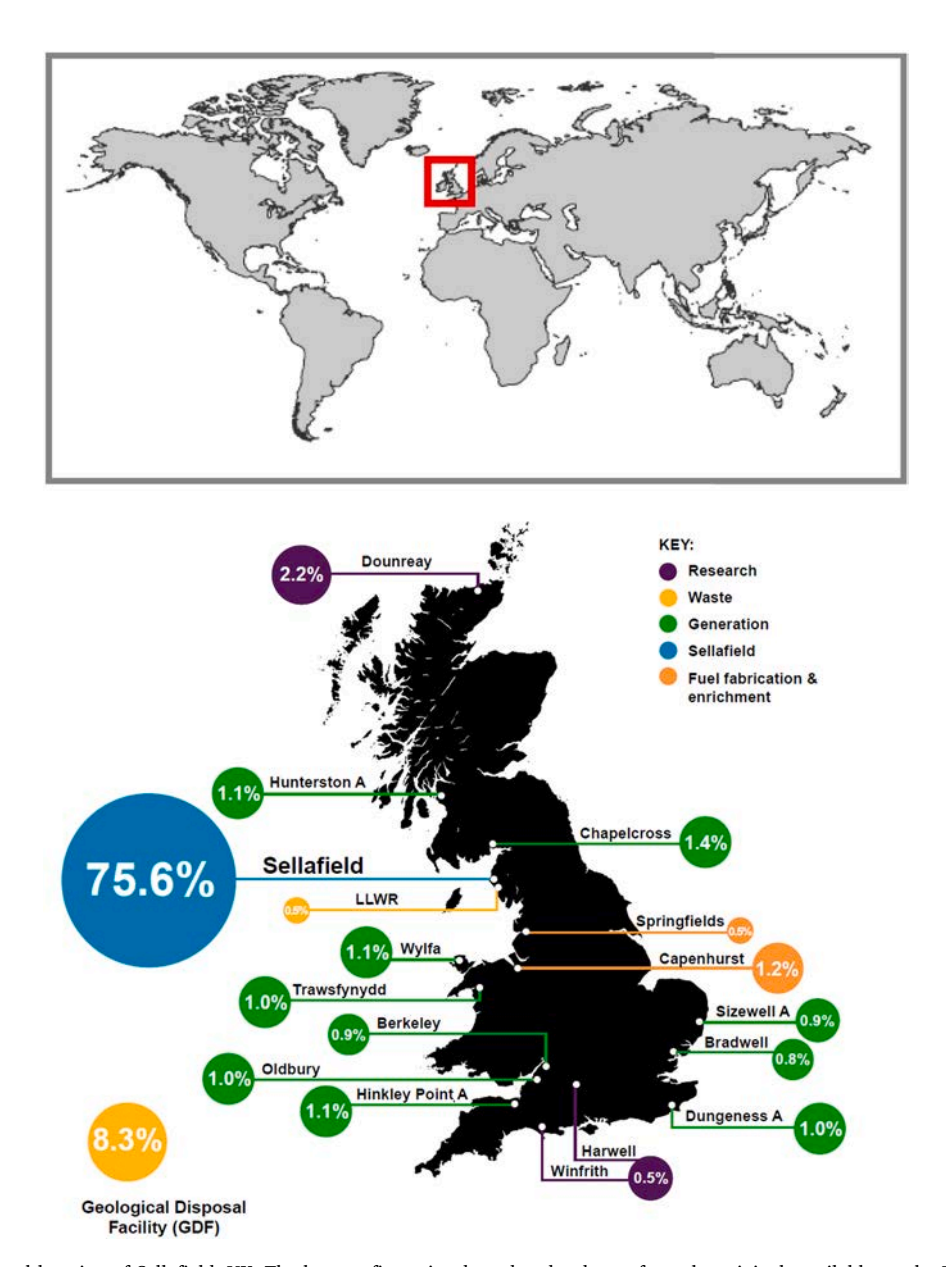


Fig. 13. Global and national location of Sellafield, UK. The bottom figure is adapted and redrawn from the original, available on the UK Government's website, (Nuclear Decommissioning Authority, 2020) where circles represent total contribution to UK nuclear remediation clean-up costs.

Targeting a nuclear end-state of 2120, the UK Government estimates decommissioning costs of *ca.* \$117 billion (£91 billion; 2018) (National Audit Office (NAO), 2018), although this has risen substantially in recent years (2009 costs were \$80 billion/£62 billion, and in 2012, \$102 billion/£79 billion) (National Audit Office (NAO), 2012) and may in fact be as high as \$210/£ 163 billion (2015, est.) (Nuclear Decommissioning Authority (NDA), 2015). Decommissioning activities at Sellafield dominate the UK nuclear legacy estate, accounting for over 75% of remediation expenditure, Fig. 13, in 2018–2019 (Nuclear Decommissioning Authority, 2020). This has risen from 74% in 2015–2016 (Nuclear Decommissioning Authority (NDA), 2015).

The subsurface of the Sellafield site is primarily superficial glacial deposits overlaying sandstone bedrock (Smith et al., 2020). Groundwater flow away from the Sellafield site tends towards the Irish Sea where, along with authorised discharges, contamination can become entrained in surrounding sediment. One such example is the Ravenglass estuary which contains ⁶⁰Co, which is amenable to EKR (Cundy and Hopkinson, 2005). A schematic cross section of the Sellafield site is given in Fig. 14.

The extensive contamination at Sellafield has driven numerous detailed investigations of EKR at the Sellafield site, led by the UK National Nuclear Laboratory (NNL). This includes its predecessors, British Nuclear Fuels Ltd. (BNFL) and Nexia Solutions Ltd. Due to the sensitive nature of these reports their results were not publicly disseminated, enabling us to present this work here for the first time.

The first example of EKR on the Sellafield site we are aware of was undertaken in the late 1990s by BNFL on three authentic Sellafield soils artificially spiked and saturated overnight with ¹³⁷Cs (caesium nitrate), ⁹⁰Sr (strontium nitrate) and transuranic alpha sources (including ²³⁹Pu; 8 kBq mL⁻¹ solution of ²³⁹Pu in 6 M nitric acid) (Eilbeck and Learmonth, 1999). Here, 'sample 1' describes a spiked, clay-rich soil under static conditions, and 'sample 2' describes a spiked, sand-rich soil under flow of water; both samples were collected from points on the Sellafield site. EKR was assessed using a set up described in Fig. 15, with radionuclide concentrations measured by scintillation after 14 days.

For both soil tests, 7 cm cores were selected and \it{ca} . 260 g material added to the soil core. The soil samples (samples 1 and 2) were treated for 14 days at 8 V with graphite electrodes. Under these conditions

 137 Cs $^+$ or 90 Sr $^{2+}$ were significantly redistributed across the length of the soil sample. For the clayey spiked soil under static conditions, sample 1, the concentrations of 137 Cs and 90 Sr nearest the cathode decreased by 69% and 93%, respectively. When the simulated effect of groundwater flow was added, sample 2, the redistribution was less effective, with reductions of 44% of 137 Cs and 50% for 90 Sr measured nearest the cathodes. Large errors in the α-spectroscopy measurements prevented an accurate assessment of 239 Pu redistribution in the cores. A modified Tessier scheme was employed for sequential leaching, showing 137 Cs and 90 Sr were predominantly in exchangeable form (calcium chloride leach) and that 239 Pu was predominantly leached with Fe and Mn oxides (hydroxylamine hydrochloride leach). Soil pH was also monitored, with the soil core and cathodic chamber becoming very basic (pH 12) after 14 days, and anodic chamber acidic (pH ca. 1.5) after the 14 day run (Eilbeck and Learmonth, 1999).

This set-up (Fig. 15) was later used to assess EKR in a 90 Sr-, 239 Pu-and 126 Sn-contaminated, brucite (Mg(OH)₂)-rich soil, representative of a real leak area beneath a Sellafield waste storage facility (Eilbeck and Lorimer, 2001). Although the authors suggested EKR was not feasible on the Sellafield site (due to high alkaline buffering of the soil), we consider this to be an overly pessimistic assessment as the release of large quantities of alkaline material is not realistic of the entire site (on which carbonate concentrations can vary considerably) (Graham, 2015). The effectiveness of EKR at many areas of the Sellafield site with lower soil buffering capacity remains poorly researched.

Concerns over scalability (e.g. the 7 cm cell shown in Fig. 15) were addressed separately on moving to a larger 40 L cell (Fig. 16), where EKR on sandy or clayey Sellafield soils contaminated with ⁹⁰Sr in simulant groundwater were examined (Brydie and Beadle, 2004).

Measured β -activity values of 0.830 ± 0.254 Bq g $^{-1}$ (sandy soil) and 0.871 ± 0.251 Bq g $^{-1}$ (clayey soil) were obtained for both soils in this pumped system. As both soils were initially contaminated with ^{90}Sr at dangerous levels, the measured β -activities suggest that EKR was effective in reducing the contamination of these systems substantially (Brydie and Beadle, 2004).

Building on earlier work by Cundy and Hopkinson (2005) scaled tests were also run to examine the potential application of EK processes to remotely generate *in-situ* iron barriers in simulated Sellafield soils and

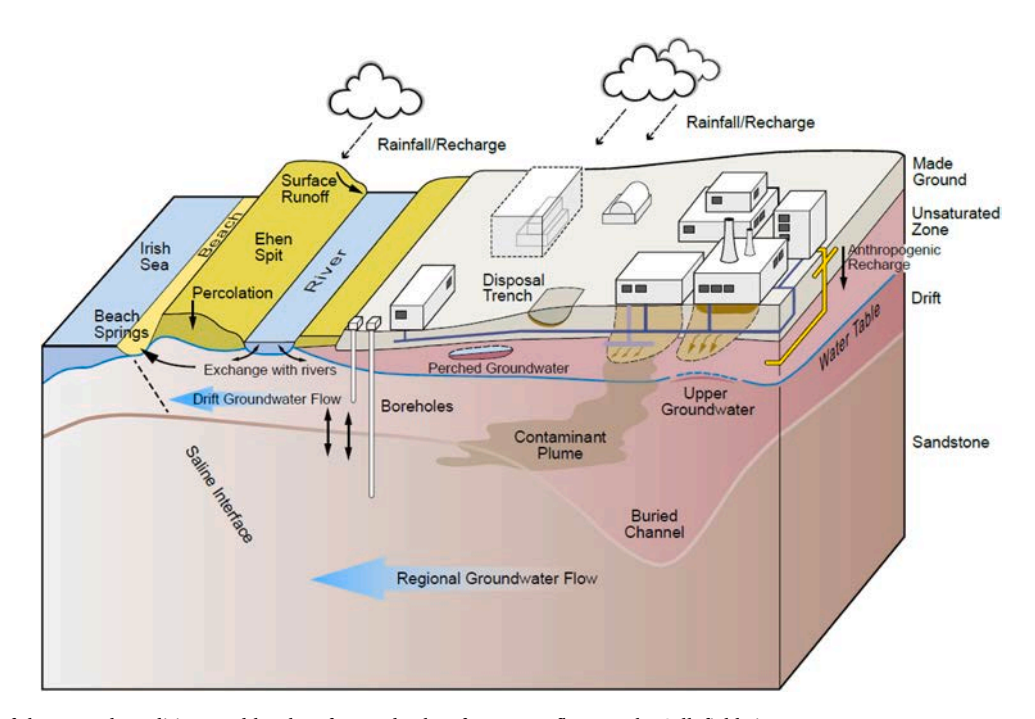


Fig. 14. Schematic of the ground conditions and local surface and subsurface water flows at the Sellafield site. Adapted and redrawn from the 2016 review of groundwater monitoring at Sellafield (Sellafield Ltd., 2016).

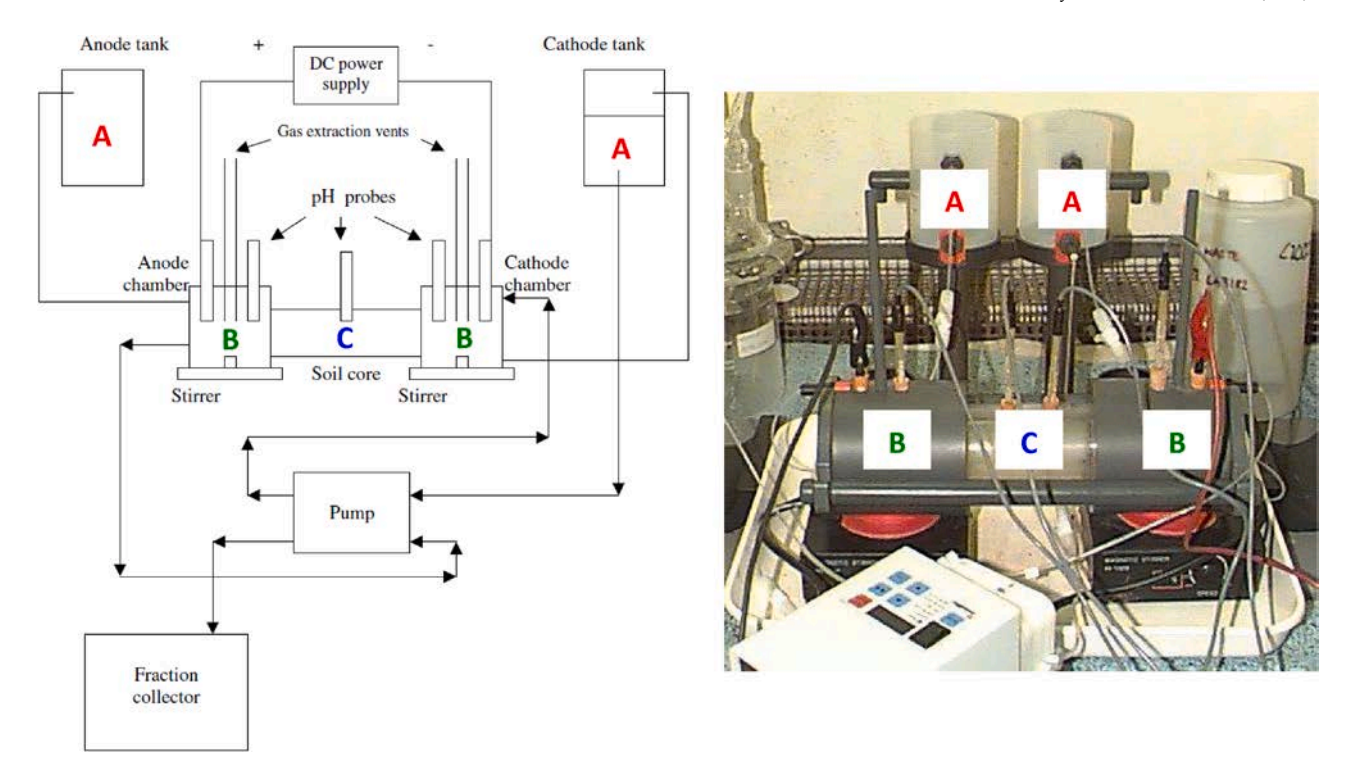


Fig. 15. Left, schematic of the EK cell used, and right, empty cell set-up utilised for the EKR analysis. The soil core (EKR chamber) was 7 cm long with an unspecified diameter. The electrolyte tanks (A), electrode chambers (B) and soil core, where the EK cell was housed (C), are highlighted (Eilbeck and Learmonth, 1999).

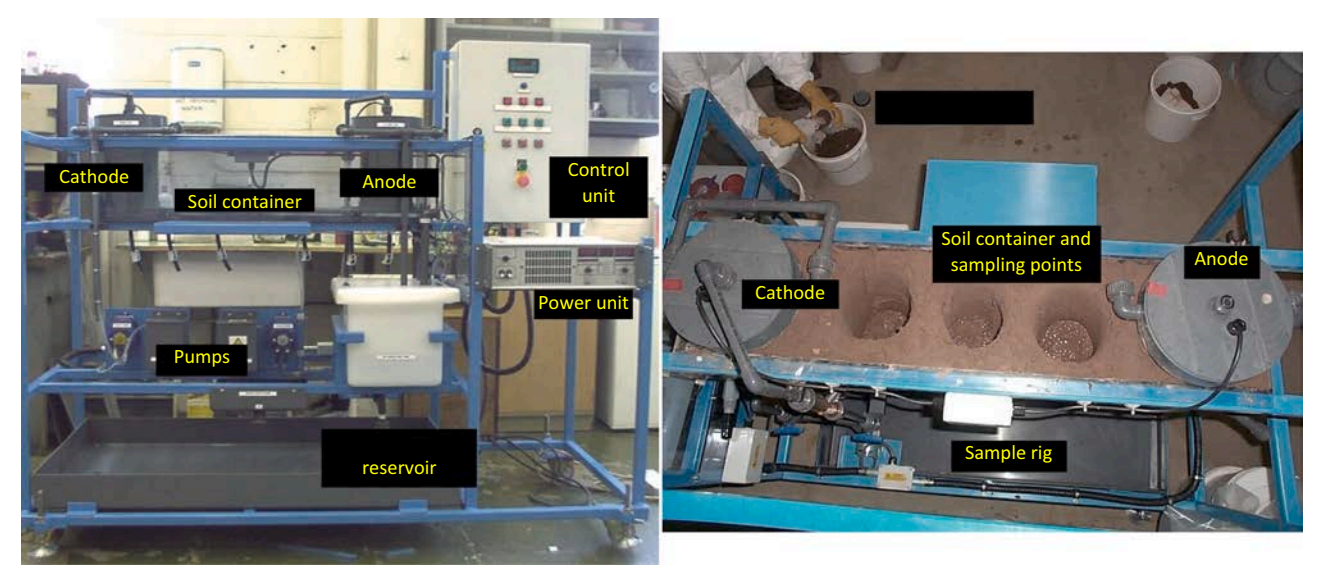


Fig. 16. Left, perspective view of the test rig used (LWH = 0.3 m x 0.75 m x 1.7 m) showing the pumping and electrical and control units, and right, birds-eye view of the test rig showing a full sample container, sample points and preparation of the soil (Brydie and Beadle, 2004).

near-surface materials, Fig. 17. This work utilises the *in-situ* generation of reactive iron barriers in soil when EKR is coupled with use of sacrificial steel electrodes.

Experiments operated up to metre-scales demonstrated the effective growth of iron rich barriers under site-relevant (ground)water salinities, at low voltages ($\leq 0.5~\rm V~cm^{-1}$) over multiple months. These *in-situ* generated iron-rich "pans" may have significant use in providing reactive, *in-situ* barriers for groundwater flow control or groundwater remediation in higher permeability subsurface materials on the Sellafield site. We are developing these systems in collaboration with the UK nuclear industry and will report further in due course.

4. Towards sustainable, integrated EKR techniques for nuclear sites

All EKR experiments discussed for these three sites are laboratory- or pilot-scale experiments, meaning that for nuclear sites the scalability of EKR remains a pressing issue. While non-nuclear electrochemical remediation technologies are becoming commercially feasible (Lacasa et al., 2019), evaluating the factors that influence the applicability of EKR is complex.

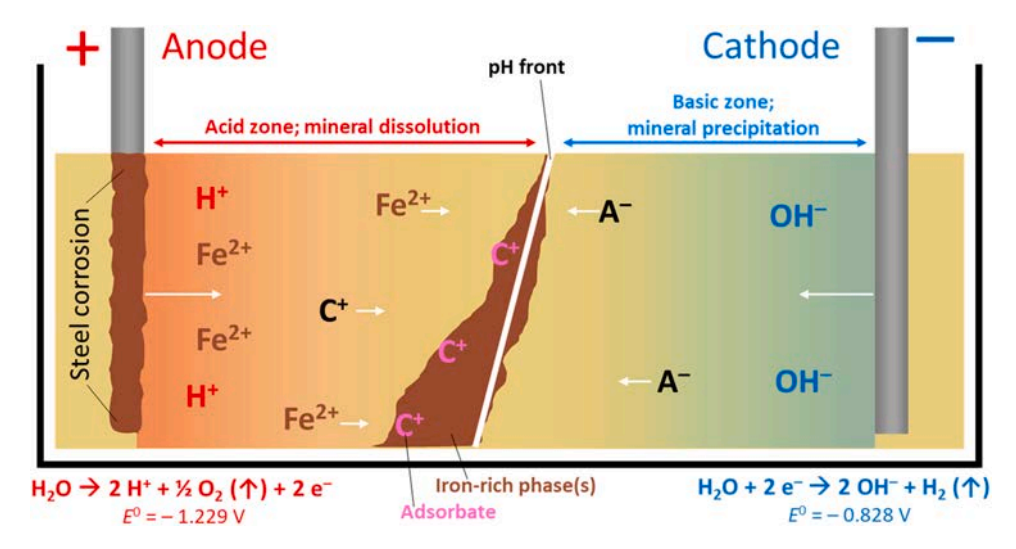


Fig. 17. A simplified EKR cell showing development of an iron-rich band in the FIRS technique and movement of ions. Cation (C⁺) and anion (A⁻) movement with pH gradient, towards electrodes of opposing charge, is shown. Water electrolysis half-cell values are vs. SHE.

4.1. Key properties of EKR for use at nuclear sites

How, for example, does cost – the need to optimise public expenditure – balance with effecting the Best Practicable Environmental Option? (O'Riordan, 1989) To answer this we have assessed previous work on the scalability of EKR (López-Vizcaíno et al., 2016; Suied et al., 2018; Lacasa et al., 2019; Yeung and Gu, 2011; Kim et al., 2011a; Yeung, 2011), and have identified four key areas (Fig. 18) that influence the effectiveness of EKR with particular relevance for nuclear sites. These include i) properties of the substrate (soil, concrete, etc.) ii) properties of the contaminant, iii) electrical inputs and electrodes, and iv) cost and sustainability. The assessment presented here builds on a previous assessment made by the predecessor organisation to the NDA, Nexia Solutions Ltd (Parton, 2007).

Firstly, consider the properties of the substrate to be remediated (Fig. 18, i and ii). Soils, concretes, and sludges, *etc.* each have differing electrical conductivities, moisture levels, particle size distributions, cation exchange capacities, porosities and rheologies. Temperature and precipitation, groundwater flow and topologies will all also affect flow rates of a contaminant through a substrate. While the properties of a substrate are almost universally unique to a particular site, factors such as cation exchange capacities may be generalised dependent on soil type. In particular, clay-rich soils such as illite, montmorillonite, and

kaolinite typically exhibit high acid/base buffering capacities, meaning strongly acidic conditions may be required to effectively transport contaminants. The physicochemical properties of a contaminant are also important (Fig. 18, ii), and can include contaminant speciation (estimated using a Pourbaix phase diagram) (Takeno, 2005) redox and pH sensitivity (e.g. Tc^{IV} vs. Tc^{VII}), adsorption behaviour (kinetics, Langmuir vs. Freundlich isotherms), and the size of a contaminant plume. The chemical form of contaminants is especially important as only dissolved solutes or colloids are amenable to EKR. It may also be necessary to inject additional reagents including weak acids, chelating agents or high ionic strength electrolytes, to enhance contaminant mobility (Wuana and Okieimen, 2011).

The electrical and electrode properties of the EKR unit (Fig. 18, iii), such as voltage and current, direct flow of the contaminants to points in the cell; the higher the voltage, the faster the remediation. This must be balanced with electrode corrosion with acid-resistant materials at the anode, with platinum, graphite or coated titanium preferred as these are (typically) inert to dissolution. Any base-resistant and electrically-conducting material is generally acceptable as a cathode. In the case of sacrificial iron electrodes, electrode dissolution may actually be beneficial (Section 3.3). Expensive or valuable electrodes may be vulnerable to theft and thus require special security, although on tightly regulated nuclear sites this is unlikely to be a problem. Machinable

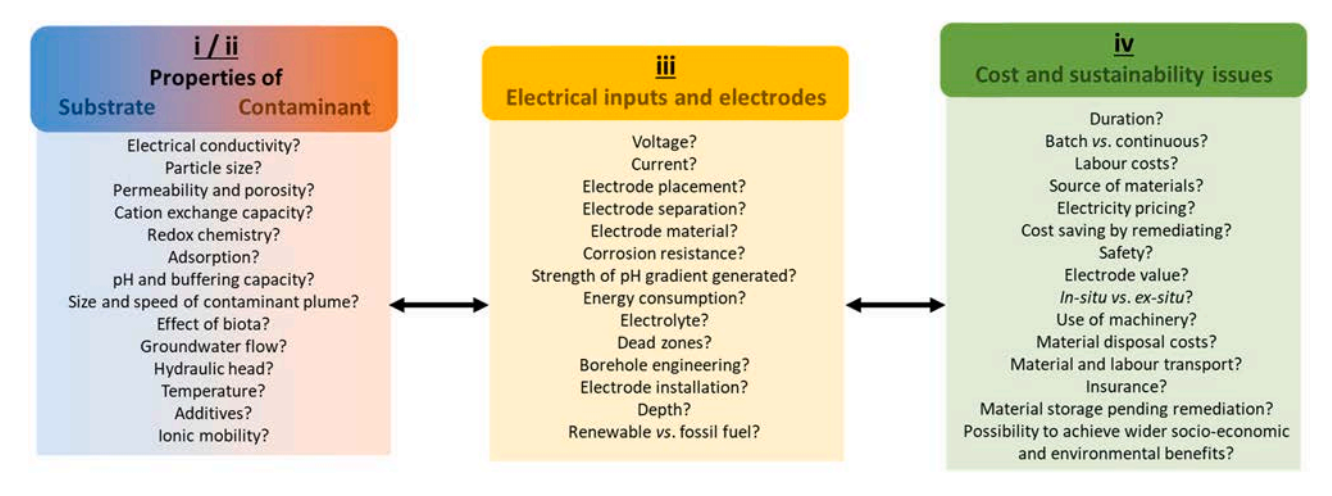


Fig. 18. Factors affecting the potential effectiveness of EKR at a specific site. Assessing these individually and understanding how all these issues affect others is key to understanding outcomes of EKR schemes.

electrodes, particularly hollow or porous ones, are beneficial as they can be combined with flushing technologies or act as PRBs in which the electrodes both migrate and trap selected contaminants. The electrochemical degradation of trichloroethylene has been achieved using machined porous graphite electrodes (Rajic et al., 2016).

A choice of vertical or horizontal electrode placement can be used to further control contaminant movement. Most experiments described here occur in only one or two-dimensions, with depth not considered. Clearly, in multi-centimetre or -metre deep soils, contaminant plume depth is important and further work is needed to establish the effect of electrode depth on contaminant remediation through a stratified soil profile. As discussed in Section 3.1, rather than actively remediating contaminated soil, it may be possible (through EKF) to passively prevent contamination in the first instance. This may be achieved by driving horizontal (sheet) electrodes into a soil but this requires carefully machined sheets of a pliable material, which are typically brittle and susceptible to fracturing if not handled carefully. Simple lines of electrode rods could alternatively be installed and, if buried to a certain depth, be used to generate horizontal fencing bands in-situ (Faulkner et al., 2005). Although this is not a new idea (López-Vizcaíno et al., 2017) we are sceptical if the challenging engineering required to apply this on-site is commercially attractive compared to more established technologies (e.g. injection grouting). Avoiding electrical 'dead zones' (where field strength rapidly diminishes, meaning EKR ceases to be effective) is also important, and although changing electrode placement (e.g. hexagonal vs. circular vs. linear electrode arrays) has been examined (Putra, 2016; Alshawabkeh et al., 1999) it remains untested at scale. Large electrode spacings reduce the borehole and installation costs but increase the time taken to remediate a large area.

Finally, there are cost issues (Fig. 18, iv) to be considered. The costs for EKR are low, rarely costing more than tens or maybe hundreds of USD for electricity or electrode and wiring materials (Purkis et al., 2021). Graphite or steel electrodes and wiring are available from home improvement stores, or *via* the Internet.⁴ Installation, labour and safety costs are the largest outlays, with borehole engineering and maintenance requiring trained operators over weeks to months. We estimate costs here to run to thousands of USD as salaries, safety, training, insurance and other costs are accounted for. Machinery, its rental or ownership, and fuel may also need to be considered, depending on site-specific considerations.

Therefore, in deciding which variables (electrode placement, additives, *etc.*) to control (to maximise EKR effectiveness), the assessor is confronted with a complex, interacting set of parameters. In order to simplify the complex nature of EKR parameters, the NNL developed modelling software, Fig. 19, within the GoldSim (Monte Carlo) package⁵ that assessed an EKR proposal on a number of technical and cost input metrics. These could be compared against output for similar models developed for other remedial techniques in order to support decisions on remedial approach, based on cost (rather than sustainability, below).

We are currently building on this GoldSIM model to develop our own tools to support the options appraisals for nuclear site decommissioning, and we discuss this further in Section 5.

4.1.1. EKR and sustainability

Within the framework of increasing international standards over

sustainable land remediation (Bardos et al., 2016) (e.g. ISO18504:2017 (International Standards Organisation (ISO), 2017) and ASTM E2893 (ASTM International, 2016)), key questions remain around the sustainability of EKR. Although cheap, the power and material requirements for EKR over prolonged periods of time can be resource intensive. To address this, EKR power inputs could be coupled to battery technology with renewable inputs (e.g. solar PV (Hassan et al., 2015) and wind). Abundant electrode materials (e.g. steel rebar) may also help reduce the sustainability footprint of the EKR process (Agnew et al., 2011).

Combining EKR with other technologies (Section 4.2) could enhance the effectiveness of EKR and realise further sustainability benefits from the remediation process. For example, advantages to combining EKR with bio- or phytoremediation could include CO2 sequestration, reduced dust emission, reduced material and resources cost, improved soil function, reduced waste generation, improved project lifespan and biodiversity benefits (Juwarkar, 2012). More generally the sustainability assessment criteria produced by the SuRF-UK (Sustainable Remediation Forum-UK), published in 2011 (Sustainable Remediation Forum (SuRF) and Contaminated Land: Application in Real Environments (CL: AIRE), 2011) and updated in 2020 (Sustainable Remediation Forum (SuRF) and Contaminated Land: Application in Real Environments (CL: AIRE), 2020), provides a clear framework against which the sustainability of remediation options for contaminated land can be assessed (Li et al., 2019a, 2019b). Gill et al. (2016) have used the SuRF-UK framework to compare the sustainability benefits of EKR-Bio, compared with alternative remediation options for a petroleum release site. The authors noted the strong performance of EKR-Bio compared to other intensive treatments, however, benefits are likely site-specific and methods to improve the sustainability of the EK-Bio treatment design (such as use of solar cells) had only a minor effect at the selected site.

4.2. Can other technologies help?

A significant advantage of EKR is that it can easily be applied in combination with other techniques. Our intention here is not to review the individual technologies but comment on how these have been or can be applied on nuclear sites with EKR.

4.2.1. EKR-Phyto and EKR-Bio

A recent contribution from Li et al. (2019b) combines phyto-remediation with **EKR** for the remediation uranium-contaminated soils using sunflower (Helianthus) and mustard (Brassicaceae) plants. Although EKR-Phyto is known for non-nuclear remediation, for example in heavy metal (and Cs) remediation in paddy fields (Mao et al., 2016), or petroleum-contaminated (Rocha et al., 2019) land its use remains rare in radionuclide-contaminated soils (Shahandeh and Hossner, 2002). In the study Li et al. spiked 0.1 g of uranium dioxide, uranium trioxide or uranyl nitrate per kilogram of Mississippi Delta soil, into which sunflowers and mustard plants were grown for 60 days. Phytoremediation without EKR after 60 days showed uranium removal efficiencies of only 0.8-4.3%. When this was repeated and combined with EKR after only 9 days, this increased to between 26% and 62% depending on the form of uranium (UO2, UO3 or uranyl nitrate) used. This increase is consistent with previous EKR-Phyto experiments using mustards in Cu-, Zn-, Cd- and Pb-contaminated paddy field soils, where similar removal efficiencies were reported (ca. 40–50%) (Yeung and Gu, 2011). Although phytoremediation is slow (limited by plant lifecycles), combining it with EKR should offer significant benefits for the remediation of large areas of soil with low levels of shallow radionuclide contamination (Chatterjee et al., 2020).

We are not aware of any EKR-Bio schemes on nuclear sites, although EKR-Bio has received significant attention in recent years, including for the remediation of organics (Gill et al., 2014). In particular, the group of Prof. E. K. Yanful (Western University, Canada) have undertaken numerous studies on the EKR-Bio of petroleum contaminated soils.

⁴ For example, Walmart.com (here) and Amazon.co.uk (here) both stock common electrode materials. These are sold to the public free of restrictions with next-day delivery options available.

⁵ The GoldSIM software package (https://www.goldsim.com/) is a probabilistic simulator that employs Monte Carlo methods used in the analysis of radioactive waste management. Here, the NNL and partners developed a bespoke simulator with pre-defined parameters such as operator cost, etc., toact as a DST when assessing the feasibility of EKR for a given site. The proprietary simulator remains the property of the NNL, NDA, and selected partners.

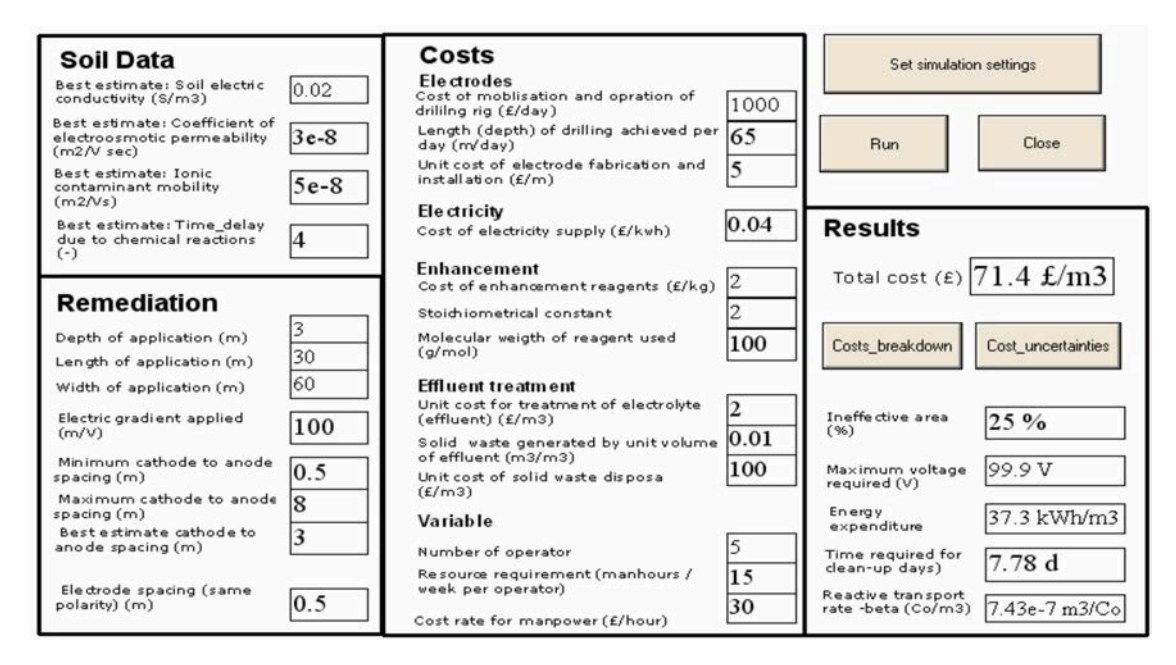


Fig. 19. Example calculation being performed in the EKR cost simulator in the GoldSim package.

Nuclear site wastes often contains organic contamination, including phenanthrene and other polyaromatic hydrocarbons (PAHs), phenols. At Sellafield, trichloroethylene, phthalates and phenols are noteworthy organic contaminants (Sellafield Ltd., 2016). Important considerations for successful site-scale implementation of EKR-Bio for organic contaminants include prolonging the lifetime of indigenous microbiota, increasing metabolic rates and ensuring that metabolic pathways are not disrupted by the application of, or chemical by-products resulting from, the electrokinetic apparatus (Hassan et al., 2018). In particular, combining EKR-Bio reactors on the laboratory scale with solar (PV) cells was shown by Hassan et al. to operate effectively in the mycobacterium-based remediation of artificially contaminated kaolinite mixtures (2 mg of phenanthrene per gram of dry soil). One month of EKR in plastic cells (LWH 35x12x10 cm) with variable voltage resulted in removal of up to 50% of pre-experiment phenanthrene levels (Hassan et al., 2017). Further work on solar-powered EKR-Bio extended this to

diesel fuel contaminated soil (Hassan et al., 2016). We are also aware of successful pilot-scale trials of EKR-Bio in low permeability soils contaminated with polychloroethylenes at a former industrial site in Denmark (e.g. Fig. 20), showing that EKR-Bio is not limited to the laboratory-scale.

Here, EKR-Bio experiments produced three to five times as much ethene (a degradation product of polychloroethylenes) compared to bioremediation without EKR (Riis et al., 2012).

4.2.2. EKR-ISCO (In-situ Chemical Oxidation)

In-situ chemical oxidation (ISCO) is a relatively well-established remediation technique where soluble oxidants are injected into a substrate to degrade (generally) organic pollutants. Similarly to EKR-Bio and EKR-Phyto, Section 4.2.1, recent developments have focused on ISCO of organic contaminants including chlorinated ethylenes and PAHs. Both are contaminants on active and legacy nuclear sites and

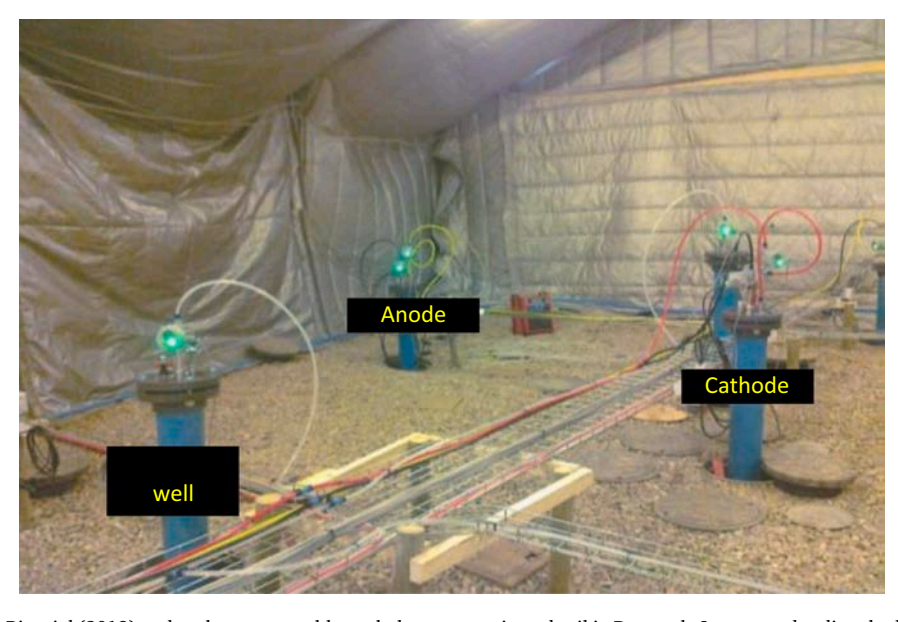


Fig. 20. Example of the EKR-Bio trial (2018) undertaken on tetrachloroethylene-contaminated soil in Denmark. Lactate and sodium hydroxide additives were used to stimulate bacterial growth (Riis et al., 2012).

recent work is of direct relevance to removing organic contaminants on nuclear sites. In particular, EKR enhances the transport of oxidants to desired points within an EKR cell by force-migrating ISCO reagents through low permeability soils (Wu et al., 2010). In laboratory tests Chowdhury et al. demonstrated that permanganate (MnVIIO4) delivery was enhanced under EK through a silt-rich soil over a 41 day period, and reduced spiked trichloroethylene contamination more effectively than either EKR or ISCO alone (Chowdhury et al., 2017). Xu et al. (2020) have also shown that persulfate $(S_2O_8^{2-})$ delivery to PAH-contaminated soil is accelerated by the use of EK apparatus. Although EKR-ISCO may be useful in low-permeability soils, the problem of residual oxidant contamination remains and as these (e.g. permanganate) are generally toxic (Kemp et al., 1966), their indiscriminate use is incompatible with a drive towards sustainable (e.g. mild) remediation technologies. We further note that redox-sensitive radionuclides (and metal contaminants) may not be amenable to EKR-ISCO as oxidation may alter the speciation of these contaminants (Crimi et al., 2011).

4.2.3. EKR-Nano, or EKR-Colloid, based technologies

As noted in Section 3.3, sacrificial iron electrodes can be used to deliver Fe-rich phases into a soil, to reduce (e.g. Cr^{VI} to Cr^{III}, possibly also for Tc^{VII} to Tc^{IV}), (Hopkinson et al., 2009) or sorb contaminants in the subsurface (Faulkner et al., 2005; Cundy and Hopkinson, 2005). There is also scope to electrophoretically "pump" or contain colloids and nanoparticles within an active treatment zone using the electric field, depending on their zeta potential. The movement of clays and colloids under an EK field is an area needing further research at nuclear sites. So-called 'electro-grouting' – where soils are stabilised through ion migration under an electric field – may also be combined with injection grouts to fill voids in building materials, again, electrophoretically

(Alshawabkeh and Sheahan, 2003).

The electro-osmotic movement of calcium chloride and sodium silicates under an electric field is known to increase the shear strength of soft silty clays, and coupling EKR with nano-remediation (Ingle et al., 2014) is effective for the degradation of organic pollutants (Gomes et al., 2016, 2014). Engineered barrier repair or ground containment are other areas where EK may be combined with injection grouting (Bani Baker et al., 2018; Wong et al., 2018), however we are not aware of any examples of EKR-Nano or electro-grouting applied on radioactively contaminated materials. We are examining combined approaches for this technology in our laboratories.

4.2.4. Electrokinetic dewatering, EKD

Electrokinetic dewatering (EKD) is the electro-osmotic flow of water from anode to cathode, from where it can be removed. Although not strictly a combined technique EKD is a medium-to-high TRL technology with wide commercial applications, having been reported first in 1966 (Adamson et al., 1966) and applied for sludge thickening and dewatering for at least thirty years, (Sunderland, 1987) and thus we include it here. It is broadly applied at scale in various sectors including mining, water purification, and civil engineering (Colin et al., 2017). This wide scalability makes it advantageous over other forms of 'combined' EKR techniques. It also aligns strongly with the waste minimisation objectives of the waste hierarchy. This was recently highlighted in work by Lamont-Black et al. on radioactively contaminated sludges on a working nuclear site (Lamont-Black et al., 2015). A schematic of the setup used is given in Fig. 21, alongside the material before and after processing, and the batch-scale setup employed.

The sludges were dewatered in batches for 6 days at 30 V, with a total electricity consumption of 864 kW h. More than 400 m^3 of



Fig. 21. Top: batch scale processing of contaminated nuclear waste sludges on site; bottom: contaminated sludge before and after processing. Figures adapted from Lamont-Black et al. (2015).

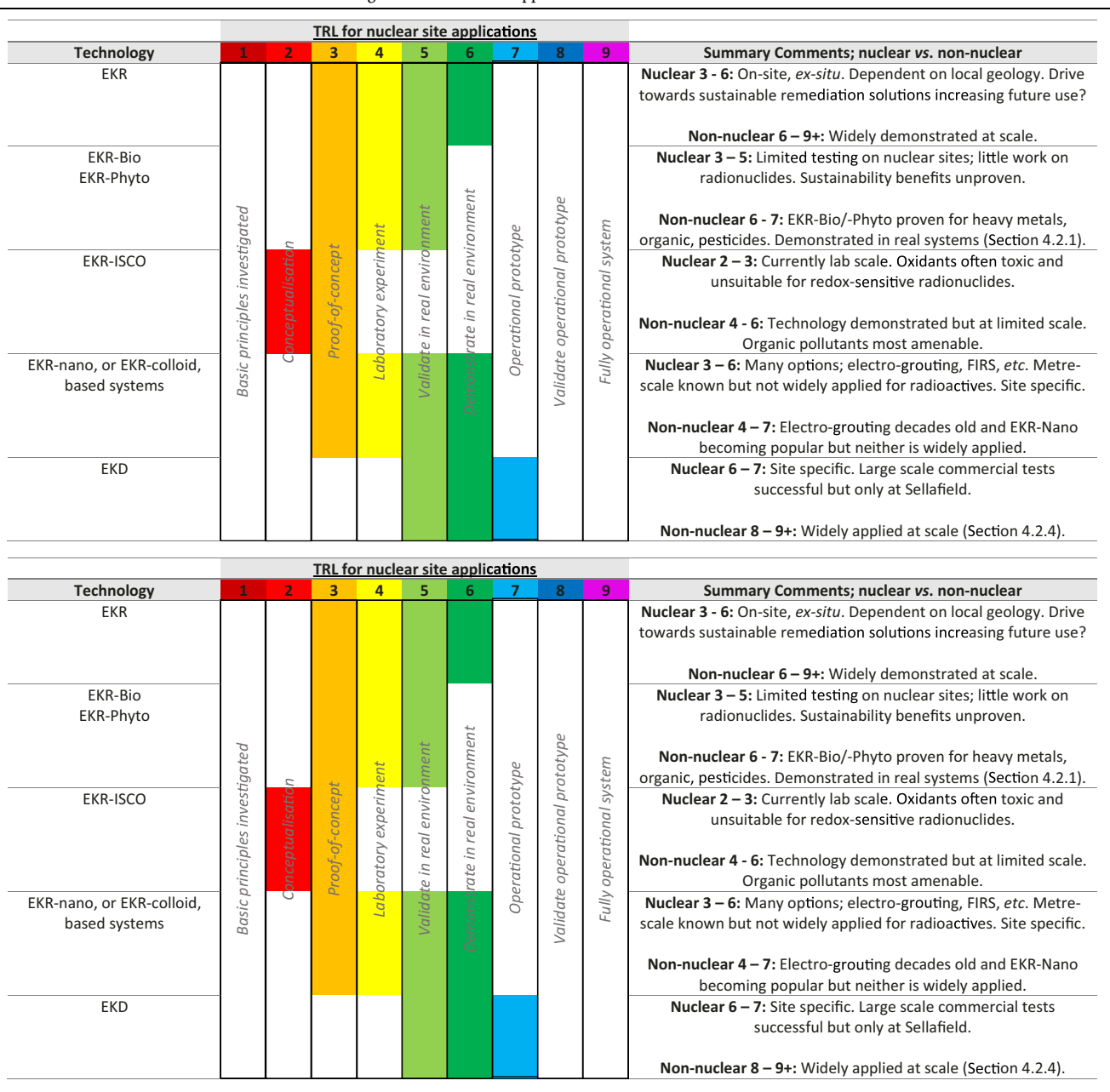
radioactively contaminated sludge was reduced to 30 m³, a volume reduction of over 90%. Although this power consumption is high there is no reason why the EKD process could not be coupled with renewable energy sources to maximise energy efficiency. Given disposal costs of *ca*. \$52,000/£ 40,000 (UK, 2015) per tonne for contaminated waste, the cost benefit of EKD, if successfully incorporated into waste treatment workflows, may be significant. Sludges are among the most significant and problematic wasteforms on nuclear sites (at Sellafield, for example, almost 3000 m³ of material is classed as 'sludge') (Department of Business, Energy and Industrial Strategy (BEIS) and Nuclear Decommissioning Authority (NDA), 2017) and EKD may offer another technique in the assessor's toolkit for remediating contaminated wastes.

4.3. TRL of EKR for nuclear site applications

While many of the technologies discussed above are technologically feasible, few have been applied at scale, particularly as readily available "turn-key" solutions. This is particularly true for nuclear sites and partly reflects the considerable logistical challenges to applying these technologies at scale on what are (rightly) very heavily regulated industrial sites, rather than the technological inferiority of the EKR process itself. Where examples of scalable EKR processes are forthcoming these are often *ex-situ* on individual batches of simulated materials, rather than *in-situ* under a continuous process on real site materials. This limits the current applicability of EKR and combined processes for use at nuclear sites. Table 3.

We assess EKR for nuclear sites as between TRL 3 and 6; that is, demonstrated at the laboratory scale with limited intermediate and pilot

Table 3Our view on the current TRL status of EKR technologies for nuclear site application.



scale work. For non-nuclear this extends to between TRL 6 and 9+, as electrokinetics are widely applied for construction and mining applications (Hansen et al., 2016). There are significant practical issues limiting the wider scale applicability of EKF and EKR-ISCO for nuclear sites (for EKR-ISCO, organic pollutants in non-nuclear applications are most applicable), although combining EKR with other approaches (*e.g.* electro-grouting or EKR-Nano) is an expanding research area with growing future scope to address on-site contamination, sustainably.

5. Concluding remarks and scaling up

To answer the first of the three questions posed in the introduction, there has been considerable progress in EKR over the last decade. Since the last major review in 2009, EKR has been studied on new wasteforms and elements, including 134/137Cs-contaminated ash, uraniumcontaminated concretes, gravels, 60 Co/ 137 Cs/ $^{152/154}$ Eu-contaminated spent graphite, and ⁹⁹Tc contaminated Mexican soil. Where reported, remediation efficiencies are high (often 90%+). Based on our assessment in Table 3, Fig. 22 indicates elements we believe are currently amenable to EKR on nuclear sites. Diagonal shading indicates elements that have radionuclides of interest, but on which EKR has not been performed, or pre-2009. These include calcium (chemically analogous to strontium), nickel (mobile in experiments on naturally occurring Ni) (Saleem et al., 2011), tin (non-nuclear mining waste, pre-2009) (Ho and Lee, 1994), iodine (Hg-selective EKR lixivant) (Suer and Allard, 2003) and radium and thorium (pre-2009 removal from clayey soils) (Acar et al., 1992).

By moving from the laboratory to intermediate and even pilot scale, a number of authors have shown that even in tonnes of contaminated material removal efficiencies remain high (*ca.* 80%+), competitive with other technologies. Although these studies are *ex-situ* and employ washing (soils) or ball milling (concretes, gravels), they are the first step in demonstrating the wider feasibility of EKR for problem nuclides (*e.g.* through on-site, *ex-situ* applications).

Further, many of the radionuclides we consider in Fig. 22 have traditionally been overlooked, because detecting low energy alpha or

beta emissions from at least one of their isotopes is challenging. These include ³H (Section 3.3), ¹⁴C, ⁴¹Ca, ⁶³Ni, ⁹⁰Sr, ⁹⁹Tc, ¹²⁹I, ^{239–241}Pu, and ²⁴⁴Cm, *via* non-destructive techniques (Hou, 2019). Although some advances have been made with these DTM radionuclides since 2009 (Section 2.3) (Agnew et al., 2011; Valdovinos et al., 2016; Leskinen et al., 2020; Warwick and Croudace, 2017), there remains a lack of research examining the remediation of these DTMs at scale, particularly EKR. This is despite being key contaminants in common materials found at nuclear sites, such as graphite, concrete, steel, water and soil (Hou, 2007). Work to expand EKR for the treatment of DTM radionuclides is currently being undertaken in our laboratories with industrial partners and will be reported in due course.

For answers to the two remaining questions (EKR at selected nuclear sites, and further application of EKR), scalability remains problematic. Examples of EKR at the site scale (Hanford, Fukushima) do not vet exist and those at the pilot scale (Sellafield) are limited by the small number of studies in real site conditions. Off-the-shelf "turn-key" EKR systems have not been applied, and given the large number of factors that can influence the success, duration and cost of EKR schemes (Fig. 18), this is not surprising. However, the most important factors are likely to include the soil type, groundwater flow, water table depth, primary (radionuclide) contaminant, presence or absence of co-contaminants, required duration, and ionic mobility of contaminants. As these vary from site to site, we suggest that site-specific modelling of EKR rather than a general approach will be most effective in scaling EKR technologies up. Effective communication with stakeholders is vital to ensure knowledge is transferred between academic and industrial stakeholders most effectively (Gill et al., 2016; Onwubuya et al., 2009; Cundy et al., 2015; Mobbs et al., 2019). Decision support tools (DSTs) are models designed to help achieve this, ensuring stakeholders have access to relevant information in a form convenient to them. Several DSTs over the last decade or so have been produced to supplement the (sustainable) remediation of contaminated land (Onwubuya et al., 2009; Cundy et al., 2015; Huysegoms and Cappuyns, 2017). Through the TRANSCEND consortium we are developing EKR DSTs with a view towards site-scale application, and we will report on this in due course.

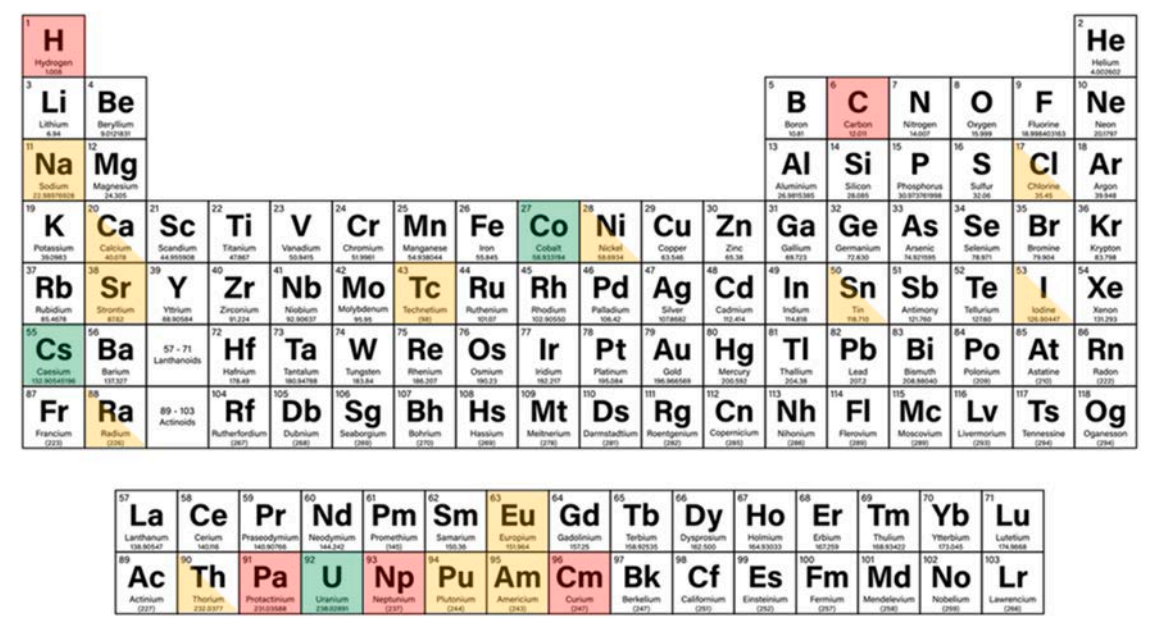


Fig. 22. Periodic table of elements with common isotopes present in nuclear sites applicable to EKR (Tables 1 and 2). Elements in **red** require further testing; yellow, limited work in past 10 years; diagonal yellow, demonstrated but not on a radionuclide and/or more than 10 years ago; and green, multiple studies showing EKR is useful in mobilising these elements. Elements with isotopes of half-lives < 1 year are excluded.

We also suggest that combining EKR with other in-situ technologies may offer enhanced benefits versus EKR alone. Options that we consider most advantageous include EKR-Bio and EKR-Phyto (long duration but high potential for wider sustainability benefits), EKR-nano (easily combined, e.g. FIRS, electro-grouting) and EKD (which has demonstrated commercial viability). There are significant barriers to practical application of large-scale EKF (e.g. high continuous power requirement) or EKR-ISCO (harmful oxidants, possibility of enhanced mobilisation of some radionuclides). In terms of sustainability, although a full sustainability assessment of EKR-Bio for use on petroleum sites was recently published (Gill et al., 2016), such an assessment for use of EKR on nuclear sites is urgently needed. This would provide assessors with the information they need to decide the best technology to remediate a given site, sustainably, reflecting the growth of sustainable remediation guidelines (Nuclear Energy Agency (NEA) of the Organisation for Cooperation and Development (OECD), 2016) and legislation (Bardos et al., 2018).

CRediT authorship contribution statement

Jamie M. Purkis: Conceptualization, Methodology, Investigation, Validation, Visualization, Writing – original draft, Writing – review & editing. Phil E. Warwick: Funding acquisition, Supervision, Writing – review & editing. James Graham: Software, Validation, Writing – review & editing. Shaun D. Hemming: Investigation, Writing – review & editing. Andy B. Cundy: Conceptualization, Methodology, Investigation, Project administration, Supervision, Validation, Writing – original draft, Writing – review & editing, Funding acquisition.

Declaration of Competing Interest

The authors declare that they have no known competing financial interests or personal relationships that could have appeared to influence the work reported in this paper.

Acknowledgements

The authors acknowledge funding from the TRANSCEND (TRANsformative SCience and Engineering for Nuclear Decommissioning) consortium (EPSRC grant number EP/S01019X/1), as well as the original authors of reports examining EKR at the Sellafield site under BNFL, Nexia Solutions, and the NNL and NDA. PW and AC acknowledge support from the EPSRC / National Nuclear User Facility Phase 2 programme (EP/T011548/1, NNUF-EXACT). The authors further thank the NDA, NNL and predecessors for kindly providing access to these reports. For redrawing and adapting many of the figures in this paper from their original source, the authors also thank Mrs. Kate Davis (National Oceanography Centre, Southampton, UK).

References

- Acar, Y.B., Alshawabkeh, A.N., 1993. Principles of electrokinetic remediation. Environ. Sci. Technol. 27, 2638–2647.
- Acar, Y.B., Gale, R.J., Ugaz, A., Puppala, S., Leonard, C., 1992. Feasibility of Removing Uranium, Thorium and Radium from Kaolinite by Electrochemical Soil Processing. Electrokinetics Inc., Baton Rouge, Louisiana, US. Report EK-BR-009-0292(Final Report-Phase I of EK-EPA Cooperative Agreement CR816828-01-0).
- Acar, Y.B., Gale, R.J., Alshawabkeh, A.N., Marks, R.E., Puppala, S., Bricka, M., Parker, R., 1995. Electrokinetic remediation: basics and technology status. J. Hazard. Mater. 40, 117–137.
- Adamson, L.G., Chilingar, G.V., Beeson, C.M., Armstrong, R.A., 1966. Electrokinetic dewatering, consolidation and stabilization of soils. Eng. Geol. 1, 291–304.
- Agnew, K., Cundy, A.B., Hopkinson, L., Croudace, I.W., Warwick, P.E., Purdie, P., 2011.
 Electrokinetic remediation of plutonium-contaminated nuclear site wastes: results from a pilot-scale on-site trial. J. Hazard. Mater. 186, 1405–1414.
- Alshawabkeh, A.N., Sheahan, T.C., 2003. Soft soil stabilisation by ionic injection under electric fields. Proc. Instit. Civ. Eng. Ground Improv. 7, 177–185.
- Alshawabkeh, A.N., Gale, R.J., Ozsu-Acar, E., Bricka, R.M., 1999. Optimization of 2-D electrode configuration for electrokinetic remediation. J. Soil Contam. 8, 617–635.

- ASTM International, 2016. ASTM E2893 16e1: Standard Guide for Greener Cleanups. ASTM International.
- Bani Baker, M., Elektorowicz, M., Hanna, A., 2018. Electrokinetic nondestructive in-situ technique for rehabilitation of liners damaged by fuels. J. Hazard. Mater. 359, 510–515.
- Bardos, R.P., Cundy, A.B., Smith, J.W.N., Harries, N., 2016. Sustainable remediation. J. Environ. Manag. 184, 1–3.
- Bardos, R.P., Thomas, H.F., Smith, J.W.N., Harries, N.D., Evans, F., Boyle, R., Howard, T., Lewis, R., Thomas, A.O., Haslam, A., 2018. The development and use of sustainability criteria in SuRF-UK's sustainable remediation framework. Sustainability 10, 1781.
- Beavers, J.A., Chawla, S., Evans, K., Rollins, B.C., Sherer, K.M., Sridhar, N., Boomer, K.D., Girardot, C.L., Venetz, T., Stock, L.M., 2019. History of the first double-shell highlevel nuclear waste tank at the Hanford site. Corrosion 75, 292–301.
- Bespala, E.V., Antonenko, M.V., Chubreev, D.O., Leonov, A.V., Novoselov, I.Y., Pavlenko, A.P., Kotov, V.N., 2019. Electrochemical treatment of irradiated nuclear graphite. J. Nucl. Mater. 526, 151759.
- Briner, W., 2010. The toxicity of depleted uranium. Int. J. Environ. Res. Public Health 7, 303–313.
- Brines, M.E., Simmons, S., Morse, J., 2013. Startup of the New 200 West Pump-and-Treat, Hanford Site, Richland, Washington presented in part at the Waste Management (WM) Symposia 2013, Phoenix, Arizona, US.
- Brydie, J.R., Beadle, I., 2004. Electrokinetic Remediation of Sellafield Soils in Preparation for Field Scale Remediation Trials. British Nuclear Fuels Ltd. (BNFL), UK. Report NSTS 4965.
- Buehler, M.F., Surma, J.E., Virden, J.W., 1994. In situ soil remediation using electrokinetics (PNL-SA-24081) presented in part at the Thirty-Third Hanford Symposium on Health and the Environment, Richland, Washington, USA.
- Cameselle, C., Gouveia, S., 2018. Electrokinetic remediation for the removal of organic contaminants in soils. Curr. Opin. Electrochem. 11, 41–47.
- Chatterjee, S., Mitra, A., Walther, C., Gupta, D.K., 2020. Plant Response Under Strontium and Phytoremediation. In: Pathak, P., Gupta, D.K. (Eds.), Strontium Contamination in the Environment. Springer International Publishing, Cham, pp. 85–97.
- Chowdhury, A.I.A., Gerhard, J.I., Reynolds, D., Sleep, B.E., O'Carroll, D.M., 2017. Electrokinetic-enhanced permanganate delivery and remediation of contaminated low permeability porous media. Water Res. 113, 215–222.
- Colin, J., John, L.-B., David, H., David, A., Stephanie, G., 2017. Electrokinetic geosynthetics: from research to hype to practice. Proc. Instit. Civ. Eng. - Civ. Eng. 170, 127–134.
- Crimi, M., Simpkin, T.J., Palaia, T., Petri, B.G., Siegrist, R.L., 2011. Systematic Approach for Site-Specific Engineering of ISCO. In: Siegrist, R.L., Crimi, M., Simpkin, T.J. (Eds.), In Situ Chemical Oxidation for Groundwater Remediation. Springer New York, New York, NY, pp. 355–412.
- Cundy, A., Bardos, P., Puschenreiter, M., Witters, N., Mench, M., Bert, V., Friesl-Hanl, W., Müller, I., Weyens, N., Vangronsveld, J., 2015. Developing effective decision support for the application of "gentle" remediation options: the GREENLAND project. Remed. J. 25, 101–114.
- Cundy, A.B., Hopkinson, L., 2005. Electrokinetic iron pan generation in unconsolidated sediments: implications for contaminated land remediation and soil engineering. Appl. Geochem. 20, 841–848.
- De Rose, A., Buna, M., Strazza, C., Olivieri, N., Stevens, T., Peeters, L., Tawil-Jamault, D., 2017. Technology Readiness Level: Guidance Principles for Renewable Energy Technologies. European Union (EU), Brussels. Report EUR 27988 EN.
- Department of Business, Energy and Industrial Strategy (BEIS) and Nuclear
 Decommissioning Authority (NDA), 2017. 2016 UK Radioactive Waste & Materials
 Inventory: UK Radioactive Waste Inventory Report, Department of Business, Energy
 and Industrial Strategy (BEIS) and Nuclear Decommissioning Authority (NDA), UK.
- Department of Energy (DoE), 2009R. Hanford Site Groundwater Monitoring and Performance Report for 2009. Department of Energy (DoE), US. Report DOE/RL-2010-11.
- Department of Energy (DoE), 2013. Hanford Site Excavating, Trenching and Shoring Procedure (HSETSP). Department of Energy (DoE), US. Report DOE-0344 Revision 3A
- Department of Energy (DoE), 2019. 2019 Hanford Lifecycle Scope, Schedule and Cost Report. Department of Energy (DoE), US. Report DOE/RL-2018-45.
- Eilbeck, A., Lorimer, K., 2001. Electrokinetic Remediation Studies on Soil Contaminated with B38 Leak Simulant. British Nuclear Fuels Ltd. (BNFL), UK. Report RAT 1307.
- Eilbeck, A.B., Learmonth, P.E., 1999. An Experimental Investigation into the Application of Electrokinetic Remediation to Contaminated Sellafield Soils. British Nuclear Fuels Ltd. (BNFL), UK. Report RDR 1717.
- Ellis, D.E., Hadley, P.W., 2009. Sustainable remediation white paper—Integrating sustainable principles, practices, and metrics into remediation projects. Remediation 19, 5–114.
- Evrard, O., Laceby, J.P., Nakao, A., 2019. Effectiveness of landscape decontamination following the Fukushima nuclear accident: a review. SOIL 5, 333–350.
- Faulkner, D.W.S., Hopkinson, L., Cundy, A.B., 2005. Electrokinetic generation of reactive iron-rich barriers in wet sediments: implications for contaminated land management. Mineral. Mag. 69, 749–757.
- Food and Agricultural Organisation (FAO) of the United Nations (UN), 2015. World Reference Base for Soil Resources 2014: International Soil Classification System for Naming Soils and Creating Legends for Soil Maps (Update 2015). Food and Agricultural Organisation (FAO) of the United Nations (UN), Rome.
- Fredrickson, J.K., Zachara, J.M., Balkwill, D.L., Kennedy, D., Li, S.-M.W.,
 Kostandarithes, H.M., Daly, M.J., Romine, M.F., Brockman, F.J., 2004.
 Geomicrobiology of high-level nuclear waste-contaminated vadose sediments at the
 Hanford Site, Washington State. Appl. Environ. Microbiol. 70, 4230–4241.

- Fuller, A.J., Shaw, S., Ward, M.B., Haigh, S.J., Mosselmans, J.F.W., Peacock, C.L., Stackhouse, S., Dent, A.J., Trivedi, D., Burke, I.T., 2015. Caesium incorporation and retention in illite interlayers. Appl. Clay Sci. 108, 128–134.
- Gallardo, A.H., Marui, A., 2016. The aftermath of the Fukushima nuclear accident: measures to contain groundwater contamination. Sci. Total Environ. 547, 261–268.
- Gavrilescu, M., Pavel, L.V., Cretescu, I., 2009. Characterization and remediation of soils contaminated with uranium. J. Hazard. Mater. 163, 475–510.
- Gill, R.T., Harbottle, M.J., Smith, J.W.N., Thornton, S.F., 2014. Electrokinetic-enhanced bioremediation of organic contaminants: a review of processes and environmental applications. Chemosphere 107, 31–42.
- Gill, R.T., Thornton, S.F., Harbottle, M.J., Smith, J.W.N., 2016. Sustainability assessment of electrokinetic bioremediation compared with alternative remediation options for a petroleum release site. J. Environ. Manag. 184, 120–131.
- Gomes, H.I., Fan, G., Mateus, E.P., Dias-Ferreira, C., Ribeiro, A.B., 2014. Assessment of combined electro–nanoremediation of molinate contaminated soil. Sci. Total Environ. 493, 178–184.
- Gomes, H.I., Fan, G., Ottosen, L.M., Dias-Ferreira, C., Ribeiro, A.B., 2016.
 Nanoremediation coupled to electrokinetics for PCB removal from soil. In:
 Ribeiro, A.B., Mateus, E.P., Couto, N. (Eds.), Electrokinetics Across Disciplines and
 Continents: New Strategies for Sustainable Development. Springer International
 Publishing, Cham, pp. 331–350.
- Graham, J., 2015. MSSS GEMS Phase 2: Characterisation of Soils and Strontium Sorption Batch Testing. National Nuclear Laboratory, NNL. Report NNL 13224.
- Hansen, H.K., Ottosen, L.M., Ribeiro, A.B., 2016. Electrokinetic soil remediation: an overview. In: Ribeiro, A.B., Mateus, E.P., Couto, N. (Eds.), Electrokinetics Across Disciplines and Continents: New Strategies for Sustainable Development. Springer International Publishing, Cham, pp. 3–18.
- Harbottle, D., Hunter, T., 2019. Electrokinetic Separation for Enhanced Decontamination of Soils and Groundwater Systems. Engineering and Physical Sciences Research Council (EPRSC), UK (grant EP/S032797/1).
- Hassan, I., Mohamedelhassan, E., Yanful, E.K., 2015. Solar powered electrokinetic remediation of Cu polluted soil using a novel anode configuration. Electrochim. Acta 181, 58–67.
- Hassan, I., Mohamedelhassan, E., Yanful, E.K., Yuan, Z.-C., 2017. Solar power enhancement of electrokinetic bioremediation of phenanthrene by Mycobacterium pallens. Bioremediat. J. 21, 53–70.
- Hassan, I., Mohamedelhassan, E., Yanful, E., Yuan, Z.-C., 2018. Enhancement of bioremediation and phytoremediation using electrokinetics. In: Shiomi, N. (Ed.), Advances in Bioremediation and Phytoremediation. IntechOpen.
- Hassan, I., Mohamedelhassan, E., Yanful, E.K., Yuan, Z.-C., 2016. Solar powered electrokinetic bioremediation of diesel fuel contamination presented in part at the International Symposium on Electrokinetic Remediation 2016 (EREM 2016), Abu Dhabi. United Arab Emirates (UAE).
- Ho, C.C., Lee, K.C., 1994. Electrokinetic behaviour of tin tailings slurries in solutions of lanthanum and thorium salts. Colloids Surf. A Physicochem. Eng. Asp. 90, 17–24.
- Ho, S.V., Athmer, C., Sheridan, P.W., Hughes, B.M., Orth, R., McKenzie, D., Brodsky, P. H., Shapiro, A., Thornton, R., Salvo, J., Schultz, D., Landis, R., Griffith, R., Shoemaker, S., 1999. The lasagna technology for in situ soil remediation. 1. Small field test. Environ. Sci. Technol. 33, 1086–1091.
- Hopkinson, L., Cundy, A.B., Faulkner, D.W.S., Hansen, A., Pollock, R., 2009.
 Electrokinetic stabilization of Cr(VI)-contaminated soils. In: Reddy, K., Cameselle, C.
 (Eds.), Electrochemical Remediation Technologies for Polluted Soils, Sediments and Groundwater. John Wiley and Sons, Inc, New York, pp. 179–193 ch. 8.
- Hou, X., 2005. Radiochemical determination of 41 Ca in nuclear reactor concrete. Radiochim. Acta 93, 611.
- Hou, X., 2007. Radiochemical analysis of radionuclides difficult to measure for waste characterization in decommissioning of nuclear facilities. J. Radioanal. Nucl. Chem. 273, 43–48
- Hou, X., 2019. Radioanalysis of ultra-low level radionuclides for environmental tracer studies and decommissioning of nuclear facilities. J. Radioanal. Nucl. Chem. 322, 1217–1245.
- Huysegoms, L., Cappuyns, V., 2017. Critical review of decision support tools for sustainability assessment of site remediation options. J. Environ. Manag. 196, 278–296.
- IAEA, 1999. Technologies for Remediation of Radioactively Contaminated Sites. IAEA, Austria. Report IAEA-TECDOC-1086.
- IAEA, 2004. Remediation of Sites with Dispersed Radioactive Contamination. IAEA, Vienna, Austria. Report STI/DOC/010/424.
- Ingle, A.P., Seabra, A.B., Duran, N., Rai, M., 2014. Nanoremediation: a new and emerging technology for the removal of toxic contaminants from environment. In: Das, S. (Ed.), Microbial Biodegradation and Bioremediation. Elsevier, Oxford, pp. 233–250.
- International Standards Organisation (ISO), 2017. ISO 18504:2017: Soil quality Sustainable remediatio. International Standards Organisation (ISO).
- Jung, H.B., Yang, J.-S., Um, W., 2015. Bench-scale electrokinetic remediation for cesium-contaminated sediment at the Hanford Site, USA. J. Radioanal. Nucl. Chem. 304, 615–625.
- Juwarkar, A.A., 2012. Microbe-assisted phytoremediation for restoration of biodiversity of degraded lands: a sustainable solution. Proc. Natl. Acad. Sci. India B 82, 313–318.
- Kemp, H.T., Fuller, R.G., Davidson, R.S., 1966. Potassium permanganate as an algicide. J. Am. Water Work. Assoc. 58, 255–263.
- Kikuchi, R., Mukai, H., Kuramata, C., Kogure, T., 2015. Cs-sorption in weathered biotite from Fukushima granitic soil. J. Mineral. Petrol. Sci. 110, 126–134.
- Kim, B.-K., Baek, K., Jo, S.-H., Yang, J.-W., 2011. Research and field experiences on electrokinetic remediation in South Korea. Sep. Purif. Technol. 79, 116–123.

- Kim, G.-N., Choi, W.-K., Lee, K.-W., 2010. Decontamination of radioactive concrete using electrokinetic technology. J. Appl. Electrochem. 40, 1209–1216.
- Kim, G.-N., Yang, B.-I., Choi, W.-K., Lee, K.-W., 2009. Development of vertical electrokinetic-flushing decontamination technology to remove 60Co and 137Cs from a Korean nuclear facility site. Sep. Purif. Technol. 68, 222–226.
- Kim, G.-N., Kim, S.-S., Park, U.-R., Moon, J.-K., 2015. Decontamination of soil contaminated with cesium using electrokinetic-electrodialytic method. Electrochim. Acta 181, 233–237.
- Kim, G.-N., Kim, S.-S., Moon, J.-K., Hyun, J.-H., 2015. Removal of uranium from soil using full-sized washing electrokinetic separation equipment. Ann. Nucl. Energy 81, 188–195.
- Kim, G.-N., Kim, I., Kim, S.-S., Choi, J.-W., 2016. Removal of uranium from contaminated soil using indoor electrokinetic decontamination. J. Radioanal. Nucl. Chem. 309, 1175–1181.
- Kim, G.-N., Yang, B.-I., Choi, W.-K., Lee, K.-W., Hyeon, J.-H., 2009. Washingelectrokinetic decontamination for concrete contaminated with cobalt and cesium. Nucl. Eng. Technol. 41, 1079–1086.
- Kim, G.-N., Lee, S.-S., Shon, D.-B., Lee, K.-W., Chung, U.-S., 2010. Development of pilot-scale electrokinetic remediation technology to remove 60Co and 137Cs from soil. J. Ind. Eng. Chem. 16, 986–991.
- Kim, G.-N., Shon, D.-B., Park, H.-M., Lee, K.-W., Chung, U.-S., 2011. Development of pilot-scale electrokinetic remediation technology for uranium removal. Sep. Purif. Technol. 80, 67–72.
- Kim, G.-N., Shon, D.-B., Park, H.-M., Kim, K.-H., Lee, K.-W., Moon, J.-K., 2011b. Precipitation-filtering method for reuse of uranium electrokinetic leachate. J. Nucl. Fuel Cycle Waste Technol. 9, 63–71 (Korean).
- Kim, G.-N., Kim, S.-S., Park, H.-M., Kim, W.-S., Park, U.-R., Moon, J.-K., 2013. Cs-137 and Cs-134 removal from radioactive ash using washing–electrokinetic equipment. Ann. Nucl. Energy 57, 311–317.
- Kim, G.-N., Park, U.-R., Kim, S.-S., Kim, W.-S., Moon, J.-K., Hyun, J.-H., 2014. Decontamination of gravels contaminated with uranium. Ann. Nucl. Energy 72, 367–372.
- Kim, S.-S., Kim, G.-N., Park, U.-R., Moon, J.-K., 2014. Development of a practical decontamination procedure for uranium-contaminated concrete waste. J. Radioanal. Nucl. Chem. 302, 611–616.
- Kim, S.-S., Kim, W.-S., Kim, G.-N., Park, H.-M., Park, U.-R., Moon, J.-K., 2013. Decontamination of uranium-contaminated concrete. J. Radioanal. Nucl. Chem. 298, 973–980.
- Kim, W.-S., Kim, S.-S., Kim, G.-N., Park, U.-R., Moon, J.-K., 2014c. Improved treatment technique for the reuse of waste solution generated from a electrokinetic decontamination system. J. Nucl. Fuel Cycle Waste Technol. 12, 1–6 (Korean).
- Koarashi, J., Nishimura, S., Atarashi-Andoh, M., Matsunaga, T., Sato, T., Nagao, S., 2018.
 Radiocesium distribution in aggregate-size fractions of cropland and forest soils affected by the Fukushima nuclear accident. Chemosphere 205, 147–155.
- Kornilovich, B., Mishchuk, N., Abbruzzese, K., Pshinko, G., LKlishchenko, R., 2005. Enhanced electrokinetic remediation of metals-contaminated clay. Colloids Surf. A Physicochem. Eng. Asp. 265, 114–123.
- Korolev, V.A., 2009. Electrokinetic removal of radionuclides, in electrochemical remediation technologies for polluted soils. In: Reddy, K.R., Cameselle, C. (Eds.), Sediments and Groundwater. John Wiley & Sons, Inc, pp. 127–139 ch. 5. (https://on linelibrary.wiley.com/doi/10.1002/9780470523650.ch5).
- Lacasa, E., Cotillas, S., Saez, C., Lobato, J., Canizares, P., Rodrigo, M.A., 2019. Environmental applications of electrochemical technology. What is needed to enable full-scale applications? Curr. Opin. Electrochem. 16, 149–156.
- Lageman, R., 2014. Demonstration Project for Seawater Purification Technologies. Lambda Consult, Netherlands.
- Lageman, R., 2014. Preliminary Assessment of the Application of an Electrokinetic Ring Fence for the Removal of Radionuclides from Groundwater at Fukushima Daiichi Nuclear Power Plant. Lambda Consult, Netherlands.
- Lamont-Black, J., Jones, C.J.F.P., White, C., 2015. Electrokinetic geosynthetic dewatering of nuclear contaminated waste. Geotext. Geomembr. 43, 359–362.
- Lee, G.T., Ro, H.M., Lee, S.M., 2007. Effects of triethyl phosphate and nitrate on electrokinetically enhanced biodegradation of diesel in low permeability soils. Environ. Technol. 28, 853–860.
- Lehto, J., Koivula, R., Leinonen, H., Tusa, E., Harjula, R., 2019. Removal of radionuclides from Fukushima Daiichi waste effluents. Sep. Purif. Rev. 48, 122–142.
- Leonard, K.S., McCubbin, D., Harvey, B.R., 1993. Chemical speciation and environmental behaviour of 60Co discharged from a nuclear establishment. J. Environ. Radioact. 20, 1–21.
- Leskinen, A., Salminen-Paatero, S., Gautier, C., Räty, A., Tanhua-Tyrkkö, M., Fichet, P., Kekki, T., Zhang, W., Bubendorff, J., Laporte, E., Lambrot, G., Brennetot, R., 2020. Intercomparison exercise on difficult to measure radionuclides in activated steel: statistical analysis of radioanalytical results and activation calculations. J. Radioanal. Nucl. Chem. 324, 1303–1316.
- Li, J., Zhang, J., Larson, S.L., Ballard, J.H., Guo, K., Arslan, Z., Ma, Y., Waggoner, C.A., White, J.R., Han, F.X., 2019a. Electrokinetic-enhanced phytoremediation of uranium-contaminated soil using sunflower and Indian mustard. Int. J. Phytoremed. 21, 1197–1204.
- Li, X., Bardos, P., Cundy, A.B., Harder, M.K., Doick, K.J., Norrman, J., Williams, S., Chen, W., 2019b. Using a conceptual site model for assessing the sustainability of brownfield regeneration for a soft reuse: a case study of Port Sunlight River Park (U. K.). Sci. Total Environ. 652, 810–821.
- Lima, A.T., Hofmann, A., Reynolds, D., Ptacek, C.J., Cappellen, P.V., Ottosen, L.M., Pamukcu, S., Alshawabekh, A., O'Carroll, D.M., Riis, C., Cox, E., Gent, D.B., Landis, R., Wang, J., Chowdhury, A.I.A., Secord, E.L., Sanchez-Hachair, A., 2017.

- Environmental electrokinetics for a sustainable subsurface. Chemosphere 181,
- Lin, C.C., 1996. Radiochemistry in Nuclear Power Reactors. National Research Council (NRC; USA), Pleasanton, California. Report NAS-NS-3119.
- López-Vizcaíno, R., Navarro, V., Léon, M.J., Risco, C., Rodrigo, M.A., Sáez, C., Canizares, P., 2016. Scale-up on electrokinetic remediation: engineering and technological parameters. J. Hazard. Mater. 315, 135–143.
- López-Vizcaíno, R., Risco, C., Isidro, J., Rodrigo, S., Saez, C., Cañizares, P., Navarro, V., Rodrigo, M.A., 2017. Scale-up of the electrokinetic fence technology for the removal of pesticides. Part II: Does size matter for removal of herbicides? Chemosphere 166, 549–555.
- Mao, X., Han, F.X., Shao, X., Guo, K., McComb, J., Arslan, Z., Zhang, Z., 2016. Electrokinetic remediation coupled with phytoremediation to remove lead, arsenic and cesium from contaminated paddy soil. Ecotoxicol. Environ. Saf. 125, 16–24.
- McKinley, J.P., Zeissler, C.J., Zachara, J.M., Serne, R.J., Lindstrom, R.M., Schaef, H.T., Orr, R.D., 2001. Distribution and retention of 137Cs in sediments at the Hanford Site, Washington. Environ. Sci. Technol. 35, 3433–3441.
- Miura, T., Kabir, M., Suzuki, M., Nakajima, S., Mori, S., 2015. Cesium removal from contaminated soil by electrokinetic process considering for slope areas of mountains. IEEJ Trans. Fundam. Mater. 135, 725–726 (translated from Japanese: Denki Gakkai Ronbunshi. A).
- Mobbs, S., Orr, P., Weber, I., 2019. Strategic considerations for the sustainable remediation of nuclear installations. J. Environ. Radioact. 196, 153–163.
- National Audit Office (NAO), 2012. Nuclear Decommissioning Authority: Managing Risk Reduction at Sellafield. National Audit Office (NAO), UK.
- National Audit Office (NAO), 2018. The Nuclear Decommissioning Authority: Progress with Reducing Risk at Sellafield. National Audit Office (NAO), UK.
- Nuclear Decommissioning Authority (NDA), 2015. Nuclear Provision Explaining the Cost of Cleaning up Britain's Nuclear Legacy. Nuclear Decommissioning Authority (NDA). UK.
- Nuclear Decommissioning Authority, Nuclear Provision: the cost of cleaning up Britain's historic nuclear sites, (https://www.gov.uk/government/publications/nuclear-provision-explaining-the-cost-of-cleaning-up-britains-nuclear-legacy/nuclear-provision-explaining-the-cost-of-cleaning-up-britains-nuclear-legacy), accessed 16 October 2020.
- Nuclear Energy Agency (NEA) of the Organisation for Economic Cooperation and Development (OECD), 2014. Nuclear Site Remediation and Restoration during Decommissioning of Nuclear Installations: A Report by the NEA Co-operative Programme on Decommissioning. Nuclear Energy Agency (NEA) of the Organisation for Economic Cooperation and Development (OECD). Report NEA No. 7192.
- O'Riordan, T., 1989. Best Practicable Environmental Option (BPEO): a case-study in partial bureaucratic adaptation. Environ. Conserv. 16, 113–122.
- Office for Nuclear Regulation (ONR), the Environment Agency, the Scottish Environment Protection Agency and Natural Resources Wales, 2015. Basic principles of radioactive waste management, Office for Nuclear Regulation (ONR), the Environment Agency, the Scottish Environment Protection Agency and Natural Resources Wales, UK.
- Office of Environmental Management, Department of Energy (DoE), 1999. In Situ Bioremediation for the Hanford Carbon Tetrachloride Plume. Office of Environmental Management, Department of Energy (DoE), US.
- Office of Environmental Management, Department of Energy (DoE), 2004. Optimization of Groundwater Pump and Treat Systems at Hanford. Office of Environmental Management, Department of Energy (DoE). Report No. 031102-027.
- Okumura, M., Kerisit, S., Bourg, I.C., Lammers, L.N., Ikeda, T., Rosso, K.M., Machida, M., 2018. Radiocesium interaction with clay minerals: theory and simulation advances Post–Fukushima. J. Environ. Radioact. 189, 135–145.
- Onwubuya, K., Cundy, A., Puschenreiter, M., Kumpiene, J., Bone, B., Greaves, J., Teasdale, P., Mench, M., Tlustos, P., Mikhalovsky, S., Waite, S., Friesl-Hanl, W., Marschner, B., Müller, I., 2009. Developing decision support tools for the selection of "gentle" remediation approaches. Sci. Total Environ. 407, 6132–6142.
- Park, U.-K., Kim, G.-N., Kim, S.-S., Moon, J.-K., 2015. Decontamination of uranium-contaminated gravel. J. Nucl. Fuel Cycle Waste Technol. 13, 35–43 (Korean).
- Parker, A.J., Joyce, M.J., Boxall, C., 2017. Remediation of 137Cs contaminated concrete using electrokinetic phenomena and ionic salt washes in nuclear energy contexts. J. Hazard. Mater. 340, 454–462.
- Parton, N., 2007. Remediation Technology Demonstrators: Availability of Version 1 of the Cost and Technology Models for Soil Washing, Permeable Reactive Barriers, Insitu Stabilisation and Electrokinetics. Nexia Solutions, UK. Report NDA 1648.4.
- Peretyazhko, T.S., Zachara, J.M., Kukkadapu, R.K., Heald, S.M., Kutnyakov, I.V., Resch, C.T., Arey, B.W., Wang, C.M., Kovarik, L., Phillips, J.L., Moore, D.A., 2012. Pertechnetate (TcO4—) reduction by reactive ferrous iron forms in naturally anoxic, redox transition zone sediments from the Hanford Site, USA. Geochim. Cosmochim. Acta 92, 48–66.
- Pham, T.D., Sillanpää, M., 2015. Electrokinetic remediation of organic contamination. Environ. Technol. Rev. 4, 103–117.
- Purkis, J.M., Tucknott, A., Croudace, I.W., Warwick, P.E., Cundy, A.B., 2021. Enhanced electrokinetic remediation of nuclear fission products in organic-rich soils. J. Appl. Geochem. 125, 104826 https://doi.org/10.1016/j.apgeochem.2020.104826.
- Putra, R.S., 2016. Development of electrokinetic remediation for caesium: a feasibility study of 2D electrode configuration system. IOP Conf. Ser. Mater. Sci. Eng. 107, 012015.
- Qafoku, N.P., Zachara, J.M., Liu, C., Gassman, P.L., Qafoku, O.S., Smith, S.C., 2005. Kinetic desorption and sorption of U(VI) during reactive transport in a contaminated Hanford sediment. Environ. Sci. Technol. 39, 3157–3165.
- UK Government, 1993. Radioactive Substances Act, UK Government.

- Rajic, L., Nazari, R., Fallahpour, N., Alshawabkeh, A.N., 2016. Electrochemical degradation of trichloroethylene in aqueous solution by bipolar graphite electrodes. J. Environ. Chem. Eng. 4, 197–202.
- Reddy, K.R., 2013. Electrokinetic remediation of soils at complex contaminated sites: technology status, challenges, and opportunities. In: Manassero, M., Dominijanni, A., Foti, S., Musso, G. (Eds.), Coupled Phenomena in Environmental Geotechnics. CRC Press, London, pp. 131–147.
- Reddy, K.R., Cameselle, C., 2009. Overview of electrochemical remediation technologies.
 In: Reddy, K.R., Cameselle, C. (Eds.), Electrochemical Remediation Technologies for Polluted Soils Sediments and Groundwater. John Wiley & Sons, Inc, pp. 1–28 ch. 1.
- Riis, C., Bymose, M., Cox, E., Wang, J., Gent, D., Terkelsen, M., 2012. Successful pilot test of electrokinetic enhanced bioremediation (EK-BIO) as an innovative remedial approach for PCE/DNAPL source area presented in part at the NORDROCS 2012: 4th Nordic Joint Meeting on Remediation of Contaminated Sites, Oslo, Norway.
- Rocha, I.M.V., Silva, K.N.O., Silva, D.R., Mártinez-Huitle, C.A., Santos, E.V., 2019. Coupling electrokinetic remediation with phytoremediation for depolluting soil with petroleum and the use of electrochemical technologies for treating the effluent generated. Sep. Purif. Technol. 208, 194–200.
- Saini, A., Bekele, D.N., Chadalavada, S., Fang, C., Naidu, R., 2020. A review of electrokinetically enhanced bioremediation technologies for PHs. J. Environ. Sci. 88, 31–45.
- Saleem, M., Chakrabarti, M.H., Irfan, M.F., Hajimolana, S.A., Hussain, M.A., Diya'uddeen, B.H., Daud, W.M.A.W., 2011. Electrokinetic remediation of nickel from low permeability soil. Int. J. Electrochem. Sci. 6, 4264–4275.
- Sellafield Ltd., 2016. Sellafield Groundwater Monitoring Annual Data Review 2016. Sellafield Ltd., UK.
- Sellafield Ltd., 2017. Context Plan (2017–2026): Explaining the Context of Sellafield's Operations. Sellafield Ltd., UK.
- Shahandeh, H., Hossner, L.R., 2002. Enhancement of uranium phytoaccumulation from contaminated soils. Soil Sci. 167, 269–280.
- Sheppard, S.C., Johnson, L.H., Goodwin, B.W., Tait, J.C., Wuschke, D.M., Davison, C.C., 1996. Chlorine-36 in nuclear waste disposal—1. Assessment results for used fuel with comparison to 129I and 14C. Waste Manag. 16, 607–614.
- Skeen, R.S., Roberson, K.R., Workman, D.J., Petersen, J.N., Shouche, M., 1992. In-situ bioremediation of Hanford groundwater presented in part at the 1992 Federal Environmental Restoration Conference, Vienna, Virgina, US.
- Smith, N.T., Shreeve, J., Kuras, O., 2020. Multi-sensor core logging (MSCL) and X-ray computed tomography imaging of borehole core to aid 3D geological modelling of poorly exposed unconsolidated superficial sediments underlying complex industrial sites: an example from Sellafield nuclear site, UK. J. Appl. Geophys. 178, 104084.
- Nuclear Energy Agency (NEA) of the Organisation for Cooperation and Development (OECD), 2016. Strategic Considerations for the Sustainable Remediation of Nuclear Installations. Nuclear Energy Agency (NEA) of the Organisation for Cooperation and Development (OECD). Report NEA No. 7290.
- Suer, P., Allard, B., 2003. Mercury transport and speciation during electrokinetic soil remediation. Water Air Soil Pollut. 143, 99–109.
- Suied, A.A., Tajudin, S.A.A., Zakaria, M.N., Madun, A., 2018. Potential electrokinetic remediation technologies of laboratory scale into field application- methodology overview. J. Phys. Conf. Ser. 995, 012083.
- Sunderland, J.G., 1987. Electrokinetic dewatering and thickening. I. Introduction and historical review of electrokinetic applications. J. Appl. Electrochem. 17, 889–898.
- Sustainable Remediation Forum (SuRF) and Contaminated Land: Application in Real Environments (CL:AIRE), 2011. Annex 1: The SuRF-UK Indicator Set for Sustainable Remediation Assessment. Sustainable Remediation Forum (SuRF) and Contaminated Land: Application in Real Environments (CL:AIRE), UK.
- Sustainable Remediation Forum (SuRF) and Contaminated Land: Application in Real Environments (CL:AIRE), 2020. Supplementary Report 1 of the SuRF-UK Framework: A General Approach to Sustainability Assessment for Use in Acheiving Sustainable Remediation, Sustainable Remediation Forum (SuRF) and Contaminated Land: Application in Real Environments (CL:AIRE), UK.
- Takeno, N., 2005. Atlas of Eh-pH Diagrams, Intercomparison of Thermodynamic Databases. National Institute of Advanced Industrial Science and Technology, Research Center for Deep Geological Environments. Geological Survey of Japan Open File Report No. 419.
- Tanaka, K., Watanabe, N., Yamasaki, S., Sakaguchi, A., Fan, Q., Takahashi, Y., 2018. Mineralogical control of the size distribution of stable Cs and radiocesium in riverbed sediments. Geochem. J. 52, 173–185.
- Tanaka, K., Takahashi, Y., Sakaguchi, A.Y.A., Umeo, M., Hayakawa, S., Tanida, H., Saito, T., Kanai, Y., 2012. Vertical profiles of Iodine-131 and Cesium-137 in soils in Fukushima Prefecture related to the Fukushima Daiichi Nuclear Power Station Accident. Geochem. J. 46, 73–76.
- Tanaka, S., 2018. Gypsum precipitation enhanced by electrokinetic method and porewater chemistry in compacted montmorillonite. Appl. Clay Sci. 161, 482–493.
- Tasutaka, T., Naito, W., 2016. Assessing cost and effectiveness of radiation decontamination in Fukushima Prefecture, Japan. J. Environ. Radioact. 151, 512–520.
- TÜV SÜD Nuclear Technologies Division and Office of Nuclear Regulation (ONR), 2020. Remediation Technologies for Radioactive Contaminated Land on Nuclear Licensed Sites, Report NT/7225002059/R2043, TÜV SÜD – Nuclear Technologies Division and Office of Nuclear Regulation (ONR), UK.
- US Environmental Protection Agency (EPA), 1996. Technology Screening Tools for Radioactively Contaminated Sites. US Environmental Protection Agency (EPA). Report EPA 402-R-96-017.
- US Environmental Protection Agency (EPA), 2007. Technology Reference Guide for Radioactively Contaminated Media. US Environmental Protection Agency (EPA). Report EPA 402-R-07-004.

- Valdovinos, V., Monroy-Guzmán, F., Bustos, E., 2016. Electrokinetic removal of radionuclides contained in scintillation liquids absorbed in soil type Phaeozem. J. Environ. Radioact. 162–163, 80–86.
- Vermeul, V.R., Szecsody, J.E., Fritz, B.G., Williams, M.D., Moore, R.C., Fruchter, J.S., 2014. An injectable apatite permeable reactive barrier for in situ 90Sr immobilization. Groundw. Monit. Remed. 34, 28–41.
- Warwick, P.E., Croudace, I.W., 2017. Rapid on-site radionuclide screening of aqueous waste streams using dip-stick technologies and liquid scintillation counting. J. Radioanal. Nucl. Chem. 314, 761–766.
- Wong, C., Pedrotti, M., Mountassir, G. El, Lunn, R.J., 2018. A study on the mechanical interaction between soil and colloidal silica gel for ground improvement. Eng. Geol. 243, 84, 100
- World Health Organisation (WHO), 2011. Guidlines for Drinking-Water Quality, Fourth Edition. World Health Organisation (WHO).
- Wu, M.Z., Reynolds, D.A., Fourie, A., Thomas, D., Prommer, H., 2010. Field Implementation of Electrokinetic-ISCO Remediation presented in part at the 2010 Fall Meeting of the American Geophysical Union, San Francisco, California, US.

- Wuana, R.A., Okieimen, F.E., 2011. Heavy metals in contaminated soils: a review of sources, chemistry, risks and best available strategies for remediation. ISRN Ecol. 2011, 1–20.
- Xu, H., Song, Y., Cang, L., Zhou, D., 2020. Ion exchange membranes enhance the electrokinetic in situ chemical oxidation of PAH-contaminated soil. J. Hazard. Mater. 382, 121042.
- Yang, G.C.C., 2019. Integrated electrokinetic processes for the remediation of phthalate esters in river sediments: a mini-review. Sci. Total Environ. 659, 963–972.
- Yeung, A.T., 2011. Milestone developments, myths, and future directions of electrokinetic remediation. Sep. Purif. Technol. 79, 124–132.
- Yeung, A.T., Gu, Y.-Y., 2011. A review on techniques to enhance electrochemical remediation of contaminated soils. J. Hazard. Mater. 195, 11–29.
- Yurchenko, A.Y., Karlin, Y.V., Nikolaev, A.N., Karlina, O.K., Barinov, A.S., 2009. Decontamination of radioactive concrete. Energy 106, 225–230.

Appendix E

Current and emerging technologies for the remediation of difficult-to-measure radionuclides at nuclear sites

Shaun D. Hemming, Jamie M. Purkis, Phillip E. Warwick, and Andrew B. Cundy

Published in: Environmental Science: Processes & Impacts 25, 1909 (2023)

Environmental Science Processes & Impacts



CRITICAL REVIEW

View Article Online
View Journal | View Issue



Cite this: Environ. Sci.: Processes Impacts, 2023, 25, 1909

Current and emerging technologies for the remediation of difficult-to-measure radionuclides at nuclear sites

Shaun D. Hemming, * Jamie M. Purkis, Phillip E. Warwick and Andrew B. Cundy * *

Difficult-to-measure radionuclides (DTMRs), defined by an absence of high energy gamma emissions during decay, are problematic in groundwaters at nuclear sites. DTMRs are common contaminants at many nuclear facilities, with (often) long half-lives and high radiotoxicities within the human body. Effective remediation is, therefore, essential if nuclear site end-state targets are to be met. However, due to a lack of techniques for in situ DTMR detection, technologies designed to remediate these nuclides are underdeveloped and tend to be environmentally invasive. With a growing agenda for sustainable remediation and reduction in nuclear decommissioning costs, there is renewed international focus on the development of less invasive technologies for DTMR clean-up. Here, we review recent developments for remediation of selected problem DTMRs (129), 99Tc, 90Sr and 3H), with a focus on industrial and sitescale applications. We find that pump and treat (P&T) is the most used technique despite efficacy issues for ¹²⁹I and ³H. Permeable reactive barriers (PRBs) are a less invasive alternative but have only been demonstrated for removal of 99Tc and 90Sr at scale. Phytoremediation shows promise for site-scale removal of ³H but is unsuitable for ¹²⁹I and ⁹⁹Tc due to biotoxicity and bioavailability hazards, respectively. No single technique can remediate all DTMRs of focus. Likewise, there has been no successful site-applied technology with high removal efficiencies for iodine species typically present in groundwaters (iodide/ I^- , iodate/ IO_3^- and organoiodine). Further work is needed to adapt and improve current techniques to field scales, as well as further research into targeted application of emerging technologies.

Received 5th May 2023 Accepted 16th October 2023

DOI: 10.1039/d3em00190c

rsc.li/espi

Environmental significance

The presence of difficult-to-measure radionuclides (DTMRs) in groundwaters at nuclear sites poses significant threats to ecosystems and human health due to their long half-lives and high radiotoxicities. Addressing this remedial challenge is vital for achieving nuclear site end-state targets and minimizing environmental impacts. Our study critically evaluates current and emerging technologies for DTMR remediation, revealing that no single technique is universally effective for all DTMRs of focus, and highlights areas for further research. This work contributes to the broader understanding of DTMR remediation in the context of sustainable environmental management, emphasising the need for continued development of less invasive and more efficient remediation technologies to protect ecosystems and public health.

1 Introduction

Groundwater contamination at nuclear sites is extensive, containing many types of organic, inorganic and radioactive contaminants e.g. Hanford Site (Washington, USA)¹ and Sellafield (Cumbria, UK).² Some of these radioactive contaminants (e.g. ¹³⁷Cs and ⁶⁰Co) emit high-energy gamma radiation during decay, making them detectable and quantfiable remotely using in situ gamma spectrometry.³ However, several isotopes found in groundwaters and soils emit alpha, beta or low-energy

gamma radiation, making them challenging to identify using conventional, non-intrusive methods.⁴ Complex laboratory analysis is needed for detailed measurements of these Difficult to Measure Radionuclides (DTMRs), which include ^{241,240,239}Pu, ¹²⁹I, ⁹⁹Tc, ⁹⁰Sr, ¹⁴C, and ³H. Further, DTMRs have varying mobilities in groundwater, making their site distributions difficult to characterise. Development of targeted remediation and risk management strategies is consequently hindered, potentially reducing their efficacy. The range of mobilities also limits the application of scaling factors, a commonly used technique at nuclear facilities that involves measuring the ratio of an easy-to-measure radionuclide to a DTMR in a material, *e.g.* ratio of ¹³⁷Cs: ⁹⁰Sr in a spent nuclear fuel container, and applies it to any on-site instance where that material is present, *e.g.*

GAU-Radioanalytical, School of Ocean and Earth Science, University of Southampton, National Oceanography Centre (Southampton), European Way, Southampton, SO14 3ZH, UK. E-mail: S.D.Hemming@soton.ac.uk; A.Cundy@soton.ac.uk spent nuclear fuel leak in the subsurface.⁴ If, in this example, ⁹⁰Sr migrates through groundwater slower than ¹³⁷Cs, the two radionuclides will eventually form separated plumes in different areas of the site. When the leak is discovered, it will be assumed that the ⁹⁰Sr is present with the ¹³⁷Cs in the ratio previously ascertained. This means that the true ⁹⁰Sr plume extent may remain undetected, whilst facility time and money is spent remediating the ¹³⁷Cs plume for ⁹⁰Sr despite its reduced activity in this area of the subsurface.

DTMRs are abundant at many nuclear sites worldwide. For example, at the Hanford Site, the most contaminated nuclear facility in the United States, 5 129 I, 99 Tc and 3 H plumes covered 58 km², 2 km² and 58 km² of land area, respectively, in 2021.6 The plume boundaries were defined by concentrations in excess of 0.037 Bq L^{-1} (1 pCi L⁻¹) of ^{129}I , 33.3 Bq L⁻¹ (900 pCi L⁻¹) of ^{99}Tc and 740.0 Bq L⁻¹ (20 000 pCi L⁻¹) of ³H, which are upper limits of the drinking water standard set by the U.S. Environmental Protection Agency (USEPA).7 Similarly, in 2016, Sellafield borehole monitoring detected up to 164 000 Bq L⁻¹ of ³H, over 16 times greater than the World Health Organisation (WHO) drinking water limits.² The same borehole continued to exceed the drinking water limits in 2021, although the exact activity was not stated.8 Many DTMRs are long-lived and will remain a significant problem over human (and site operation and decommissioning) lifetimes, making effective remediation at nuclear sites a necessity for the protection of local populations and for eventual, successful, release of this land to public use following decommissioning.

Although all forms of land remediation were once considered beneficial (or their costs considered acceptable), it is now recognised that remediation technologies require careful planning and management to avoid excessive negative impacts on the environment.9 The Sustainable Remediation Forum UK (SuRF-UK) define sustainable remediation as "the practice of demonstrating, in terms of environmental, economic and social indicators, that the benefit of undertaking remediation is greater than its impact and that the optimum remediation solution is selected through the use of a balanced decisionmaking process". 10 International guidelines have produced to encourage standard practices in sustainable remediation e.g. the American Society for Testing and Materials (ASTM) Standard Guide for Greener Cleanups¹¹ for Standardization the International Organization (ISO) Soil Quality - Sustainable Remediation procedures, 12 incorporating a wider socio-economic outlook alongside assessment of a technology's feasibility implementation at a particular site. Sustainable approaches to remediation are also being introduced to nuclear decommissioning documentation e.g. Section 8.2 of the Nuclear Decommissioning Authority Strategy 2021,13 encouraging standard practices at a number of sites. Responsible clean-up in the nuclear sector is especially important, owing to the hazardous nature of materials held on-site, making sustainable remedia-tion an important area for development.

Several reviews have been published on nuclear site remediation, including those by Hossain, ¹⁴ Alby et al., ¹⁵ Sharma et al. ¹⁶ and the International Atomic Energy Agency (IAEA), ¹⁷ with the development of more sustainable techniques in recent years well-documented. However, DTMR-specific work focuses

mostly on laboratory analyses e.g. IAEA4 and Thierfeldt and Deckert¹⁸ rather than in situ detection and removal, and consequently there are no comprehensive reviews on remediation for these nuclides. Technologies and applications focussing on in situ DTMR removal from groundwater remain underdeveloped compared to radionuclides that are easier to detect. This knowledge gap hinders the ability of assessors to fully remediate a site effectively, as numerous groundwater and soil samples must be obtained and tested. This is a slow, expensive, and labour-intensive process, as laboratory analysis increases the time taken for DTMR data to be collated and acted upon, slowing the implementation of immediate measures such as locating and isolating radionuclide leaks. Greater subsurface sampling also increases the risk to site operators, as working in close proximity to radionuclides for prolonged periods may expose workers to substantial dose.

Today, many nuclear sites are nearing or have reached the end of their operational lifetimes,19 and require decommissioning in order to achieve end-state land quality targets. At a number of these facilities, DTMRs comprise large proportions of the remaining radionuclides (examples given above), making effective, low-cost clean-up technologies vitally important for achieving remediation targets. Here, we review both conventional and sustainable remediation techniques at site-scale for four DTMRs that are highly mobile in groundwaters and compare advantages and disadvantages for each technology. Techniques such as subsurface walls (for example, as applied at the Fukushima Daiichi Nuclear Power Plant to limit off-site ³H transport²⁰) have been excluded from this review as they do not actively remediate groundwater, but instead channel plumes to allow further radioactive decay to occur before off-site migration can happen. We aim to highlight knowledge gaps in DTMR remediation and inform future work by addressing key issues that remain in the management of these radionuclides and their risk. The reviewed DTMRs are ¹²⁹I, ⁹⁹Tc, ⁹⁰Sr and ³H. These radionuclides have been selected as they either emit gamma radiation of <100 keV or do not produce gamma emissions during decay.21 In addition, 129I and 99Tc both have high abundances in nuclear wastes^{22–24} and long half-lives of 15.7 × 10^6 years and 2.11×10^5 years, respectively. As a result, hazard mitigation through natural attenuation is not feasible over human lifetimes, making effective nuclide remediation the only option for achieving nuclear site end-state targets. In comparison, 90Sr and 3H have much shorter half-lives and are likely to only present issues over decadal to century timescales but are included here due to their presence in large quantities at a number of nuclear facilities internationally. High abundances in wastes are especially pertinent for ³H and make development in its remediation globally important; frequent progression reviews can enhance the growth and implementation of new technologies to combat this problem.

2 DTMRs in the environment

2.1 Interaction between soils and groundwater

The movement of nuclides in the environment can vary depending on the conditions and materials present. The degree

of ion mobility can be described using the partition coefficient $(K_d; eqn\ (1))$, which shows the ability of an ion to adsorb onto a given medium, rather than remaining in solution. $K_d\ (mL\ g^{-1})$ is defined as:

$$K_{\rm d} = {{\rm radionuclide~on~adsorbent~at~equilibrium~(mg~g^{-1})}\over{{\rm radionuclide~in~solution~at~equilibrium~(mg~mL^{-1})}}~(1)$$

A K_d of <1 mL g^{-1} shows that negligible adsorption is occurring and the radionuclides are remaining in solution, whilst high K_d values (e.g. $1000 \ \text{mL} \ g^{-1}$ or greater) indicate a high level of contaminant sorption.

While the K_d test approach can provide a simple method for demonstrating the proportion of an ion in groundwater and soil, the approach has drawbacks. It is highly dependent on the starting concentrations of radionuclide, as a greater abundance of the contaminant will likely bind to the adsorption sites more quickly and result in the adsorbent reaching capacity in smaller volume of solution. The method is also influenced by various factors of environmental aqueous geochemistry (e.g. the preferential uptake of competing ions onto adsorption sites, pH. redox potential etc.),25 and groups additional attenuation processes, such as precipitation and diffusion into pores, into a single 'sorption' term.26 The Kd test method also assumes that adsorption is instantaneous and fully reversible which may not be true under real-world conditions. 25 Despite the limitations, K_d test methods provide an intuitive method for comparing the extent of elemental partitioning between two media and are consequently popular in sorption-based literature (and are therefore utilised in this review).

2.2 DTMRs of focus

2.2.1 Iodine. ¹²⁹I is a fission product of ²³⁵U (0.71% yield) with a half-life of 1.57 × 10⁷ years.²¹ Significant groundwater contamination from 129I exists at the Hanford Site and Savannah River Site (SRS) nuclear facilities in the USA,6,27 although the isotope is also found in smaller concentrations at other facilities, such as Sellafield.2 The dominant forms of iodine in the environment are iodate (IO₃ ⁻) and iodide (I⁻).²⁸ Laboratory studies have shown that reactions between iodine and organic material in soils and groundwater (e.g. humic and fulvic acids^{29,30}) lead to the formation of organoiodine (org-I) compounds, which can increase or decrease the environmental mobility of iodine depending on the products created.31 IO₃ [−], Γ and org-I compounds can co-exist in groundwaters, further complicating the behaviour and mobility of iodine in these environments.²⁷ Typical Hanford sediments of quartzand feldspar-rich sands have a low I sorption, with K_ds of 0-8.1 mL g⁻¹ and 0.8–7.6 mL g⁻¹ for I⁻ and IO₃⁻, respectively.^{32–34} Quartz-rich surface aquifer sediments from SRS also have low I K_{ds} , ranging from 0.06 to 8.8 in starting solutions of 10^{-2} to 10^{3} mM I . 31 These high mobilities in groundwater are a result of IO₃ and I existing as anions, which are repelled by the negative surface charges of material in soils at typical environmental pHs.35 Laboratory experiments have shown that IO3 can have K_ds up to 90 times greater than I when mineral

phases such as iron oxides are present in soils. 36,37 However, the aforementioned nuclear sites generally have low abundances of these in the subsurface, as reflected by the low iron content in experimental samples e.g. SRS³¹ and Hanford. 34 Further, Γ K_ds remain almost unaffected in comparison to Hanford and SRS values, suggesting that iodine migration in groundwater would still be a concern at nuclear sites with higher iron oxide concentrations within the subsurface where Γ is the dominant form of I present.

2.2.2 Technetium. ⁹⁹Tc is a high-yield fission product of 235 U (6.13%), with a half-life of 2.11 \times 10 5 years. 21,22 In oxidising conditions, Tc(vII) is the dominant species in the form of per-technetate, TcO $_4$, whereas reducing conditions produce Tc(IV) and primarily form TcO $_2$.nH $_2$ O, 38 where n can range between 0.44 and 4.22. 39 Tc(vII) has a high solubility and, hence, high mobility in water, with an approximate K_d of 0–1 mL g^{-1} , 22,32,40 but Tc(IV) is only sparingly soluble e.g. K_d s of 15–280 mL g^{-1} have been estimated for sediment at Forsmark and Laxemar-Simpevarp sites in Sweden. 41

2.2.3 Strontium. ⁹⁰Sr is another high-yield ²³⁵U fission product (5.73%) with a 28.91 year half-life. ²¹The chemistry of Sr is similar to that of Ca, ⁴² with Sr often existing in aqueous environments as a divalent ion that is either hydrated or bound to small organic compounds. ⁴³ Sr(II) has been found to have K_d s of 10–25 mL g^{-1} in quartz-rich Hanford sediment. ⁴⁴ However, mobility can be reduced through sorption onto fulvic and humic acids ⁴⁵ and clays, resulting in much higher K_d s e.g. $\sim 10^3$ estimated for the subsurface at Sellafield. ⁴⁶

2.2.4 Tritium. ³H is an activation product with a half-life of 12.32 years.21 It results from collisions between neutrons and stable ²H nuclei found within reactor materials, such as control rods and water coolant.24 These materials are commonplace at nuclear facilities, and so ³H remobilisation and leakage during storage is a risk for sites globally.⁴⁷ ³H is also generated through ternary fission, or through neutron interaction with boric acid dissolved in the coolant/moderator of pressurised water reactors. ³H exists as tritiated groundwater at nuclear sites, ^{2,48} resulting from isotopic exchange between ³H and ¹H₂O already present in groundwater.40 As a result, the Kd for 3H is considered to be 0 mL g⁻¹, although slight sorption in sandy soils (K_d range of 0.04–1 mL g⁻¹) has been previously reported.⁴⁹ In some circumstances, where organically-bound tritium (OBT) is the dominant form of ³H present (e.g. in discharges from radiopharmaceutical facilities), greater retention of ³H on solid phase materials may be observed.50

Key characteristics of each of the above DTMRs are given in Table 1. All of ¹²⁹I, ⁹⁹Tc, ⁹⁰Sr and ³H emit beta particles, ²¹ which can result in health issues for humans if significant quantities build in the body through ingestion or inhalation. For example, thyroid cancers can be caused by both ¹²⁹I⁵¹ and ⁹⁹Tc⁵² exposure, and skeletal abnormalities can develop as a result of ⁹⁰Sr incorporation into bones.⁵³ Whilst ³H does not accumulate in specific parts of the body, the 10 day and 40 day biological half-lives of tritiated water and OBT, respectively, make the radio-nuclide a potential hazard once inside humans.⁵⁴ Defining the specific risk that DTMRs pose can be complex due to a number of variables, including the exposure pathway to an individual

Table 1 Summary of the radionuclides of focus

	^{129}I	⁹⁹ Tc	⁹⁰ Sr	³ H
Half-life (years) ²¹	15.7 million	211 100	28.91	12.32
Gamma decay energy (keV) [absolute intensity (%)] ²¹	39.6 [7.51]	$89.5 \left[6.5 \times 10^{-4}\right]$	No gamma emitted	No gamma emitted
Oxidation state(s) in groundwater [speciation]	$+5 \left[IO_3^{-} \right]^{28}$	+7 [TcO ₄ ⁻] ²²	+2 [Sr(II)] ⁴³	$0 [^{3}H^{1}HO]^{2}$
	$-1 [I^{-}]^{28}$	+4 [typically TcO ₂] ³⁸		$0 [^{3}H_{2}O]^{2}$
Typical K_{ds} (mL g ⁻¹)	0.8-7.6 [IO ₃ ⁻] ³³	0-1 [Tc(vII)] ³²	10–25 [quartz-rich] ⁴⁴	0–1 [all sediment] ⁴⁹
	$0-8.1 [I^-]^{32,33}$	15–280 [Tc(IV)] ⁴¹	$\sim \! 10^3 [{ m clays}]^{46}$	

(inhalation, ingestion, skin contact, etc.), the body part(s) that come into contact with radiation, the age of the person (chil-dren and the elderly may potentially be more affected compared to adults), etc. 55 This has led to differences in the dose limits and risk management guidelines given by regulatory bodies at both national and international levels. Many countries regulate radiation exposure based on IAEA recommendations and WHO guidelines, although the USA is a notable exception to this with the Environmental Protection Agency (EPA), Department of Energy (DOE) and Nuclear Regulatory Commission (NRC) overseeing public and nuclear site worker protection. The limits and recommendations set by these organisations provide clarity on the end-state targets for remediation projects and can also determine the suitability of a particular technology for the cleanup or risk schemes implemented.

3 Current treatment methods

3.1 Pump and treat

Pump and treat (P&T) is the most commonly applied method for ex situ groundwater clean-up at nuclear sites. 56,57 The technique works by pumping groundwater from the subsurface and treating it through adsorption, ion-exchange or chemical (e.g. redox) processes (Fig. 1). Decontaminated water can then be discharged at the surface or pumped back into the ground.⁵⁸ The present-day appeal of the technique for site remediators is its proven track record of generally remediating facilities to a desired level.⁵⁹ P&T can be very effective at removing groundwater-mobile elements (e.g. Cr(vI)60) but is less effective for elements that strongly sorb to sediments (e.g. Pu and Am⁶¹). Subsurface permeability can also affect remedial efficiencies, with finer-grained media requiring longer time periods to reach the same clean-up goals as coarser sediment. 62 This can further complicate remediation in substrates with dual porosities (caused either through materials with differing permeabilities or as a result of a variation between matrix and fracture porosities). The technology also incurs large financial costs during both the initial setup and operation and maintenance phases, making only long-term projects economically viable.

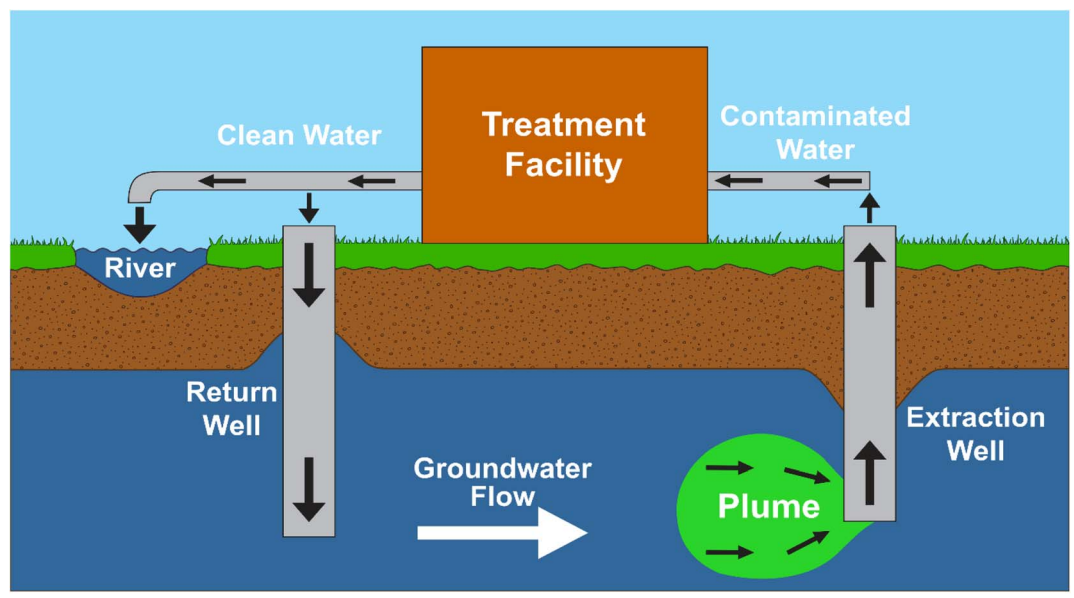
Adsorption is performed by pumping extracted groundwater through a column filled with one or more adsorbent materials such as clay minerals, activated carbon, iron oxides and metalorganic frameworks.^{63,64}

Radionuclides bind to the surface of the adsorbents, whilst groundwater passes through the column. Ion exchange is a similar process, but the adsorbent contains a non-toxic ion, such as Cl⁻, ⁶⁵ that counter-balances the charge of the adsorption sites. ⁶⁶ If the radionuclide has a greater electrochemical potential than the starting ion, the two are exchanged and the radionuclide is retained on the adsorbent.

Site-scale iodine remediation through P&T has not been effectively implemented at nuclear facilities, despite ^{129}I plumes being present at sites such as Hanford and SRS. Laboratory trials of various materials including Purolite A530E ion exchange resin and granular activated carbon (GAC) were performed at Hanford, with $K_{\rm d}s$ of 78 and 76 mg L^{-1} observed, respectively (in simulated Hanford groundwater containing 1.0 mg $L^{-1}\,IO_3^{-}$). 67,68 However, none of the tested adsorbents will be efficient enough to decrease the activity below 0.037 Bq $L^{-1}\,(1$ pCi L^{-1} ; 6 mg L^{-1}) – the USEPA drinking water standard 67

− before the area's active remediation period ceases in 2047. ⁶⁹ The poor ¹²⁹I uptakes were generally caused by the adsorbents' preference for Γ over IO_3 , whilst on-site groundwater conditions favour IO_3 speciation over Γ (77.5% of stable iodine at the site exists as IO_3 , 19.6% as Γ and 2.6% as org-I). ⁶⁷ Due to being only a small percentage of total ¹²⁹I speciation ⁶⁷ and having a variety of potential properties depending the organic molecules present, ⁷⁰ laboratory studies do not focus of determining K_d s for org-I for Hanford. As a result of the poor adsorbent uptake capacities, as well as alternative remedial technologies also being ineffective, there is no current strategy for long-term ¹²⁹I clean-up of the Hanford site. ⁷¹ A Technical Impracticability waiver has therefore been drafted for the USEPA. ⁷²

Adsorption of technetium, in combination with other contaminants, onto Purolite A532E and DOWEX 21K ion exchange resins is being utilised at the Hanford Site. 73,74 Groundwater P&T influent streams are pumped into the facility where they are passed through a train of DOWEX columns followed by A532E columns, before being released back into the subsurface. 73,75 DOWEX was first installed into the P&T system in 2015 and is used primarily for U adsorption.75 As a result, despite laboratory K_ds measuring 1800-19 800 mg L⁻¹ in double deionised water (DDI) containing NO3 - (90-99% uptake to resin; 0–104 mM NO₃⁻; all with 200 ppb 99 Tc) and >19 800 mL g^{-1} in DDI containing SO_4^{2-} (>99% uptake; 0–10 mM SO_4^{2-} ; all with 200 ppb 99Tc),74 resin used in the Hanford P&T columns between 2015 and 2017 showed no Tc adsorption.75 By contrast, Purolite A532E has been chosen for targeted ⁹⁹Tc uptake, and is the successor to the A530E resin, a microporous form of the A532E⁷³ which had a 92.1% ⁹⁹Tc removal efficiency in the Hanford P&T facility in 2020.76 No information on A532E Tc





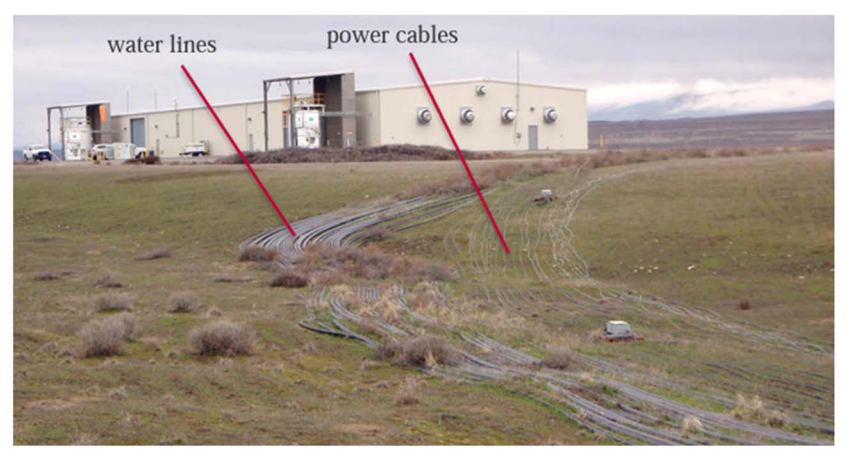


Fig. 1 Top – Diagram illustrating the P&T process. The plume of contaminated groundwater (green) is extracted and treated, before being either pumped back into the subsurface or released as surface waters. Middle – Photo from Mackley *et al.*⁵⁸ showing a typical P&T extraction well at Hanford, with monitoring equipment attached. Bottom – Photo from Mackley *et al.*⁵⁸ showing water pipes and power cables running between a Hanford P&T facility and monitoring wells.

uptakes in the same P&T system could be found, although Saslow and coworkers have recorded $K_{\rm d}s$ of >19 800 mL g^{-1} (>99% resin uptake) in double deionised water containing 200 ppb $^{99}{\rm Tc.}^{73}$ This figure remained constant with NO₃ $^-$ and

 ${
m SO_4}^{2-}$ present at concentrations up to 20 mM and 10 mM, respectively, exceeding the levels seen in P&T influent streams (1.61 and 0.60 mM for ${
m NO_3}^-$ and ${
m SO_4}^{2-}$, respectively) between 1st June 2021 and 30th May 2022 (data cited in ref. 73). Whilst this

high degree of ⁹⁹Tc selectivity shows promise for A532E's application at site scales, there is a need for larger pilot trials to support results of simplified laboratory set ups. As the P&T system continues to operate at Hanford, future work by Saslow and coworkers will look at the performance of both A532E and DOWEX 21K with flowing groundwater, and scale up models to predict the efficacy with varying P&T influent chemistry.

P&T remediation was also attempted for the removal of ⁹⁰Sr plumes from the Brookhaven Graphite Research Reactor (BGRR), former Pile Fan Sump (PFS) and the Waste Concentration Facility (WCF) areas at Brookhaven National Laborato-

ries (BNL) in 2005. 77 Although Sr Kds in the sediment were high enough to indicate that plume migration off site was unlikely, the project was initiated to avoid public concerns over a managed natural attenuation approach.⁷⁸ Maximum pretreatment 90Sr activities for the BGRR, PFS and WCF plumes were 116.6 Bq L⁻¹ (3150 pCi L⁻¹; recorded in 2003), 20.9 Bq L⁻¹ $(566 \text{ pCi L}^{-1}; \text{ recorded in 1997}) \text{ and } 57.7 \text{ Bq L}^{-1} (1560 \text{ pCi L}^{-1};$ recorded in 2003), respectively.⁷⁷ By the end of 2021, borehole activities had decreased to 0.47 Bq L⁻¹ (12.7 pCi L⁻¹), 0.88 Bq L $^{-1}$ (23.9 pCi L⁻¹) and 1.93 Bq L⁻¹ (52.2 pCi L⁻¹) in the BGRR, PFS and WCF - reductions of 99.5%, 96% and 97%, respectively.79 The ion exchange resin used, and its respective K_d, have not been disclosed publicly by the site. Plume remediation efforts were assisted by the low mobility of Sr in the sediment, allowing the most contaminated subsurface areas to be easily identified and targeted. However, between 2003 and 2021 the plumes split into multiple smaller entities, possibly as a result of remediation efforts targeting and removing the highestactivity zones which are typically in the middle of plumes, making the residual contamination difficult to track. Further, plumes had migrated underneath buildings which complicated monitoring. As a result, 90Sr activities are anticipated to be higher in certain areas where monitoring wells are not currently set up, although the areal extent of these high-activity regions are thought to have decreased significantly compared to 2004 plume boundaries.⁷⁹ The remediation project aims to reduce ⁹⁰Sr activities to below the 0.3 Bq L⁻¹ (8 pCi L⁻¹) drinking water standard by 2070.

P&T is ineffective for ³H remediation as the radionuclide can be exchanged with protons in water.^{2,48} Adsorbents and ion exchange resins cannot distinguish between ¹H₂O, ³H₂O and ³H¹HO, rendering P&T unsuitable for ³H clean-up projects. Despite this, sites such as SRS and Brookhaven have previously attempted to pump tritiated water up-gradient of a plume and keep it in a continuous loop until radioactive decay reduces the activities to acceptable levels.⁸⁰ However, the SRS system was costing \$1 000 000 per month to maintain and, in the process, was potentially mobilising more contamination.⁸⁰ The operations were ceased after 6 years, with approximately \$50 million having been spent on setup and \$100 million on maintenance over their lifetimes.

3.2 Permeable reactive barriers

Permeable Reactive Barriers (PRBs) are a relatively inexpensive, passive and in situ remediation method for groundwater. They

consist of a reactive medium that is placed into the subsurface, perpendicular to the direction of groundwater flow (Fig. 2).^{81,82} The reactive medium converts contaminants into an immobile or less harmful form, whilst allowing groundwater to pass through the barrier.^{81,83}

Records of iodine remediation through PRBs at nuclear sites could not be found. This is surprising considering substances such as organic material may appear as good candidates for a low-cost reactive medium. Covalent bonding and complexation of I onto organic material such as humic acid has been observed at bench scale^{84,85} and in field observations at facilities such as Hanford⁸⁶ and SRS.⁵ However, the lack of application is likely due to a poor understanding of interactions between iodine and natural organic matter87 in addition to its susceptibility to redox reactions within organic compounds, caused by microorganisms and materials within the subsurface.88 Benchscale experiments performed on organic-rich SRS soil have shown conversion of inorganic I into particulates, colloids and dissolved org-I after a 31 day equilibration period.89 This is thought to be caused by the oxidising and reducing capacity for I and IO_3^- in the soil, creating reactive intermediates such as I_2 and HOI during the conversion between the iodine +5 and -1 species. These intermediates may subsequently react with organic material before they can be converted back to I and IO₃ -. Due to the variety of water solubilities that organic molecules can have, long-term iodine immobilization could be compromised depending on the organic material present, making it an unsuitable adsorbent.

⁹⁹Tc is amenable to PRB remediation via reduction due to the variation in solubility between Tc(VII) (as TcO₄; soluble in water) and Tc(IV) (as TcO₂; solid).³⁸ When Tc(VII) in groundwater comes into contact with a suitable reactive barrier, it may be reduced to Tc(IV) which facilitates precipitation, immobilising the Tc and limiting its environmental spread. 90 Examples of suitable reactive barrier materials include zero-valent iron (ZVI), a cheap, frequently used medium in PRBs. 91 Laboratory experiments on ZVI obtained a K_d of 2700 mL g⁻¹ for ⁹⁹Tc at an initial concentration of 38.2 Bq L⁻¹ (1031 pCi L⁻¹).⁹² ZVI adsorbents have been deployed at scale, for example, in two PRBs at the Oak Ridge Site, Tennessee, 1997, to chemically reduce and immobilise Tc.93 In this study the radionuclide was found within the Bear Creek Valley and Upper East Fork Poplar Creek watersheds, both comprising of Maynardville Limestone. 94 The first PRB, referred to here as 'PRB 1' (for configuration see Fig. 2a), was a 68 m long × 6-9 m deep section comprising of 80 tonnes of ZVI, and the second, 'PRB 2' (for configuration see Fig. 2b), was a 67 m long × 8 m deep trench containing 1500 L of ZVI and peat moss.⁹³ Monthly testing over a 3 year period established that the two PRBs reduced Tc levels in groundwater, although final concentrations were not publicly reported. However, precipitation of iron-based minerals decreased permeability in both barriers, reducing the lifespan of PRB 1 to between 15 and 30 years, whilst causing PRB 2 to completely cease operations within an unspecified time period.

A typical setup for a PRB requires infrastructure to contain the reactive medium, with optional features such concrete walls (Fig. 2b) that channel water flow to be added at the site

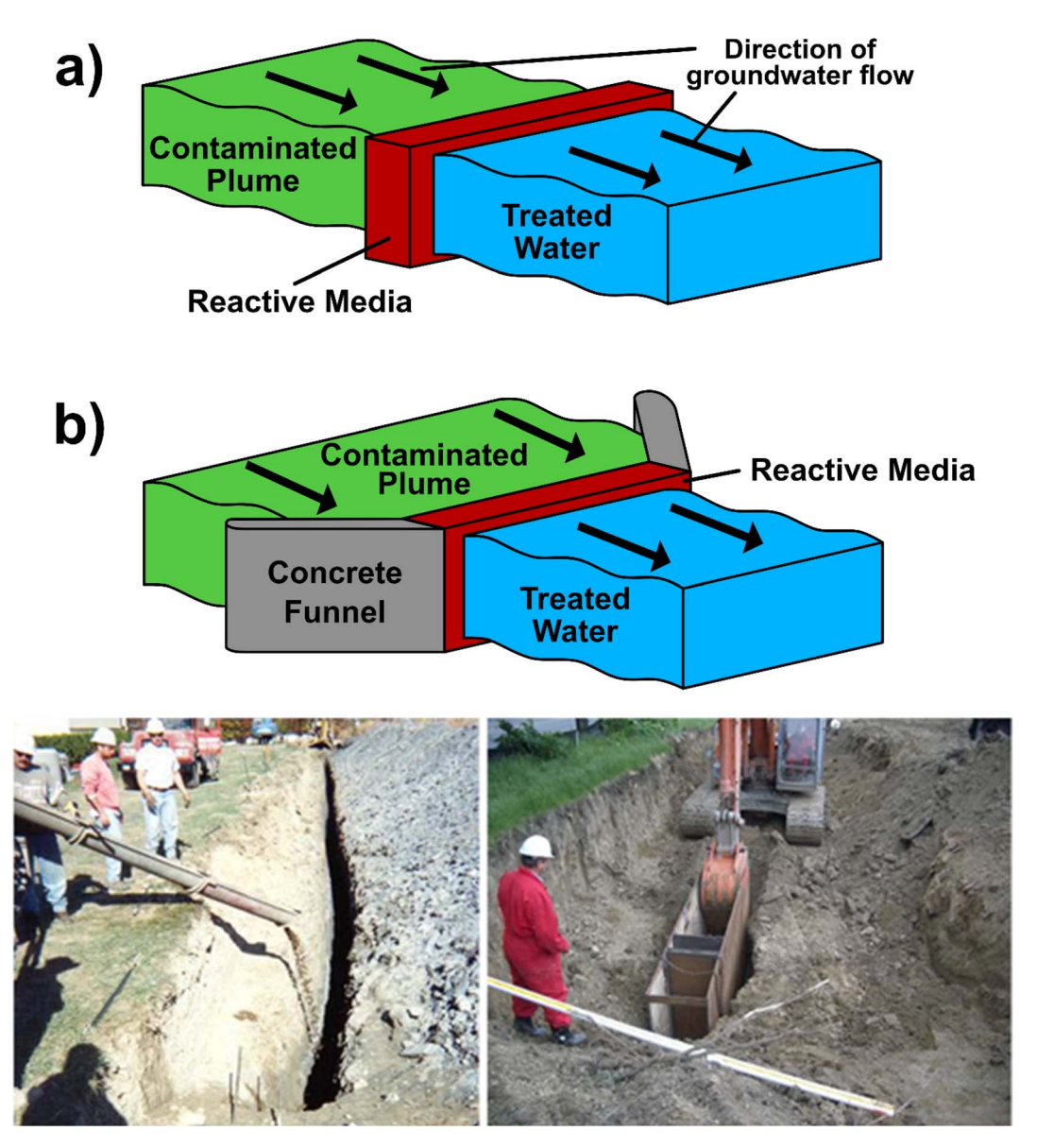


Fig. 2 Top – Diagram illustrating permeable reactive barriers in (a) continuous and (b) funnel and gate configurations at the Oak Ridge Y-12 Site, Tennessee. In both instances, contaminated groundwater passes through a reactive medium, where contaminants are removed, and clean water passes out the other side. Funnel and gate configurations have the addition of concrete barriers to channel groundwater flow. Bottom – Photos from ITRC⁸² showing unsupported (left) and temporary trench box (right) excavation during PRB installation at non-nuclear industrial sites. Reactive media is poured into the hole to complete the PRB.

remediators' discretion. However, a less invasive approach was adopted at the Hanford site to reduce the 90 Sr activity reaching the Columbia River. 95 A solution of Ca, citrate and PO_4^- was added to the groundwater through boreholes, 96,97 creating a diffuse, continuous calcium phosphate (apatite) barrier that formed *in situ* from a series of discrete points at the surface. 98 Once formed, Ca in the apatite will substitute with Sr in the plume, as the existence of strontiapatite is more thermodynamically favourable than the initial hydroxyapatite. 99 Four pilot boreholes were initially injected between 2006 and 2008, with pre-barrier activities ranging from 36.5 Bq L $^{-1}$ to 171.3 Bq L $^{-1}$ (972 pCi L $^{-1}$ to 4630 pCi L $^{-1}$) 90 Sr. 6 As of 2021, activities within the boreholes have dropped to 4.1–23.5 Bq L $^{-1}$ (111–635

pCi L⁻¹) – a decrease of 77–91% compared to the respective prebarrier maximum ⁹⁰Sr activities. The variance in reduction efficiencies is likely caused by a variability in the apatite concentrations surrounding the boreholes. To avoid a significant loss of apatite over time, the mineral constituents are reinjected into boreholes with increasing ⁹⁰Sr activities, allowing specific areas of the barrier to be targeted and rejuvenated without the need to dig up large sections of the barrier. ³H is not amenable to PRB attenuation for two reasons; the technique is typically limited to redox-sensitive elements that have variable solubilities in groundwaters, and tritiated groundwater is permeable to PRBs.

3.3 Phytoremediation

Phytoremediation is an *in situ*, passive and low-cost method that uses plants (and their associated microorganisms) for remediation over medium- to long-term periods.^{100,101} The technique involves the use of at least one of the following main processes^{102,103} (Fig. 3):

- (1) Phytoextraction removal of contaminants from soils and shallow groundwaters and accumulating them in above-ground shoots.
- (2) Phytovolatilization extraction of volatile radionuclides from soils and subsequently releasing them in a gaseous form.

- (3) Phytostabilisation reduction of a contaminant's bioavailability within the subsurface.
- (4) Phytofiltration filtration of contaminants by plant roots or seedlings through adsorption or absorption.
- (5) Phytostimulation removal of contaminants through plant roots and their rhizospheric microorganisms.
- (6) Phyto/rhizodegradation degradation of organic contaminants by plants/rhizospheric microorganisms.
- ¹²⁹I has been considered as a target contaminant for phytovolatilization, but concerns have been raised over the health risks associated with its bioaccumulation within humansif

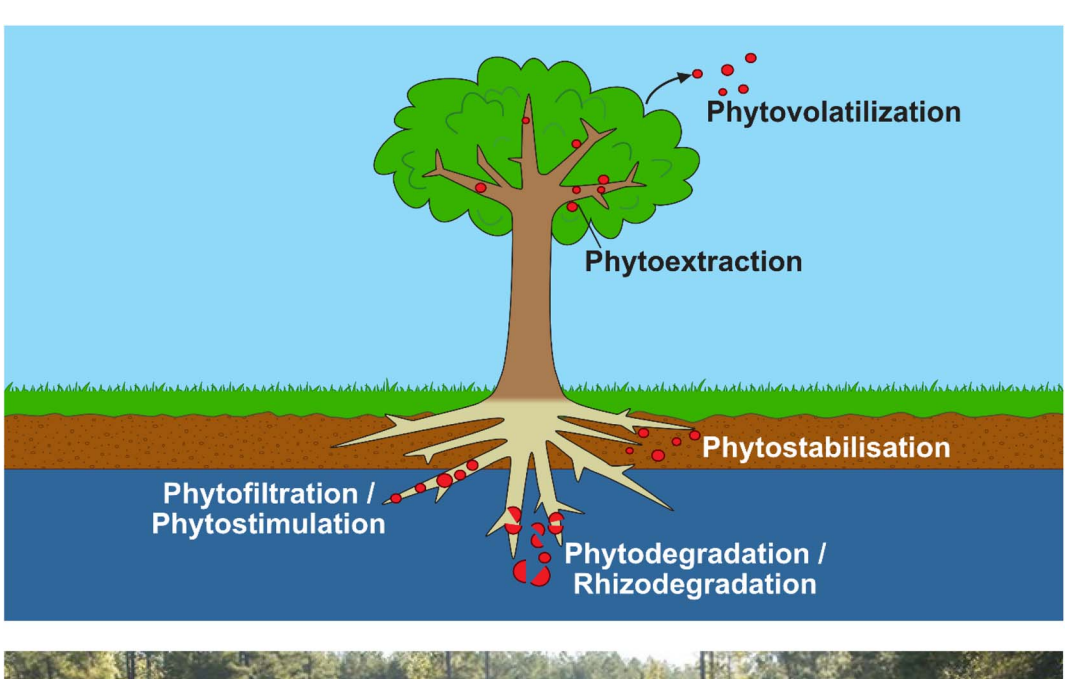




Fig. 3 Top – Sub-processes of phytoremediation, showing phytovolatilization, phytoextraction, rhizofiltration and phytostabilization. ³H is released into the environment through the former-most option, diffusing into the atmosphere through leaves rather than being expelled by the roots. Bottom – Photo from DOE¹¹² showing Savannah River Nuclear Solutions engineers examining pumping equipment next to the ³H-contaminated groundwater storage pond. Water is pumped from the pond and used to irrigate the surrounding woodland, where evaporation and phytovolatilization release ³H into the atmosphere.

inhaled.¹⁰⁴ As a result, phytoremediation of ¹²⁹I has not been performed at nuclear sites. ⁹⁹Tc can also be theoretically remediated through phytoextraction, but is hindered by sulfate competition caused by preferential SO_4^{2-} binding over TcO_4^{-} in amino acids residues within the roots.¹⁰⁵

Whilst a number of phytoremediation schemes have been performed in proximity to nuclear sites (e.g. Fukushima¹⁰⁶ and Chernobyl⁵⁷), fewer examples exist for direct on-site applications. However, a 1999 investigation at Sellafie ld examined the use of spear thistles (Cirsium vulgare) and broad-leaved docks (Rumex obtusifolius) for ⁹⁰Sr uptake.¹⁰⁷ It was found that the thistles removed 64–89% of ⁹⁰Sr, with a mean efficiency of 84%, whilst the docks extracted 50–87% of ⁹⁰Sr, with a mean removal rate of 76%. The large variation in Sr removal for both species is likely caused by intra-specific competition, in addition to site heterogeneities including microbial activity and soil composition. Further discussion and additional examples of ⁹⁰Sr phytoremediation are described in Purkis et al.¹⁰⁸

Phytovolatilization of ³H has been utilised at the SRS, South Carolina, in conjunction with evaporation. 109,110 Tritiated groundwater from the on-site Old Radioactive Waste Burial Ground was continuously brought to the surface by a spring, discharging between 15 170 Bq L^{-1} and 24 235 Bq L^{-1} (410 000 pCi L⁻¹ and 655 000 pCi L⁻¹) of ³H into the nearby stream, the Fourmile Branch.¹⁰⁹ These levels are between 20 and 32 times the 740.0 Bq L⁻¹ (20 000 pCi L⁻¹) ³H Environmental Protection Agency drinking water standard.111 A dam was built downstream of the spring which diverted water into a storage pond used for irrigation of the surrounding 89 000 m² of mixed woodland^{80,112,113} (Fig. 3). During the irrigation process, ³H is released into the atmosphere through a combination of phytovolatilization, after being taken up by tree roots, and evaporation from the dam and woodland floor. Closure of the dam in 2000 caused a 71% decrease in ³H levels (to 7067 Bq L⁻¹; 191 000 pCi L ⁻¹) in the stream within 2 weeks, and a 82% decrease (to 4329 Bq L⁻¹;117 000pCi L⁻¹)within 10 months. 109 The longterm success of the system resulted in an additional 78 acres of pine trees being planted, greatly expanding the irrigation project.¹¹⁰ The general downward trend of average

³H activity in the Fourmile Branch has continued over the last decade, with 2021 data showing only ~629 Bq m⁻³ (~17 000 pCi L⁻¹) of ³H¹¹¹ − a 97% reduction from the 24 235 Bq L⁻¹ of 3H recorded shortly before the dam closure in 2000. In addition, the volatilization of 3H poses minimal risk to human health, as shown by a 2019 maximum on-site concentration of 28.19 Bq m⁻³ (762 pCi m⁻³) in air, decreasing to a maximum of 0.99 Bq L⁻¹ (26.7 pCi m⁻³) in air at the site perimeter. The 97% reduction to 629 Bq L⁻¹ in the Fourmile Branch is enough to reduce concentrations belowthe 740.0 BqL⁻¹ Environmental Protection Agency drinking water standard for ³H.¹¹¹ Furthermore, because this project also utilises evaporation, ³H remediation caused exclusively by the phytovolatilization component is difficult to practically determine and, hence, is not specifically reported in the literature.

4 Emerging Treating Methods

In efforts to produce more effective and sustainable remediation, additional techniques have been applied at nuclear sites over recent decades. These technologies have been used less extensively than those previously mentioned but could provide an alternative, viable, approach if more traditional remediation strategies are deemed unsuitable for a given scenario.

4.1 Bioimmobilization

Bioimmobilization involves the use of bacteria or plants to decrease the water solubility of aqueous contaminants through changes in oxidation state and therefore promoting precipita-tion of solid phases. 114,115 The process can be performed either through the introduction of new organisms to an area or by promoting the growth of organisms already present in the target environment.^{114,116} Field-scale, in situ bioimmobilization of ⁹⁹Tc was conducted at the Oak Ridge site by Istok and coworkers in 2004.¹¹⁴ It was suggested that chemical reduction of radionuclides including Tc could be performed by microbial colonies already present within facility sediments. Although the microorganisms required for this are apparently present within the subsurface, 117 factors such as competing electron acceptors (e.g. NO³⁻) and numbers of microbial colonies within the sediments limit the efficiency of Tc reduction. 118 Further, reducing conditions are required within the subsurface, both for promoting the growth of metal-reducing bacteria (e.g. Geobacter) and for maintaining Tc in its insoluble 4+ oxidation state. 114 These anaerobic conditions can be generated by the addition of elec-tron donors into a system, allowing bacteria to reduce NO³⁻ and, subsequently, metals for respiration in the absence of O2. In this field trial, single-well, push-pull tests were used to inject multiple rounds of ethanol (acting as an electron donor) into a shallow aguifer to monitor 99Tc reduction. All results were corrected to account for the Tc dilution that occurred when the clean test solution mixed with contaminated borehole ground-water. Initial tests showed that Tc(VII) could not be reduced when NO3- was present, as microorganisms would preferen-tially reduce NO³⁻ during respiration. However, the first ethanol injection resulted in Tc(VII) concentrations reducing from 13 200 pM to 5800 pM (56.1% reduction) within 400 hours and to ~3700 pM (72.0%) reduction) within 600 hours. In comparison, NO3- concentrations dropped from ~140 mM to ~40 mM (71.4% reduction) within 400 hours and ~25 mM (82.1% reduction) by 600 hours. Multiple injections were performed into the same borehole over several months, with the seventh ethanol injection causing a Tc(VII) reduction from ~12 000 pM to ~1000 pM (91.7% reduction) within 400 hours, although no further data were collected after this time period. Concurrently, the initial ~125 mM of NO³dropped to negligible levels (~100% reduction) after ~35 hours and stayed constant for the following ~365 hours. After the seven biostimulating ethanol injections, a test solution was created without the electron donor, and inserted into the borehole. The absence of ethanol had no negative effect on Tc(VII) reduction, with concentrations decreasing from ~11 000 pM to ~1000 pM (90.9% reduction) within 400 hours and remaining constant for up to 500 hours postinjection. Initial NO³-concentrations of ~120 mM dropped to ~70 mM (41.7% reduction) within 400 hours and ~35 mM (70.8% reduction) by 600 hours. These experiments

show that in situ 99Tc reduction is possible when NO₃ is simultaneously consumed through bacterial denitrification; promoted via the use of cheap electron donors such as ethanol. Despite this, there does not appear to have been further work on this at site scales. In addition, pilot-scale bioimmobilization studies for 129I, 90Sr and 3H could not be found. In addition to the reasons given for their unsuitability regarding phytoremediation (see Section 3.3) the absence of 129I, 90Sr and 3H studies is likely because the dominant chemical species present in water for ¹²⁹I (5+ and 1-) and ⁹⁰Sr (2+) are all highly soluble and would therefore have further requisites for immobilization to occur (adsorption sites, reactive media, etc.), whilst tritiated water would not be immobilised as it cannot be distinguished from light water with this technique.

Chemical/colloid injection

Injection is the process of inserting a material into the subsurface that can either manipulate the oxidation states of pollutants to promote their precipitation, or provide active sites for contaminants to adsorb onto. 119 The injected material can be chosen to remove multiple compounds simultaneously, such as variants of zeolites that can treat heavy metals, 120 or to target specific contaminants, such as Savannah River Site's project for multiple submicron AgCl injections to treat a migrating 129I plume.121 AgCl was intruded into the subsurface as it can react with this radionuclide to form Ag129I, which is insoluble in water and, thus, is immobilised and retained within the aquifer. 122 The first set of injections occurred throughout 2011, in 7 temporary boreholes that were distributed in an approximately semi-circular shape with a diameter of ~70 m. Only the well closest to the injection sites showed a definitive 129I decrease after treatment. Activities for this well between October 2009 and October 2011 averaged at 5.0 Bg L⁻¹ (135 pCi L⁻¹), but decreased to 2.9 Bq L⁻¹ (77 pCi L⁻¹) shortly before the injections. 121 Measurements of 1.7-2.6 Bq L-1 (46-70 pCi L-1) were recorded in the first 6 months, before a sharp increase to 3.7 Bq L^{-1} (99 pCi L⁻¹) in the 7th month. A range of 2.9 to 4.0 Bq L⁻¹ (79 to 109 pCi L⁻¹) was reported for the remaining 5 months of monitoring. All other wells, which were further away from the injection boreholes, show ambiguous or no evidence of 129I activity reductions, suggesting that remediation is only effective within close proximity to the injection sites. Ag migration data indicated limited particle movement after subsurface deposition. Of the total AgCl solution volume that was permitted to be injected in 2011, only half was used. As a result, the remaining volume was used in 2015 to boost the project's long-term efficiency. 122 7 new boreholes were used to concentrate the AgCl barrier to the east of the original wells, with the 2015 group spaced across \sim 35 m. It was reported that 5 of the 7 wells had ¹²⁹I decreases between 25% and 65% and one well upgradient of the barrier detected no change, with the final borehole not discussed. 122,123 However, activities for each of the wells were not provided in these reports, and other possible sources for raw borehole data are not publicly available, meaning the

percentage reductions given here could not be independently verified. Given the apparent success of both 2011 and 2015

injectionsthirdound as approved in 21 and performed in 2019. 123 Theinsertionsite distribution consisted of 15 wells with a broadly linear configration spanning ~35 m, aligned perpendicular to groundwater flow. This was based on the 1.2-2.4 m AgCl diffusion radius that formed around previous boreholes, allowing the formation of a single, continuous zone in the subsurface¹²² comparable to Hanford's ⁹⁰Sr permeable treatmentbarrier(seeSection 3.2). Results from the most recent injections will be disclosed in the site's 2022 Corrective Action Report. 123 Subsurface AgCl insertion will continue until 2040, when the area will transition to natural monitored attenuation.110 However, whilst this technique shows promise at SRS, applications on other nuclear sites may not be feasible due to the toxic nature of Ag,88 and so careful consideration and planning mustbetakentoavoidadverseconsequencesontheecologyand surroundingenvironmentsofnuclearfacilities.

4.3 Combined electrolysis catalytic exchange

Combined Electrolysis Catalytic Exchange (CECE) is a ³H remediation technique for detritiating effluent and groundwaters. 124 Contaminated feed water is pumped into a containment cell and electrolysed, converting liquid H2O into H2 and O2 gases. The energy required to electrolyse tritiated water is greater than that required for light water, meaning that ³H will concentrate in the remaining feed solution whilst light water is driven off. Deionised water is also added to the system to recapture any 3H that is electrolysed, as the radionuclide will preferentially exist as liquid H₂O over gaseous H₂. ¹²⁵ Pilot-scale trials have shown high detritiation factors e.g. >100;126 1000 when used with heavy water - a more difficult separation than with light water. 127 However, the system is expensive to operate and at present is not able to remediate large volumes of water, making it unsuitable for processing large water flows or volumes with relatively low 3H activities. 126 The application of CECE has been evaluated for ³H contaminated groundwater at the Fukushima site (known as ALPS-treated water) but, due to the high cost and small treatment volumes, the technology was deemed unsuitable for ³H remediation¹²⁶ and these waters will instead be discharged to sea.¹²⁸ For similar reasons, the 2022 Hanford ³H wastewater treatment review determined that whilst the Modular Detritiation System® (a commercialised version of the CECE process) shows promise for effective ³H removal in the future, the modifications required for use with large volumes of liquid make it currently infeasible for on-site application with groundwaters. 129

5 Comparison of main techniques

The "tried and tested" attitude towards P&T at nuclear sites makes it appealing for site remediators. Many government-funded remediation projects are ultimately paid for by the taxpayer, who want cheap and effective technologies that opti-mise project efficiencies. The financial, and potentially political, consequences of a technique that is ineffective or that mobilises additional contaminants could be high, often make P&T the most attractive option. In addition, the technique allows for

convenient testing of groundwater before discharge, ensuring that remediation targets are always being met. However, P&T can be expensive to operate due to the infrastructure required for an ex situ technique. This was highlighted in a 2001 study on 32 United States Environmental Protection Agency (USEPA) P&T sites in North America, where the average capital and yearly operational costs were \$4 900 000 and \$770 000, respectively at 2001 prices. 130 Site selection criteria included the presence of a full-scale remediation system and operator reports on aquifer clean-up targets and technology costings. Although the tech-nique is expensive, the total cost for each project will depend on the price per unit of reactive medium as well as the frequency at which the medium needs to be replaced. Further, multiple types of reactive media may be required if different contaminants are to be treated simultaneously, further increasing operational costs, but this can reduce the remediation timeframe in comparison to using a single, less selective medium that removes a lower proportion of radionuclides in favour of competing ions such as HCO₃, NO₃ etc.

The passive nature of PRBs offers benefits over P&T including a decrease in the number of staff required for daily operation, lowering the long-term function and maintenance costs, and minimal infrastructure, which reduces initial costs. 15 USEPA facilities in North America and an additional site in Northern Ireland were also examined in the EPA¹³⁰ P&T study, and their costings compared. The selection criteria for the survey required a full-scale system with capital costs provided, although annual maintenance costs were a necessity as only 2 of the sites had been operating long enough for accurate prices to be determined. The average capital costs for the 16 PRB sites was \$730 000 - more than 6 times cheaper than the average P&T capital costs, as determined by the same study. Annual operational and maintenance costs of \$78 000 and \$120 000 were recorded for the US National Coast Guard Support Centre (North Carolina) and the Intersil (California) sites. Although the lack of case studies reduces the certainty as to whether these costs are truly reflective of PRB projects, both available examples are \sim 7 times lower than the \$770 000 equivalent for P&T.

From this study, PRBs appear to be a much cheaper alternative to P&T but multiple factors can influence the fin al cost, including the price of the reactive medium and the lifetimes of both the barrier and the wider remediation project. PRB placement is important for financial and remedial success, as the technique can only remediate groundwater that passes through it, making it unsuitable for contamination spread over large areas. Consequently, the decision as to whether a PRB or P&T is the best remediation approach will be highly sitespecific. An updated version of a cost comparison report for different remediation techniques could not be found. Further, no list of remediation techniques deployed specifically at nuclear sites could be obtained, and only one site in the EPA report included radionuclide clean-up (Oak Ridge Site, Ten-nessee (see Section 4): capital costs of \$900 000). This highlights the absence of financial data available to site operators when designing remedial strategies and demonstrates the need for readily accessible information to promote more sustainable options in the nuclear industry.

The primary appeal to phytoremediation is its passive nature, although active enhancements such as the SRS irrigation system can boost the removal efficiency (and may be necessary in some cases to allow plant establishment and growth). A direct result of passive techniques are the relatively low costs compared to conventional pump and treat methods. For example, implementation of the irrigation system at the SRS came at an initial cost of \$5 000 000, with an additional \$500 000 needed per year. 80 In comparison, the average set up cost for 32 American P&T sites was \$4 900 000, followed by \$770 000 per annum. Although these gures are similar, phytoremediation without an irrigation system would drastically reduce the overall cost and make the technique much more financially favourable. Additional, unique benefit s can come from phytoremediation projects, including greater protection from flooding, improved site aesthetics and supporting or reintroducing native plant and animal species to the local area. 131 However, the depth at which remediation can occur is limited to the depth of plant roots, only making it a suitable alternative to P&T in shallow groundwaters. The same constraint applies to areal extent, meaning that large areas of contaminated land would require large numbers of plants for remediation to be effective. The long-term chemical and physical forms of targeted radionuclides must be understood before implementation, as processes such as phytovolatilization may mobilise contaminants that pose a greater risk to wildlife and humans in air than when retained within sediments (or within the subsurface). Further, phytoremediation is only able to extract radionuclides that are taken up by the plants' roots, resulting in contaminants with lower bioavailabilities remaining in the subsurface. In comparison, P&T can extract any radionuclides that are mobile in groundwater regardless of their bioavailability, takes up less space at a site and extracts groundwater from any depth, although higher costs may be associated with deeper extraction wells.

Both phytoremediation and PRBs had a range of field-scale pilot projects performed in the late 1990s and early 2000s, 48,93,132 likely as a result of the globally increasing costs and tightening of restrictions associated with the 'dig and dump' approach to contaminated materials.¹³³ Although each technique on its own is unlikely to be used in favour of P&T for simultaneous treatment of all DTMRs discussed here, a combination of these more sustainable methods may be superior to conventional remediation; for example, phytovolatilization and PRBs could be used to remove 99Tc, 90Sr and 3H with minimal upkeep and maintenance. However, limitations of these practices, such as the area of land available and radionuclide selectivity of each technique, make this unsuitable for groundwater application on the majority of nuclear sites. This highlights the need for new techniques that can be used in combination with PRBs and phytoremediation to enhance the number of DTMRs that can be remediated in a sustainable way. Emerging in situ technologies under active development for DTMRs include electrokinetic remediation¹³⁴ and silica grouting,135 although further work is needed to show efficacy for both DTMRs and for field-scale application.

6 Conclusions

In line with the growing demand for sustainable remediation at nuclear sites, we have reported on techniques for the removal of DTMRs from groundwaters. Whilst a variety of possible remediation techniques exist for ¹²⁹I, ⁹⁹Tc, ⁹⁰Sr and ³H, the differing physical and chemical properties of these DTMRs result in a need for site-specific implementations. P&T is, by far, the most commonly applied technique and can effectively remediate ⁹⁹Tc and 90Sr. However, 129I and 3H cannot be treated by this method, as current adsorbents are not capable of effective 129I uptake, and ³H₂O and ³H¹HO are not differentiable from groundwater H₂O. In situ techniques can also be applied for remediation, although their application should be evaluated to determine their suitability on a site-by-site basis. PRBs (including colloidal or chemical injection systems, such as that applied at the Hanford site for ⁹⁰Sr) can be a more financially favourable technology in comparison to P&T due to the minimal infrastructure required but offer fewer advantages for less sensitive radionuclides and depend upon the selection of an appropriate reactive media. Phytoremediation is a low-cost method for ³H removal and offers secondary environmental and social benefits but operates over long timescales and is not suitable for elements with low bioavailabilities (99Tc) or where bioaccumulation presents a risk to humans (129I).

Of the examined technologies, none are effective at removing all of ¹²⁹I, ⁹⁹Tc, ⁹⁰Sr and ³H. This highlights the need for simultaneous growth in research areas looking at improving the efficiency of current techniques, enhancing the development of "treatment train" approaches (potentially including natural attenuation for shorter-lived DTMRs), and continued progression of emerging technologies to minimise scenarios where no remediation strategies are appropriate. Alternative techniques such as electrokinetic remediation and silica grouting are being developed but their application towards DTMRs (with the exception of 90Sr134,136) remains unreported, particularly at larger (field or field pilot) scale. The need for advancement in this area is clear but current progress is hindered due to the difficulty associated with measuring DTMRs in situ. Although rapid screening techniques for these radionuclides is a developing area (e.g. studies by Hou, 137 Warwick et al. 138 and Zaffora et al. 139), a coevolution with the advancement of remediation technologies would help to optimise both research fields. If this were to occur, site operators would be able to make better-informed decisions on remediation strategies using real-time, highresolution plume data, leading to more intelligent groundwater clean-up. This synergy would greatly benefit the capability of remedial projects globally, consequently reducing the financial burden for nuclear sites and governments as more effective action can be taken to ensure that thorough and comprehensive DTMR removal occurs.

Conflicts of interest

There are no conflicts to declare.

Acknowledgements

We thank two anonymous reviewers for helpful comments which improved the overall quality of the information and arguments presented in this paper. We are grateful for comments and information from Dr James Graham from the National Nuclear Laboratory (UK) on remediation strategies at the Sellafield facility (UK), and to the TRANSCEND Consortium (EPSRC grant number EP/S01019X/1) for funding support. Shaun Hemming is also grateful to the INSPIRE Doctoral Training Partnership (NERC grant number NE/S007210/1) for PhD funding.

References

- 1 DOE, *Hanford Site RCRA Groundwater Monitoring Report For 2022*, U.S. Department of Energy, Richland, Washington, 2023.
- 2 Sellafield Ltd., *Groundwater Monitoring Annual Data Review* 2016, Sellafield Ltd., 2017.
- 3 N. M. Hassan, Y. J. Kim, J. Jang, B. U. Chang and J. S. Chae, Comparative study of precise measurements of natural radionuclides and radiation dose using in-situ and laboratory γ-ray spectroscopy techniques, *Sci. Rep.*, 2018, **8**, 14115.
- 4 IAEA, Determination and Use of Scaling Factors for Waste Characterization in Nuclear Power Plants, International Atomic Energy Agency, Vienna, 2009.
- 5 S. Zhang, C. Xu, D. Creeley, Y.-F. Ho, H.-P. Li, R. Grandbois, K. A. Schwehr, D. I. Kaplan, C. M. Yeager, D. Wellman and P. H. Santschi, Iodine-129 and Iodine-127 Speciation in Groundwater at the Hanford Site, U.S.: Iodate Incorporation into Calcite, *Environ. Sci. Technol.*, 2013, 47, 9635–9642.
- DOE, Hanford Site Groundwater Monitoring Report for 2021,
 U.S. Department of Energy, Richland, Washington, 2022.
- 7 DOE, *Hanford Site Groundwater Monitoring Report for 2019*, U.S. Department of Energy, Richland, Washington, 2020.
- 8 Sellafield Ltd., *Monitoring Our Environment Discharges and Environmental Monitoring 2021*, Sellafield Ltd., Cumbria, UK, 2022.
- 9 D. Hou, P. Guthrie and M. Rigby, Assessing the trend in sustainable remediation: A questionnaire survey of remediation professionals in various countries, *J. Environ. Manage.*, 2016, **184**, 18–26.
- 10 CL:AIRE, A Framework for Assessing the Sustainability of Soil and Groundwater Remediation, Contaminated Land: Applications in Real Environments, London, 2010.
- 11 ASTM International, ASTM E2893 16e1: Standard Guide for Greener Cleanups, ASTM International, 2016.
- 12 ISO, ISO 18504:2017: Soil quality Sustainable remediation, International Standards Organisation, 2017.
- 13 NDA, *Nuclear Decommissioning Authority Strategy* 2021, Nuclear Decommissioning Authority, Cumbria, UK, 2021.
- 14 F. Hossain, Natural and anthropogenic radionuclides in water and wastewater: Sources, treatments and recoveries, *J. Environ. Radioact.*, 2020, 225, 106423.

- 15 D. Alby, C. Charnay, M. Heran, B. Prelot and J. Zajac, Recent developments in nanostructured inorganic materials for sorption of cesium and strontium: Synthesis and shaping, sorption capacity, mechanisms, and selectivity-A review, *J. Hazard. Mater.*, 2018, 344, 511–530.
- 16 S. Sharma, B. Singh and V. K. Manchanda, Phytoremediation: role of terrestrial plants and aquatic macrophytes in the remediation of radionuclides and heavy metal contaminated soil and water, *Environ. Sci. Pollut. Res.*, 2015, 22, 946–962.
- 17 IAEA, Technologies for remediation of radioactively contaminated sites, International Atomic Energy Agency, Vienna, 1999.
- 18 S. Thierfeldt and A. Deckert, Radionuclides Difficult to Measure in Waste Packages, Swedish Nuclear Power Inspectorate, Stockholm, 1995.
- 19 IAEA, Nuclear Power Reactors in the World 2022 Edition, International Atomic Energy Agency, Vienna, 2022.
- 20 K. Shozugawa, M. Hori, T. E. Johnson, N. Takahata, Y. Sano, N. Kavasi, S. K. Sahoo and M. Matsuo, Landside tritium leakage over through years from Fukushima Dai-ichi nuclear plant and relationship between countermeasures and contaminated water, *Sci. Rep.*, 2020, 10, 19925.
- 21 IAEA, IAEA Nuclear Data Services, https://www-nds.iaea.org/, accessed 6 October 2023.
- 22 D. Banerjee, D. Kim, M. J. Schweiger, A. A. Kruger and P. K. Thallapally, Removal of TcO₄⁻ ions from solution: materials and future outlook, *Chem. Soc. Rev.*, 2016, 45, 2724–2739.
- 23 B. J. Riley, J. D. Vienna, D. M. Strachan, J. S. McCloy and J. L. Jerden, Materials and processes for the effective capture and immobilization of radioiodine: A review, *J. Nucl. Mater.*, 2016, 470, 307–326.
- 24 IAEA, Management of Waste Containing Tritium and Carbon-14, International Atomic Energy Agency, Vienna, 2004.
- 25 D. Bugai, J. Smith and M. A. Hoque, Solid-liquid distribution coefficients (Kd-s) of geological deposits at the Chernobyl Nuclear Power Plant site with respect to Sr, Cs and Pu radionuclides: A short review, *Chemosphere*, 2020, 242, 125175.
- 26 S. Sheppard, G. Sohlenius, L. G. Omberg, M. Borgiel, S. Grolander and S. Nordén, Solid/liquid partition coefficients (Kd) and plant/soil concentration ratios (CR) for selected soils, tills and sediments at Forsmark, Swedish Nuclear Fuel and Waste Management Co., Stockholm, 2011.
- 27 M. Denham, D. Kaplan and C. Yeager, *Groundwater Radioiodine: Prevalence, Biogeochemistry, and Potential Remedial Approaches*, Savannah River National Laboratory, South Carolina, 2009.
- 28 D. I. Kaplan, M. E. Denham, S. Zhang, C. Yeager, C. Xu, K. A. Schwehr, H. P. Li, Y. F. Ho, D. Wellman and P. H. Santschi, Radioiodine Biogeochemistry and Prevalence in Groundwater, Crit. Rev. Environ. Sci. Technol., 2014, 44, 2287–2335.
- 29 F. Keppler, H. Biester, A. Putschew, P. J. Silk, H. F. Schöler and G. Müller, Organoiodine formation during

- humification in peatlands, *Environ. Chem. Lett.*, 2003, 1, 219–223.
- 30 V. Moulin, P. Reiller, B. Amekraz and C. Moulin, Direct characterization of iodine covalently bound to fulvic acids by electrospray mass spectrometry, *Rapid Commun. Mass Spectrom.*, 2001, 15, 2488–2496.
- 31 K. A. Schwehr, P. H. Santschi, D. I. Kaplan, C. M. Yeager and R. Brinkmeyer, Organo-Iodine Formation in Soils and Aquifer Sediments at Ambient Concentrations, *Environ. Sci. Technol.*, 2009, 43, 7258–7264.
- 32 K. J. Cantrell, R. J. Serne and G. V. Last, *Hanford Contaminant Distribution Coefficient Database and Users Guide*, Pacific Northwest National Laboratory, Richland, Washington, 2003.
- 33 D. I. Kaplan, K. A. Roberts, K. A. Schwehr, M. S. Lilley, R. Brinkmeyer, M. E. Denham, D. DiPrete, H.-P. Li, B. A. Powell, C. Xu, C. M. Yeager, S. Zhang and P. H. Santschi, Evaluation of a Radioiodine Plume Increasing in Concentration at the Savannah River Site, *Environ. Sci. Technol.*, 2011, 45, 489–495.
- 34 C. Xu, D. I. Kaplan, S. Zhang, M. Athon, Y.-F. Ho, H.-P. Li, C. M. Yeager, K. A. Schwehr, R. Grandbois, D. Wellman and P. H. Santschi, Radioiodine sorption/desorption and speciation transformation by subsurface sediments from the Hanford Site, *J. Environ. Radioact.*, 2015, 139, 43–55.
- 35 R. Naidu, N. S. Bolan, R. S. Kookana and K. G. Tiller, Ionic-strength and pH effects on the sorption of cadmium and the surface charge of soils, *Eurasian J. Soil Sci.*, 1994, 45, 419–429.
- 36 J. L. Dai, M. Zhang, Q. H. Hu, Y. Z. Huang, R. Q. Wang and Y. G. Zhu, Adsorption and desorption of iodine by various Chinese soils: II. Iodide and iodate, *Geoderma*, 2009, **153**, 130–135.
- 37 J.-L. Dai, M. Zhang and Y.-G. Zhu, Adsorption and desorption of iodine by various Chinese soils: I. Iodate, *Environ. Int.*, 2004, **30**, 525–530.
- 38 D. Fan, R. P. Anitori, B. M. Tebo, P. G. Tratnyek, J. S. Lezama Pacheco, R.K.Kukkadapu, L.Kovarik, M.H.Engelhard and M. E. Bowden, Oxidative Remobilization of Technetium Sequestered by Sulfide Transformed Nano Zerovalent Iron, Environ. Sci. Technol., 2014, 48, 7409–7417.
- 39 R. E. Meyer, W. D. Arnold, F. I. Case and G. D. O'Kelley, Solubilities of Tc(IV) Oxides, *Radiochim. Acta*, 1991, 55, 11–18.
- 40 R. J. Serne, Kd Values for Agricultural and Surface Soils for Use in Hanford Site Farm, Residential, and River Shoreline Scenarios, U.S Department of Energy, 2007.
- 41 S. Sheppard, J. Long, B. Sanipelli and G. Sohlenius, *Solid/liquid partition coefficients (Kd) for selected soils and sediments at Forsmark and Laxemar-Simpevarp*, Swedish Nuclear Fuel and Waste Management Co., Stockholm, 2009.
- 42 A. Cleary, J. R. Lloyd, L. Newsome, S. Shaw, C. Boothman, G. Boshoff, N. Atherton and K. Morris, Bioremediation of strontium and technetium contaminated groundwater using glycerol phosphate, *Chem. Geol.*, 2019, **509**, 213–222.

- 43 D. K. Gupta, W. Schulz, G. Steinhauser and C. Walther, Radiostrontium transport in plants and phytoremediation, *Environ. Sci. Pollut. Res.*, 2018, 25, 29996–30008.
- 44 R. J. Serne, V. L. LeGore, K. J. Cantrell, C. W. Lindenmeiser, J. A. Campbell, J. E. Amonette and J. L. Conca, Solid-waste leach characteristics and contaminant-sediment interactions. Volume 1, Batch leach and adsorption tests and sediment characterization, Pacific Northwest Lab., Richland, Washington, 1993.
- 45 J. Guillén, A. Baeza, J. A. Corbacho and J. G. Muñoz-Muñoz, Migration of ¹³⁷Cs, ⁹⁰Sr, and ²³⁹⁺²⁴⁰Pu in Mediterranean forests: influence of bioavailability and association with organicacidsinsoil, *J. Environ. Radioact.*, 2015, 144, 96–102.
- 46 S. H. Wallace, S. Shaw, K. Morris, J. S. Small, A. J. Fuller and I. T. Burke, Effect of groundwater pH and ionic strength on strontium sorption in aquifer sediments: Implications for ⁹⁰Sr mobility at contaminated nuclear sites, *Appl. Geochem.*, 2012, 27, 1482–1491.
- 47 M.-S. Yim and F. Caron, Life cycle and management of carbon-14 from nuclear power generation, *Prog. Nucl. Energy*, 2006, **48**, 2–36.
- 48 M. C. Negri, R. Hinchman and J. Wozniak, *Capturing a 'Mixed' Contaminant Plume: Tritium Phytoevaporation at Argonne National Laboratory's Area 319*, Argonne National Laboratory, Argonne, Illinois, 2000.
- 49 D. H. Thibault, M. I. Sheppard and P. A. Smith, *A Critical Compilation and Review of Default Soil Solid/Liquid Partition Coefficients, Kd, for Use in Environmental Assessments*, Whiteshell Nuclear Research Establishment, Pinawa, Manitoba, Canada, 1990.
- 50 I. W. Croudace, P. E. Warwick and J. E. Morris, Evidence for the Preservation of Technogenic Tritiated Organic Compounds in an Estuarine Sedimentary Environment, *Environ. Sci. Technol.*, 2012, 46, 5704–5712.
- 51 S. Masiuk, M. Chepurny, V. Buderatska, A. Kukush, S. Shklyar, O. Ivanova, Z. Boiko, N. Zhadan, G. Fedosenko, A. Bilonyk, T. Lev, M. Talerko, S. Kutsen, V. Minenko, K. Viarenich and V. Drozdovitch, Thyroid doses in Ukraine due to 131I intake after the Chornobyl accident. Report I: revision of direct thyroid measurements, Radiat. Environ. Biophys., 2021, 60, 267–288.
- 52 IAEA, Technetium-99m Radiopharmaceuticals: Status and Trends, International Atomic Energy Agency, Vienna, 2009.
- 53 S. G. Dahl, P. Allain, P. J. Marie, Y. Mauras, G. Boivin, P. Ammann, Y. Tsouderos, P. D. Delmas and C. Christiansen, Incorporation and distribution of strontium in bone, *Bone*, 2001, 28, 446–453.
- 54 H. Matsumoto, Y. Shimada, A. J. Nakamura, N. Usami, M. Ojima, S. Kakinuma, M. Shimada, M. Sunaoshi, R. Hirayama and H. Tauchi, Health effects triggered by tritium: how do we get public understanding based on scientificallysupportedevidence? *J. Radiat. Res.*, 2021, 62,557– 563.
- 55 J. L. Downs, B. A. Napier, M. J. Truex and A. L. Bunn, Evaluation of Dose- and Risk-Based Groundwater Cleanup

- Levels for Low Energy Beta Radioisotopes, Pacific Northwest National Laboratory, Richland, Washington, 2020.
- 56 C. I. Pearce, R. C. Moore, J. W. Morad, R. M. Asmussen, S. Chatterjee, A. R. Lawter, T. G. Levitskaia, J. J. Neeway, N. P. Qafoku, M. J. Rigali, S. A. Saslow, J. E. Szecsody, P. K. Thallapally, G. Wang and V. L. Freedman, Technetium immobilization by materials through sorption and redox-driven processes: A literature review, *Sci. Total Environ.*, 2020, 716, 132849.
- 57 S. Dushenkov, Trends in phytoremediation of radionuclides, *Plant Soil*, 2003, **249**, 167–175.
- 58 R. D. Mackley, D. M. Anderson, J. N. Thonle and C. E. Strickland, Technical and Economic Assessment of Solar Photovoltaic for Groundwater Extraction on the Hanford Site, Pacific Northwest National Laboratory, Richland, Washington, 2015.
- 59 O. Al-Hashimi, K. Hashim, E. Loffill, T. Marolt Cebasek, I. Nakouti, A. A. H. Faisal and N. Al-Ansari, A Comprehensive Review for Groundwater Contamination and Remediation: Occurrence, Migration and Adsorption Modelling, *Molecules*, 2021, 26, 5913.
- 60 EPA, Pump and Treat and In Situ Chemical Treatment of Contaminated Groundwater at the Odessa Chromium II South Plume Superfund Site Odessa, Ector County, Texas, U. S. Environmental Protection Agency, 2005.
- 61 R. V. Fox and B. Mincher, *Supercritical Fluid Extraction of Plutonium and Americium from Soil*, Idaho National Engineering and Environmental Laboratory, 2002.
- 62 CRC CARE, *Technology guide: Pump and treat*, Cooperative Research Centre for Contamination Assessment and Remediation of the Environment, 2018.
- 63 W. C. Jolin and M. Kaminski, Sorbent Materials for Rapid Remediation of Wash Water during Radiological Event Relief, *Chemosphere*, 2016, **162**, 165–171.
- 64 C. I. Pearce, E. A. Cordova, W. L. Garcia, S. A. Saslow, K. J. Cantrell, J. W. Morad, O. Qafoku, J. Matyás, A. E. Plymale, S. Chatterjee, J. Kang, F. C. Colon, T. G. Levitskaia, M. J. Rigali, J. E. Szecsody, S. M. Heald, M. Balasubramanian, S. Wang, D. T. Sun, W. L. Queen, R. Bontchev, R. C. Moore and V. L. Freedman, Evaluation of materials for iodine and technetium immobilization through sorption and redox-driven processes, *Sci. Total Environ.*, 2020, 716, 136167.
- 65 D. Banerjee, W. Xu, Z. Nie, L. E. V. Johnson, C. Coghlan, M. L. Sushko, D. Kim, M. J. Schweiger, A. A. Kruger, C. J. Doonan and P. K. Thallapally, Zirconium-Based Metal-Organic Framework for Removal of Perrhenate from Water, *Inorg. Chem.*, 2016, 55, 8241–8243.
- 66 ONR, Remediation Techniques for Radioactive Contaminated Land on Nuclear Licensed Sites, Office for Nuclear Regulation, 2020.
- 67 M. J. Truex, V. L. Freedman, C. I. Pearce and J. E. Szecsody, Assessment of Technologies for I-129 Remediation in the 200UP-1 Operable Unit, Pacific Northwest National Laboratory, Richland, Washington, 2019.
- 68 J. E. Szecsody, C. Pearce, K. J. Cantrell, N. P. Qafoku, G. Wang, E. C. Gillispie, A. R. Lawter, B. N. Gartman and

- C. M. Brown, Evaluation of Remediation Technologies for Iodine-129: FY18 Bench Scale Results, Pacific Northwest National Laboratory, Richland, Washington, 2018.
- 69 USEPA, Washington State Department of Ecology and USDOE, *Record of Decision for Interim Remedial Action Hanford 200 Area Superfund Site 200-UP-1 Operable Unit.*, U. S. Environmental Protection Agency, Olympia, Washington, 2012.
- 70 J. J. Neeway, D. I. Kaplan, C. E. Bagwell, M. L. Rockhold, J. E. Szecsody, M. J. Truex and N. P. Qafoku, A review of the behavior of radioiodine in the subsurface at two DOE sites, *Sci. Total Environ.*, 2019, 691, 466–475.
- 71 M. L. Rockhold, S. R. Waichler, J. L. Downs, X. He, J. D. Tagestad, Y. Fang, V. L. Freedman, M. J. Truex and C. M. R. Yonkofski, Information on Technical Impracticability for Remediation of Iodine-129 Contamination, Pacific Northwest National Laboratory, Richland, Washington, 2019.
- 72 M. L. Rockhold, J. L. Downs, S. R. Waichler, C. M. R. Yonkofski, V. L. Freedman and M. J. Truex, Draft Technical Impracticability Evaluation for Iodine-129 in Groundwater at Hanford: 200-UP-1 Operable Unit, Pacific Northwest National Laboratory, Richland, Washington, 2018.
- 73 S. A. Saslow, T. G. Levitskaia, E. A. Cordova, N. M. Avalos, D. Boglaienko, Y. Fang, X. Song, A. Lawter, H. Emerson, J. Szecsody, C. D. Johnson, C. I. Pearce, V. L. Freedman and R. D. Mackley, Part I: Predicting performance of Purolite A532E resins for remediation of comingled contaminants in groundwater, *J. Environ. Chem. Eng.*, 2023, 11, 109618.
- 74 S. A. Saslow, T. G. Levitskaia, E. A. Cordova, N. M. Avalos, D. Boglaienko, Y. Fang, X. Song, A. Lawter, H. Emerson, J. Szecsody, C. D. Johnson, C. I. Pearce, V. L. Freedman and R. D. Mackley, Part II: Predicting performance of DOWEX 21K resin for remediation of comingled contaminants in groundwater, *J. Environ. Chem. Eng.*, 2023, 11, 109620.
- 75 E. L. Campbell, T. G. Levitskaia, M. S. Fujimoto, V. E. Holfeltz, S. D. Chatterjee and G. B. Hall, Analysis of Uranium Ion Exchange Resin from the 200 West Pump-and-Treat Facility, Pacific Northwest National Laboratory, Richland, Washington, 2018.
- 76 DOE, Calendar Year 2020 Annual Summary Report For Pump And Treat Operations In the Hanford Central Plateau Operable Units, U.S. Department of Energy, Richland, Washington, 2022.
- 77 BNL, 2005 Site Environmental Report Volume II Groundwater Status Report, Brookhaven National Laboratory, Upton, New York, 2006.
- 78 T. Sullivan, M. Hauptmann and W. Gunther, Lessons Learned in Detecting, Monitoring, Modeling and Remediating Radioactive Ground-Water Contamination, United States Nuclear Regulatory Commission, Upton, New York, 2011.
- 79 BNL, 2021 Site Environmental Report Volume II Groundwater Status Report (Appendix C), Brookhaven National Laboratory, Upton, New York, 2022.

- 80 G. Blount, J. Thibault, M. Millings and P. Prater, 25 Years Of Environmental Remediation In The General Separations Area Of The Savannah River Site: Lessons Learned About What Worked And What Did Not Work In Soil And Groundwater Cleanup 15270, Waste Management Symposia, Phoenix, Arizona, 2015.
- 81 A. A. H. Faisal, A. H. Sulaymon and Q. M. Khaliefa, A review of permeable reactive barrier as passive sustainable technology for groundwater remediation, *Int. J. Environ. Sci. Technol.*, 2018, **15**, 1123–1138.
- 82 ITRC, Permeable Reactive Barrier: Technology Update, International Technology and Regulatory Council, Washington D.C., 2011.
- 83 F. Obiri-Nyarko, S. J. Grajales-Mesa and G. Malina, An overview of permeable reactive barriers for *in situ* sustainable groundwater remediation, *Chemosphere*, 2014, 111, 243–259.
- 84 S. Smoleń, I. Ledwożyw-Smoleń and W. Sady, The role of exogenous humic and fulvic acids in iodine biofortification in spinach (Spinacia oleracea L.), Plant Soil, 2016, 402, 129–143.
- 85 S. M. Steinberg, G. T. Schmett, G. Kimble, D. W. Emerson, M. F. Turner and M. Rudin, Immobilization of fission iodine by reaction with insoluble natural organic matter, J. Radioanal. Nucl. Chem., 2008, 277, 175–183.
- 86 N. P. Qafoku, C. Bagwell, A. R. Lawter, M. J. Truex, J. E. Szecsody, O. Qafoku, L. Kovarik, L. Zhong, A. Mitroshkov and V. Freedman, Conceptual Model of Subsurface Processes for Iodine at the Hanford Site, Pacific Northwest National Laboratory, Richland, Washington, 2018.
- 87 P. H. Santschi and D. I. Kaplan, *Using Radioiodine Speciation* to Address Environmental Remediation and Waste Stream Sequestration Problems at the Fukushima Daiichi Nuclear Power Plant and a DOE Site, Texas A&M University, Galveston, Texas, 2020.
- 88 R. C. Moore, C. I. Pearce, J. W. Morad, S. Chatterjee, T. G. Levitskaia, R. M. Asmussen, A. R. Lawter, J. J. Neeway, N. P. Qafoku, M. J. Rigali, S. A. Saslow, J. E. Szecsody, P. K. Thallapally, G. Wang and V. L. Freedman, Iodine immobilization by materials through sorption and redox-driven processes: A literature review, Sci. Total Environ., 2020, 716, 132820.
- 89 C. Xu, E. J. Miller, S. Zhang, H.-P. Li, Y.-F. Ho, K. A. Schwehr, D. I. Kaplan, S. Otosaka, K. A. Roberts, R. Brinkmeyer, C. M. Yeager and P. H. Santschi, Sequestration and Remobilization of Radioiodine (129I) by Soil Organic Matter and Possible Consequences of the Remedial Action at Savannah River Site, Environ. Sci. Technol., 2011, 45, 9975–9983.
- 90 L. Newsome, K. Morris, A. Cleary, N. K. Masters-Waage, C. Boothman, N. Joshi, N. Atherton and J. R. Lloyd, The impact of iron nanoparticles on technetium-contaminated groundwater and sediment microbial communities, *J. Hazard. Mater.*, 2019, 364, 134–142.
- 91 D. Boglaienko, O. Qafoku, R. K. Kukkadapu, L. Kovarik, Y. P. Katsenovich, D. E. Cherkasov, H. P. Emerson and

- T. G. Levitskaia, Elemental iron: reduction of pertechnetate in the presence of silica and periodicity of precipitated nano-structures, *Environ. Sci.: Nano*, 2020, **8**, 97–109.
- 92 L. Liang, B. Gu and X. Yin, Removal of technetium-99 from contaminated groundwater with sorbents and reductive materials, *Sep. Technol.*, 1996, **6**, 111–122.
- 93 K. Bronstein, *Permeable Reactive Barriers for Inorganic and Radionuclide Contamination*, National Network of Environmental Studies, Washington, DC, 2005.
- 94 Bechtel Jacobs Company LLC, Bechtel Jacobs Company LLC Sampling and Analysis Plan for the Water Resources Restoration Program for Fiscal Year 2009 Oak Ridge Reservation, Oak Ridge, Tennessee, Bechtel Jacobs Company LLC, Oak Ridge, Tennessee, 2008.
- 95 DOE, *Hanford Site Groundwater Monitoring Report for 2020*, U.S. Department of Energy, Richland, Washington, 2021.
- 96 V. M. Vermeul, B. G. Fritz, J. S. Fruchter, J. E. Szecsody and M. D. Williams, 100-NR-2 Apatite Treatability Test: High-Concentration Calcium-Citrate-Phosphate Solution Injection for In Situ Strontium-90 Immobilization Final Report, Pacific Northwest National Laboratory, Richland, Washington, 2010.
- 97 V. R. Vermeul, J. E. Szecsody, B. G. Fritz, M. D. Williams, R. C. Moore and J. S. Fruchter, An Injectable Apatite Permeable Reactive Barrier for *In Situ* ⁹⁰Sr Immobilization, *Groundwater Monit. Rem.*, 2014, 34, 28–41.
- 98 USEPA, US Department of Energy 100-NR-1 and 100-NR-2 Operable Units Hanford Site 100 Area Benton County Washington Amended Record of Decision Decision Summary and Responsiveness Summary September 2010, United States Environmental Protection Agency, Seattle, Washington, 2010.
- 99 R. M. H. Verbeeck, M. Hauben, H. P. Thun and F. Verbeek, Solubility and Solution Behaviour of Strontiumhydroxyapatite, *Z. Phys. Chem.*, 1977, **108**, 203–215.
- 100 C. Macci, E. Peruzzi, S. Doni and G. Masciandaro, Monitoring of a long term phytoremediation process of a soil contaminated by heavy metals and hydrocarbons in Tuscany, *Environ. Sci. Pollut. Res.*, 2020, 27, 424–437.
- 101 D. E. Salt, M. Blaylock, N. P. B. A. Kumar, V. Dushenkov, B. D. Ensley, I. Chet and I. Raskin, Phytoremediation: A Novel Strategy for the Removal of Toxic Metals from the Environment Using Plants, *Bio/Technology*, 1995, 13, 468– 474.
- 102 H. Ali, E. Khan and M. A. Sajad, Phytoremediation of heavy metals—Concepts and applications, *Chemosphere*, 2013, 91, 869–881.
- 103 I. Alkorta, J. Hernández-Allica, J. M. Becerril, I. Amezaga, I. Albizu and C. Garbisu, Recent Findings on the Phytoremediation of Soils Contaminated with Environmentally Toxic Heavy Metals and Metalloids Such as Zinc, Cadmium, Lead, and Arsenic, Rev. Environ. Sci. Bio/Technol., 2004, 3, 71–90.
- 104 J. T. Brown, G. Matthern, A. Glenn, J. Kauffman, S. Rock, M. Kuperberg, C. Ainsworth and J. Waugh, Proceedings from the Workshop on Phytoremediation of Inorganic

- Contaminants, Idaho National Engineering and Environmental Laboratory, Chicago, Illinois, 2000.
- 105 R. Bennett and N. Willey, Soil availability, plant uptake and soil to plant transfer of 99Tc—A review, *J. Environ. Radioact.*, 2003, 65, 215–231.
- 106 M. Tamaoki, T. Yabe, J. Furukawa, M. Watanabe, K. Ikeda, I. Yasutani and T. Nishizawa, Comparison of Potentials of Higher Plants for Phytoremediation of Radioactive Cesium from Contaminated Soil, *Environ. Control Biol.*, 2016, 54, 65–69.
- 107 M. V. Dutton, Accumulation of Caesium and Strontium by Cirsium vulgare and Rumex obtusifolius on the Southern Soil Disposal Tip at Sellafield: Part I, Westlake Scientific Consultin, Cumbria, UK, 2000.
- 108 J. M. Purkis, R. P. Bardos, J. Graham and A. B. Cundy, Developing field-scale, gentle remediation options for nuclear sites contaminated with ¹³⁷Cs and ⁹⁰Sr: The role of Nature-Based Solutions, J. Environ. Manage., 2022, 308, 114620.
- 109 C. Lewis and R. Van Pelt, Natural Remediation at Savannah River Site, Waste Management Symposia, Tucson, Arizona, 2002
- 110 SRNS, Savannah River Site Groundwater Management Strategy and Implementation Plan (U), Savannah River Nuclear Solutions, LLC, Aiken, South Carolina, 2006 (updated 2020).
- 111 SRNS, Savannah River Site Environmental Report 2021, Savannah River Nuclear Solutions, LLC, Aiken, South Carolina, 2022.
- 112 DOE, Trees Help Clean Groundwater in SRS Project, 2016, https://www.energy.gov/management/articles/trees-help-clean-groundwater-srs-project, accessed 6 October 2023.
- 113 D. R. Hitchcock, C. D. Barton, K. T. Rebel, J. Singer, J. C. Seaman, J. D. Strawbridge, S. J. Riha and J. I. Blake, A containment and disposition strategy for tritiumcontaminated groundwater at the Savannah River Site, South Carolina, United States, *Environ. Geosci.*, 2005, 12, 17–28.
- 114 J. D. Istok, J. M. Senko, L. R. Krumholz, D. Watson, M. A. Bogle, A. Peacock, Y.-J. Chang and D. C. White, *In Situ* Bioreduction of Technetium and Uranium in a Nitrate-Contaminated Aquifer, *Environ. Sci. Technol.*, 2004, 38, 468–475.
- 115 M. Radziemska, M. Z. Gusiatin, A. Cydzik-Kwiatkowska, G. Majewski, A. Blazejczyk and M. Brtnicky, New approach strategy for heavy metals immobilization and microbiome structure long-term industrially contaminated soils, *Chemosphere*, 2022, **308**, 136332.
- 116 W. Qiao, Y. Zhang, H. Xia, Y. Luo, S. Liu, S. Wang and W. Wang, Bioimmobilization of lead by Bacillus subtilis X3 biomass isolated from lead mine soil under promotion of multiple adsorption mechanisms, R. Soc. Open Sci., 2019, 6, 181701.
- 117 D. R. Lovley, E. J. P. Phillips, Y. A. Gorby and E. R. Landa, Microbial reduction of uranium, *Nature*, 1991, **350**, 413–416.

- 118 I. T. Burke, C. Boothman, J. R. Lloyd, R. J. G. Mortimer, F. R. Livens and K. Morris, Effects of Progressive Anoxia on the Solubility of Technetium in Sediments, *Environ. Sci. Technol.*, 2005, **39**, 4109–4116.
- 119 J. Wikström, S. Bonaglia, R. Rämö, G. Renman, J. Walve, J. Hedberg and J. S. Gunnarsson, Sediment Remediation with New Composite Sorbent Amendments to Sequester Phosphorus, Organic Contaminants, and Metals, *Environ. Sci. Technol.*, 2021, 55, 11937–11947.
- 120 C. Xiong, D. Wang, N. F. Tam, Y. Dai, X. Zhang, X. Tang and Y. Yang, Enhancement of active thin-layer capping with natural zeolite to simultaneously inhibit nutrient and heavy metal release from sediments, *Ecol. Eng.*, 2018, **119**, 64–72.
- 121 M. E. Denham, H. Gonzalez-Raymat and C. A. Eddy-Dilek, Applied Science Investigations to Facilitate Closure of the F-Area and H-Area Seepage Basins, Savannah River National Laboratory, Aiken, South Carolina, 2020.
- 122 K. Boerstler, J. Thibault, D. Stefanko and P. Prater, *The Use of Silver Chloride Injection in Remediation of Iodine-129 by In Situ Capture as Silver Iodide at the F-Area Seepage Basin 20225*, Waste Management Symposia, Phoenix, Arizona, 2020.
- 123 SRNS, Annual Corrective Action Report for the F-Area Hazardous Waste Management Facility, the H-Area Hazardous Waste Management Facility, and the Mixed Waste Management Facility (U), Savannah River Nuclear Solutions, LLC, Aiken, South Carolina, 2021.
- 124 D. J. Geniesse and G. E. Stegen, 2009 Evaluation of Tritium Removal and Mitigation Technologies for Wastewater Treatment, U.S. Department of Energy, Richland, Washington, 2009.
- 125 C. J. Sienkiewicz and J. E. Lentz, Recovery of Tritium from Water, *Fusion Technol.*, 1988, **14**, 444–449.
- 126 T. Yamanishi, H. Kakiuchi, H. Tauchi, T. Yamamoto and I. Yamamoto, Discussions on Tritiated Water Treatment for Fukushima Daiichi Nuclear Power Station, *Fusion Sci. Technol.*, 2020, 76, 430-438.
- 127 S. D. Bondarenko, I. A. Alekseev, O. A. Fedorchenko, T. V. Vasyanina, K. A. Konoplev, E. A. Arkhipov and V. V. Uborsky, Improvement of PNPI Experimental Industrial Plant Based on CECE Process for Heavy Water Detritiation, *Fusion Sci. Technol.*, 2008, 54, 446–449.
- 128 Government of Japan, Events and highlights on the progress related to recovery operations at TEPCO's Fukushima Daiichi Nuclear Power Station, Government of Japan, 2022.

- 129 DOE, Evaluation of Tritium Removal and Mitigation Technologies for Wastewater Treatment, U.S. Department of Energy, Richland, Washington, 2022.
- 130 EPA, Cost Analyses for Selected Groundwater Cleanup Projects: Pump and Treat Systems and Permeable Reactive Barriers, U. S. Environmental Protection Agency, 2001.
- 131 A. B. Cundy, L. LaFreniere, R. P. Bardos, E. Yan, R. Sedivy and C. Roe, Integrated phytomanagement of a carbon tetrachloride-contaminated site in Murdock, Nebraska (USA), J. Cleaner Prod., 2021, 290, 125190.
- 132 M. C. Negri, G. Gopalakrishnan and C. Hamilton, 317/319 Phytoremediation Site Monitoring Report - 2003 Growing Season, Argonne National Laboratory, Argonne, Illinois, 2004
- 133 S. Withana, P. Ten Brink, A. Illes, S. Nanni and E. Watkins, Environmental Tax Reform in Europe: Opportunities for the future, Institute for European Environmental Policy, Brussels, 2014.
- 134 J. M. Purkis, P. E. Warwick, J. Graham, S. D. Hemming and A. B. Cundy, Towards the application of electrokinetic remediation for nuclear site decommissioning, *J. Hazard. Mater.*, 2021, 413, 125274.
- 135 M. Pedrotti, C. Wong, G. El Mountassir, J. C. Renshaw and R. J. Lunn, Desiccation behaviour of colloidal silica grouted sand: A new material for the creation of near surface hydraulic barriers, *Eng. Geol.*, 2020, **270**, 105579.
- 136 P. Bots, J. C. Renshaw, T. E. Payne, M. J. Comarmond, A. E. P. Schellenger, M. Pedrotti, E. Calì and R. J. Lunn, Geochemical evidence for the application of nanoparticulate colloidal silica gel for *in situ* containment of legacy nuclear wastes, *Environ. Sci.: Nano*, 2020, 7, 1481–1495.
- 137 X. Hou, Radiochemical analysis of radionuclides difficult to measure for waste characterization in decommissioning of nuclear facilities, *J. Radioanal. Nucl. Chem.*, 2007, 273, 43– 48.
- 138 P. E. Warwick, B. C. Russell, I. W. Croudace and Z. Zacharauskas, Evaluation of inductively coupled plasma tandem mass spectrometry for radionuclide assay in nuclear waste characterisation, *J. Anal. At. Spectrom.*, 2019, 34, 1810–1821.
- 139 B. Zaffora, M. Magistris, J.-P. Chevalier, C. Luccioni, G. Saporta and L. Ulrici, A new approach to characterize very-low-level radioactive waste produced at hadron accelerators, *Appl. Radiat. Isot.*, 2017, **122**, 141–147.